# INVESTIGATIONS ON SLOT-LOADED SQUARE MICROSTRIP PATCH ANTENNAS FOR COMPACT DUAL FREQUENCY DUAL POLARIZED OPERATIONS

*Thesis submitted by*

BINOY G S

*in partial fulfilment of the requirements*
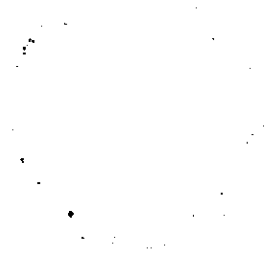
*for the award of the degree of*

*DOCTOR OF PHILOSOPHY*

DEPARTMENT OF ELECTRONICS
FACULTY OF TECHNOLOGY
COCHIN UNIVERSITY OF SCIENCE AND TECHNOLOGY
COCHIN 682 022, INDIA

JUNE 2002

*Dedicated to my parents and teachers.........*

# CERTIFICATE

This is to certify that this thesis entitled **"INVESTIGATIONS ON SLOT-LOADED SQUARE MICROSTRIP PATCH ANTENNAS FOR COMPACT DUAL FREQUENCY DUAL POLARIZED OPERATIONS"** is a bona fide record of the doctoral research work carried out by Mr.Binoy GS, under my supervision in the Department of Electronics, Cochin University of Science & Technology. The results presented in thesis or part of it have not been presented for any other degree.

**Dr.K Vasudevan**
Supervising Teacher
Professor

Cochin 682 022
5th June 2002

Department of Electronics
Cochin University of Science and Technology

# DECLARATION

I hereby declare that the work presented in this thesis entitled "**INVESTIGATIONS ON SLOT-LOADED SQUARE MICROSTRIP PATCH ANTENNAS FOR COMPACT DUAL FREQUENCY DUAL POLARIZED OPERATIONS**" is based on the original work done by me under the supervision of Dr. K Vasudevan in the Department of Electronics, Cochin University of Science & Technology, and that no part thereof has been presented for any other degree.

Cochin 682 022                                                          **BINOY GS**
5<sup>th</sup> June 2002

# Acknowledgements

**BINOY G.S**

# CONTENTS

# CHAPTER 1

---

# INTRODUCTION

# INTRODUCTION

*Since the first light of civilization, communication has been of prime significance to human beings. Depending upon the distance of communication, various acoustic methods such as drums, horns and optical communication methods like smoke signals and fire works, utilizing the visible portion of the electromagnetic spectrum, were used. As technology advanced further, communication using the electromagnetic spectrum outside the visible region has been explored.*

*It is strongly believed that electromagnetic theory is one of the chief intellectual achievements of human species over the last two centuries. James Clark Maxwell (1831-1879) predicted that light and electromagnetic waves are due to one and the same physical phenomenon and both can be explained by the waves travelling at the same speed. Maxwell's partial differential equations of Electrodynamics represent a fundamental unification of electric and magnetic fields predicting an electromagnetic wave phenomenon [1].*

The notion of antenna was first conceived in 1886, by Heinrich Rudolph Hertz, the father of Electromagnetics, in his Laboratory at the Technical Institute of Kalsruhe. Hertz proved experimentally that the electrical disturbances could be detected with a secondary circuit of proper dimensions for resonance and containing an air gap for sparks to occur. He generated, transmitted and received electromagnetic energy by means of an end loaded half-wave dipole (Hertzian Dipole) as transmitter and a resonant square loop antenna as receiver.

Antennas are like Electronic eyes and ears [2]. They act as interface between free space and circuitry. IEEE standards define an antenna as "a means for radiating or receiving electromagnetic waves" [3]. An antenna is an integral part of any communication device.

The talented Indian scientist Sir. Jagadis Chunder Bose (1858-1937) conducted pioneering research work with millimeter waves in the 60-GHz range [4]. He developed a new type of antenna named as Horn antenna in1897 during his studies with millimeter wave propagation. Even though Bose has contributed substantially to the millimeter and microwave detection, his contributions were not adequately publicized and appreciated by the large electronic community in general. Although neglected somewhat in the early 1900s, the horn antenna has drawn immense popularity in the late 1930s, due to the interest in microwaves and waveguide transmission lines during the period of World War II. The horn is widely used as a feed element for radio astronomy and satellite tracking antennas installed all over the world. In addition to that they form an integral part of phased arrays and serves as a universal standard for calibration and gain measurements.

The challenging works by Bose and Hertz inspired Guglielmo Marconi (1874-1937), an Italian Electrical Engineer to use the Hertzian waves for communication purposes. Marconi startled the scientific community in 1901 through his transatlantic radio communication link. The set up consisted of a transmitting antenna made out of a spark transmitter connected between the ground and a system of 50 vertical wires. The antenna used in a radio can radiate or receive electromagnetic waves, thereby can

transfer information between different locations without any intervening structures. Radio has been the first technological product that percolated into the common man's life.

The contributions of the Ohio University professor, Dr.J.D. Kraus to the field of antennas are outstanding. He invented the helical and corner reflector antennas, which has got wide applications in space communication as well as television reception. Kraus is the author of the classic textbook 'Antennas', considered as the 'Antenna Bible'. He made extensive studies on the performance of various antennas and classified them as discussed in the following section.

## 1.1 GENERAL CLASSIFICATION OF ANTENNAS

J D Kraus [2,5] has suggested a basic classification for antenna types depending on their design peculiarities, mode of operation and applications in which they can be employed;

(i) Wire antennas: dipoles, monopoles, helical antennas and Yagi-Uda antennas, commonly used in lower frequency

(ii) Aperture antennas: waveguide horn, slot in waveguide, cavity or ground plane, generally used in microwave frequency.

(iii) Printed planar antennas: microstrip antennas, used in microwave frequency and MMIC Applications.

(iv) Reflector antennas: parabolic reflector antenna and Cassegrain antenna operating at microwave frequencies.

The main objective of this thesis is the design and characterization of printed antennas having dual frequency dual polarized mode of operation.

## 1.2 PRINTED STRUCTURES

Printed geometries drastically reduced the size of the waveguide or other communication components, which find wide application in this era of micro fabrication techniques. Printed structures are composed of one or more dielectric layers with metallic traces printed on it. Early designs were made of triplate or strip lines with one thin metallic strip enclosed by two dielectric layers with metallic patches. As technology of printed circuits advances further more and more sophisticated designs were implemented. Some of the commonly used printed structures are microstrip lines (here, one of the dielectric layers are removed) slotlines (in which only one side of the dielectric is metallic), the inverted line and the finline. The most widely used printed geometry is the microstrip line. It is comparatively easy to fabricate and can be easily incorporated into circuit designs.

Microstrips are printed circuits operating in the microwave range, over the Giga Hertz region of the electromagnetic spectrum. Realized by the photolithographic process, they let designers reduce the size, weight and cost of components and systems for low-signal-level applications by replacing the more cumbersome waveguide components and assemblies. The fabrication process is well suited for series production of circuits and antennas. At microwave frequencies, all dimensions become important, so the realization of microstrip requires more care than that of low-frequency printed circuits.

Based on design and application, four types of waves can be excited in a planar microstrip geometry; they are

    i.      Space waves: - Ideal for Antennas

    ii.     Guided waves: - For transmission Line structures

    iii.    Surface waves

    iv.    Leaky Waves

For effective transmission in an antenna, most of the energy has to be converted in to a space wave, whereas in transmission lines, most of the energy should be stored in a guided wave. The other two wave types, the surface and the leaky wave account for the unwanted radiation losses. As the height of the microstrip substrate increases, surface waves are introduced which usually are not desirable since they extract power from the total power available for direct radiation (space waves). The surface waves travel within the substrate and they are scattered at bends and surface discontinuity, such as the truncation of the dielectric and the ground plane, which degrade the antenna pattern and polarization characteristics.

## 1.3 MICROSTRIP ANTENNAS

The microstrip antenna uses the microstrip structure to make an antenna. Microwave engineers earlier used strip lines to fabricate feed lines from circuit board. Strip line uses two ground planes and a flat strip in between, to guide RF. The major drawback of these type of circuits is unwanted radiation. The idea of microstrip antennas occurred to microwave engineers as a positive utilization of this radiated undesired power in the case of strip line circuits. The microstrip Antenna concept was first proposed by Deschamps [6] in 1953. Since then, it took nearly 20 years for the first practical microstrip antenna to come up. The first practical microstrip antennas were developed by Howell [7] and Munson [8] in the early 1970's, which resulted in the evolution of a new branch of antenna engineering called Printed Patch Antennas, which find enormous applications in satellite and mobile communication systems owing to its compact structure and low profile.

The basic configuration of a microstrip antenna consists of a planar radiating structure of desired geometrical shape on one side of a dielectric substrate and a ground plane on the other. Commonly used microstrip radiating geometries are rectangular and circular [9]. However, other shapes are also considered depending upon the application. A simple microstrip antenna configuration is shown in figure 1.1.
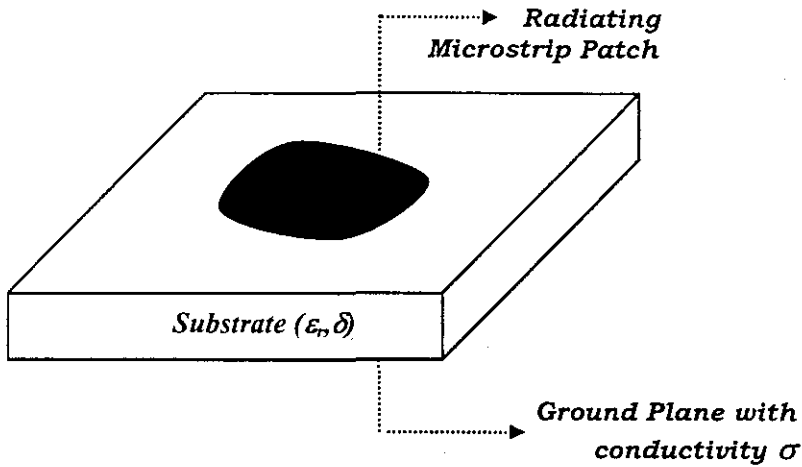
*Figure 1.1* Microstrip Antenna Configuration

## 1.3.1 Radiation from a Microstrip Antenna

In microstrip antennas, the radiation is from the periphery of the patch, where the fringing field is maximum. Portions of the patch act like slots, with respect to the ground plane. The exciting dipole launches guided modes in the parallel plate region under the patch. The surface current distributions can be computed on the conducting and dielectric surfaces of the antenna to understand their behaviour. The radiation from microstrip antennas occurs from the fringing fields between the edge of the microstrip antenna conductor and the ground plane [9]. For a rectangular microstrip antenna fabricated on thin dielectric substrate and operating in the fundamental mode, there is no field variation along the width and thickness. The fields vary along the length, with a period of half a wavelength. The radiation from a microstrip patch is shown in figure 1.2.

The radiation mechanism can be explained by resolving the fringing fields at the open circuited edges into the normal and tangential components with respect to the ground plane. The normal components are out of phase (as the patch is half wavelength long) and hence the far fields produced by them cancel each other. The tangential components are in phase and the resulting fields are combined to give maximum radiation in the broadside direction.

6
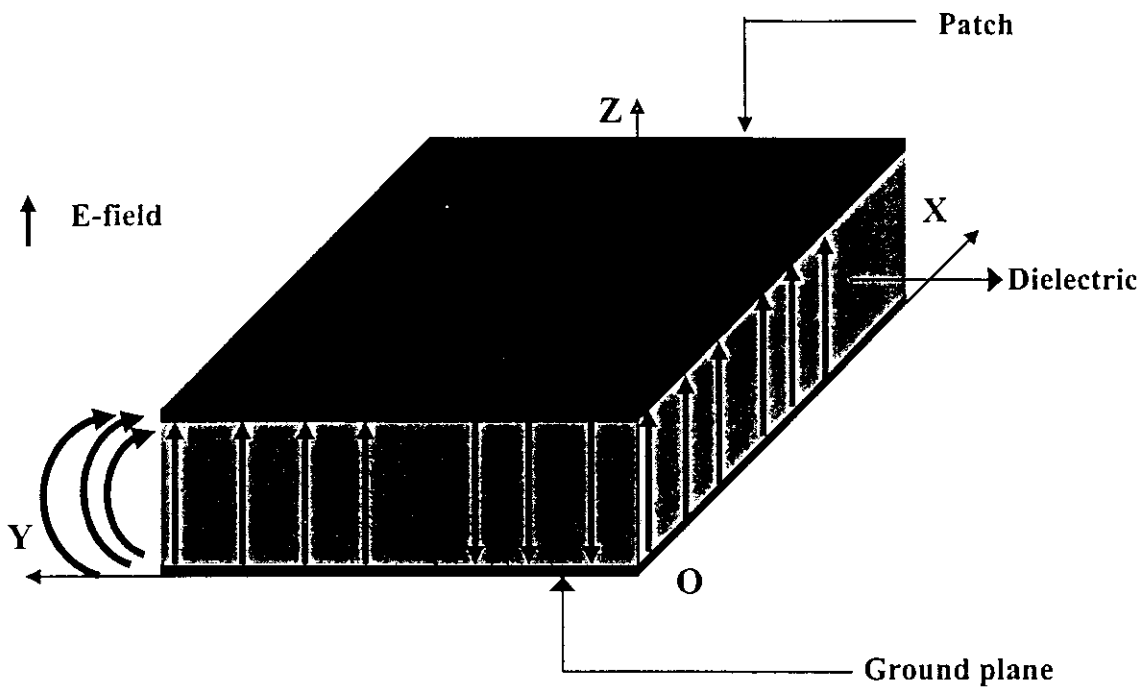
*Figure 1.2 Radiations from a Microstrip Patch Antenna*


## 1.3.2 Advantages and Disadvantages

In high-performance aircraft, spacecraft, satellite and missile applications, where size, weight, cost, performance, ease of installation and aerodynamic profile are constraints, low profile antennas may be required. At present, there are many other applications, such as mobile radio and wireless communication that has similar specifications. To meet these requirements, microstrip antennas can be used. These antennas are low profile, conformable to planar and non-planar surfaces, simple and inexpensive to manufacture using modern printed circuit technology, mechanically robust when mounted on rigid surfaces and compatible with MMIC designs. When the particular patch shape and mode are selected they are very versatile in terms of resonance frequency, polarization, impedance and broad radiation characteristics. In addition, by mounting active components like pins, varactor diodes and chip-capacitors antenna elements with variable resonance frequency, impedance, polarization and pattern can be designed.

Microstrip antennas also suffer from certain operational disadvantages, which limit their application in certain specified areas. The major drawbacks are their low efficiency, low

power, high Q, poor polarization purity, poor scan performance, spurious feed radiation and narrow impedance bandwidth. The power handling capacity as well as gain is lower than that of conventional microwave antennas. In certain cases, the isolation between the radiating patch and the feed element is also poor.

### 1.3.3 Selection of Substrate Materials

Substrate materials play an essential role in microstrip antenna design. For optimum performance, substrate characteristics and evaluation must be compatible with design objectives. Several aspects of the materials such as dielectric constant ($\varepsilon_r$) and loss tangent (tan $\delta$) and their variation with temperature and frequency, uniformity of thickness of substrate, dimensional stability with processing, thermal coefficient, temperature range etc., must be considered in the design stage when the substrates are selected [10]. There is no single ideal substrate; the choice rather depends on the application. Conformal microstrip antennas require flexible substrates, while low frequency applications require high dielectric constants to keep the size small. Microstrip patch antennas use low dielectric substrates [9]. Generally, this selection procedure is a compromise to get the best balance of desirable features for a given application.

The most commonly used substrates for antenna designs are Glass Micro Fiber reinforced PTFE (RT Duroid), Alumina, copper clad laminates and Teflon Glass cloth laminates. A wide variety of these substrates with dielectric constants varying from 2 to 25 and loss tangent below 0.0004 over the entire microwave frequency range, with considerable mechanical flexibility are available [9].

Substrate technology thus offers a challenge to material manufacturers to craft high-performance stable substrates at a reduced price.

## 1.3.4 Excitation Techniques

The selection of an appropriate feeding mechanism to couple power to a microstrip antenna is as important as the selection of a suitable geometry for a particular application.

A variety of feeding mechanisms are available and some important among them are explained here.

## 1.3.4.1 Microstrip Feed

This is the simplest way to feed electromagnetic power to a microstrip antenna. Here, the antenna and the feed line are fabricated simultaneously on the same side of the substrate as shown in figure 1.3 and this makes it very attractive in array environments.



To SMA Connector
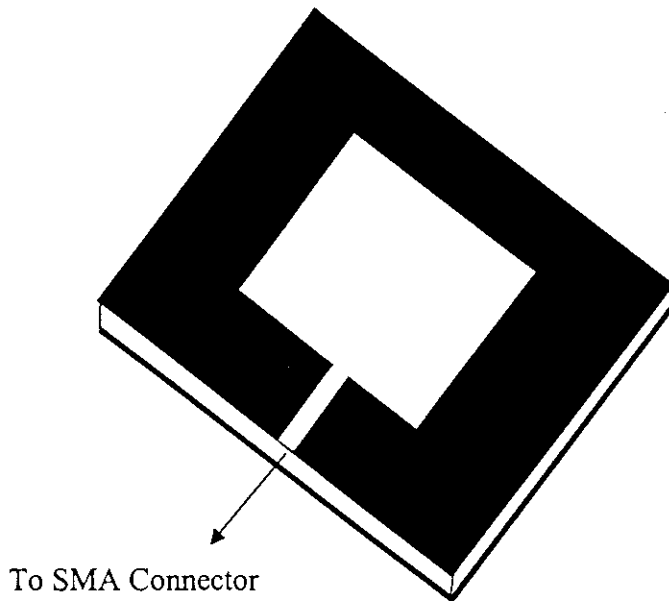
*Figure 1.3 Microstrip feeding Arrangement*

The most undesirable feature of this feeding mechanism is the spurious radiation from bends, transitions, junctions etc. These radiations adversely affect the side-lobe level and the cross-polarization characteristics of the antenna. This drawback may be compensated by suitably selecting a high dielectric constant substrate. This will also reduce the radiation efficiency of the antenna. A compromise between the two is to be made depending upon the applications.

## 1.3.4.2 Coaxial Feed
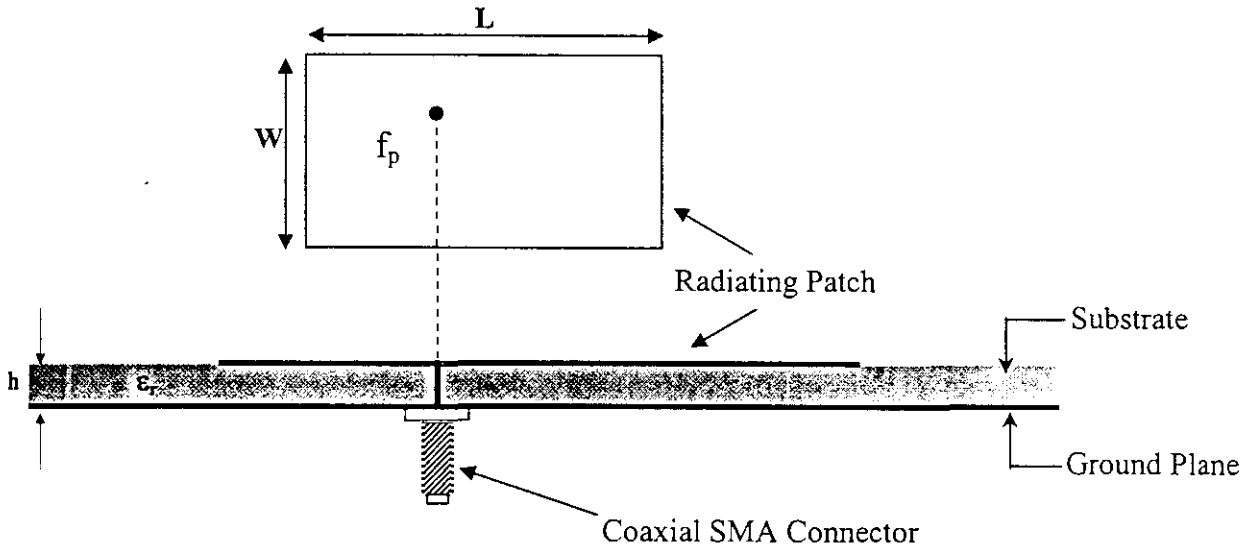


*Figure 1.4 Coaxial (probe) feeding for a Microstrip Antenna*

It is a convenient method of feeding a single patch. Here, the coaxial connector is attached to the backside of the printed circuit board and the centre conductor is attached to the antenna at the desired point. The coaxial (probe) feeding arrangement is shown in figure 1.4. As the feed lies behind the radiating surface, there is no chance of unwanted radiation from the feed for thin substrates. For thick substrates, the coupling between adjacent feeds may deteriorate the performance of the antenna. In array environment, the complete antenna design and feeding arrangement cannot be fabricated simultaneously. This increases the feeding complexity, especially in large arrays. At high frequencies, it becomes very difficult to realize these types of feeding as it involves drilling holes through the substrate and proper soldering of the centre conductor to the patch. For coaxial feeds, the feed location is usually selected to provide a good impedance match. Since the excitation by an electric dipole is simulated, the impedance of the feed can be ignored and the effect of its location on the excitation efficiency of various modes can be investigated. The various modes have different radiation patterns and affect the overall radiation pattern at different angular positions.

## 1.3.4.3 Buried Feed (Electromagnetic Coupling)

This is the most popular feeding mechanism for microstrip antenna. Here, the antenna and the feed are placed at two separate levels. The feed system is a covered microstrip line and radiating element is fabricated on the covering substrate immediately above the open-ended feed line. The system can be considered as a single patch on a double layered substrate sharing a common ground plane with the feed as shown in figure 1.5. Similar to the microstrip feed, in this method also, performance is affected by spurious radiation from the feed network. This can be minimized by using substrates of high dielectric constant for the feed line.
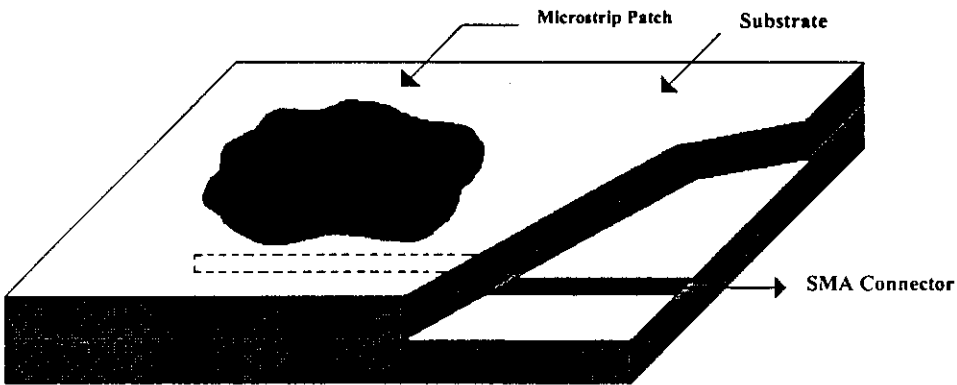


*Figure 1.5 Electromagnetic Coupling Arrangement*

## 1.3.4.4 Aperture Coupling Feed

Microstrip structures possess inherent asymmetries that generate higher order modes and cross-polarized radiation. To overcome this, non-contact aperture coupling feeds as shown in figure 1.6 is implemented. This feed arrangement is easy to model and has moderate spurious radiation effects. The aperture coupling consists of two substrates separated by a ground plane. On the bottom side of the lower substrate there is a microstrip feed line through which energy is coupled to the patch via a slot

separating the two substrates. This technique allows independent optimization of the feed mechanism and the radiating element. A high dielectric material is used for the bottom substrate, and thick low dielectric constant material for the top substrate. The ground plane between the substrates isolates the feed from the radiating element and minimizes interference of spurious radiation for pattern formation and polarization purity.

The spurious radiation from the line is physically separated from that of the patch and can be completely avoided by enclosing the feed within a box. To avoid radiation towards the backside of the antenna, the slot must not resonate within the operating frequency band of the patch and should be placed far enough from the edge of the patch.

The design is optimized by substrate electrical properties, feed line width, slot size and its position. Matching is obtained by controlling the width of the feed line and length of the slot.
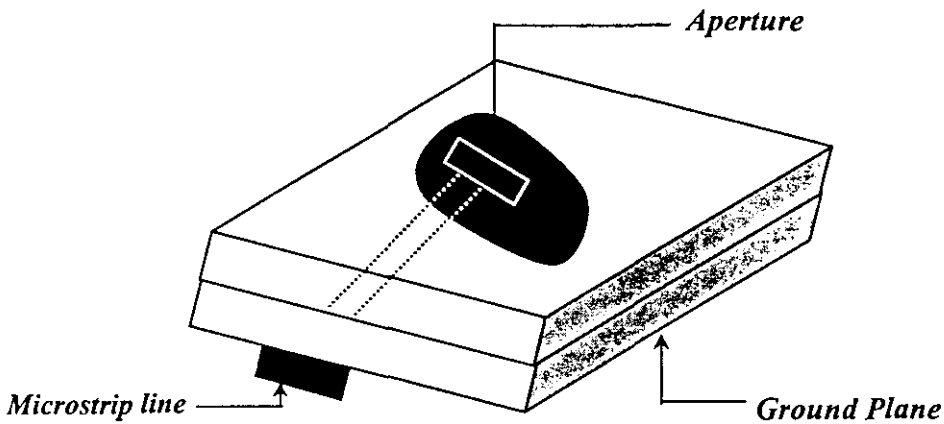


*Figure 1.6 Aperture (slot) feeding method*

## 1.3.5 Various Microstrip Antenna Configurations

Microstrip antennas are mainly categorized into three basic categories:

### 1.3.5.1 Microstrip patch antenna

A microstrip patch antenna consists of a very thin conducting metallic patch ($t \ll \lambda_0$, where $\lambda_0$ is the free-space wavelength) of desired planar geometry on one side of a dielectric substrate backed by a ground plane on the other side. The microstrip patch is so designed that its pattern maximum is normal to the patch (broadside radiator) [3]. This is accomplished by properly selecting the field configuration of excitation beneath the patch. Certain conventional patch antenna configurations are shown in figure 1.7.
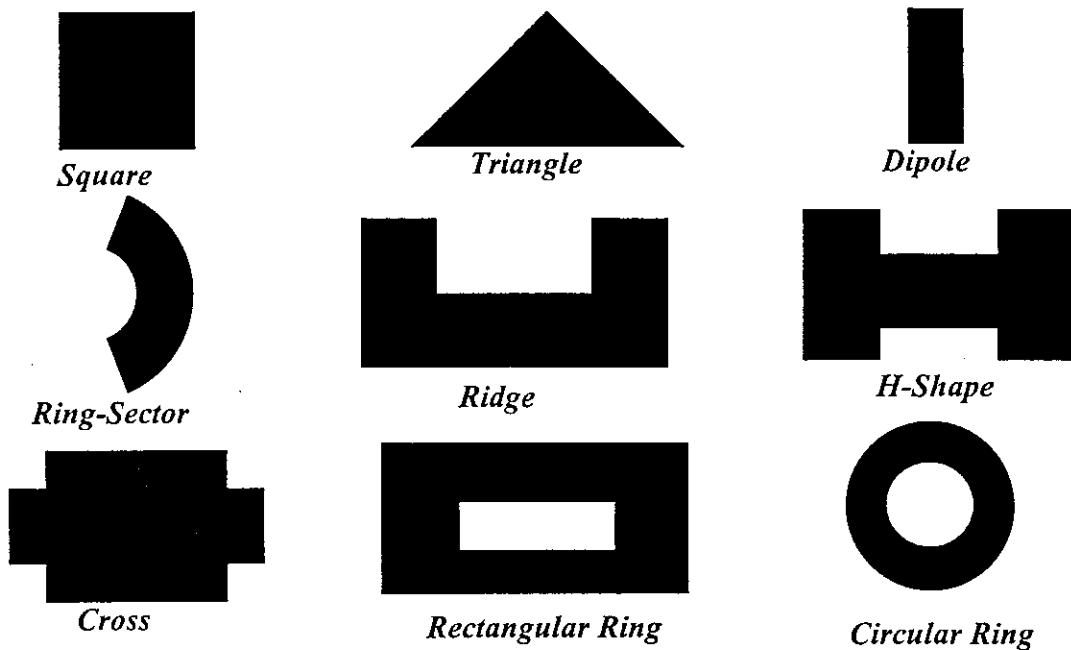
*Figure 1.7 Representative Shapes of Microstrip Patch Elements*

## 1.3.5.2 Microstrip Traveling wave antenna (MTA)

MTA consists of a chain-of periodic conductors or an ordinary long TEM line which also supports a TE mode, on a substrate backed by a ground plane. The open end of the TEM line is terminated in a matched resistive load [9]. As antenna supports traveling wave, their structures may be designed so that the main beam lies in any direction from broadside to end fire. Certain typical MTA geometries are shown in figure1.8.
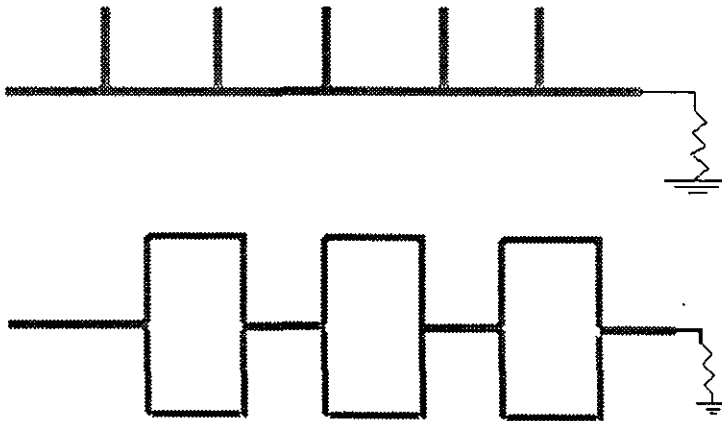


*Figure 1.8 Geometry of a couple of typical Microstrip Traveling wave* antennas

## 1.3.5.3 Microstrip Slot Antenna

Microstrip slot antenna consists of a slot in the ground plane fed by a microstrip feed line. They have the advantages of being able to produce bi-directional and unidirectional radiation patterns. Patch and slot combinations offer an additional degree of freedom in the design of microstrip antennas. This design criterion facilitates the design of antennas with desired polarization and they are less sensitive to manufacturing tolerances than are microstrip patch antennas. The slot can have the shape of a rectangle (narrow or wide), a circle or a ring slot as shown in figure 1.8. Microstrip slot antennas are generating wide interest owing to its characteristic features like compactness and dual-frequency operation.
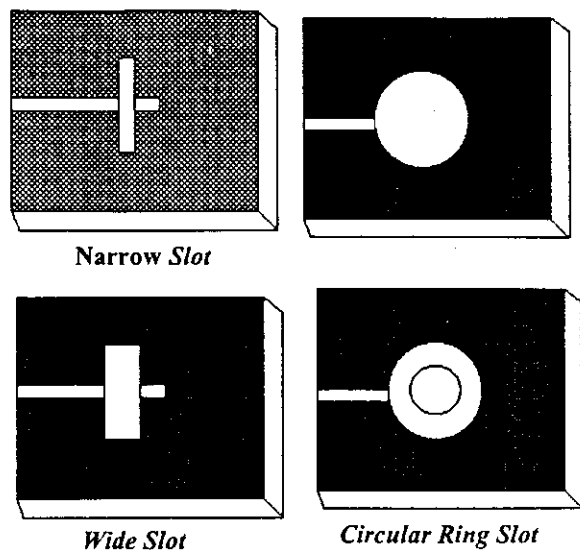
**Narrow** *Slot*

**Wide Slot**          *Circular Ring Slot*

*Figure 1.8 Microstrip Slot Antennas*

## 1.3.6 Broadband Microstrip Antennas

One of the major drawbacks of microstrip antennas, which limit its widespread application, is the narrow impedance bandwidth. There are different approaches for improving the impedance bandwidth of microstrip antennas. They include using thicker substrates with low dielectric constant, addition of a parasitic patch on top of the original patch with low dielectric constant, using multiple patches in one plane, or by means of proximity coupling of feed line to the patch antenna.

The use of thicker substrates for bandwidth enhancement is not usually preferred due to the excitation of surface waves. In the case of parasitic patches, each element resonates at adjacent frequencies and as a result the impedance bandwidth improves. Parasites can be mounted coplanar as thin resonators, as additional patches either gap or line coupled to the square patches. But, the disadvantage is that the parasitic loading will usually increase the overall surface area.

## 1.3.7 Compact Microstrip Antennas

Depending upon the application, microstrip antennas having different geometrical shapes are used [10]. However, recent developments in personal communication systems (PCS) demand more and more compact microstrip antennas. The important approaches for reducing the size of microstrip patch antennas include:

15

the use of new geometrical shapes, use of shorting posts and use of high dielectric constant substrate.

A detailed review of the research work, towards the development of compact microstrip antennas with dual frequency operation is presented in chapter 2.

The electric field and magnetic surface current distributions on the sidewall of the waveguide cavity for $TM_{10}$, $TM_{01}$ and $TM_{20}$ modes are demonstrated in fig 1.9. For the $TM_{10}$ mode, the magnetic currents along the width 'b' are constant and in phase while, those along length 'a' vary sinusoidally and they are out of phase. Because of this, the edge 'b' is known as the radiating edge since it contributes primarily to the radiation. Edge 'a' is termed as the non-radiating edge. For the $TM_{01}$ mode, the magnetic currents are constant and in phase along edge 'a', which is the radiating edge and 'b' acts as non-radiating edge, since the magnetic currents are not in phase.

## 1.3.8 Dual Frequency Dual Polarized Microstrip Patch Antennas

Dual frequency patch antennas have received much attention due to its capability to radiate at two separate frequencies from a single radiating structure, which finds wide applications in radar and aerospace systems. Similarly, Dual polarized antennas are also creating great interest owing to the recent developments in wireless communication. They can be applied in satellite communication systems to realize frequency reuse for doubling the system capability. They also can be used in mobile communication systems to obtain polarization diversity for good performance of reception and transmission or to integrate the receiving and transmitting functions into one antenna for reducing the antenna size. The single layer square patch antenna fed by a coaxial probe is highly desirable due to its thin profile, lightness, conformity, low cost and capability of being integrated with active devices. The diagonally fed patch operates on two orthogonally polarized modes, $TM_{10}$ and $TM_{01}$, normal to the patch edges.
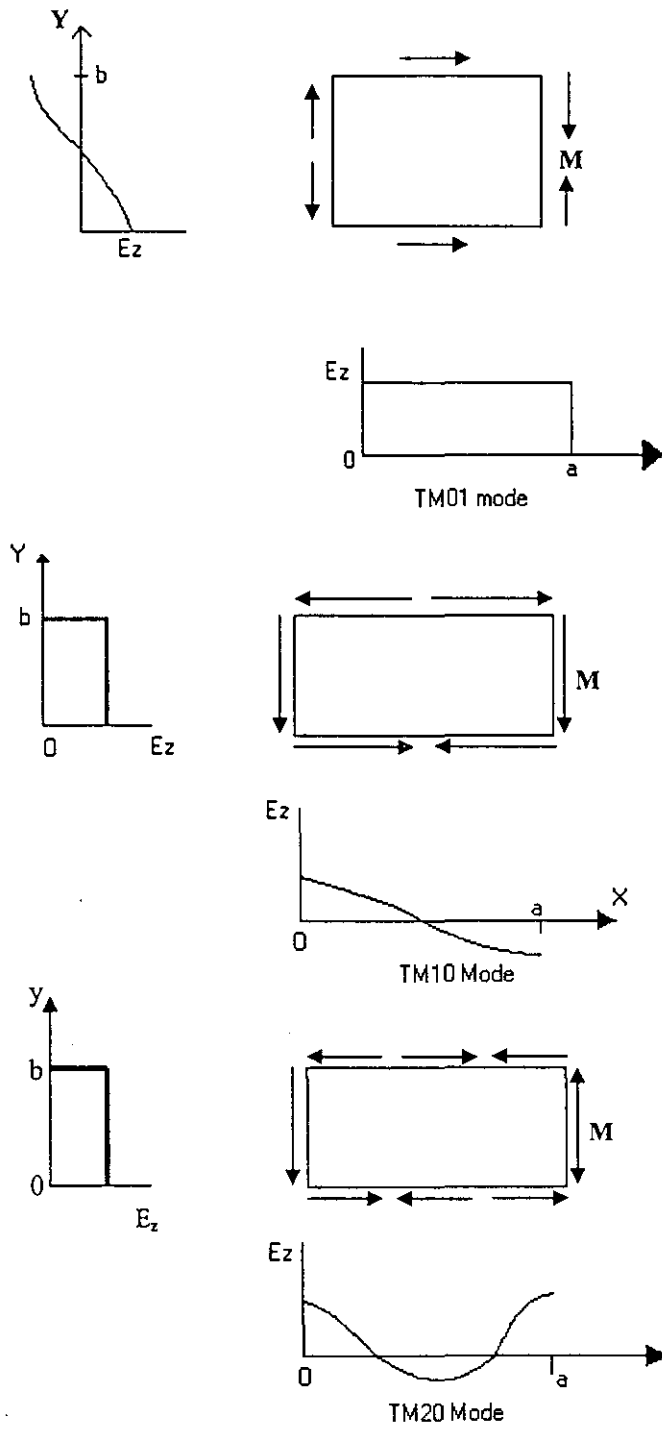
*Figure 1.9* $TM_{01}$, $TM_{10}$, and $TM_{20}$ modes generated in a microstrip Patch

## 1.3.9 Theoretical methods used in the analysis of microstrip antennas

Different theoretical approaches are available in literature for the analysis of microstrip antennas. For antennas having regular geometrical shapes (rectangular), analytical methods could be applied with segmentation technique. These techniques are unsuitable in the case of arbitrary shaped patches and slotted geometries. Here numerical techniques like Finite Element Method (FEM) or Finite Difference Time Domain method (FDTD) could be used. Some important techniques used for the analysis of microstrip antennas are briefly described in the following sections.

### 1.3.9.1 Transmission Line Model

This model was proposed by Munson [8] and Derbeyd [11]. Here the microstrip resonator is represented by two radiating slots (corresponding to the two radiating edges) separated and connected by an approximately half wavelength ideal transmission line. The input impedance is determined as a function of the distance from the edge of the patch to the feed point. The different radiation characteristics are determined by assuming that the fields vary along the length of the patch and remain constant across the width. The main inadequacy of this model is that, it is applicable only to rectangular (or square) patch geometries.

### 1.3.9.2 Cavity Model

Here, the microstrip geometry is considered as a cavity bounded at its top and bottom by electric walls and on its sides by a magnetic wall. The magnetic current flowing on the cavity side-walls radiate at the resonant frequencies of the cavity, which is assumed to be surrounded by free space. This model is suitable for geometries in which the Helmholtz equation possesses an analytical solution such as discs, rectangles, triangles, ellipses etc.

### 1.3.9.3 Method of Moments

In method of moments, the dielectric surface currents flowing over the patch metallization and the ground planes are evaluated by using Richmond's reaction methods [12]. The reaction integral equation is solved using the boundary conditions

and method of moments. Now, using suitable expansion functions, for electric surface currents, the integral equations are reduced to algebraic equations. These equations, are then solved for the unknown coefficients using any of the known numerical techniques. This technique is analytically simple and versatile, but it requires large amount of computation. The limitation of this technique is usually the speed and storage capacity of the computer.

### 1.3.9.4 Finite Element Method

The finite element method is a computer aided mathematical technique for obtaining approximate solutions for the abstract equations of calculus that predict the response of physical systems subjected to external influences. In the case of microstrip antennas, the fields interior to the antenna cavity can be determined by this method. Here the region of interest is sub-divided in to small areas or volumes depending upon the dimensions of the region. Usually these small regions are polygons such as triangles and rectangles for two-dimensional problems and tetrahedral elements for three-dimensional problems. The interior electric field, satisfying the inhomogeneous wave equation along with an impedance boundary condition on the perimeter walls, is solved for each of the elements, subdividing the region of interest. This method is applicable to arbitrary shaped patches also.

### 1.3.9.5 Finite Difference Time Domain (FDTD) Method

The Finite-Difference Time-Domain computational modeling provides a means to prototype a complex antenna design on the computer and spot troublesome microstrip calculations before any fabrication is done [13]. This method can be applied for all types of feeds [14]. FDTD method consists of the discretisation and solution of the Maxwell's curl equations directly in the time domain. In FDTD, microstrip antennas are treated in the time domain for analysis. The frequency dependence of the different parameters is determined from the Fourier transform of the Transient current. However, this method becomes computationally difficult and requires large amount of memory when the structure becomes complex. The method takes into account the full-wave effects of distributed electromagnetic wave coupling, radiation, ground loops and ground bounce. The time-domain measurements [1] are found to be far advantageous

19

compared to the frequency-domain measurements in analyzing complex electromagnetic problems.

### 1.3.9.6 Green's Function Method

This method can be employed when the shape of the microstrip radiating structure is simple, such as rectangle, triangle or circle. The electric field inside the cavity is evaluated using Green's function that in turn is used for the evaluation of the input impedance. This method is not suitable in the case of arbitrary geometrical shapes, since the Green's functions are not available for such shapes.

When the dimensions of the radiating system are of many wavelengths, low frequency methods is not that much computationally efficient. However, asymptotic methods are more efficient and stable.

### 1.4 ELECTROMAGNETIC SIMULATION

Electromagnetic simulation model is a new technology to yield high accuracy analysis and design of complicated microwave and RF printed circuits. Today there are a number of Electromagnetic modeling tools available in market such as SONET, ENSEMBLE, HFSS, MICRO-STRIPES etc. IE3D is an integrated full wave electromagnetic simulation and optimization package for the analysis and design of 3-dimensional microstrip antennas. The primary formulation of IE3D is an integral equation obtained through the use of Green's functions [15].

For the analysis, the new geometry is simulated using the IE3D simulation package. Here moment method codes using the roof-top functions are implemented, which is very accurate in predicting the total current on the transverse direction.
One of the major advantages of electromagnetic simulation is that the field and the current distribution from a simulated structure can be easily obtained. This is valuable to circuit and antenna designers. Here, we can model both the electric current on a metallic structure and a magnetic current representing the field distribution on a metallic structure. For antenna designers, the most interesting parameters are the S-parameters. These parameters are directly related to the total current on the transverse direction at a

port. The radiation pattern that is also a weighted integral of current density of the antenna, can also be precisely simulated using this technique.

## 1.5 SUMMARY OF THE PRESENT WORK

Microstrip antennas are being increasingly used in communication and radar systems due to their inherent advantages over conventional antennas of being lightweight, compact, and conformal. Recently, patch antenna research has been focused on reducing the size of the patch for their applications in mobile communications and monolithic microwave integrated circuits. One of the most effective approaches towards this is to increase the electric length by optimizing the shape of the microstrip antenna by inserting slots and reactive components in the antenna. In this study, the experimental and theoretical investigations towards the development of a new compact microstrip antenna are presented. The experimental investigations revealed that the newly proposed antenna requires much lesser area compared to the conventional microstrip antennas. It also provides methods like insertion of slots and microwave chip-capacitors within the antenna geometry without increasing the over all area of the patch. The investigations also exposed that the reduction of size can be achieved without significant reduction in gain. Another important design concern is the frequency tuning capability of the geometry through the embedded tuning stubs, which can tune the frequency of operation over a broad range. The operating frequencies are found to be having a systematic variation with respect to the stub length, and hence the criteria of frequency tuning can be fulfilled. Dual polarized antennas are finding wide applications in mobile communication systems to integrate the receiving and transmitting functions into one antenna for reducing the overall size.

## 1.6 CHAPTER ORGANIZATION

In chapter 2, a brief review of work carried out in the field of microstrip antennas during the past few decades by researchers all over the world is presented. This chapter also portrays some of the relevant works in the field of compact microstrip antennas for dual frequency operation.

In chapter 3, the methodology adopted for the investigations are described. The techniques used for the measurement of different antenna characteristics like resonance frequency, input impedance, bandwidth, radiation pattern, gain and field variation over the patch surface are explained. The IE3D electromagnetic modeling technique is also introduced in this chapter.

The important outcome of the experimental investigations carried out on the characteristics of the different slot loaded compact microstrip antenna configurations are described in chapter 4.

Chapter 5 describes the theoretical interpretations of the antenna. The theoretical approach is based on the FDTD modeling technique. The theoretical results are confirmed by comparison with the experimental results. In the last section, the antenna characteristics are also analyzed using the IE3D electromagnetic simulation technique.

The conclusions drawn from the experimental and theoretical investigations are discussed in Chapter 6. The dual resonant frequencies are found to be tunable with the dimensions of the central tuning stub. The scope for further work in the field is also suggested in this chapter.

The experimental work done by the author to study the electromagnetic scattering from various dielectric substrates is described in Appendix A.
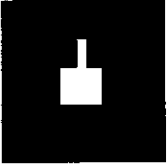
# EARLIER WORK IN THE FIELD-
# A BRIEF REVIEW

*The idea of utilizing the radiation characteristics of printed microstrip structures was suggested several years ago. Since then, research into the use of microstrip patch antennas for a broad range of applications has flourished, with microstrip antennas emerging as a separate field within Microwave Antenna Engineering.*

*During the past few decades the researchers all over the world have studied the theoretical and experimental aspects of different types of microstrip antennas. Recently, development and analysis of compact microstrip antennas have become an interesting area in personal communications systems due to the miniaturization of communication equipment. The significant works in the field of microstrip antennas, especially on dual frequency dual polarization characteristics, are reviewed with emphasis given to compact microstrip antennas.*

## 2.1 MICROSTRIP ANTENNAS – BRIEF REVIEW

Microstrip antennas started receiving considerable attention in the early 1970s [7], although the idea of a microstrip antenna can be traced to 1953 [6] by Deschamps and a patent in 1955 by Gulton [16]. During the past few decades, there was a growing need for the development of low profile antennas on the emerging new generation of missiles and spacecrafts. Revolution in electronic circuit miniaturization, brought forward by the developments in large Scale Integration (LSI), made conventional antennas massive and expensive part of the equipment. These two factors prompted the scientists for the design and development of compact and efficient microstrip radiators. Extensive research and development of microstrip antennas and arrays, exploiting the numerous advantages such as light weight, low volume, low cost, low scattering cross section, planar configuration and compatibility with MMIC's have led to diversified applications over a broad frequency range from ~100 MHz to 50 GHz.

The idea of a conducting strip radiator separated from a ground plane by a dielectric substrate was suggested by Byron [17] in the early 1970, and it was the first reported microstrip antenna in open literature. It consisted of a strip radiator having length of several wavelengths and width of half wavelength. It was fed at periodic intervals along the radiating edges and separated from a ground plane by a dielectric strip. The strip was fed at periodic space points using coaxial connectors along the radiating edges and was used as an array. Howell [7] in 1972, presented some really useful data on the basic rectangular and circular patches. His low profile antenna consisted of planar resonating element separated from a ground plane by a dielectric substrate whose thickness was small compared to wavelength. Feeding to the line was effected either by coaxial line or by a stripline feed deposited on the same. Lewin studied the radiation from the discontinuities in striplines. Munson [8] in 1974 demonstrated a new class of microstrip wraparound antenna suitable for missiles using microstrip radiator and microstrip feed networks on the same substrate. This low profile microstrip array offered nearly 90% efficiency and almost omni directional coverage. Sanford [18] reported the use of conformal microstrip array for L-band communication from KC-135 aircraft to the ATS-6 satellite.

Weinschel [19] constructed a practical pentagonal antenna in 1975. He demonstrated its use in a S-band cylindrical array producing circular array patterns for a telemetry link from a sounding rocket. Similar array designs were reported by James & Wilson [20], when they constructed flush mounted low profile antennas for missiles.

The first step in designing a microstrip antenna is to choose an appropriate substrate. Many substrate properties play a decisive role in this design procedure. Dielectric constant, loss tangent and their variation with frequency, homogeneity, isotropicity, thermal coefficient, temperature range etc are important parameters in the selection of a proper substrate. A detailed study on different dielectric materials available in the market was done by Nowicki [21].

Polytetraflouroethylene substrates reinforced with glass random fiber or glass woven web were reported by Traut [22]. These filler materials occupy preferred orientations in the polymer matrix during the manufacture process and give necessary mechanical and electrical properties desirable for antenna construction.

Theoretical analysis through mathematical modeling of microstrip antennas was first carried out by applying transmission line analogies to simple rectangular patches fed at the centre of a radiating wall. It was first proposed independently by Munson [8] and Demeryd [11,23]. The radiating edges were considered as slots that are approximately separated by a half wavelength and connected by an ideal transmission line. This model provides expressions for the radiated fields, radiation resistance, input impedance etc. This model is applicable only for patches of rectangular shape and not adaptable for the inclusion of feed point. James and Wilson used the vector Kirchoff relationship for the known aperture fields of an open circuited microstrip line and analysis of its radiation mechanism [20]. They observed that the terminal plane region is the dominant radiating aperture. Theoretical and experimental pattern analysis of different radiating elements showed that they are similar to that of the slot radiators.

Agarwal and Bailey [24] suggested the wire grid model for the evaluation of microstrip antenna characteristics. Here, the microstrip radiating structure was modeled as fine grid of wire segments and solved for the current on them using Richmond's reaction theorem. From these current values, all the antenna characteristics of interest

were obtained. This method is useful for the design of different microstrip antenna geometries like circular disc, circular segment and triangular patches.

A more accurate mathematical technique, known as cavity model, was suggested for the analysis of microstrip antennas by Lo et al. [25-27]. Here, the upper patch and the section of the ground plane located below it are joined by a magnetic wall under the edge of the patch. The structure now behaves as a dielectric resonator. The antenna characteristics of different patch geometries with arbitrary feed points can be calculated using this approach. The effects of radiation and other losses are introduced in terms of either an artificially increased substrate loss tangent [27] or by employing the impedance boundary conditions.

Alexopoulos et al [28] discussed a Dyadic green's function technique for calculating the field radiated by a Hertzian dipole printed on a grounded substrate.

Mosig and Gardiol [29] generated a vector potential approach and applied the numerical techniques to evaluate the fields produced by microstrip antennas of any arbitrary shape.

Newmann et al [30,31] suggested the method of moments for the numerical analysis of microstrip antennas. They used the Richmond's reaction method in connection with method of moments for calculating the unknown surface currents flowing on the walls forming the microstrip patch, ground plane and magnetic walls. This method can be adopted for the calculation of input impedance of microstrip antennas of arbitrary patch shapes.

Hammer et al [32] proposed an aperture model for calculating the radiation fields of microstrip antennas. This model accounts radiation from all the edges of the patch and can give the radiation field and the radiation resistance of any mode in a microstrip resonator antenna.

Carver et al [33] suggested a numerical analysis based on the finite element method for deciding the field interior to the microstrip antenna cavity. This is a variational method that gives a solution closest to the true analytical solution. The problem can be solved with the help of the Eigen value problem. A pentagonal shaped patch was analyzed using this method.

The circular microstrip patch has been rigorously treated by Butler [34]. He solved the problem of center fed circular microstrip antenna by considering the patch as a radiating annular slot, in which the radius of the outer ring is very large. Butler and Yung [35] analyzed the rectangular microstrip antenna using this technique.

The rectangular patch is the most regularly used microstrip antenna, and is distinguished by its length and width. The literature covers well-established studies on its far-field radiation pattern, losses, quality factor, input impedance and other electrical parameters. Another design is the circular patch antenna and its geometry is characterized by a single parameter, namely its radius. The expressions for its electrical characteristics are also studied in literature and suggested by Bahl and Bhartia [9].

Long et al [36,37], measured the driving point impedance of a printed circuit antenna consisting of a circular disc separated by a dielectric from a ground plane. A theoretical RLC model is proposed for calculating the variation of input impedance with frequency and disc parameters.

A linear array consisting of 16 square elements each fed at two orthogonal points from an underlying stripline layer was developed by Bartely et al [38]. This array generated two independent orthogonally polarized beams. Yee and Furlong [39] made a 2 x 16 element multilayered phased array operating at 970 MHz for remote piloted vehicle. The feed used was 16 way stripline power divider. Azimuth scanning of $\pm 60^0$ was provided by four bit phase shifter. The designs of a 7.5 GHz receive array for satellite communication was given by Cipolla [40]. In this array, radiating elements were placed on one board and feedline, phase shifter and bias line are all placed on a second board. Murphy [41] suggested a special purpose array used for ocean and land surveillance in a space born radar imaging system. Here substrate materials for specialized applications such as in aircrafts, where weight reduction is very important, is reported by Murphy. They were the 10.7 x 2.2 m SEASAT array at 1275 MHz and 9.4 x 2.2 m SIR-A array at 1278 MHz. The peak power handled by these antennas are 3000W and 1800 W respectively. A 32 x 32 element array for 38.4 GHz, where, the E and H plane side-lobes were minimized by proper amplitude tapering, was suggested by Weiss [42].

Carver [43] analyzed the circular microstrip antenna and gave an accurate formula for its resonant frequency. He showed that for the radiating patch, the resonant frequency is complex since the wall admittance is complex. He conducted some thorough investigations on the dependence of resonant frequency on the various substrate parameters.

Wood [44] suggested a new technique for the production of circular polarization from a compact microstrip antenna based on a radiation from curved microstrip transmission lines supporting a single traveling wave. He gave the theoretical and experimental radiation patterns of circular sector antenna and a spiral antenna. Using these antennas he achieved an impedance bandwidth of 40 % at 10GHz.

Mink [45] developed a circular ring microstrip antenna, which operates at a substantially low frequency compared to a circular patch antenna at the same size.

Chadha [46] reported Green's functions for triangular segments in microwave planar circuits. This work enabled the analysis of certain triangular shaped antenna using Green's function method. Shen [47], analyzed the elliptical microstrip antenna and showed that the radiation from this antenna is circularly polarized in a narrow band when the eccentricity of the ellipse is small. Here only a single feed is necessary to achieve circular polarization. Long et al [48] experimentally verified this result.

Chadha and K C Gupta [49] developed Green's functions of circular sector, annular ring and annular sector shaped segments in microwave planar circuits and microstrip antennas.

This also helped the analysis of microstrip antennas using Green's function method or segmentation / desegmentation method.

Newman et al [50] used moment method for the analysis of microstrip patch antennas of different shapes. The patch is modeled by surface currents and the dielectric by polarization current. This method is accurate, but requires precise computation.

A comprehensive review of the microstrip antenna technology till 1981 is provided by Carver and Mink [51]. Here, the dielectric constant was varied from 1.7 to 1.14 depending upon the thickness of the dielectric layers. Certain numerical and analytical techniques for the analysis of microstrip antennas are briefed in this study. The substrates available are also discussed. Design procedures for the most popular

geometries (rectangular and circular) are given and the necessity for further research is also discussed.

A full wave method for the analysis of open printed circuit structures is presented by Itoh et al [52]. From the spectral domain equivalent circuits the spectral domain immittance matrix is derived and it forms the basis of this method. Finally numerical results are compared with experimental results. This method is also applicable to coplanar and slotline printed structures, structures involving stratified substrates, several radiating elements and conductor elements at different interfaces of stratified substrates.

Gupta et al [53] presented a review of two-dimensional analysis approach applicable to circuits, resonators and antennas. Methods like Green's function approach, segmentation method, de-segmentation method, numerical methods for arbitrary shaped structures etc. are discussed here.

Some of the researchers worldwide, started working towards overcoming the inherent disadvantage of narrow impedance bandwidth and came out with interesting results.

A method for doubling the bandwidth of rectangular patch antennas was proposed by Wood [54]. He used two $\lambda/4$ short circuited parasitic elements placed parallel to the radiating edges. The antenna characteristics are explained in terms of antiphase mode of a pair of coupled resonators. He also noted that the bandwidth improvement of the coupling capacitance.

Wilkinson [55] discussed the radiation from microstrip dipoles. He presented a structure with one arm of the dipole on one side of the substrate and the other arm on the opposite side and spacing the substrate dipole, one-quarter wavelength from a ground plane.

Oltman [56] pointed out that thin resonant microstrip dipoles can be efficiently excited by electromagnetic proximity coupling to a microstrip transmission line embedded in the substrate.

Deshpande and Bailey [57] derived an expression for the input impedance of microstrip patch antennas. Both microstrip and coaxial type feeding can be considered. This method considers the effects of dielectric constant, dielectric losses, substrate thickness, surface waves and dielectric cover. The input impedance of a rectangular microstrip antenna is computed and compared with experimental result to check the

validity of the method. This technique can be extended to other microstrip antenna geometries like circular, triangular, elliptical etc.

Poddar et al [58], presented microstrip antennas fabricated on stepped and wedge –shaped dielectric substrates. They observed significant improvement in antenna impedance bandwidth compared to that of an equivalent rectangular microstrip antenna.

Lo et al [59] developed an array with two port rectangles and discs, as the array element. Here one port was fed and other loaded to achieve tuning, matching or modification in the element pattern.

A modified circular patch antenna configuration by slightly depressing the patch conically into the substrate was suggested by Das et al [60]. This antenna gives a much larger bandwidth compared to ordinary antenna.

Lo and Richards applied the perturbation model approach to the design of circularly polarized microstrip antennas. Critical dimensions needed to produce circular polarization from nearly circular patches, were determined by trial and error method.

Das and Chatterjee [61] constructed a quarter wave microstrip antenna on a ferromagnetic substrate. The efficiency of the antenna can be increased by proper choice of w/h ratio.

Lee et al [62] reported the design of a quasi-log-periodic microstrip antenna for enhanced bandwidth.

Detailed work on the design of microstrip antennas was carried out by Henderson and James [63]. A canonical transition model was developed to estimate the unwanted radiation loss from the transitions between the feedpoint and the incoming coaxial line or triplate line. It was proved that the level of radiation loss is a constraint on the performance where the sidelobe level, polarization purity and constructional simplicity are of prime importance.

Wood [64] reported an analysis of a circular microstrip patch antenna using the orthogonal mode of representation of the current distribution on the disc. Accuracy of the resonant frequency calculation was found to be less than 1 percent. The influence of surface waves were considered and it was concluded that they might limit the upper frequency at which the substrate may be used.

Brown [65] investigated the cross-polarization characteristics of linear comb line microstrip antennas. He derived the condition for cross polarization suppression for particular board characteristics at 4.3 GHz. It was noted that for achieving cross-

polarization suppression below a certain level, low radiation efficiency has to be tolerated.

The design of a microstrip antenna covered with a dielectric layer was reported by Bahl et al [66].

The rectangular microstrip antenna has been extensively analyzed by E.Lier et al. [67] for both the finite and infinite ground plane extensions. For the case of infinite ground plane, existing formulas have been improved. In the finite ground plane case, contribution from ground plane edge diffraction is also accounted in the analysis. The accuracy of the method is tested through comparison with experimental results. They suggested appropriate corrections to be considered in calculating the resonant frequency of a microstrip antenna coated with a protective dielectric layer. The fractional change in resonant frequency observed, matched with the theoretical value.

Kuester et al [68] reported a thin substrate approximation applied to microstrip antennas. The formulas obtained were found to be useful in simplifying the expressions for the microstrip antenna parameters considerably. The closed form expressions derived for the resonant frequency and unloaded Q of the antenna were valid when commonly used quasistatic formulae were no longer valid.

A moment method solution to calculate the input impedance and mutual coupling of microstrip antenna elements was discussed by Pozar [69]. The presence of the substrate and surface waves is accounted by suitable Green's function. Calculated values agree well with the theoretically predicted results.

P C Sharma et al. [70] presented the analysis and designs of three types of circularly polarized microstrip antennas. The antenna configurations were analyzed by using the Green's function approach and de-segmentation technique. The axial ratio bandwidths, VSWR bandwidths and radiation patterns are evaluated and verified experimentally.

A systematic analysis of a probe fed microstrip patch phased array is discussed by Liu et al [71]. The analysis of the E-plane scan performance of this two-dimensional array is based on an infinite array model.

Jones et al [72] described the design parameters of a series fed microstrip patch array to produce a shaped pattern.

Analysis of an arbitrary shaped microstrip antenna with multi terminals is presented by Y.Suzuki and T.Chiba [73]. An approach based on variational method and

modal-expansion technique uses Rayleigh-Ritz method for the determination of Eigen values and Eigen functions. The input impedance and other antenna parameters are computed at non resonance and the theoretical results are compared with experimental results for a pentagonal patch. This method can be applied to microstrip antennas with arbitrary shaped boundaries and multiple terminals.

The input impedance of rectangular and circular microstrip patch antennas have been accurately analyzed by Lier [74]. The theory included the effects of antenna patches due to fringe fields at the edge, and the surface roughness of the dielectric substrate. This extended cavity model provided considerably improved results.

For the calculation of resonant frequencies and the Q-factor of triangular printed circuit antenna, a geometrical theory has been developed by Kuester and Chang [75].

Katehi and Alexopoulos [76] traced the effect of substrate thickness and relative permittivity of the substrate on the radiation properties of the printed dipoles. The analysis is presented in the case of PTFE glass random fiber substrate.

Ashkenazy [77] suggested a method for the design of medium gain microstrip array antenna. Using a modular approach, X-band antennas of 15-25 dB were designed and the results validate the usefulness of the theory.

C M Krowne [78] analyzed the field distribution within a cylindrical rectangular microstrip antenna using cavity model for the TE and TM modes. The Eigen frequencies for the modes were calculated using the resonant frequency Eigen value equations.

Mosig and Gardiol [79] developed a theory for the calculation of the electromagnetic fields and potentials created by an arbitrary surface current distribution on microstrip. The mode theory of wave propagation was used to establish the Green's functions associated with the microstrip structure. Fields and potentials were expressed as Sommerfield integrals and the numerical and analytic evaluations of these integrals were derived.

Delyser et al [80] suggested the design of a log periodic Strip Grating Microstrip Antenna which features narrow patches coupled along non-radiating edges, a double layer geometry with mounting on the antenna above a through line allowing electromagnetic coupling to all elements of the antenna. This 12 element grating antenna is compact and has a measured power bandwidth of 22%.

Dahele and Lee [81] examined the effect of substrate thickness on the characteristics of a circular disc microstrip antenna. It was shown that even below 1 GHz the change in substrate thickness from 0.158 to 0.08 significantly alters the resonant frequency, bandwidth and impedance of the antenna.

Prasad and Mahapatra [82] presented the design of a microwave integrated circuit slot line antenna. Compared to the conventional dipole and resonator antennas, this antenna has a narrow beam for the same order of gain.

The edge-diffracted fields from the finite ground plane of a patch antenna was calculated by Huang [83], by applying the uniform geometrical theory of diffraction. The effect on the radiation patterns due to the finite ground plane was investigated using slot theory and modal expansion theory.

Sharma and Gupta [84] presented the optimized designs of single feed circularly polarized microstrip antennas. Using the desegmentation method the resonant frequencies for two orthogonal modes were calculated for the shapes like diagonally fed square, truncated corners square and the square with diagonal slot. It was observed that for truncated corners, antenna exhibits a 0.02 dB axial ratio but it has narrow bandwidth.

Pozar [85] tried the performance of printed antennas on electrically thick substrates. The resonant length, resonant resistance, bandwidth, losses and mutual coupling were considered for printed dipoles and patch antennas. A moment method solution was given for the analysis of a multielement antenna array.

Theoretical and experimental investigations on the annular, annular sector and circular sector microstrip antennas were presented by W.F.Richards et al [86]. They analyzed the structures after the full expansion of resonant modes within the cavity formed by the radiating patch and the ground plane. For comparison, experimental results were also presented. The same authors has modified this technique by using microstrip stub instead if coaxial stub. Here, the inset distance of the stub was also a decisive parameter.

Pues et al, [87] presented a more accurate and efficient method for the analysis of rectangular microstrip antennas. They modified transmission line model by incorporating the mutual coupling between the equivalent slots and by considering the influences of the side slots on the radiation conductance. For a rectangular microstrip

33

antenna fed with a single microstrip feed line, the method showed very good agreement with available experimental and theoretical results.

V Palaniswami and R Garg [88] presented two new geometries that could be used as substitutes for regular microstrip antennas. They presented the theoretical and experimental results of rectangular ring and H-Shaped antennas. A comparison with the characteristics of ordinary rectangular patch antenna is also given.

Sengupta [89] derived an expression for the resonant frequency of a rectangular microstrip antenna. Accuracy of the expressions of the patches of different sizes were compared with the measured results.

Wu and Kauffman [90] used the modal expansion cavity model to compute the radiation pattern of patch antennas mounted on spherical or cylindrical bodies such as missiles and spacecrafts.

Sabhani and Rao [91] derived simple analytic expressions for the characteristic wave resistance and effective dielectric constant of microstrip dipole antenna in mixed dielectric medium. They assumed the quasi TEM mode of wave propagation.

Bhatnagar [92] et al proposed a broadband microstrip antenna configuration for wideband operation. The configuration consisted of one triangular patch placed parasitically over a driven patch.

Fong et al [93] reported a wide band coaxial fed microstrip antenna element on electrically thick multilayer substrate incorporating an additional technique for feeding thick substrates.

Das et al [94] analyzed the modal fields and radiation characteristics of microstrip ring antennas. The experiments conducted at 1.8 GHz were compared with the theoretical patterns.

Prior et al [95] showed that the placement of short circuited annular ring near a disc antenna enhances the bandwidth of the disc. Nearly two times enhancement in bandwidth is achieved with slight reduction in gain.

Mosig and Gardiol [96] reported a study on placing a parasitic parallel to the non-radiating edge of a microstrip antenna.

G Kumar et al [97] studied the bandwidth enhancement using parasitic elements. They observed significant improvement in impedance bandwidth when the driven patch and the parasitic elements were resonating at adjacent frequencies.

Morioka et al [98] looked in to a slot antenna with parasitic element for dual band operation. It consists of three types of dual band antenna combining a slot and a parasitic wire. Characteristics such as VSWR, and radiation pattern are calculated by the method moments. Slot and the parasite must be designed to resonate at a high and low frequency band, respectively.

V Palanisamy et al [99] performed the analysis of circularly polarized square ring and crossed strip microstrip patch antennas based on cavity model.

C K Aanandan and K G Nair, [100] presented the development of a compact and broadband microstrip antenna. They used a number of parasitic elements, gap coupled to a driven patch to get improvement in bandwidth.

Operation of microstrip antennas over multioctave bandwidth has been shown to be possible by using electromagnetically coupled patches in a log period series fed array by P S Hall [101]. The measured results showed that the array bandwidth is greater than two octaves.

A two port rectangular patch antenna providing an accurate control of the radiated power is described by Benalla and Gupta [102] .They analyzed the ports with the input and output ports on the non radiating edges by using transmission line model.

Pozar and Voda [103] presented a rigorous solution for a rectangular microstrip antenna fed by a microstrip feed line. The currents on the feed line and the patch are expanded in a suitable set of modes and a moment method solution is formulated in the spectral domain. Here, the analysis is performed on patches fed at the radiating edge as well as the non-radiating edges. He also analyzed proximity coupled patches. He observed that the results are not good if the feeding is at the non-radiating edge.

Yang and Alexopoulos [104] demonstrated the use of multiple superstrates for gain enhancement. They observed that through the proper selection of the substrate and superstrate, high directivity gain can be obtained in any desired scan angle. The reciprocity theorem and transmission line method are used for the analysis of such antenna configurations.

Reineix and Jecko [105] used the Finite Difference Time Domain Method (FDTD) for the analysis of microstrip antennas. The method is so flexible that almost all types of antennas and all types of feeding can be treated by this method. Here, the antenna is treated directly in the time domain. The frequency dependence of the relevant

parameters can be determined by taking the Fourier transform of the transient currents after deciding a proper excitation.

The multiport network model has been extended to incorporate the mutual coupling between the two edges of a rectangular patch antenna by Benalla and Gupta [106]. An admittance matrix is used to model the mutual coupling among the edges. The obtained results were compared with the data available in the literature for validation.

Drewniak and Mayes [107] proposed a simple, low profile, broadband antenna with circularly polarized radiation pattern. Both senses of circular polarization can be transmitted or received from the same structure. The antenna is proposed to have 30 % impedance bandwidth.

Wang and Tripp [108] demonstrated a spiral mode microstrip antenna with a bandwidth of 6:1 for patterns and wider for VSWR. This new antenna did not require a cavity loaded with absorbing materials and hence is not bulky and lossy. The gain of the antenna was also found to be greater for a 5:1 band compared to a loaded cavity spiral.

Green Lee et al [109] studied the characteristics of millimeter wave rectangular patch antennas excited using irises. Relationship of coupling to the antenna as a function of the position and size of irises were also studied.

Penard and Daniel [110] used the cavity model for the analysis of open and hybrid microstrip antennas.

Sungupta [111] applied the uniform transmission line model to determine the resonant frequency of a rectangular patch antenna that is tuned by metallic posts placed within the antenna boundary. This technique has been extended in the case of circular patch antennas also by Lan and Sengupta.

Alexopoulse [112] experimented the criteria for producing the omnidirectional E and H-Plane radiation patterns from printed antennas. Design graphs were presented for the microstrip antenna geometry that give omnidirectional patterns. It was observed that the omnidirectional bandwidth is very narrow.

Zhang et al [113] studied the suspended patch antenna excited by electromagnetic coupling from an inverted microstrip feed. The analysis was based on full wave transmission line analysis in conjunction with microwave network theory.
Hara [114] reported a three faced microstrip slot array, which gives vertically polarized radiation.

Venkataraman and Chang [115] proposed a new theory for calculating the input impedance of a probe fed patch antenna. It was shown that the input impedance depends largely on the short-lived waves confined to the vicinity of the probe while the input resistance is associated with the excitation of resonant mode.

Pozar [116] invented a new method of feeding the antennas. Here a patch antenna on one substrate is coupled to a microstrip line feed on another parallel substrate through an aperture in the ground plane, which separates the two substrates.

## 2.2 COMPACT MICROSTRIP ANTENNAS

Many researchers have studied dual frequency operation of microstrip antennas at this time. Kerr et al. [117] suggested a dual frequency microstrip antennas dish feed consisting of a microstrip element that resonates at one frequency embedded within another element that resonates at a lower frequency. Schaubert et al. [118] suggested a piggy back antenna for dual frequency operation. They used two trapezoidal shaped patches stacked one over the other. McIlevenna et al. [119] achieved dual frequency operation from a circular patch antenna by etching two ears (bunny antenna) along with the patch at an angular separation of $60^0$.

Long and Walton [120] investigated the dual frequency behaviour of stacked circular disc printed circuit antenna. Here, two discs of slightly different size were stacked together to obtain the dual frequency operation. Expressions for input impedance were also given in terms of the disc parameters.

Weinschel and Carver [121] reported the results of a novel frequency array using piggyback elements. The array operated at 401.8 and 468.8 MHz and provided a gain of 12 dB. It was used as a link from Buoy or Ship to a satellite.

Itoh and Goto [122] modified the printed antenna with slots and strips to obtain dual frequency circularly polarized nature. The antenna consisted of two different length strips and a slot excited by a microstrip feed. The optimum parameters for the dual frequency operation were theoretically obtained.

A technique for achieving dual frequency operation in microstrip antennas was suggested by Wang and Lo [123]. By placing shorting pins at appropriate locations within the patch, they were able to vary the ratio of the two band frequencies from 3 to

1.8. By introducing slots in the patch geometry, this ratio can be reduced. A hybrid multiport theory was also developed to predict the antenna characteristics.

Suzuki and Chiba [124] reported that single fed circularly polarized microstrip antenna was able to provide Circularly Polarized (CP) waves at two different frequencies. A numerical method for determining the optimum feed location is also proposed.

Svitak et al [125] demonstrated a new technique for feeding microstrip antenna through RF modulated light wave signals via an optical fiber. A module containing a photodiode, RF circuitry and a microstrip antenna element performs the light wave-to-RF conversion. They have designed and tested three transmitting antenna configurations each containing an aperture coupled microstrip patch as the radiating element. Here the connections to the antenna modules were through an optical fiber.

Kishk [126] presented the analysis of a spherical annular microstrip antenna. The input impedance of the patch is computed using the generalized transmission line model. Method of moments has been used for the computation of the radiation patterns. He observed that the sphere radius has significant influence on the input impedance and the resonant frequency.

Kashiwa et al [127] demonstrated the analysis of rectangular microstrip antennas mounted on the curved surface using the curvilinear FDTD method. The numerical results agreed well with almost all experimental results and this confirms with the validity of the technique.

Results of an iterative procedure for the determination of an effective loss tangent is presented by Lee et al [128]. They observed that the final value of $\delta_{eff}$ depended on the value of the initially taken substrate loss tangent (tan $\delta$).

Dey et al [129] analyzed the effect of flaring and end loading of the arms of a cavity backed printed dipole on the impedance bandwidth. Here, the closed form expressions for the radiated power of a half-wave microstrip patch is modified to calculate the impedance bandwidth of a printed dipole.

Tong et al [130] suggested an aperture coupled five patch broadband microstrip antenna, which made use of stacked, and coplanar techniques, which in turn can help to attain a bandwidth of 45%. The SWR characteristic and radiation pattern of the antenna

at several frequencies based on the theoretical analysis and experimental measurement are compared.

Gavriel Elazar and M.Kisliuk [131] reported a microstrip linear slot antenna array as an attempt to achieve moderate bandwidth and overcome the problems of radiation from microstrip feed lines and surface waves in the dielectric.
One of the major operational drawbacks of microstrip antenna is the very narrow frequency bandwidth. Several methods are being tried like U-slot insertion, reported by Huynh and Lee [132].

An et al [133] introduced a new approach for the design of broadband active antennas by using a simplified technique. They presented a sequential design procedure for the optimal design of transmitting and receiving antennas with multiple active stages, taking into account of input and output matching, the gain vs. frequency curve and the noise performance.

D M Pozar and S M Duffy [134] presented the test results of an aperture coupled circularly polarized antenna for GPS. The antenna operates both in the $L_1$ and $L_2$ frequencies of 1575 and 1227 MHz required for differential GPS to provide maximum positioning accuracy. It offers a relatively narrow beamwidth (10dB) of the order of 120 to $140^0$.

K L Wong and Wen-Hsiu Hsu [135] suggested broadband triangular microstrip antenna with a U-shaped slot. With a foam substrate of thickness ~0.08 $\lambda_0$, a slotted triangular microstrip antenna with an operating bandwidth of ~18 % is obtained, which is 1.8 times that of a corresponding simple triangular patch antenna.

Jui Han Lu [136] demonstrated that by using a pair of step slots embedded close to the non-radiating edges of the rectangular patch, dual frequency operation can be achieved.

The two operating frequencies have the same polarization planes and similar broadband radiation characteristics. He further designed a [137] novel dual-frequency design of a single feed equilateral triangle microstrip antenna by loading a bent slot of $60^0$ close to each triangle tip.

Kai-Ping Yang [138] et al reported a compact triangular microstrip antenna with a 'Y' shaped slot giving circular polarization. The Y-shaped slot is cut in the patch with its upper two arms facing either the triangle trip or the bottom side of the triangular

patch. The present design provides an antenna reduction up to about 19% for operation t a given frequency.

Jui-Han Lu [139] proposed another novel CP design, based on patch size modification technique, for an equilateral triangle microstrip antenna. By zigzagging two side edges of an equilateral triangle microstrip antenna with an indent of a small length of ~0.01 times the patch side length at the centre of the edges.

Experimental studies on a U-slot circular patch antenna with L-Probe feeding is reported by Guo et al [140]. The antenna, using a foam substrate of 0.1 $\lambda_0$, has an impedance bandwidth of 38 % and a gain of 6.8 dBi. The far field radiation patterns are stable across the passband.

Bafrooei and Shafai [141] investigated a method for miniaturization of microstrip patch antenna without degrading its radiation characteristics. It involves perforating the patch to form a microstrip square ring antenna, which is analyzed numerically and experimentally. The ring geometry introduces parameters to the antenna to control its impedance, frequency and bandwidth.

A novel dual frequency design of a single layer, single feed circular microstrip antenna with an open ring slot has been reported by Jen-Yea Jan and K L Wong [142]. The proposed dual frequency design is achieved by embedding an open ring slot, which has a small gap between the slot's two open ends, close to the boundary of the circular patch.

Jui-Han Lu and K L Wong [143] presented a new, compact, dual-frequency of single feed circular microstrip antenna with an offset circular slot placed close to the patch boundary. It is found that, when the radius of the offset slot is about 0.38 −0.62 times the radius of the circular patch, dual frequency operation can be attained. By selecting various sizes of the circular slot, the fundamental resonant mode of $TM_{11}$ for an unslotted microstrip antenna can be split up in to two separate resonant modes with orthogonal polarization planes.

Jia-Yi Sze and K L Wong [144] reported a bandwidth enhancement technique for a single layer single patch, rectangular microstrip patch antenna by embedding a pair of double bent slots close to the patch's center line. This is a modified approach for a work done by the same authors [145] by embedding a pair of toothbrush-shaped slots in which a group of three closely spaced slots in parallel to the radiating edges. It is replaced by a single narrow slot with an inclined angle of $75^0$ to the nonradiating

structures, resulting in a pair of double bent slots with bent angles $15^0$ and $75^0$.Also, where the length of the three closely spaced slots all need to be carefully tuned in the design process to make the first two resonant modes excite at frequencies close to each other to form a wider operating bandwidth.

Jui-Han Lu and Wong KL [146] presented another novel frequency design whose frequency ratio of the two operating frequencies can be as low as about 1.1. Here a pair of spur lines at the nonradiating edges and an integrated reactive loading at one of the radiating edges of a rectangular microstrip antenna is proposed. This design finds application where a low frequency design is required.

Kai-Ping Ying and Wong [147] proposed an inclined slot coupled compact dual frequency microstrip patch antenna with a cross slot which gives a antenna size reduction of ~ 40%. Also, the frequency ratio is very slightly affected by the cross-slot length, mainly determined by the aspect ratio of the patch. The polarization planes remain perpendicular to each other.

Proximity feeding is another widely used feeding technique for microstrip antennas. Mak et al [148] reported a proximity coupled U-slot patch antenna whose impedance bandwidth is 20%, centered at 4.3 GHz. It has an average gain of 7.5 dBi and a cross-polarization of about –20 dB. A novel Π-shaped stub is introduced which is connected at the end of the microstrip feed line for wide band performance.

Horng Dean Chen [149] cut a circular slot in a rectangular patch and, using a coaxial feed, generated dual frequency operation. A 20 % antenna size reduction is achieved with this modification.

Huang et al [150] reported an inclined slot-coupled microstrip antenna for broadband circular polarization operation. This non-linear slot, end-loaded with two V-slots significantly broadens the CP bandwidth to about 2.1 times than that obtained using a simple inclined slot for CP operation.

Chen et al [151] reported a microstrip antenna with a group of four bent slots in a corner truncated square patch antenna. It provides circular polarization operation and an area reduction of more than 50 % as compared to a conventional design of a corner truncated square patch without bent slots.

Wong et al [152] reported yet another dual-frequency design of equilateral-triangular microstrip antennas. This dual frequency operation is achieved by inserting a narrow slit at the bottom of the triangular patch. Two operating frequencies are

orthogonal polarization planes and the frequency ratio can be easily controlled by adjusting the slit position and slit length.

Chun-Kun Wu et al [153] reported a design using meandered rectangular patch and a slot-coupling feed to generate dual-frequency operation, which can be controlled by patch dimensions. The insetting slit length provides more freedom of operation. At the same time, Jui-Han Lu and Wong [154] analyzed meandered rectangular patch loaded with two parallel slots, for compact dual-frequency operation. The two operating frequencies have parallel polarization planes and, by varying the insetting slit length, the frequency ratio of the two frequencies is tunable in the range of ~1.8-2.4.

A novel dual frequency operation of microstrip antennas by embedding a pair of properly-bent narrow slots close to the non-radiating edges of a rectangular microstrip patch antenna, has been proposed Wong and Sze [155]. The two frequencies have parallel polarization planes and similar broadside radiation characteristics and the frequency ratio of the two frequencies can be controlled by the bent angle of the embedded slots.

Tseng et al [156] proposed an X-band planar reflector with a responding spectrum, developed using Van Atta retrodirective antenna array. The reflector contained four sub-arrays, each with six dual slot antennas appropriately fed and paired by microstrip lines.

Wong and Chen [157] reported a Slot-loaded bow-tie microstrip antenna using a single probe feed for dual frequency operation. Here a pair of narrow slots are embedded close to the radiating edges of the bow-tie patch. By varying the flare angle of the bow-tie patch, different perturbation effects on the excited patch surface current paths can be generated.

Luk et al [158] explored a novel folded small rectangular patch antenna, which provides an area reduction of 37% and a cross-polarization level of approx. −20 dB.

Xie et al [159] reported an efficient modeling of multiple wide slots on a coaxial antenna by considering the mutual coupling and the non-uniform distribution of the electric fields in the slots.

Many technologies have been used to miniaturize microstrip patch antenna area operating at a fixed frequency by introducing a shorting pin at the edge of the patch,

meandering the patch or by loading reactive components like chip capacitors and resistors over the patch.

Waterhouse [160] reported a microstrip antenna operating at a fixed frequency loaded with a shorting pin at the edge of the patch to reduce the frequency of operation considerably. But, this design as well as that by Dey and Mittra [161] caused the antenna gain and impedance bandwidths to deteriorate.

Baligar et al [162] reported a novel microstrip antenna, which contains a stacked annular ring coupled to a shorted circular patch. This design offers enhanced bandwidth, higher gain and low cross-polarization levels.

Hong [163] explored a small-size annular slot antenna with a miniaturized slot shrunk by a loaded capacitor, which offered a patch area reduction of 23.4%. The antenna has the advantages of a good impedance bandwidth and good linearly polarized radiation patterns.

Lee, [164] et al reported a compact dual band dual polarized microstrip patch antenna loaded with a slab capacitor, capable of handling two distinct frequencies. This antenna can work as a data communicator for certain specific terrestrial and satellite mobile communication systems.

C Luxey et al [165] reported the dual frequency operation of coplanar waveguide fed antenna controlled by PIN diodes. This design provides simplicity of the biasing circuitry and the similarities in the radiation patterns and return loss performances for both frequencies. The electrical length of the excitation slot is altered with pin diodes instead of the electrical dimensions of the radiating element, which greatly simplifies the biasing circuitry.

Wong and Lin [166] analyzed characteristics of a probe fed small broadband microstrip antenna with chip-resistor loading. By replacing the shorting pin with a chip-resistor of low resistance, the patch dimension can be significantly reduced for operation at a fixed frequency. The antenna bandwidth can also be considerably enhanced in this case.

Y X Guo [167] demonstrated a compact dual band patch antenna using slot loaded and short-circuited technique. By controlling the short-plane width, the two resonant frequencies, $f_{10}$ and $f_{30}$ can be significantly reduced and the frequency ratio $f_{10}/f_{30}$ can be tuned effectively.

Liang et al [168] recommended a frequency varying circular patch antenna design with a loaded capacitor, which does not considerably affect the radiated power efficiency of the antenna. In some cases, it is observed that the maximum radiated power can be improved. By assigning a chip-capacitor of proper value and location the operating frequency of the patch can be tuned over as much as 65% of the dynamic range of the original resonance frequency.

Chiou et al [169] proposed a dual polarized wideband circular patch antenna excited by both using an aperture coupled feed and a gap-coupled feed. The use of hybrid feeds is found to be very effective in obtaining high isolation between the two feeding ports. Since, there is no backward radiation for the gap-coupled feed, the coupling below the ground plane can be ignored, when a reflecting plate is added to the antenna design for practical applications.

Tong et al [170] suggested a broadband U-slot rectangular patch antenna printed on a microwave substrate. The coaxially fed antenna is analyzed using FDTD technique, which is found to be in good agreement with the experimentally observed results for the input impedance and radiation pattern. A maximum impedance bandwidth of 27% is achieved centered around 3.1 GHz, with good radiation pattern characteristics.

Desclos [171] put forward a size reduction scheme for planar patch antennas by slot insertion. Both single layer and double layer substrates are shown for the S-band with linear polarization , which helps to reduce the patch dimensions by 20%.

Tang et al [172] reported yet another dual-frequency design of a V-shaped patch antenna, supported by a non-conducting post, placed above the ground plane. An H-shaped coupling slot is cut in the ground plane and centered below the V-shaped patch. The two operating frequencies have the same polarization planes and have good radiation characteristics, notably for the low frequency mode.

The above review makes it obvious that design and development of Compact Dual Frequency Microstrip Antenna is a vibrant research topic of contemporary

relevance. Compactness and Patch area reduction can be achieved through suitable frequency tuning techniques. With this perception in mind, the author of this work has designed a set of new geometries for patch area reduction. It also provides a dual polarized frequency tuning method. The present thesis is the outcome of the experimental, simulated and theoretical investigations carried out on a novel stub loaded slotted square microstrip antenna.

# CHAPTER III

## METHODOLOGY– EXPERIMENTAL SET-UP, MEASUREMENT TECHNIQUES AND ELECTROMAGNETIC MODELLING

# METHODOLOGY– EXPERIMENTAL SET-UP, MEASUREMENT TECHNIQUES AND ELECTROMAGNETIC MODELLING

*This chapter presents the fabrication processes, experimental facilities and measurement techniques used for the investigation. An analysis of the various parameters of the antenna under investigation is also given in this chapter. The chapter concludes with a brief description of the theoretical and simulation approaches employed to analyze different antenna characteristics.*

## 3.1 FABRICATION OF MICROSTRIP ANTENNA

The selection of the proper substrate matching the required application has already been discussed in section 1.3.3. Once a suitable substrate has been chosen for the fabrication of microstrip antennas, two different techniques are employed depending upon the dimensional tolerance.

### 3.1.1 Photolithographic Process

Most commonly used method for the fabrication of microstrip antenna is the Photolithographic technique. The major procedure included in this technique is explained in brief.

### 3.1.1.1 Resist Coating

There are two types of photo-resist, a negative in which an exposed area remains after development, and a positive type in which an exposed area is removed after development. Required characteristics for resist are sensitivity, resolution, adhesiveness to the substrate, uniformity of coating and resistance against etching solution. Resist is coated on the patch with a spinner. The resist films are pre-baked in an oven after coating to vaporize the solvent completely and to enhance adhesion to the substrate. A highly pressurized mercury lamp that has a peak spectrum at a wavelength of 365 nm is used for the U-V ray exposure. After exposure, resist is developed either by dipping or by spraying with the developer solution. In the case of negative resist, the exposed area is melted away during development, and the unexposed area remains unaffected. The sensitivity depends on the developer and the temperature.

This technique is employed for the fabrication of patch antennas where the tolerance of fabrication is more critical.

**3.1.2 Fast-fabrication process**



(1)

(2)

(3)

(4)

(5)

(6)

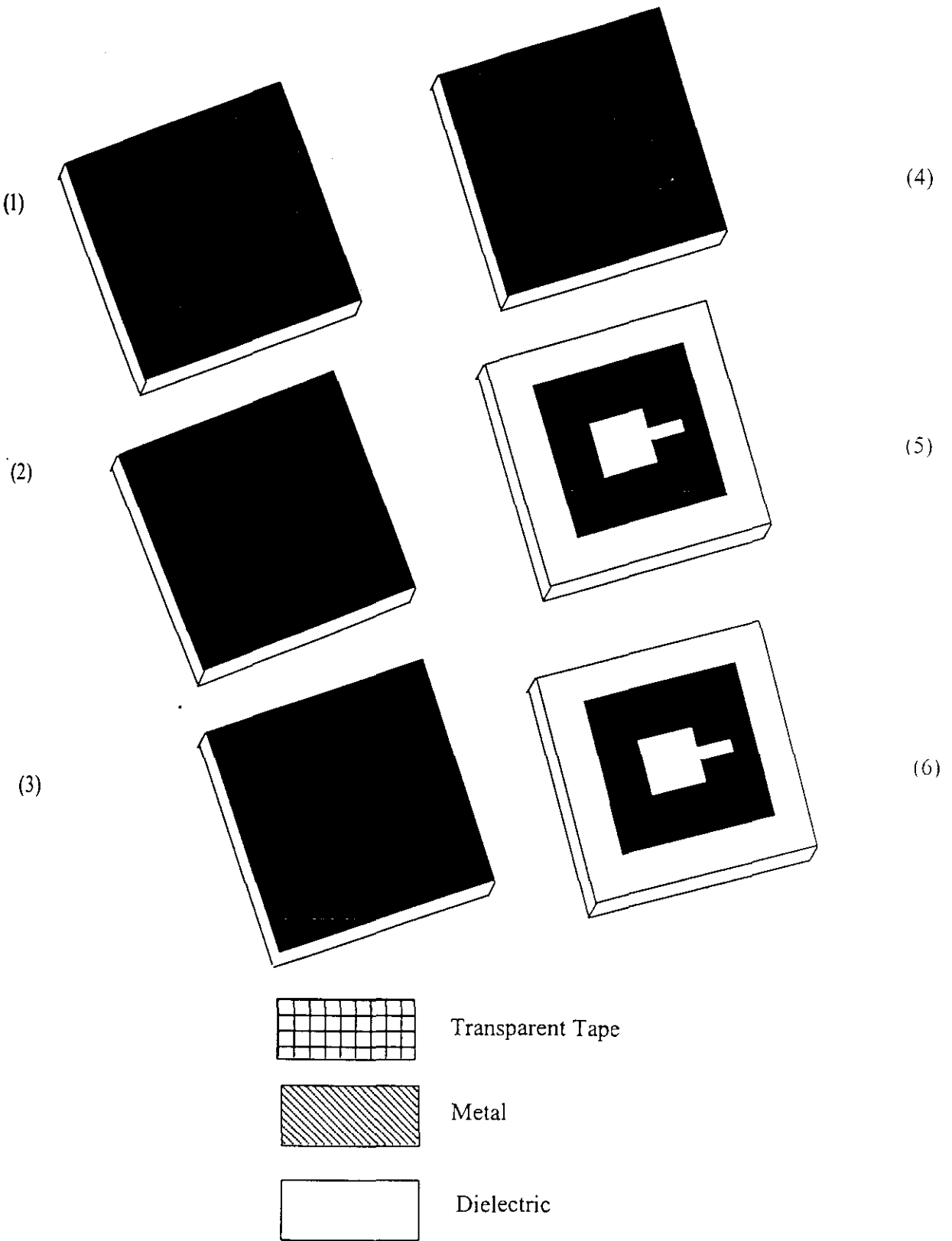Transparent Tape

Metal

Dielectric

*Figure 3.1 Different Steps in the fast fabrication process*

For fast and reasonably accurate fabrication of microstrip antennas, an alternate method is used. The different steps in this process are shown in figure3.1. Here the copper clad substrate is cleaned thoroughly (1) and a drawing of the slot antenna geometry is made on one side (2). The entire top and bottom metallisation are covered with transparent cellophane tape (3). The tape is then selectively removed from the top metallisation layer (4) by means of a sharp diamond tipped cutting tool in such a manner that the tape over the antenna geometry is unaltered. The exposed metallic regions (5) are etched out. After the etching process, tape is removed from both the surfaces and cleaned once again to get the antenna ready for test. This simple and faster technique is used to etch out microstrip patch antennas used for investigation in this work. At higher wavelengths this technique yields fabrication tolerance within acceptable limits.

This method is very fast and simple compared to the photolithographic technique mentioned earlier. The validity of this technique has been established by etching conventional rectangular patch antennas. Dielectric foam materials, which are now available with very low dielectric constant and remarkable mechanical properties, are used for the antenna fabrication.

In the case of the stub mounted slotted antenna, periphery is constituted by few square segments and can be easily fabricated by this method with acceptable tolerances of fabrication.

## 3.2 EXCITATION TECHNIQUES

Two types of feeding mechanisms are used for the excitation of the present microstrip antenna. They are

a. **Coaxial feed**
b. **Electromagnetic feed**

The general nature of these feeding mechanisms is already discussed in section 1.3.4. of Chapter 1. As in the case of a rectangular microstrip antenna, the input impedance of the slot loaded square patch antenna varies from zero to a maximum value as we move from the center towards the edges and thereby provides a simple means for matching the 50 $\Omega$ feed line. In this study, coaxial type feed is employed for almost all cases.

# 3.3 MEASUREMENT OF RETURN LOSS, RESONANT FREQUENCY AND BANDWIDTH

## 3.3.1 Network Analyzer

A Network analyzer is frequency sweep measurement equipment for completely characterizing the complex network parameters without any degradation of precision and in a reduced amount of time. A vector network analyzer measures both the magnitude and phase of the reflection and transmission coefficients. Here, the ratio of the magnitudes and phase angles of the response and excitation signals with respect to a reference plane is accurately measured and displayed.

The HP 8510 C Vector Network Analyzer is used for all the measurements of return loss, resonant frequency, bandwidth and radiation characteristics. The basic block diagram of the constituents of a Network Analyzer is shown in figure 3.2. It consists of a microwave source, an S-Parameter test set and an IF detector interfaced with a display unit.
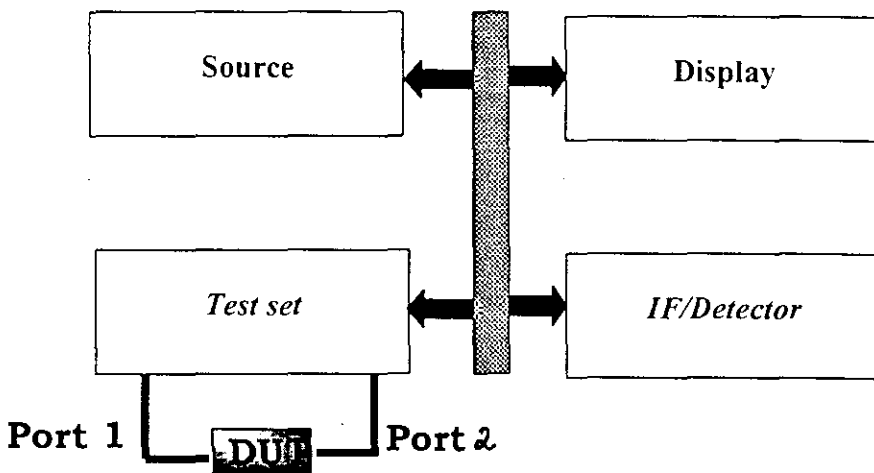


*Figure 3.2 Block Diagram of Network Analyzer*

The synthesized source or the sweep oscillator will provide the RF stimulus. It can operate from 45 MHz to 50 GHz. The source can operate in ramp or step sweep mode. In the ramp mode the network analyzer directs the source to sweep in a linear ramp over the selected frequency range. In the step sweep mode, which provides the maximum precision, although at reduced measurement speed, the synthesizer frequency accuracy and repeatability is obtained by phase locking the source at each frequency over the selected frequency range. Network analyzer is calibrated for one full port (PORT 1) and the test antenna is connected to port 1 of the S-parameter test set. The block diagram of the experimental setup for the automatic measurement setup controlled by an IBM PC interfaced to the network analyzer is given in figure 3.3. The Vector network analyzer is an embedded device constituted by the systems like Microwave Source, test set, Vector signal processor and Display unit.

The microwave power generated at the source is fed to the S-parameter test set device. Here the different scattering parameters are separated and down converted to 20 MHz and fed to the IF detector. The schematic diagram of the experimental set-up is given in figure 3.4. The detected signal is processed and fed to the display unit for output. All the devices are connected using HPIB interface. The measured $S_{11}$ LOGMAG data in the network analyzer is acquired and stored in ASCII format in the interfaced computer using the MERLsoft (A software indigenously developed by the microwave group of the department for Antenna studies).
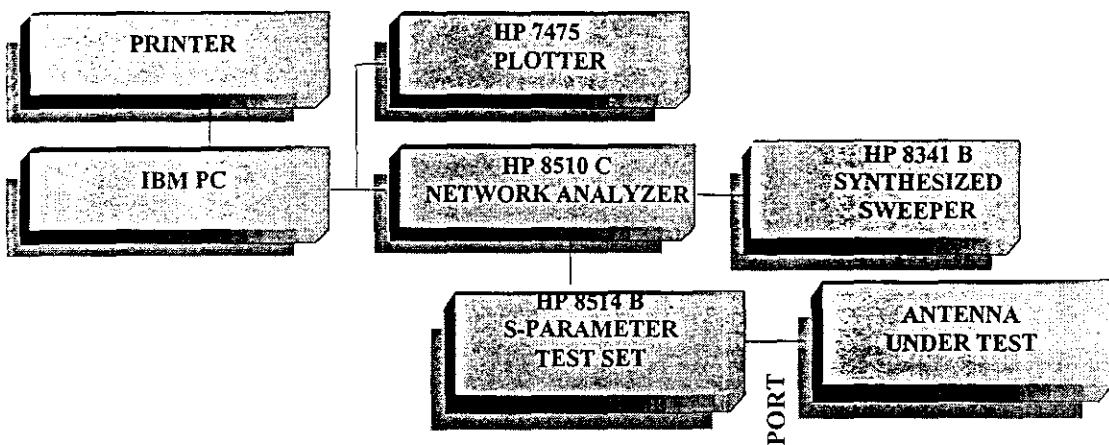


*Figure 3.3 Experimental set-up for the measurement of return loss and resonant frequency*

**PRINTER/PLOTTER**

**SOURCE HP 83651B**

**DISPLAY/PROCESSOR**

RF
INPUT

**SYSTEM BUS**

**HP 8510C**

**HP 8514B
S-PARAMETER
TEST SET**

20 MHz

PORT 1

PORT 2

Tr Antenna  Rr Antenna
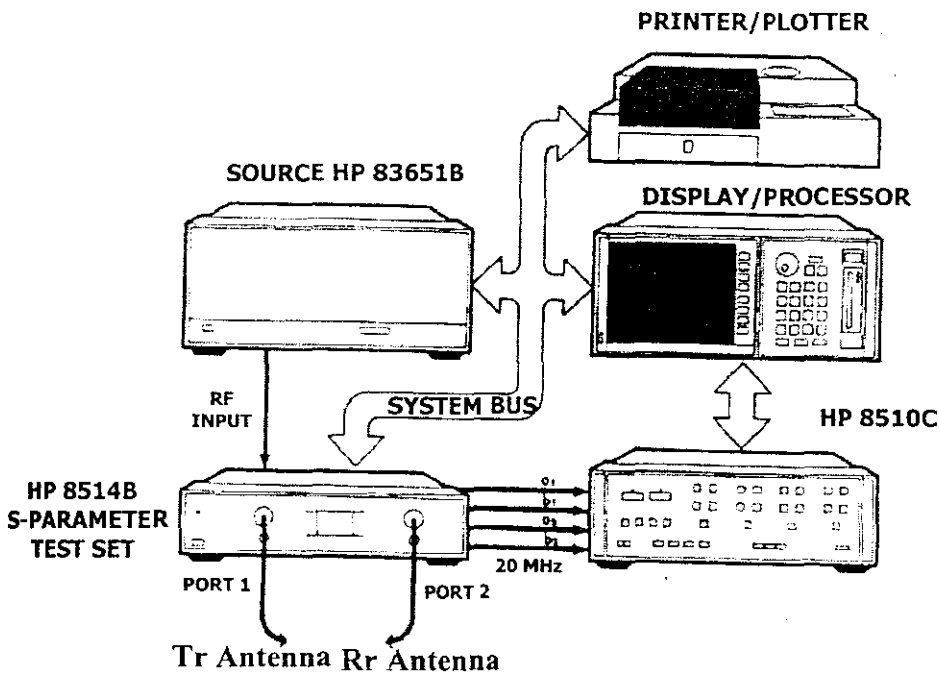
*Figure 3.4 Schematic Diagram of the Experimental set-up*

The resonant frequency of the antenna for a particular mode is determined from the dip of the return loss curve for that mode. The bandwidth can be directly obtained from the return loss data by noting the range of frequencies ($\Delta f_r$), over which the return loss is less than or equal to -10 dB. Now, percentage bandwidth is given by, $\dfrac{\Delta f_r}{f_r} 100$

where $f_r$ is the center frequency of the operating band. The stored return loss data in ASCII format is analyzed for determining the bandwidth and resonant frequency using MERLSoft.

## 3.4 ANECHOIC CHAMBER

An antenna is a device that is usually operated in a free space environment. Such an operating condition cannot be normally achieved in the case of a test antenna in a laboratory environment. The reflected power from the walls and the various instruments of the laboratory may interfere with the power radiated by the test antenna and may end up in analyzing an untrue radiation pattern. The electromagnetic interference (EMI), from the various instruments operating inside the laboratory, may also cause performance degradation. The free space can be artificially simulated inside the laboratory atmosphere by an anechoic chamber. Even though exact free space conditions may not be achieved, the chamber minimizes the spurious signals during pattern measurements.

An anechoic chamber is constructed by covering the entire interior surface of a room of specified dimensions with pyramidal or wedge shaped polyurethane foam based microwave absorbers having good coefficient of absorption in the frequency range of interest.

## 3.5 MEASUREMENT OF RADIATION PATTERN

An antenna radiation pattern is formed by its radiating currents. The multidimensional Fourier transform of the currents, results in a pattern. In a patch antenna, each edge has a nearly constant radiation current along the entire width, since the resonance is in the quadrature dimensions. The transform of the rectangular current pattern will give more gain per width. The principal E and H-plane radiation patterns (both co-polar and cross-polar) of the test antenna are measured by keeping the test antenna inside an anechoic chamber in the receiving mode. The block diagram of the experimental set-up to measure radiation pattern is shown in figure 3.5. A standard wideband ridged horn is used as the transmitter.

HP 8510 C Vector Network Analyzer, interfaced to an IBM PC, is used for the pattern measurement. The PC is also attached to a STIC 310 C antenna positioner controller. The test antenna is mounted on the antenna positioner kept inside the

chamber as shown in the test-setup shown in fig 3.5. The fully automated antenna analysis measurement system including the HP 8510C Vector Network Analyzer is shown on figure 3.6.

All the measurements are performed in a microwave anechoic chamber where a perfect free space environment is generated to avoid any external signal interference and unwanted reflections as shown in fig. 3.7
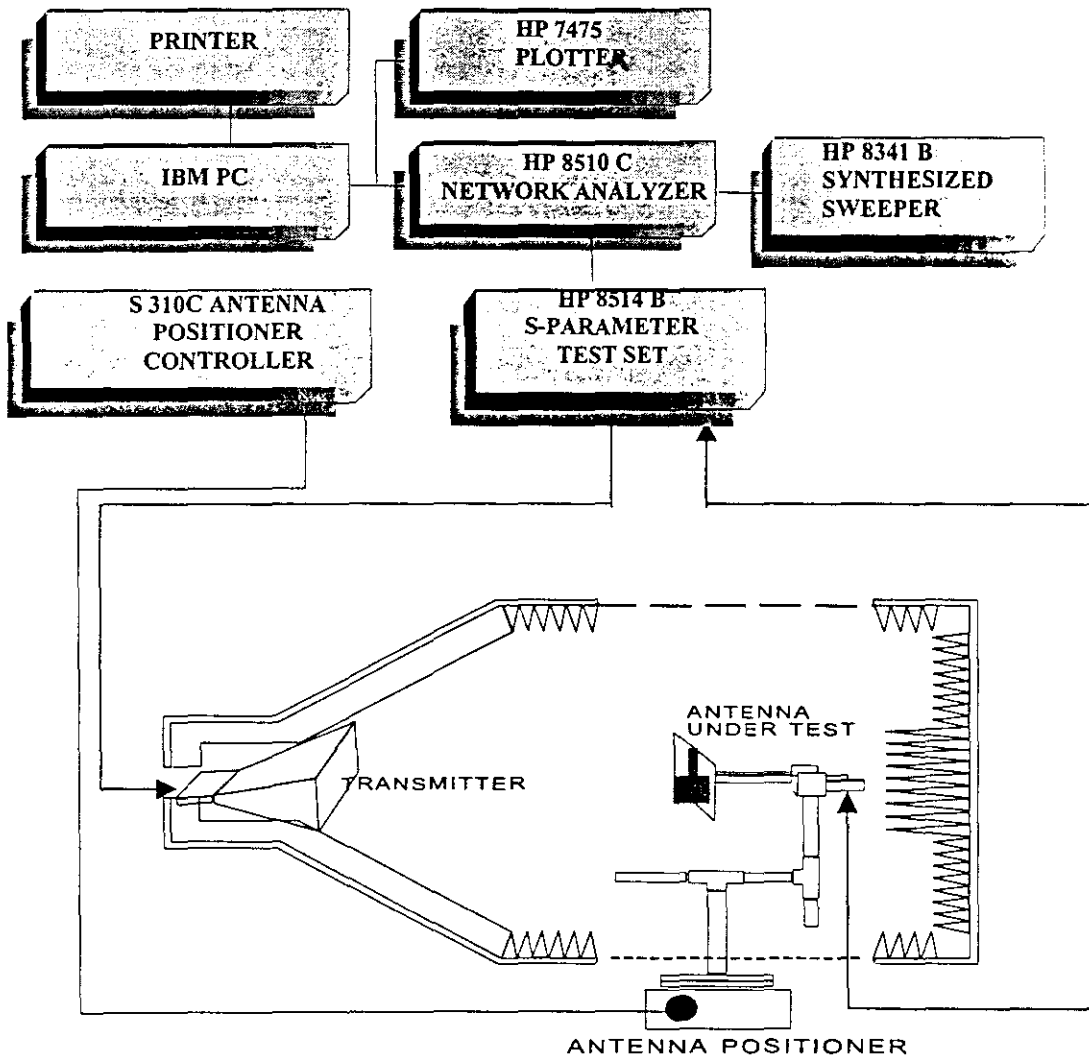


*Figure 3.5 Experimental Set-up for the measurement of Return Loss and Resonant Frequency*

54

Figure 3.6. *Antenna Analysis and Measurement system*



**Figure 3.7** *Microwave Anechoic Chamber where the antenna measurements are made. The antenna positioner interfaced to the network analyzer is also shown*

The test and standard transmitting antennas are connected to port 2 and port 1 respectively of the network analyzer.

The radiation pattern of the antenna at multiple frequency points can be measured in a single rotation of the test antenna by using the antenna positioner setup. The positioner will stop at each step angle and will take $S_{21}$ measurements till it reaches the stop angle. The entire measured values are stored in data format and can be used for further process like analysis and plotting. The different radiation pattern characteristics like half power beam width, cross-polar level, etc, are obtained after analysis of the stored patterns.

## 3.6 MEASUREMENT OF GAIN

The setup for the measurement of gain is same as that used for radiation measurement pattern. A comparative measurement of gain of the new antenna is made with standard rectangular patch antenna operating at the same frequency and fabricated on the same substrate.

## 3.7 MEASUREMENT OF ELECTRIC FIELD INTENSITY

The probe assembly for sampling the field intensity over the patch is shown in figure 3.8. The probe is fabricated by removing the outer conductor and the dielectric from a 2 mm section at the end of a long semi-rigid cable as given in [173]. The probe assembly is now mounted on a precision XY positioner, which can position the probe at any point over the patch surface with an accuracy of 1 mm. The length of the probe $P_L$ is 2 mm and the height of the probe above the patch surface is 2.5 mm. The dimensions of the probe plate are 5 cm x 5 cm.

For the measurement of electric field variation, the probe is connected to port 2 and the test antenna to port 1 of the network analyzer. The probe is moved over the entire patch area with a resolution of 1mm and the entire $S_{21}$ data at the resonant frequency is stored. The stored data are normalized and plotted to get the electric field magnitude.

PROBE-PLAT
SEMIGRID CABLE
RADIATING PATCH

**Angular View**                    **Cross-sectional View**
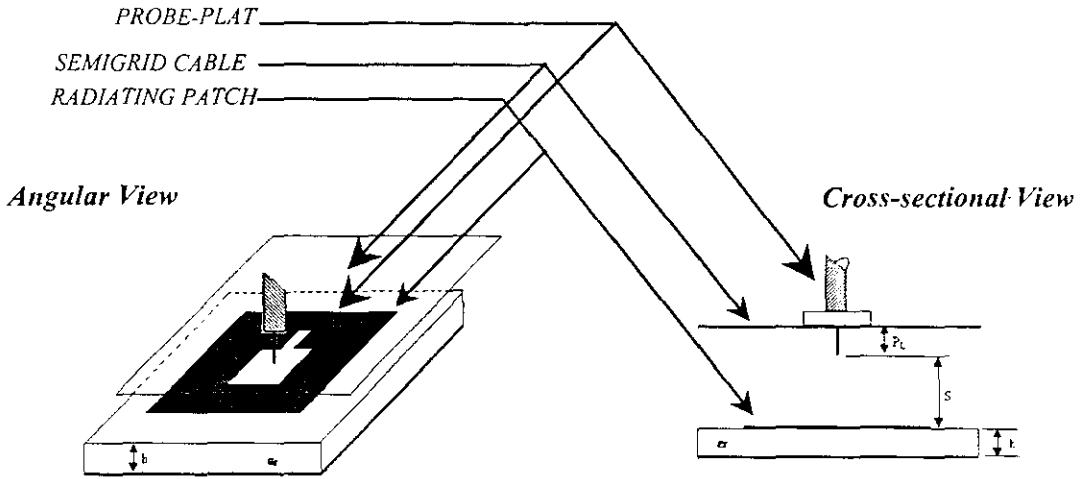
**Figure 3.8** *Set-up for measuring the electric field variation over the patch*

## 3.8 MEASUREMENT OF POLARIZATION

Polarization studies are an important factor in the analysis of any antenna system. The measurement set-up used for this is same as that for the radiation pattern. The standard wide band horn is connected to the port 2 of the network analyzer. It is then rotated clock-wise to get the maximum transmitted power and the corresponding co-polar power is noted. Now, the transmitting antenna is gradually rotated by an angle of 180° to get the other orthogonal mode of polarization.

## 3.9 THEORETICAL ANALYSIS OF THE ANTENNA

Experimental and simulated results are verified theoretically using FDTD technique. The FDTD technique was originally developed by Kane S Yee [179], which suggested a three-dimensional central difference approximation for Maxwell's curl equations, both in space and time. FDTD is a time-domain method in which transient fields are computed as a function of time. FDTD enables the accurate characterization of complex inhomogemous structures for which analytical methods are ill suited.

Numerical computation is accomplished by applying a 3-dimensional excitation to an object in a space and calculating the fields as time progresses. The method has

been proven to be an efficient tool for modeling complicated microstrip circuit geometries and microstrip antennas.

The FDTD method is formulated by discretizing Maxwell's curl equations, over a finite volume and approximating the derivatives with centered difference approximations. The conducting surfaces are treated by setting tangential electric field components to 0. The elaborate steps followed for the theoretical analysis are described in chapter5.

For the theoretical analysis of the antenna, the FDTD codes are written in Matlab 5.3 [174]. From the geometrical dimensions and substrate parameters, the code will compute the resonant frequency, electric field variation along the periphery, input impedance etc.

The experimental results were analyzed based on FDTD technique and it is observed to have good agreement between the two results.

The analysis can predict antenna characteristics like resonant frequency, mode of resonance, radiation pattern, input impedance, transmission characteristics etc. The simulated results are validated through experimental results for different antenna geometry configurations.

## 3.10 ELECTROMAGNETIC MODELING OF RETURN LOSS AND RADIATION PATTERN USING IE3D SIMULATION

Electromagnetic simulation is an entirely new concept to yield high accuracy analysis and design of microstrip antennas and MMIC's. IE3D is an integrated full-wave electromagnetic simulation and optimization package for the analysis and design of 3-dimensional microstrip antennas and high frequency printed circuits. The menu-driven graphic interface allows interactive construction of 3D and multi-layered metallic structures as a set of polygons. Numerous editing capabilities are implemented to ease the construction and manipulation of polygons and vertices. The primary concept is based on an integral equation obtained through the use of Green's functions. In IE3D one can model both the electric current on a metallic structure and a magnetic current representing the field distribution on a metallic aperture [175].

The simulation menu consists of a MGRID simulator, MODUA, a post processor for display of S, Y, and Z-parameters in data list, rectangular graphs and Smith Chart. MODUA is also a circuit simulator. One can graphically connect different S-parameter modules and lumped elements to perform a simulation, and a CURVIEW post processor that provides 3D and 2D display of current distribution and radiation patterns. It also provides information such as directivity, return loss, polarization loss, efficiency, mono-static RCS and bi-static RCS.

Using the MGRID Simulator the desired geometry is designed. A plot showing the MGRID simulator window is given in figure 3.9.
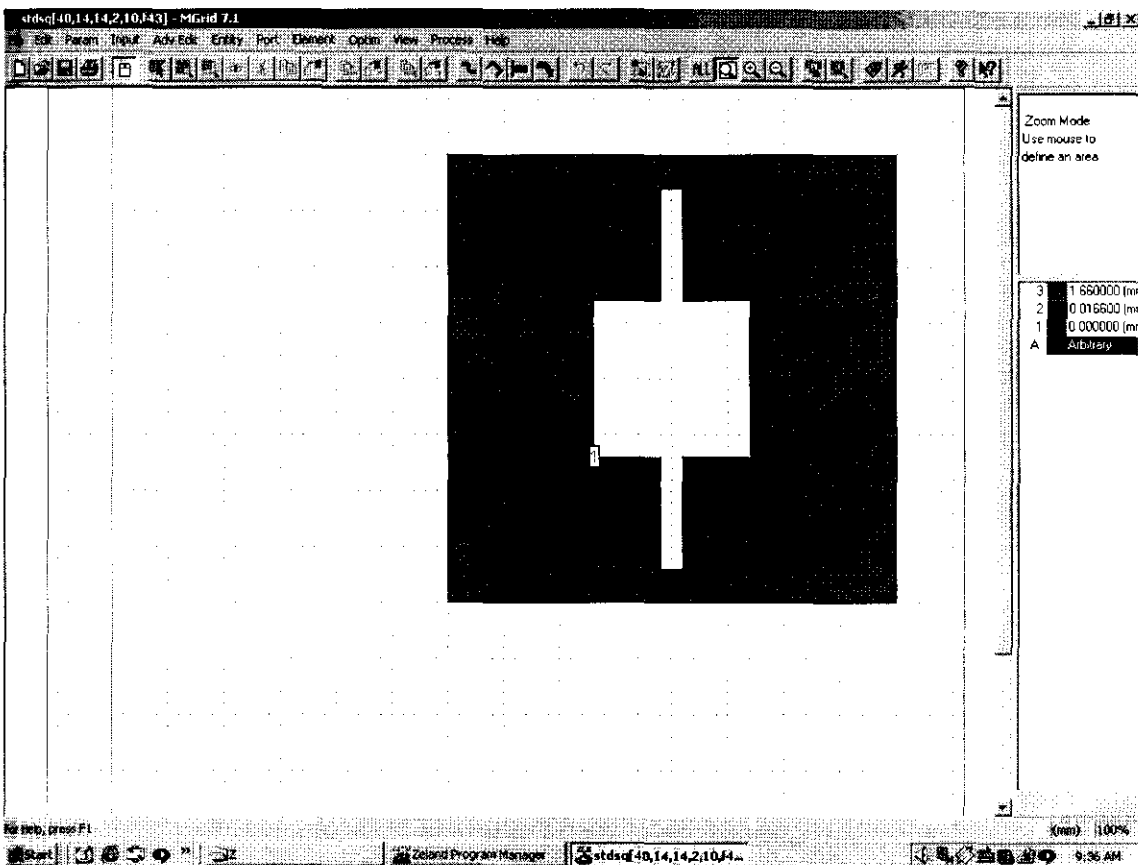


***Figure 3.9*** *IE3D MGRID Simulator window showing the DSMA modeling with a coaxial feed*

Numerical simulation requires sub-dividing a circuit into small cells. Both rectangular and triangular cells are employed here. Rectangular cells are used in the regular region for the best efficiency (each rectangular cell is equivalent to at least 2 triangles).

Triangular cells at any angle are utilized to fit the irregular boundary. The polygon formation for the analysis and port definition is carried out as illustrated in figure 3.10.
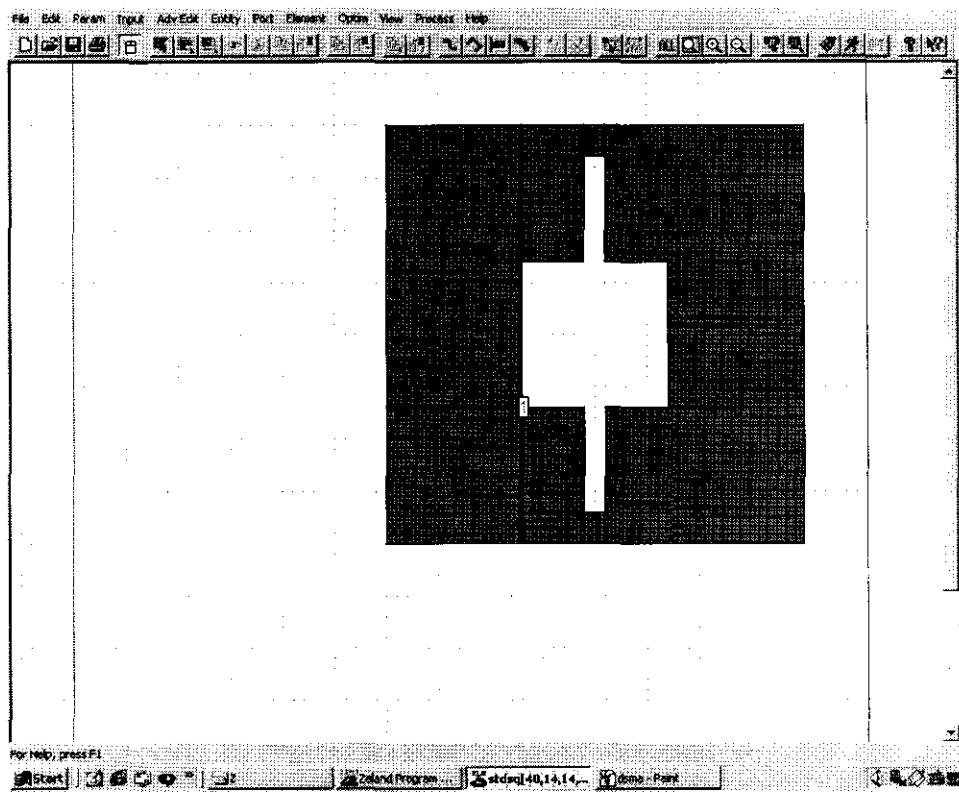


***Figure 3.10*** *Simulator window showing the SSMA gridding performed on the Dual Stub Microstrip Antenna (DSMA)*

The simulation setup window as shown in Figure 3.11 appears. Enter start frequency, stop frequency and the number of frequency points. To simulate frequency responses Adaptive Intelli-Fit option is to be enabled for fast and accurate response. To calculate the current distribution and field distribution, check it in the simulation setup window. In that case uncheck Adaptive Intelli- Fit. The IE3D simulation command is invoked to perform the simulation. IE3D will complete the simulation in a few seconds. The output will automatically appear in the **MODUA** window. The MODUA window reads the data and display the $S_{11}$, $S_{21}$ and $S_{22}$ on the smith chart as shown in Figure 3.12.

60
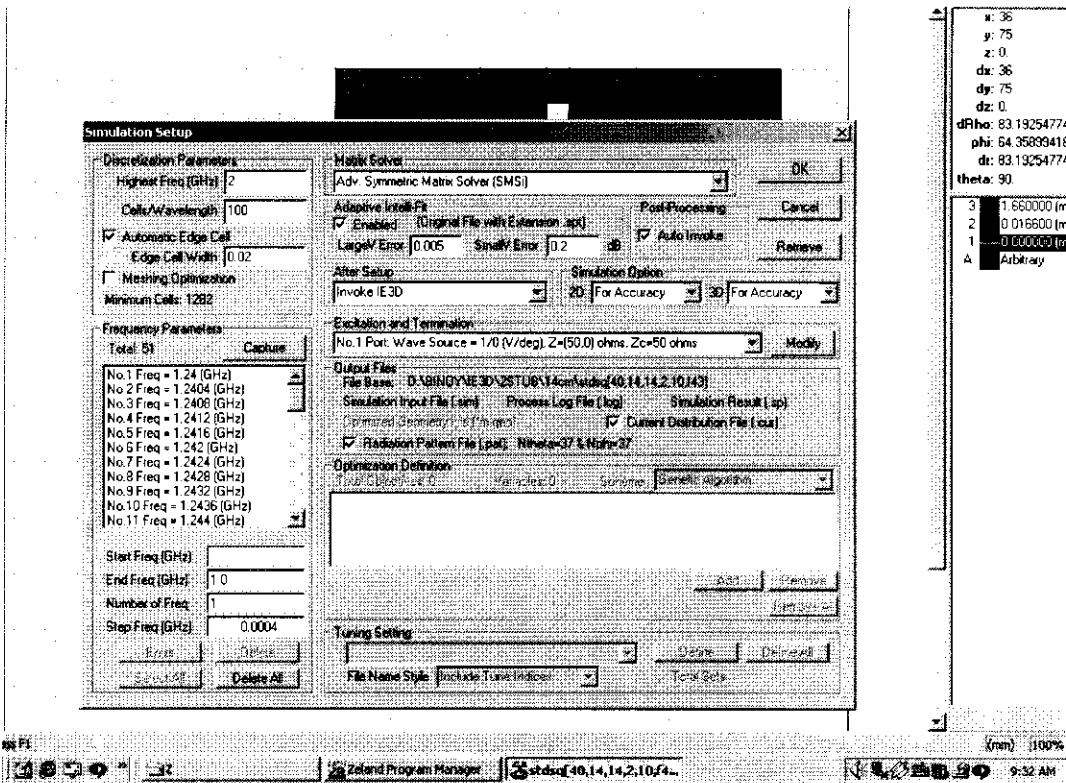
***Figure 3.11** The simulation Configuration set-up window*

To plot the radiation pattern file and current distribution file in the simulation setup dialog box, files having '*.cur' and '*.pat' extension will be created. On **CURVIEW** we can display the 3D view of a discretized structure, field and the current distribution on the structure. The application **PATTERNVIEW** can be used to compare the radiation patterns at different frequencies. The radiation pattern and the current distribution as obtained from IE3D simulation is shown in Figure 3.13.
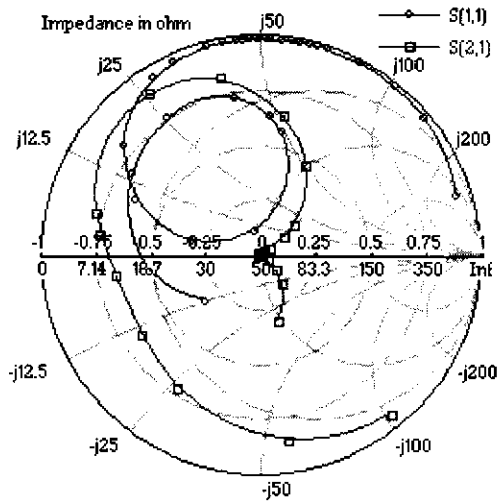
*Figure 3.12 Display of S, Y, and Z-parameters in Smith Chart*
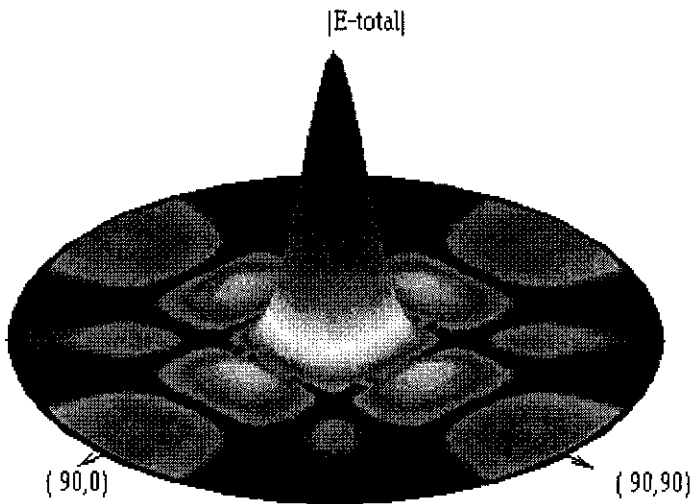


*Figure 3.13 3D Mapped IE3D Radiation Pattern of an Antenna*

IE3D can model current on the four sides of a metallic strip exactly. One can model true 3D structures such as MMIC's, patch antennas, wire bonds and other 3D structures of general shapes. IE3Dcan be used to build and simulate a wide range of planar and 3D microwave and RF structures.

---

# EXPERIMENTAL RESULTS AND OBSERVATIONS

# EXPERIMENTAL RESULTS AND
# OBSERVATIONS

*This chapter deals with the outcome of the elaborate experimental investigations performed on novel slotted microstrip patch antennas. The aim of the study is to develop compact microstrip antennas that can find applications in communication systems. The important design consideration throughout this study is reduction in effective patch area and frequency tuning by varying the antenna parameters. A dual frequency dual polarized antenna with a shaped slot embedded with tuning stubs is developed. Effect of a capacitor mounted frequency-tuning method is introduced through various antenna models. These designs have been simulated using Zeland IE3D electromagnetic modelling package to get an optimum configuration for a particular antenna characteristic. The outline of the studies conducted in this chapter is as follows:*

1. *Dual frequency dual polarized excitation from the slotted square patch antennas having a tuning stub*

2. *Development of a frequency tuning technique by varying the stub arm parameters and the subsequent insertion of additional tuning stubs for patch area reduction*

3. *A capacitor loading technique for enhanced cross-polar performance and frequency tunability*

4. *Extension of capacitor loading technique to multiple stub geometries for enhanced antenna Radiation performance*

# 4.1 SINGLE STUB SQUARE MICROSTRIP PATCH ANTENNA FOR DUAL FREQUENCY DUAL POLARIZED OPERATION

### 4.1.1 Antenna Geometry

The geometry of the new compact microstrip antenna is shown in figure 4.1. The basic design consists of a square patch of side dimensions '$L_P$', etched on a low loss dielectric substrate of dielectric constant '$\varepsilon_r$' and thickness 'h'. A placard shaped slot is inserted in the square microstrip patch antenna. It consists of a square slot of side dimensions $L_S$, with a tuning stub arm having length $L_a$ and width $W_a$ ($L_a >> W_a$). The slot is placed in the centre of the patch in order to maximize the tuning of the dominant mode of the antenna. The stub dimensions, as would be revealed in the following discussion mainly control the antenna characteristics. Hence, the antenna can be aptly named as 'Single Stub Microstrip Antenna (SSMA). The procedure for selection of proper substrate and appropriate feeding mechanism are explained in chapter 1.
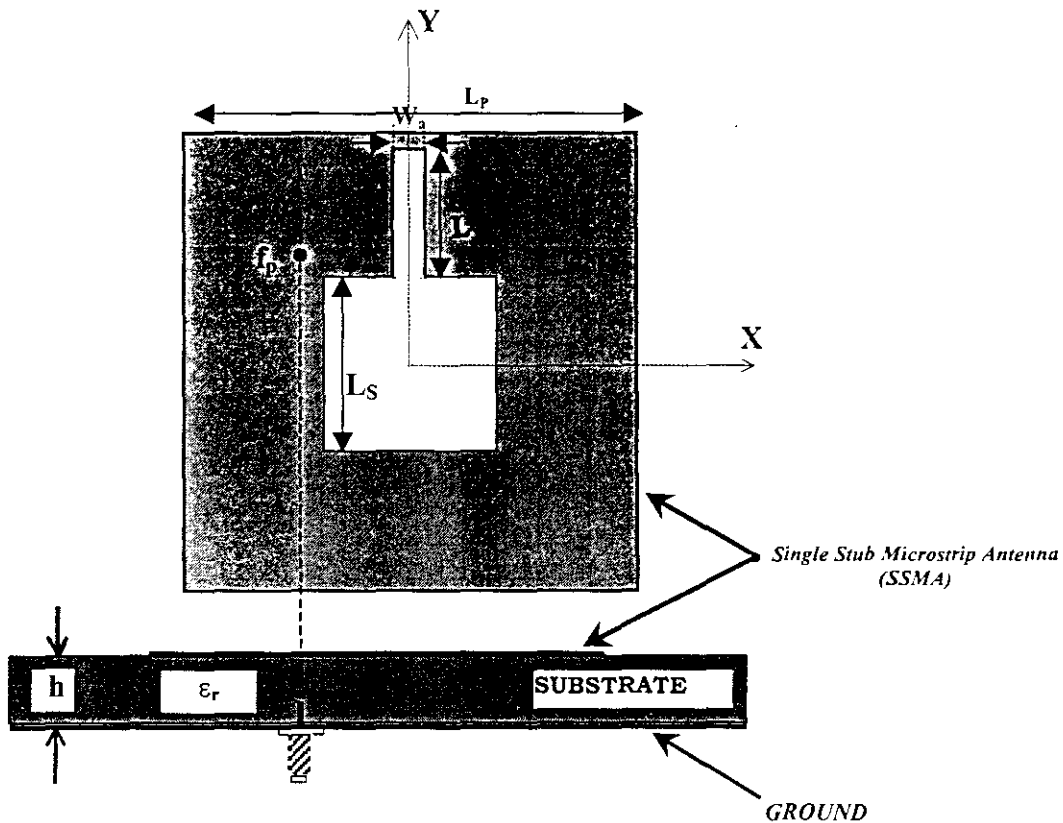


*Figure 4.1* Geometry of the compact Single Stub Microstrip Antenna with probe feed $L_P=4$ cm, $L_s=1.2cm, La=1.2$ cm $W_a=0.2$ cm, h=0.16 cm, $\varepsilon_r=4.28$

## 4.1.2 Frequency Tuning Mechanism

The frequency tuning is effected by controlling the dimensions of the tuning stub attached to the central slot. Coaxial feeding is located along the diagonal of the patch, very close to the corner of the square slot as shown in figure 4.1. In the absence of the stub arm (i.e., $L_S$=13mm. $L_a$, $W_a$ = 0), the antenna exhibits only one resonance, corresponding to its fundamental frequency characterized by its resonating length. By properly selecting the parameters of the stub arm, i.e., $L_a$ and $W_a$, two orthogonally polarized modes can be excited.

It is seen that the two resonant frequencies of SSMA are much lower as compared to the fundamental resonant frequency (*f*) of the square patch antenna. This is because the effective lengths of the two resonant edges are significantly increased. It can also be observed that the excited patch surface current densities are perturbed in such a way that these two modes at different frequencies are excited for dual-frequency operation. By controlling stub arm length, the frequency ratio of the two operating frequencies can be varied.

In each design, the effects of variation in the following patch configurations on frequency tuning are studied. They are: -
1. Square Patch Length–$L_P$
2. Central slot length –$L_S$
3. Stub arm length–$L_a$
4. Stub arm width –$W_a$

For each configuration, the following antenna characteristics are studied in detail for both $TM_{10}$ and $TM_{01}$ Modes:
    a. Variation of resonant frequency with stub-length and slot area
    b. Different antenna radiation characteristics like Impedance bandwidth, radiation pattern, gain and beam width with stub length (*$L_a$*)
    c. Mode identification by means of near field probing
    d. Typical radiation patterns and their characteristics.

The above studies enabled the development of a slot loaded square patch antenna that provides dual frequency operation with reduced patch size compared to standard rectangular patch antenna operating at the same frequency. Before going to the detailed experimental results and analysis, the important basic resonant modes and the excitation techniques adopted in each case are discussed in the next section.

### 4.1.3 Antenna Resonant modes and its variation with Antenna Dimensions

The resonant frequency of the antenna is one of the important characteristics to be studied initially. The resonant frequency depends on the length 'L$_P$' of the patch antenna. This length could be termed as the resonating length as in the case of rectangular microstrip antenna. For a rectangular patch antenna, the resonant frequencies of TM$_{10}$ and TM$_{01}$ modes are determined by its length and width respectively. It is modified here due to the square patch geometry of dimensions 'L$_P$' with a square slot on the centre with side dimension 'L$_S$'. A stub arm with dimensions 'L$_a$' and 'W$_a$' is also incorporated into the patch geometry. In this case, it is found that the antenna resonates at two different frequencies much lower than its original frequency similar to a rectangular patch of dimensions $L_{eff}$ and $W_{eff}$. These modifications increase the effective resonating length and a lower frequency (TM$_{10}$) is excited and hence significant patch area reduction is achieved. It seen that the effective resonating length ($L_{eff}$) for TM$_{10}$ mode depends on the stub parameters 'L$_a$' and 'W$_a$'. '$L_{eff}$' increases with increase in stub arm parameters. It is observed that as the effective resonating length increases, the resonant frequency decreases. The decrease in resonance frequency results in the reduction of total antenna size, making it compact.

In the case of TM$_{01}$ mode the resonance frequency is dependent on the effective width 'W$_{eff}$' of the patch, which is a combined contribution from the patch side ($L_P$) and the central square slot length ($L_S$). Here the resonating length is modified by the slot parameters making its effective value greater than the actual physical length.

### 4.1.3.1 Excitation Techniques

Like other microstrip patch antennas, impedance matching can be achieved by the appropriate selection of the feed point. The input impedance is found to vary with

the location of the feed point along the diagonal. Either a microstrip or coaxial type feed can be used for the $TM_{10}$ mode excitation (half wave variation of electric field along the length of the patch). Figure 4.2 shows the impedance loci of a typical antenna with a coaxial feed along the diagonal line of the antenna.



*Start=1300MHz*
*Stop=1700MHz*
*Centre=1500MHz*
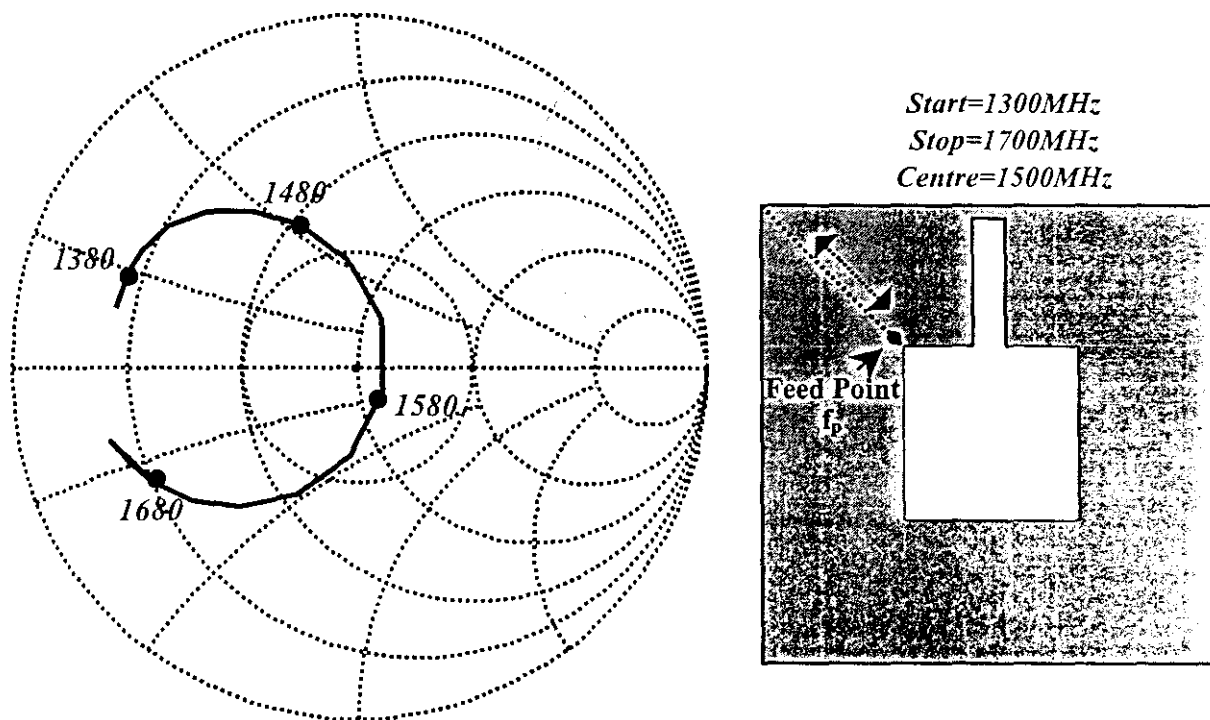
**Figure 4.2** *Variation of Input Impedance*
$L_P=4cm$, $L_S=1.2cm$, $La=1.2cm$  $W_a=0.2$ cm, $h=0.16$ cm, $\varepsilon_r=4.28$

The input impedance is found to be varying from a minimum to a maximum value, when the feed is moved from the centre towards the corner along the diagonal.

It is observed that when the feed point is near the centre, the impedance is very low. When we move from the centre to the corners, the impedance is gradually increasing. Hence, by the proper selection of the feed point, the antenna can be properly matched to 50Ω transmission lines. When the feed point is moved along one side, the $TM_{10}$ impedance varies and $TM_{01}$ remains constant and vice versa, when the feed point is moved along the other side. Hence, we are selecting a feed point along the diagonal to match for both the resonance modes.

### 4.1.3.2 Characteristics of $TM_{10}$ and $TM_{01}$ modes

By moving the feed point along the diagonal line, a change in input impedance is observed. A feed point that provides good matching for both $TM_{10}$ and $TM_{01}$ modes to the 50$\Omega$ feed line is selected. Selection of the feed point along the diagonal line of the slotted patch initiates the excitation of the $TM_{10}$ along with the $TM_{01}$ mode. The radiated fields of this mode are orthogonally polarised.

Here the antennas are fabricated on a dielectric substrate of dielectric constant $\varepsilon_r$ = 4.28 and thickness 0.16 cm. The experiments were also conducted using substrates of dielectric constants $\varepsilon_r$ = 10.2 and $\varepsilon_r$ = 2.2 RT/Duroid with thickness 0.0667 cm and 0.055 cm respectively.

### 4.1.3.3 Variation of Resonant Frequency with respect to slot geometry

The resonant frequency of the proposed antenna is affected by its central slot and the stub arm dimensions $L_S$, $L_a$, and $W_a$. When the central width is increased, the effective resonating length increases, and as a result the resonant frequency is found to be decreasing. These observations have been studied in detail by varying individual parameters and the return loss variation with respect to frequency in each case is analyzed. The experimentally measured return loss characteristics for the proposed Single Stub Microstrip Antenna (SSMA) is compared with that of the unslotted standard square microstrip patch antenna as illustrated in Figure 4.3.

### 4.1.3.4 Variation of resonant frequencies with square patch length '$L_p$', central slot length '$L_s$' and Stub arm length '$L_a$'

Variation of $TM_{10}$ *(f_1)* and $TM_{01}$ *(f_2)* mode frequencies with the tuning stub arm length $L_a$ of the antenna is shown in Table 4.1. The measurements are repeated for two different square patch dimensions ($L_p$). However, studies are concentrated on a typical 4 x 4 cm$^2$ standard square patch for easier comparison. It is observed that the first resonant

frequency decreases with the stub-length ($L_a$). By changing the length of the stub arm ($L_a$), the frequency ratio of the proposed antenna can be tuned in the range of 1.06 – 1.2.

The results also indicate that, by increasing the stub-arm length, only the lower resonance frequency ($f_1$) is decreased, and it is much lower than the fundamental frequency of the standard 4 x 4 cm$^2$ square patch (f=1.79GHz) as evident from fig 4.3. The higher resonance frequency ($f_2$) is only slightly affected by the stub arm length variations. The optimum feed position remains practically the same even when the slot arm length is changed. Figure 4.4 shows the frequency variation with respect to the stub arm length '$L_a$'.

The area requirements of the standard equivalent rectangular patches operating at frequencies $f_1$ and $f_2$ are found to be more; i.e., the dimensions of the patches operating at 1.41 GHz and 1.61 GHz are 32 cm$^2$ and 24 cm$^2$ respectively. The proposed Single Stub Microstrip Antenna (SSMA) geometry occupies only an area of 16 cm$^2$. Typically, when $f_1$ = 1.41 GHz and $f_2$ = 1.61 GHz, the reduction in patch area are 50 % and 36 % respectively in comparison to equivalent rectangular patch antennas. It is observed that the percentage bandwidth remains almost invariant even when the stub arm dimensions are changed for reducing the operating frequencies.

*Table 4.1(i): Variation of $TM_{10}$ ($f_1$) and $TM_{01}$ ($f_2$) mode frequencies with central slot length '$L_S$' and stub arm length '$L_a$'*

| $L_P$ (cm) | $L_S$ (cm) | $W_a$ (cm) | $L_a$ (cm) | h (cm) | $\epsilon_r$ | Frequency $f_1$ (GHz) | Frequency $f_2$ (GHz) | Frequency Ratio ($f_2/f_1$) |
|---|---|---|---|---|---|---|---|---|
| 4 | 0.8 | 0.2 | 0.2 | 0.16 | 4.28 | 1.525 | 1.631 | 1.069 |
|   |   |   | 0.4 |   |   | 1.514 | 1.623 | 1.071 |
|   |   |   | 0.6 |   |   | 1.472 | 1.619 | 1.099 |
|   |   |   | 0.8 |   |   | 1.463 | 1.622 | 1.107 |
|   |   |   | 1.0 |   |   | 1.443 | 1.623 | 1.124 |
|   |   |   | 1.2 |   |   | 1.426 | 1.620 | 1.136 |
| 4 | 1.0 | 0.2 | 0.2 | 0.16 | 4.28 | 1.507 | 1.611 | 1.068 |
|   |   |   | 0.4 |   |   | 1.480 | 1.610 | 1.081 |
|   |   |   | 0.6 |   |   | 1.450 | 1.592 | 1.118 |
|   |   |   | 0.8 |   |   | 1.433 | 1.604 | 1.124 |
|   |   |   | 1.0 |   |   | 1.411 | 1.611 | 1.141 |
|   |   |   | 1.2 |   |   | 1.390 | 1.618 | 1.160 |
| 4 | 1.2 | 0.2 | 0.2 | 0.16 | 4.28 | 1.487 | 1.594 | 1.071 |
|   |   |   | 0.4 |   |   | 1.459 | 1.589 | 1.089 |
|   |   |   | 0.6 |   |   | 1.441 | 1.577 | 1.094 |
|   |   |   | 0.8 |   |   | 1.419 | 1.561 | 1.1 |
|   |   |   | 1.0 |   |   | 1.407 | 1.560 | 1.109 |
|   |   |   | 1.2 |   |   | 1.387 | 1.553 | 1.119 |

Table 4.1(ii) shown below gives the results for a square patch with length '$L_p$=5 cm. Here also the characteristic of frequency tunability is obtained with an almost constant frequency ratio.

**Table 4.1(ii)** *Variation of $TM_{10}$ ($f_1$) and $TM_{01}$ ($f_2$) mode frequencies with central slot length '$L_S$' and stub arm length '$L_a$'*

| $L_P$ (cm) | $L_S$ (cm) | $W_a$ (cm) | $L_a$ (cm) | h (cm) | $\epsilon_r$ | Frequency $f_1$ (GHz) | Frequency $f_2$ (GHz) | Frequency Ratio ($f_2/f_1$) |
|---|---|---|---|---|---|---|---|---|
| 5 | 1.0 | 0.2 | 0.4 | 0.16 | 4.28 | 1.245 | 1.437 | 1.155 |
|   |     |     | 0.6 |      |      | 1.239 | 1.431 | 1.155 |
|   |     |     | 0.8 |      |      | 1.231 | 1.420 | 1.153 |
|   |     |     | 1.0 |      |      | 1.224 | 1.417 | 1.158 |
|   |     |     | 1.2 |      |      | 1.214 | 1.419 | 1.168 |
|   |     |     | 1.4 |      |      | 1.181 | 1.416 | 1.198 |
|   |     |     | 1.6 |      |      | 1.167 | 1.419 | 1.21 |
| 5 | 1.2 | 0.2 | 0.4 | 0.16 | 4.28 | 1.224 | 1.419 | 1.159 |
|   |     |     | 0.6 |      |      | 1.196 | 1.416 | 1.184 |
|   |     |     | 0.8 |      |      | 1.169 | 1.414 | 1.209 |
|   |     |     | 1.0 |      |      | 1.148 | 1.415 | 1.232 |
|   |     |     | 1.2 |      |      | 1.127 | 1.411 | 1.252 |
|   |     |     | 1.4 |      |      | 1.11  | 1.402 | 1.26 |
|   |     |     | 1.6 |      |      | 1.087 | 1.408 | 1.295 |
| 5 | 1.4 | 0.2 | 0.4 | 0.16 | 4.28 | 1.205 | 1.412 | 1.171 |
|   |     |     | 0.6 |      |      | 1.172 | 1.407 | 1.2 |
|   |     |     | 0.8 |      |      | 1.151 | 1.403 | 1.219 |
|   |     |     | 1.0 |      |      | 1.137 | 1.396 | 1.227 |
|   |     |     | 1.2 |      |      | 1.115 | 1.393 | 1.249 |
|   |     |     | 1.4 |      |      | 1.096 | 1.399 | 1.276 |
|   |     |     | 1.6 |      |      | 1.074 | 1.391 | 1.295 |

*Figure 4.3*
*Return Loss*
*Characteristics*

$L_p$=4 cm
$L_s$=1.2 cm
$L_a$=1.2 cm

............... *Standard Square Patch*
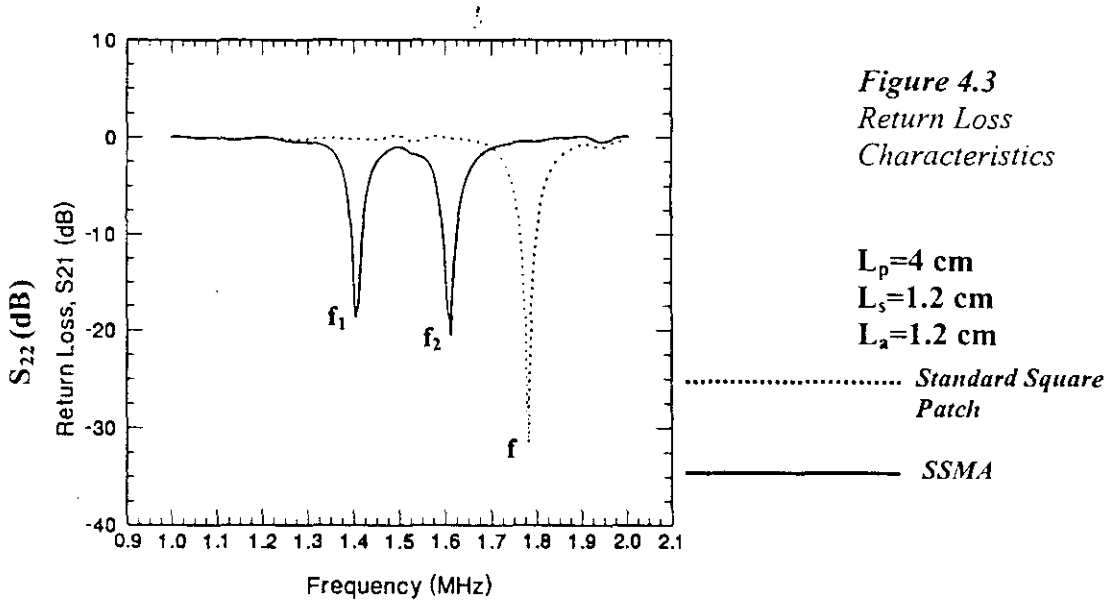
————— *SSMA*

## 4.1.3.5 Variation of Resonance frequencies with slot arm width ($W_a$)

Table 4.2 shows the variation of $TM_{10}$ and $TM_{01}$ mode frequencies with Wa for selected values of '$L_S$'.
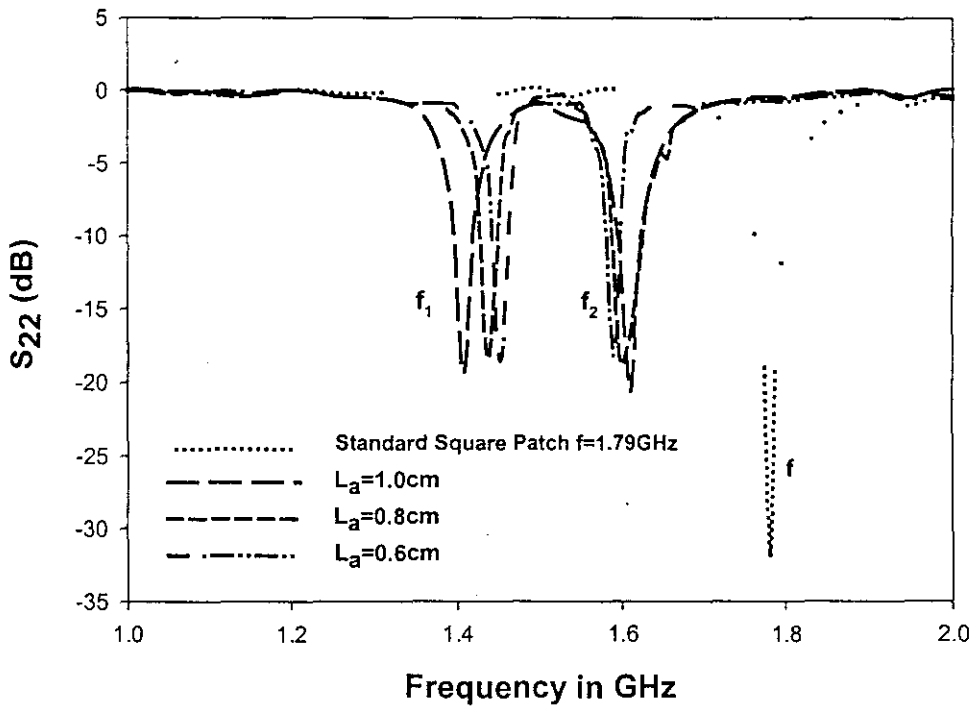


*Figure 4.4 Resonance frequency Curves of the SSMA design for various stub arm lengths '$L_a$'*
*h=0.16 cm, $L_P$=4 cm, $L_S$=1.2 cm, $W_a$=0.2 cm, $\varepsilon_r$=4.28*

72

**Table 4.2** *Variation of TM$_{10}$ (f$_1$) and TM$_{01}$ (f$_2$) mode frequencies with 'W$_a$'*

| L$_p$ (cm) | L$_s$ (cm) | L$_a$ (cm) | W$_a$ (cm) | h (cm) | ε$_r$ | Frequency f$_1$ (GHz) | Frequency f$_2$ (GHz) |
|---|---|---|---|---|---|---|---|
| 4 | 0.8 | 0.8 | 0.1 | 0.16 | 4.28 | 1.445 | 1.64 |
| | | | 0.15 | | | 1.444 | 1.639 |
| | | | 0.2 | | | 1.443 | 1.623 |
| | | | 025 | | | 1.444 | 1.615 |
| | | | 0.3 | | | 1.446 | 1.601 |
| 4 | 1.0 | 0.8 | 0.1 | 0.16 | 4.28 | 1.436 | 1.622 |
| | | | 0.15 | | | 1.433 | 1.615 |
| | | | 0.2 | | | 1.433 | 1.604 |
| | | | 0.25 | | | 1.429 | 1.586 |
| | | | 0.3 | | | 1.432 | 1.576 |

The table shown above show that the resonant frequency decrease with increasing slot arm width (W$_a$).

Figure 4.5 shows the transmission characteristics of the SSMA, which reveals the dual polarized nature of the proposed patch antenna. Dual polarized antennas are creating great interest due to the development of wireless personal communication in recent years. They find application in wireless communication systems to realize the frequency reuse for doubling the system capability. They can also be used in mobile communication systems to obtain polarization diversity for good performance of reception and transmission or to integrate the receiving and transmitting functions into one antenna for reducing the antenna size. The single layer square patch antenna, suggested in this study is highly desirable due to its thin profile, conformity, low cost and capability of being integrated with active devices. Figure 4.6 shows the measured resonant frequencies f$_1$, f$_2$ and the frequency ratio f$_2$ /f$_1$ against the slot-arm length for the proposed antenna. From the analysis, it can be seen that the frequency ratio varies from 1.06 to 1.2. By changing the slot arm dimensions we can merge or shift apart the resonating frequencies.
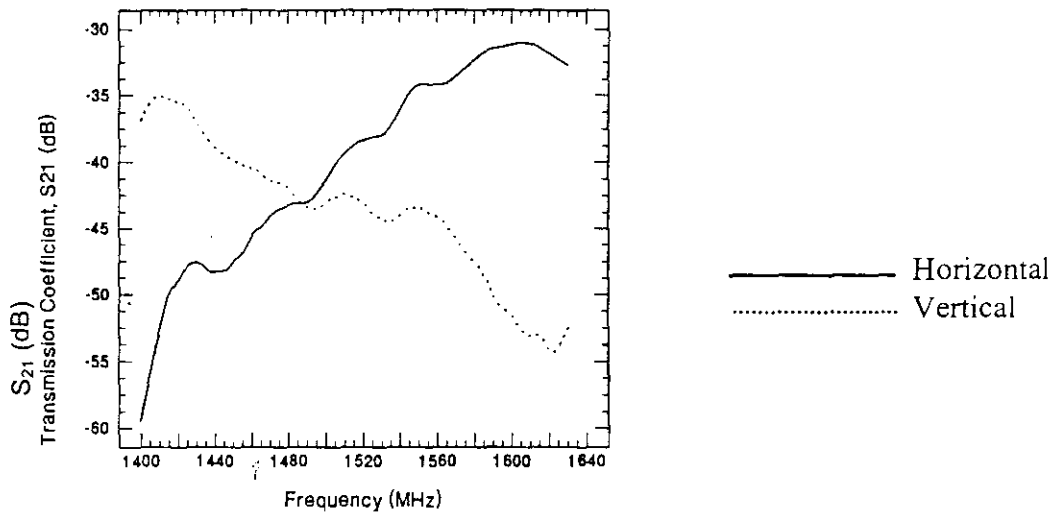
**Figure 4.5** *Transmission Characteristics showing the orthogonal Polarizatio for the Slotted Patch Antenna $L_P=4$ cm,$L_S=1.2$ cm $W_a=0.2$ cm $h=0.16$ cm, $\varepsilon_r=4.28$*
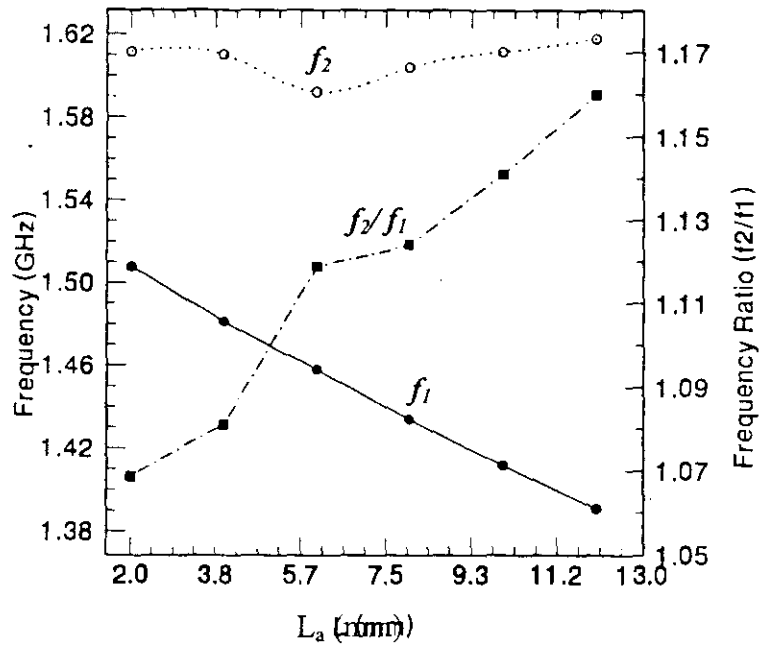


**Figure 4.6** *Measured Resonant frequencies $f_1$, $f_2$ and frequency ratio ($f_2/f_1$) against stub length with $h=0.16$ cm, $L_p=4$ cm, $L_s=1.2$ cm, $W_a=0.2$ cm, $\varepsilon_r=4.28$*

The variation of the two resonance frequencies for three selected central slot length ($L_s$) variations is illustrated in figure 4.7. From the figure it is clear that the fundamental frequency ($f_I$) is mainly affected by the stub length '$L_a$'.
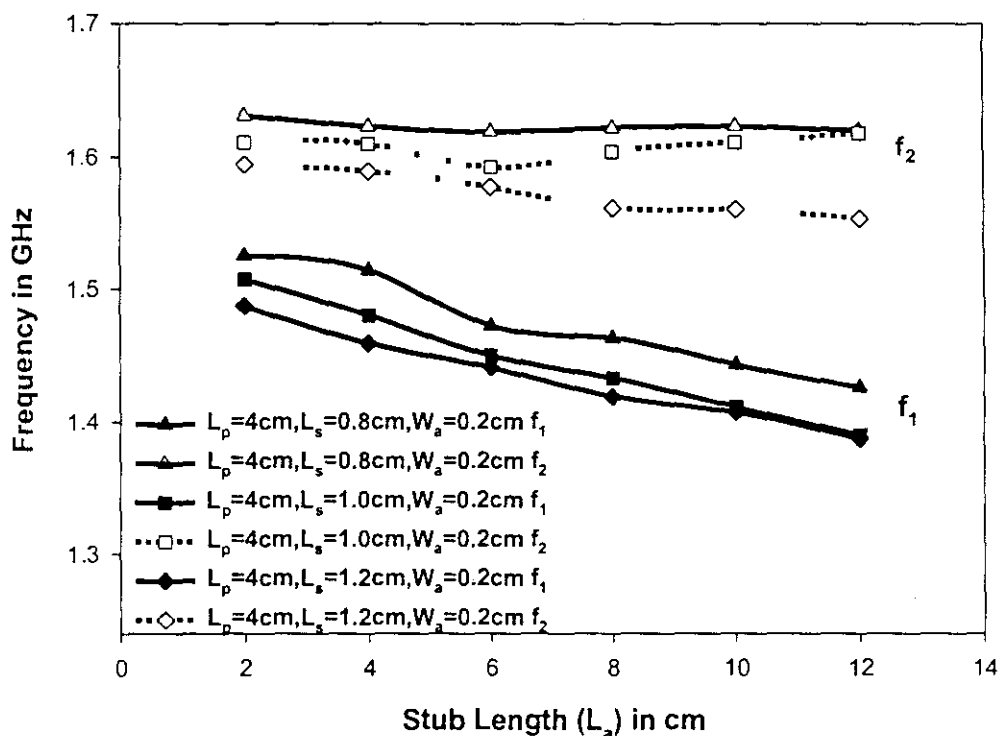


*Figure 4.7* Plot showing the experimental variation of $f_I$ and $f_2$
frequencies with stub arm length ($L_a$). $L_p=4cm$, $W_a=0.2cm$, $h=0.16cm$

#### 4.1.3.6 Variation of Resonant Frequency with respect to Dielectric Constant '$\varepsilon_r$'

The properties are very much dependent on the dielectric constant '$\varepsilon_r$' and height 'h' of the substrate.

Variation of $TM_{10}$ and $TM_{01}$ mode frequencies with height 'h' and dielectric constant '$\varepsilon_r$' is shown in Table 4.3. It shows that both the frequencies decrease with increase in dielectric constant '$\varepsilon_r$'.

*Table 4.3 Variation of TM$_{10}$ (f$_1$ )and TM$_{01}$ (f$_2$) mode frequencies with height 'h' and dielectric constant 'ε$_r$'*

| L$_P$ (cm) | L$_S$ (cm) | L$_a$ (cm) | W$_a$ (cm) | h (cm) | ε$_r$ | Frequency f$_1$ (GHz) | Frequency f$_2$ (GHz) |
|---|---|---|---|---|---|---|---|
| | | 0.2 | | 0.067 | 10.2 | 0.943 | 1.21 |
| | | 0.4 | | 0.067 | 10.2 | 0.931 | 1.16 |
| | | 0.6 | | 0.067 | 10.2 | 0.920 | 1.10 |
| 4 | 0.8 | 0.8 | 0.2 | 0.067 | 10.2 | 0.906 | 1.012 |
| | | 1.0 | | 0.067 | 10.2 | 0.880 | 1.006 |
| | | 1.2 | | 0.067 | 10.2 | 0.863 | 1.001 |
| | | 0.2 | | 0.318 | 2.20 | 1.853 | 1.206 |
| | | 0.4 | | 0.318 | 2.20 | 1.844 | 1.209 |
| 4 | 1.0 | 0.6 | 0.2 | 0.318 | 2.20 | 1.829 | 2.214 |
| | | 0.8 | | 0.318 | 2.20 | 1.814 | 2.205 |
| | | 1.0 | | 0.318 | 2.20 | 1.801 | 2.191 |
| | | 1.2 | | 0.318 | 2.20 | 1.793 | 2.195 |
| | | | | 0.067 | 10.2 | 0.926 | 0.906 |
| 5 | 1.2 | 1.0 | 0.2 | 0.16 | 4.28 | 1.148 | 1.415 |
| | | | | 0.16 | 2.20 | 1.51 | 1.694 |

## 4.1.3.7 Impedance Bandwidth

The bandwidth of a microstrip antenna is usually specified as the range of frequencies over which the return loss is better than 10 dB. Like other microstrip antennas, these antennas are also narrow banded. The bandwidth can be appropriately expressed as a percentage of the frequency difference over the centre frequency of the band. Table 4.4 illustrates the impedance bandwidth variation for the designed antenna. From the table one can easily infer that the impedance bandwidth is maintaining a constant value over the two operating frequencies, even when the antenna stub dimensions are changed for frequency tuning.

*Table 4.4 Table showing impedance Bandwidth corresponding to selected SSMA configurations of different central slot length 'Ls' and stub arm length 'La'.*

| $L_p$, $L_s$, $W_a$ (cm) | $L_a$ (cm) | Frequency $f_1$ (GHz) | Frequency $f_2$ (GHz) | Percentage Impedance Bandwidth $f_1$ | $f_2$ |
|---|---|---|---|---|---|
| 4,0.8,0.2 | 0.2 | 1.525 | 1.631 | 1.55 | 1.66 |
|  | 0.4 | 1.515 | 1.623 | 1.61 | 1.63 |
|  | 0.6 | 1.472 | 1.619 | 1.54 | 1.71 |
|  | 0.8 | 1.463 | 1.622 | 1.51 | 1.74 |
|  | 1.0 | 1.443 | 1.623 | 1.48 | 1.86 |
|  | 1.2 | 1.426 | 1.620 | 1.59 | 1.88 |
| 4,1.0,0.2 | 0.2 | 1.507 | 1.611 | 1.61 | 1.63 |
|  | 0.4 | 1.480 | 1.610 | 1.68 | 1.67 |
|  | 0.6 | 1.450 | 1.592 | 1.73 | 1.79 |
|  | 0.8 | 1.433 | 1.604 | 1.81 | 1.94 |
|  | 1.0 | 1.411 | 1.611 | 1.74 | 2.08 |
|  | 1.2 | 1.390 | 1.618 | 1.68 | 1.96 |
| 4, 1.2, 0.2 | 0.2 | 1.487 | 1.594 | 1.62 | 1.96 |
|  | 0.4 | 1.459 | 1.589 | 1.58 | 1.74 |
|  | 0.6 | 1.441 | 1.577 | 1.7 | 2.09 |
|  | 0.8 | 1.419 | 1.561 | 1.62 | 1.99 |
|  | 1.0 | 1.407 | 1.560 | 1.77 | 2.02 |
|  | 1.2 | 1.387 | 1.553 | 1.81 | 1.94 |

## 4.1.4 Radiation Pattern

An antenna radiation pattern is defined as the graphical representation of the radiated power of the antenna as a function of space coordinates. Being a novel type of microstrip antenna, radiation pattern of the SSMA has been studied in detail. The co-polar and cross-polar radiation patterns of different antenna configurations in the principal planes are taken at different frequency points in the operating frequency band. The measured co-polar and cross-polar radiation pattern at the corresponding central

frequencies of a typical configuration is shown in figure 4.8. The antenna radiation pattern is plotted using the experimental set-up described earlier in methodology chapter, inside the anechoice chamber for an antenna with dimensions $L_p=4cm$, $L_S=1.0cm$, $L_a=1.0cm$ and $W_a=0.2cm$. Radiation pattern for the proposed antenna with a single tuning stub is illustrated in fig 4.8. Similar to a rectangular or square patch, it is observed that the beam width is also large for the proposed antenna. The beam width along the E and H planes at 1.61 GHz are 112° and 82° respectively; the corresponding values at 1.41 GHz are 124° and 88°, respectively. Impedance Bandwidths of 1.8% and 2 % respectively is obtained in the two operating frequencies.
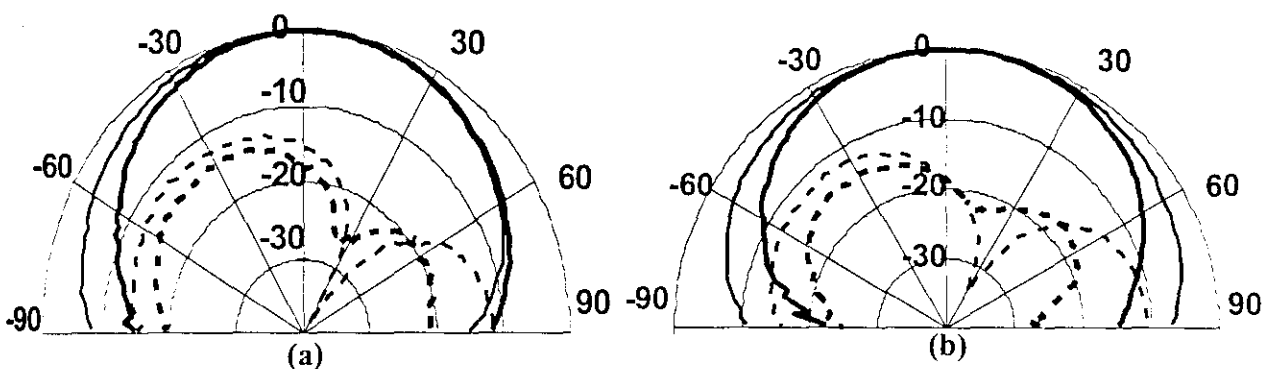


*8 Measured E-plane and H-plane radiation patterns for the single stub antenna:* (a) $f_1$ = 1411MHz (b) $f_2$= 1611GHz. _____  _ _ _ _ _ _ _ _ _ _ _ _ _   E-Plane _____ copolar
H-Plane .............. Cross

$L_p=4.0cm$, $L_s=1.0cm$, $L_a=1.0cm$ $W_a=0.2cm$, $h=0.16cm$

## 4.1.5 Gain

Gain transfer method has been utilised for measuring the relative gain of the newly proposed antennas. Few antenna configurations have been selected for the gain studies. Rectangular microstrip antennas resonating at the same frequency as that of the selected antennas have been fabricated on the same substrate. By using a standard wideband ridged horn as the transmitter, and $S_{21}$ THRU calibration is done using the rectangular patch as the receiver. The SSMA design then replaces this antenna and the transmission characteristic is measured.

The measured $S_{21}$ will give the relative gain of the new antenna with respect to the standard rectangular patch antenna. The results are plotted in figure 4.9.
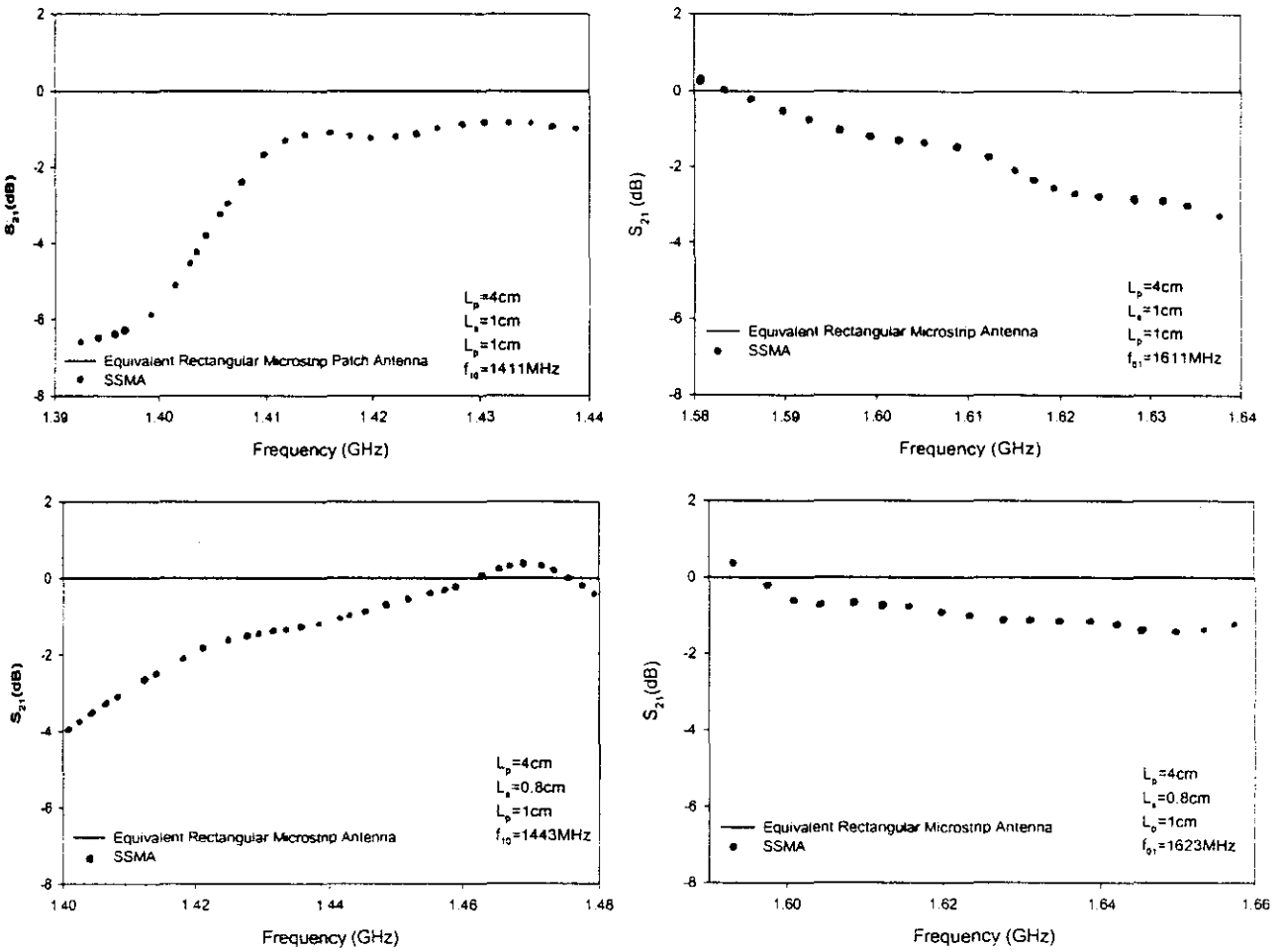


***Figure 4.9*** *$S_{21}$ plots for the Single Stub Microstrip Antenna configurations for different central slot and stub arm lengths with respect to standard rectangular microstrip patch antennas fabricated on the same substrate and resonating at the same frequency*

The resonance frequency and its percentage reduction, physical area of the Single Stub Microstrip Antenna ($A_{SSMA}$) and the equivalent rectangular patch antenna ($A_{eqnt.rect}$) etc., are given in table 4.5. The effective reduction in patch area is calculated using the formula $\dfrac{A_{eqnt.rect} - A_{SSMA}}{A_{eqnt.rect}}$, where $A_{eqnt.rect}$ is the area of the equivalent rectangular microstrip antenna having same length and width as those of the corresponding resonance frequencies $f_{1SSMA}$ and $f_{2SSMA}$ of the Single Stub Microstrip Antenna. From table it can be seen that the metallisation area of the new antenna decreases as the resonant frequency decreases. Whereas, in the case of rectangular antennas the metallisation area increases with decrease of resonance frequency. For operation at 1.411 GHz and 1.611 GHz we need to design two conventional rectangular patch antennas having overall area of 32 $cm^2$ and 25 $cm^2$ respectively. However, the introduction of this design helps to excite the two frequencies from a single square planar radiating structure with a placard shaped slot inserted in to a square patch having overall dimension of 16 $cm^2$.

Another property of this design that is evident from table 4.5 is the frequency tuning technique developed without increasing the overall size. Frequency tuning through reduction of resonant frequencies can be achieved by adjusting the length '$L_a$' and width '$W_a$' (no need to fabricate a new antenna) of the proposed antenna geometry, whereas in the case of rectangular patch antenna, resonant frequency reduction requires an extension of resonant length which necessitates the fabrication of a new antenna. Frequency tuning through the increase of resonant frequency can be achieved by reducing the stub parameters.

The stub arm dimension is controlling the antenna resonance and range of dual frequency operation. The patch and the central slot dimension affect the second frequency, whereas the fundamental resonance mode is fully characterized by the stub arm parameters.

*Table 4.5* The resonant frequencies, percentage of area reduction, physical area of the Single Stub Microstrip SSMA ($A_{SSMA}$) and corresponding equivalent rectangular patch antenna area ($A_{eqnt\cdot rect}$) for various dimensions (h=0.16cm, $\varepsilon_r$=4.28)

| $L_p, L_S, W_a$ (cm) | $L_a$ (cm) | Frequency $f_{1SSMA}$ (GHz) | Frequency $f_{2SSMA}$ (GHz) | Area of the rectangular patch ($A_{eqnt.rect}$) cm$^2$ | | Area of the SSMA ($A_{SSMA}$) cm$^2$ | Percentage Reduction in Patch area | |
|---|---|---|---|---|---|---|---|---|
| | | | | $f_1$ | $f_2$ | | $f_{1SSMA}$ | $f_{2SSMA}$ |
| 4,0.8,0.2 | 0.2 | 1.525 | 1.631 | 27.35 | 23.89 | 16.0 | 42 | 33 |
| | 0.4 | 1.515 | 1.623 | 27.72 | 24.13 | 16.0 | 42.3 | 33.7 |
| | 0.6 | 1.472 | 1.619 | 29.37 | 24.25 | 16.0 | 45.5 | 34 |
| | 0.8 | 1.463 | 1.622 | 29.73 | 24.16 | 16.0 | 46.2 | 33.7 |
| | 1.0 | 1.443 | 1.623 | 30.56 | 24.13 | 16.0 | 47.6 | 7 |
| | 1.2 | 1.426 | 1.620 | 31.3 | 24.22 | 16.0 | 48.9 | 33.7 |
| 4,1.0,0.2 | 0.2 | 1.507 | 1.611 | 28.01 | 24.49 | 16.0 | 43 | 35 |
| | 0.4 | 1.48 | 1.610 | 29.05 | 24.53 | 16.0 | 45 | 34.77 |
| | 0.6 | 1.45 | 1.592 | 30.27 | 25.09 | 16.0 | 47.1 | 36 |
| | 0.8 | 1.433 | 1.604 | 30.99 | 24.71 | 16.0 | 48.3 | 35.24 |
| | 1.0 | 1.411 | 1.611 | 32 | 25 | 16.0 | 50 | 36 |
| | 1.2 | 1.39 | 1.618 | 33 | 24.28 | 16.0 | 51.51 | 34 |
| 4, 1.2, 0.2 | 0.2 | 1.487 | 1.594 | 28.77 | 25 | 16.0 | 44.4 | 36 |
| | 0.4 | 1.459 | 1.589 | 29.90 | 25.18 | 16.0 | 46.5 | 36.45 |
| | 0.6 | 1.441 | 1.577 | 30.65 | 26 | 16.0 | 47.8 | 38.46 |
| | 0.8 | 1.419 | 1.561 | 31.6 | 26.1 | 16.0 | 49.4 | 38.7 |
| | 1.0 | 1.407 | 1.560 | 32.15 | 26.13 | 16.0 | 50.2 | 38.76 |
| | 1.2 | 1.387 | 1.553 | 33.09 | 26.37 | 16.0 | 51.6 | 39.3 |

## 4.1.6 Mode Identification through near probe feeding

The mode structure supported by planar microstrip antennas could be analysed through near field probe measurements. Since, antennas are open structures, field probing could be performed very easily. The electric field intensity just above and perpendicular to the top conductor is measured as described in [10,173]. These field values will give a clear idea of the fields that are expected to lie on the other side of the patch. We can see the current distribution along the edges. The experimental set-up for the field calculation is depicted in figure 3.8 of the methodology chapter. The analysis of the current distribution reveals that two resonant modes exist in the patch. At the first frequency, the variation represents a $TM_{10}$ mode and the second frequency the mode excited is $TM_{01}$ mode, as there is a variation along the opposite direction.

## 4.2 DUAL-STUB SQUARE MICROSTRIP ANTENNA (DSMA)

Through the studies conducted in section 4.1 it is concluded that the tuning stub is having an important role in the frequency-trimming technique of the patch antenna design. The geometry is modified to further trim the antenna area reduction features. However, the basic geometry of the $4 \times 4$ cm$^2$ square patch has been retained in order to have a comparison with earlier results. It has been found that the resonant frequency '$f_I$' depends mainly on the length '$L_a$', of the tuning stub.

### 4.2.1 Antenna Geometry

The structure of the Dual Stub Microstrip Antenna with two identical frequency-tuning stubs placed symmetrically opposite to each other is shown in figure 4.10.
The geometry is simulated using the IE3D electromagnetic modeling package, and a typical design with dimensions $L_P$= 4 cm, $L_S$=1.2 cm, $L_a$=1.0 cm, and Wa=0.2 cm is fabricated on a substrate of thickness h=0.16 cm and permittivity $\varepsilon_r$=4.28. Its characteristics are analyzed using the HP 8510C Vector Network Analyzer measurement set-up.

By exciting the patch using a coaxial probe feed along the diagonal line of the square patch, it is seen that dual frequency operation based on the two resonant frequencies ($f_{10}$ and $f_{01}$) of the perturbed $TM_{10}$ and $TM_{01}$ modes can be generated. The measured and simulated return loss ($S_{11}$) characteristics are illustrated in Figure 4.11. The two resonance frequencies, $f_1$ and $f_2$ obtained in the case of DSMA are found to be much below the resonance of the SSMA. The detailed IE3D simulation analysis is presented in section 5.9.2

The new proposed DSMA has a greater area reduction compared to the SSMA design described earlier with a single tuning stub. Also due to the shaped slot embedded with two tuning stubs inside the patch the effective lengths of the two resonant modes are greatly increased, the two resonant frequencies are much lower as compared to the fundamental resonant frequency (f) of the standard unslotted square patch antenna. By etching the central square slot alone ($L_S$=1.2 cm, $L_a$=$W_a$=0) the antenna is found to be resonating at 1.63 GHz; whereas the introduction of the dual slot arms excites a lower resonance at 1.26GHz ($f_1$). It is also observed that there is a second resonance frequency ($f_2$) at 1.48GHz (with $L_a$=1.0 cm).

The antenna stub parameters are systematically varied over the length of the patch and the corresponding operating frequencies are analysed. From the results it can be seen that the two resonant frequencies decrease with increasing stub arm dimensions (presented in detail in section 4.2.2.1). The experimental results reveal that the excited patch surface current densities are perturbed in such a way that these two modes are excited for dual frequency operation. By choosing equal stub arm lengths the frequency ratio of the two operating frequencies can be maintained almost constant. This design provides two close frequencies of different polarization and has a patch area reduction of 61% for the first frequency and 45% for the second frequency compared to standard rectangular patch. The field is mainly concentrated in the slot centre and the slot dimensions act as tuning impedances. The length of the stub extensions ($L_a$) is controlling the resonance frequency tuning. The dual frequency characteristics and impedance bandwidth of the dual stub loaded patch antenna with various stub arm lengths are shown in Table 4.6.
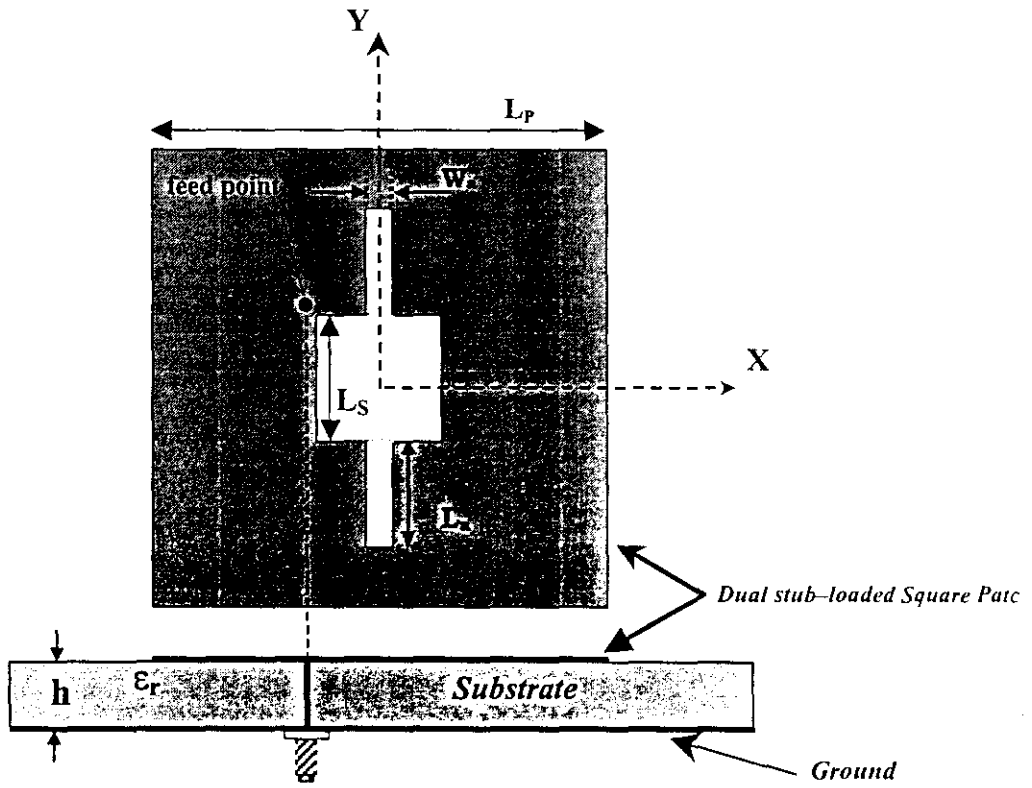
**Figure 4.10** *Geometry of the dual stub Microstrip Patch Antenna*
$L_P$= 4 cm, $L_S$=1.0 cm, $L_a$=1.0 cm, Wa=0.2 cm,h=0.16cm,$\varepsilon_r$=4.28
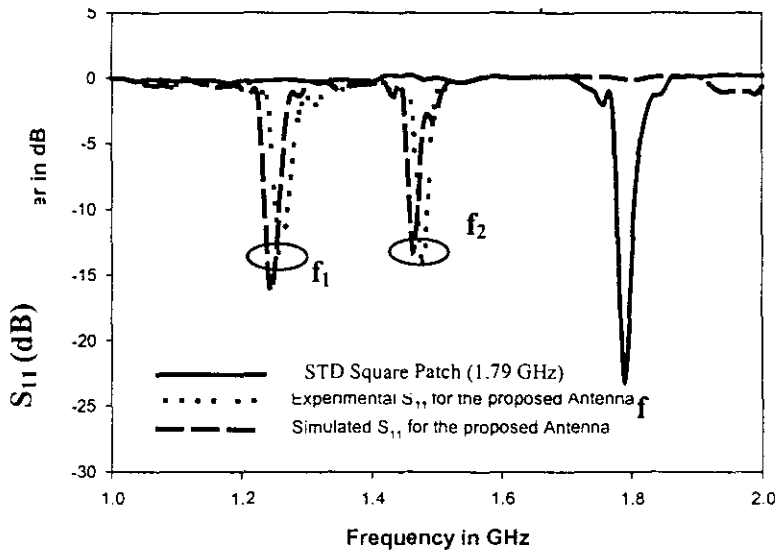
**Figure 4.11** *The measured and simulated return loss ($S_{11}$) characteristics*
*$L_P$=4 cm, $L_S$=1.0 cm, $L_a$=1.0 cm, Wa=0.2 cm, h=0.16 cm, $\varepsilon_r$=4.28*

## 4.2.2 Characteristic Resonant modes and its variation with Antenna Parameters

Both the resonant frequencies generated in the of the slot antenna geometry are affected by the central slot dimension and dual stub arm dimensions. The following section illustrates the variation of the dual resonant frequencies with respect to variation in these parameters.

### 4.2.2.1 Variation of resonant frequencies with central slot width '$L_s$' and stub arm length '$L_a$'

Variation of $TM_{10}$ ($f_1$) and $TM_{01}$ ($f_2$) mode frequencies with tuning stub length '$L_a$' of the stub microstrip antenna is studied. Here both the stub arm dimensions are varied uniformly to study the frequency tuning mechanism with the dual stub geometry. Table 4.6 gives the experimental results of the return loss by systematically varying $L_S$ *and* $L_a$. Figure 4.12 illustrates variations in frequency with the above-mentioned parameters.

*Table 4.6* *Experimental Variation of* $TM_{10}$ $(f_1)$ *and* $TM_{01}$ $(f_2)$ *mode frequencies with Central slot length* '$L_S$' *and stub arm length* '$L_a$'

| $L_P$ (cm) | $L_S$ (cm) | $W_a$ (cm) | $L_{a1}=L_{a2}$ $=L_a$ (cm) | h (cm) | $e_r$ | Frequency $f_1$ (GHz) | Frequency $f_2$ (GHz) | Frequency Ratio $(f_2/f_1)$ |
|---|---|---|---|---|---|---|---|---|
| 4 | 0.8 | 0.2 | 0.2 | 0.16 | 4.28 | 1.345 | 1.576 | 1.171 |
|   |   |   | 0.4 |   |   | 1.339 | 1.569 | 1.172 |
|   |   |   | 0.6 |   |   | 1.327 | 1.544 | 1.164 |
|   |   |   | 0.8 |   |   | 1.311 | 1.531 | 1.167 |
|   |   |   | 1.0 |   |   | 1.304 | 1.519 | 1.165 |
|   |   |   | 1.2 |   |   | 1.292 | 1.491 | 1.154 |
| 4 | 1.0 | 0.2 | 0.2 | 0.16 | 4.28 | 1.322 | 1.549 | 1.171 |
|   |   |   | 0.4 |   |   | 1.301 | 1.530 | 1.179 |
|   |   |   | 0.6 |   |   | 1.292 | 1.512 | 1.186 |
|   |   |   | 0.8 |   |   | 1.278 | 1.497 | 1.18 |
|   |   |   | 1.0 |   |   | 1.262 | 1.492 | 1.03 |
|   |   |   | 1.2 |   |   | 1.253 | 1.489 | 1.188 |
| 4 | 1.2 | 0.2 | 0.2 | 0.16 | 4.28 | 1.315 | 1.533 | 1.165 |
|   |   |   | 0.4 |   |   | 1.297 | 1.518 | 1.167 |
|   |   |   | 0.6 |   |   | 1.274 | 1.503 | 1.163 |
|   |   |   | 0.8 |   |   | 1.268 | 1.489 | 1.165 |
|   |   |   | 1.0 |   |   | 1.254 | 1.477 | 1.17 |
|   |   |   | 1.2 |   |   | 1.250 | 1.461 | 1.166 |

From the above table as well as from the following figure it is clear that in the case of DSMA also the dominant mode frequency decreases with increase in stub arm length '$L_a$'.
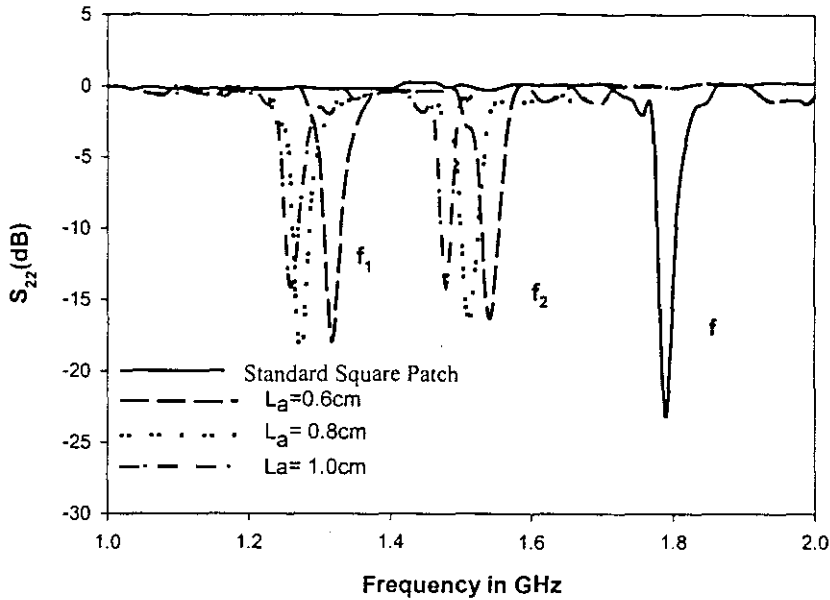
*Figure 4.12 Return loss plot of the dual stub antenna for selected central slot lengths (Ls) and stub arm lengths (La). Lp=4 cm, Ls=1.0 cm, Wa=0.2 cm, $\varepsilon_r$=4.28*

## 4.2.2.2 Impedance Bandwidth

The impedance bandwidth and ratio of the operating frequencies is studied by varying the stub arm length ($L_a$). Table 4.7 depicts the impedance bandwidth and frequency ratio for the modified Dual Stub Microstrip Antenna. By choosing equal stub arm lengths, the frequency ratio of the two resonant frequencies can be maintained almost constant.

*Table 4.7 Showing the variation of the $TM_{10}$ and $TM_{01}$ resonant frequencies and impedance bandwidth against stub arm length ($L_a$) for the dual stub slot loaded Antenna Lp=4 cm, Ls=1.3 cm, Wa=0.17 cm, h=0.16 cm, $\varepsilon_r$=4.28*

| Tuning Stub length (cm) ($L_a$) | 0.2 | 0.4 | 0.6 | 0.8 | 1.0 |
|---|---|---|---|---|---|
| $f_1$ (MHz) | 1322 | 1297 | 1274 | 1268 | 1254 |
| $BW_1$ (%) | 1.86 | 1.81 | 1.75 | 1.75 | 1.72 |
| $f_2$ (MHz) | 1549 | 1530 | 1512 | 1497 | 1482 |
| $BW_2$ (%) | 2.06 | 1.94 | 1.94 | 1.87 | 1.85 |
| $f_2/f_1$ | 1.171 | 1.179 | 1.186 | 1.180 | 1.181 |

### 4.2.2.3 Variation of Resonant Frequencies with stub arm width ($W_a$)

Table 4.8 shows the variation of $TM_{10}$ and $TM_{01}$ mode frequencies with respect to stub arm width '$W_a$'. Figure 4.13 represents the variation of resonant frequencies for different stub arm length ($L_a$).

*Table 4.8 Variation of $TM_{10}$ ($f_1$) and $TM_{01}$ mode ($f_2$) frequencies with '$W_a$' for constant '$L_a$' values*

| $L_P$ (cm) | $L_S$ (cm) | $L_a$ (cm) | $W_a$ (cm) | h (cm) | $\epsilon_r$ | Frequency $f_{10}$ (GHz) | Frequency $f_{01}$ (GHz) |
|---|---|---|---|---|---|---|---|
| 4 | 0.8 | 0.8 | 0.1 | 0.16 | 4.28 | 1.317 | 1.62 |
|   |   |   | 0.15 |   |   | 1.314 | 1.562 |
|   |   |   | 0.2 |   |   | 1.311 | 1.531 |
|   |   |   | 025 |   |   | 1.304 | 1.518 |
|   |   |   | 0.3 |   |   | 1.303 | 1.496 |
| 4 | 1.0 | 0.8 | 0.1 | 0.16 | 4.28 | 1.285 | 1.597 |
|   |   |   | 0.15 |   |   | 1.283 | 1.531 |
|   |   |   | 0.2 |   |   | 1.278 | 1.497 |
|   |   |   | 0.25 |   |   | 1.269 | 1.461 |
|   |   |   | 0.3 |   |   | 1.261 | 1.432 |

The transmission characteristic ($S_{21}$) of the designed antenna in the horizontal and vertical polarisations is measured and is shown in Fig 4.14. From the figure one can infer that in the case of Dual Stub Microstrip Antenna also dual polarisation characteristics is observed that finds wide applications in communication systems.

### 4.2.3 Radiation Pattern

The radiation characteristics for the two frequencies were also measured. The E-Plane and H-plane radiation patterns for the stub length, $L_a$ = 10mm are plotted in Fig. 4.15. The antenna pattern is plotted using the anechoic chamber set-up presented in the chapter III for the dual stub antenna with dimensions $L_p$=4cm, $L_s$=1.2cm, $L_a$=1cm and $W_a$=0.2cm. The beam width along the E and H-planes at 1.48 GHz are 118° and 91°, respectively; the corresponding values at 1.27 GHz are 114° and 92° respectively. Cross-polar levels better than −20 dB is observed over the entire range of operation.
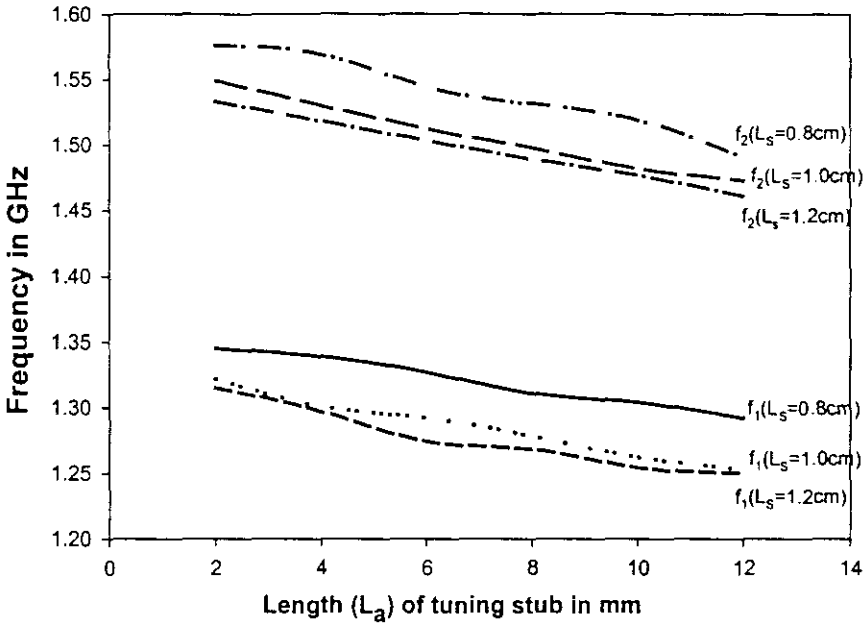
**Figure 4.13** *Plot showing the experimental variation of $TM_{10}$ and $TM_{01}$ resonant frequencies with stub arm length $(L_a)$ $L_P=4$ cm, $W_a=0.2cm$, $h=0.16cm, \varepsilon_r=4.28$*
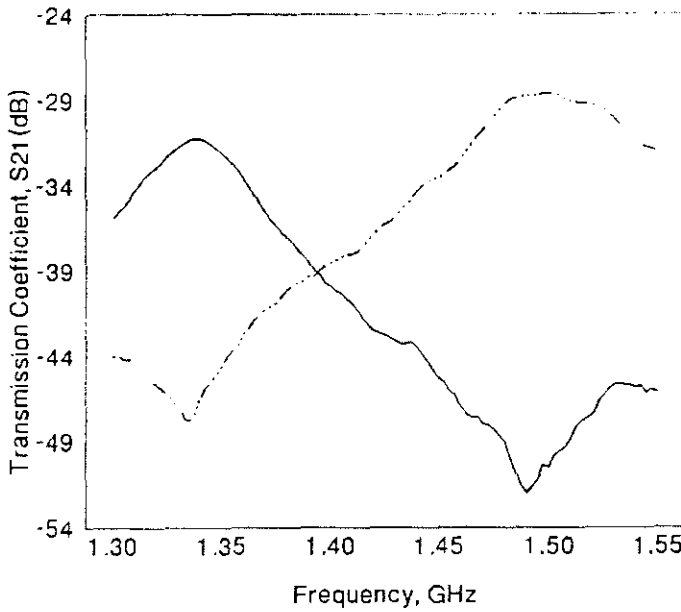


**Figure 4.14** *Variation of received power with frequency for the orthogonal*
polarization planes
*$L_P=4$ cm, $L_S=1.2$ cm, $L_a=1$ cm, $W_a=0.2$ cm, $h=0.16$ cm, $\varepsilon_r=4.28$*

———————————— *Vertical* ▬ ·· ▬ ·· *Horizontal*

H-plane

E-plane



$f_1$=1262MHz

$f_2$=1492 MHz
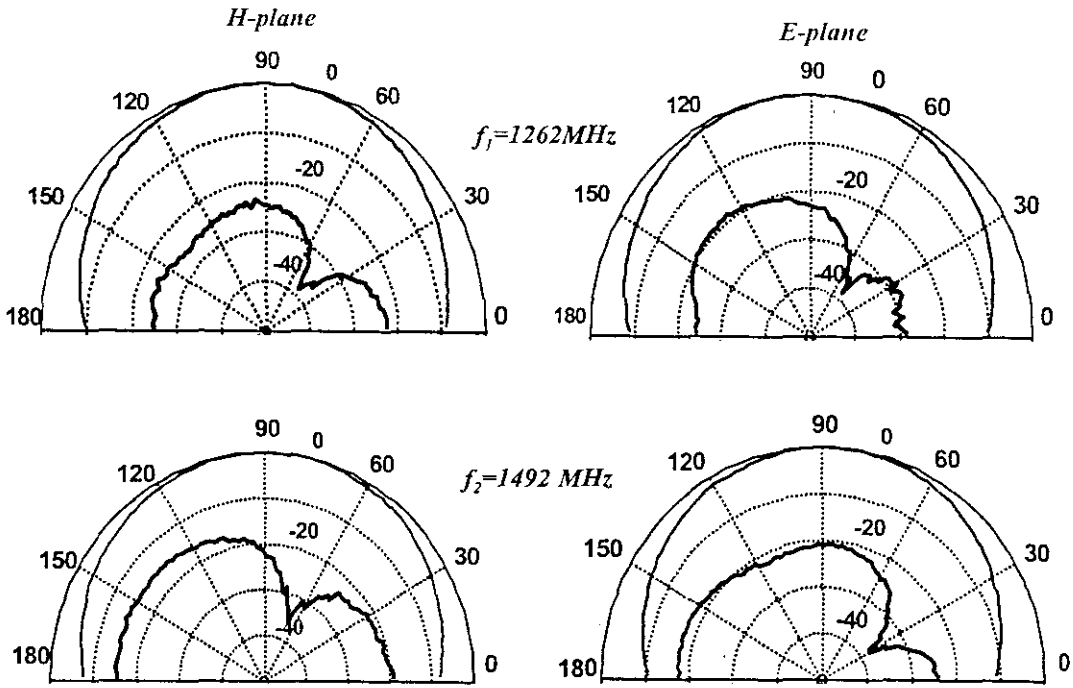
**Figure 4.15** *Measured E-plane and H-plane radiation pattern for the Dual Stub Microstri*
*antenna at the two operating frequencies Lp=4cm, Ls=1.0 cm, La=1.0 cm,*
*Wa=0.2cm,h=0.16cm, ε=4.28*  _____ Copolar

_____ Cross-polar

### 4.2.4 Antenna Gain

As described in section 4.1.5, the SSMA relative gain of the dual stub antenna
can be measured. The typical gain plots of a standard DSMA has been measured and is
plotted in figure 4.16.
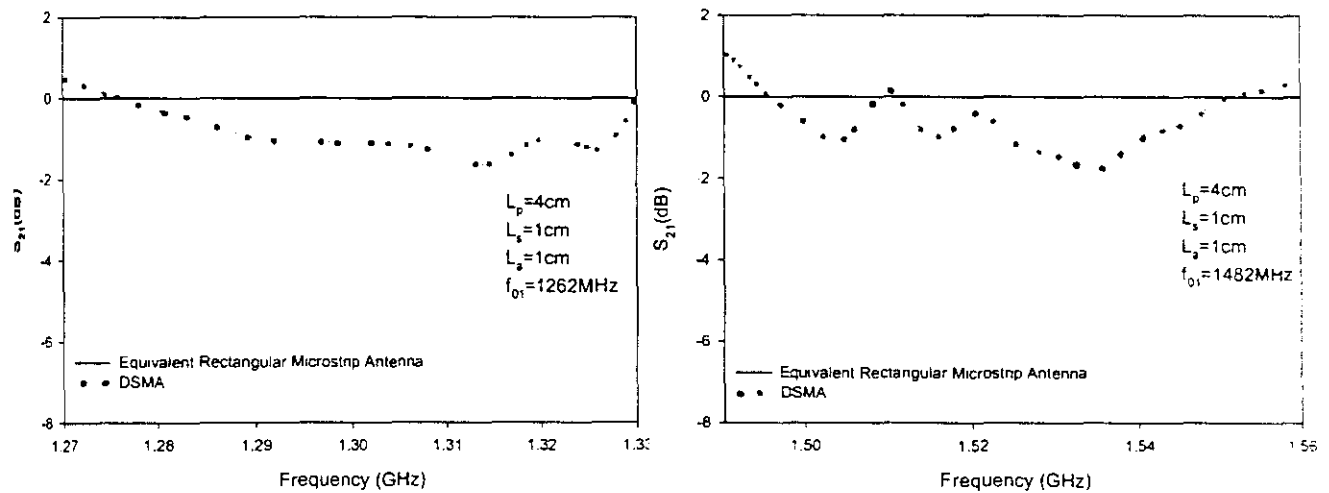


**re 4.16** *S21 plots for a typical Dual Stub Microstrip (DSM) antenna configuration with respect to*
*standard rectangular microstrip patch antenna fabricated on the same substrate and*
*resonating at the same frequency*

90
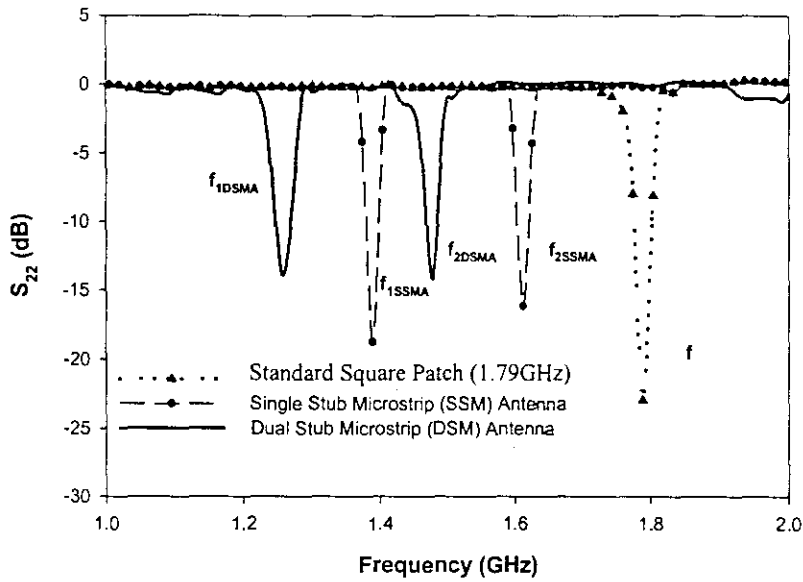
*Figure 4.17 Comparison of Resonance frequencies of the Single Stub and Dual stub Microstrip Antenna.*

The deterioration in gain as observed from the figure 4.16 is negligible in comparison to the over all patch area reduction achievement.

Figure 4.17 shows the operating frequency comparison of the single and dual stub microstrip antennas. From the figure, it is observed that the antenna resonance can be tuned considerably through the insertion of slotted geometry.

The resonance frequency and its percentage area reduction, physical area of the Dual Stub Microstrip Antenna ($A_{DSMA}$) and the equivalent rectangular microstrip patch antenna ($A_{eqnt.rect}$) etc., are given in table 4.9. From the table we can infer that the metallisation area of the new antenna decreases as the resonant frequency decreases. In the case of rectangular antennas the metallic patch area increases with decrease of resonance frequency. For operation at 1.25 GHz and 1.482 GHz we need to design two conventional rectangular patch antennas having overall area of 49 cm$^2$ and 29 cm$^2$ respectively. But, the introduction of this dual stub design helps us to excite the two frequencies from a single planar radiating structure having overall dimension of 16 cm$^2$. The DSMA design is providing enhanced area reduction features in comparison to the SSMA design introduced in the section 4.1.

Another characteristic property of this design that is evident from table 4.9 is the frequency tuning technique developed without increasing the overall size. Here, frequency tuning through reduction of resonant frequencies can be achieved by adjusting the length $L_a$ and width $W_a$ of the dual tuning stubs of this antenna geometry.

*Table 4.9* *The resonant frequencies, percentage of area reduction, physical area of the DSMA ($A_{DSMA}$) and corresponding equivalent rectangular patch antenna ($A_{eqnt.rect}$) for selected dimensions (h=0.16 cm, $\varepsilon_r$=4.28)*

| $L_p, L_s, W_a$ (cm) | $L_a$ (cm) | Frequency $f_{1DSMA}$ (GHz) | Frequency $f_{2DSMA}$ (GHz) | Area of the rectangular patch ($A_{eqnt.rect}$) cm$^2$ | | Area of the DSMA ($A_{DSMA}$) cm$^2$ | Percentage Reduction in Patch area | |
|---|---|---|---|---|---|---|---|---|
| | | | | $f_1$ | $f_2$ | | $f_1$ | $f_2$ |
| 4,0.8,0.2 | 0.2 | 1.345 | 1.576 | 35.2 | 25.6 | 16.0 | 54.5 | 37.5 |
| | 0.4 | 1.339 | 1.569 | 35.5 | 25.8 | 16.0 | 55 | 38 |
| | 0.6 | 1.327 | 1.544 | 36.2 | 26.7 | 16.0 | 55.8 | 40 |
| | 0.8 | 1.311 | 1.531 | 37 | 27.14 | 16.0 | 57 | 41 |
| | 1.0 | 1.304 | 1.519 | 37.5 | 27.6 | 16.0 | 57.3 | 42 |
| | 1.2 | 1.292 | 1.491 | 38.2 | 28.62 | 16.0 | 58 | 44 |
| 4,1.0,0.2 | 0.2 | 1.322 | 1.549 | 36.44 | 26.5 | 16.0 | 56 | 39.6 |
| | 0.4 | 1.301 | 1.530 | 37.63 | 27.17 | 16.0 | 57.5 | 41 |
| | 0.6 | 1.292 | 1.512 | 38.2 | 27.82 | 16.0 | 58 | 42.5 |
| | 0.8 | 1.278 | 1.497 | 39 | 28.4 | 16.0 | 59 | 43.7 |
| | 1.0 | 1.262 | 1.482 | 40 | 29 | 16.0 | 60 | 44.8 |
| | 1.2 | 1.253 | 1.473 | 40.58 | 29.3 | 16.0 | 60.6 | 45.4 |
| 4, 1.2, 0.2 | 0.2 | 1.315 | 1.533 | 36.83 | 27.1 | 16.0 | 56.6 | 41 |
| | 0.4 | 1.297 | 1.518 | 37.9 | 27.6 | 16.0 | 57.8 | 42 |
| | 0.6 | 1.274 | 1.503 | 39.2 | 28.2 | 16.0 | 59.2 | 43 |
| | 0.8 | 1.268 | 1.489 | 39.62 | 28.7 | 16.0 | 59.6 | 44.2 |
| | 1.0 | 1.254 | 1.477 | 40.5 | 29.2 | 16.0 | 60.5 | 45 |
| | 1.2 | 1.250 | 1.461 | 40.77 | 29.8 | 16.0 | 60.6 | 46.3 |

The dual stub arm is found to be the key element in controlling the antenna resonance and range of dual frequency tuning operation. The antenna radiation and impedance characteristics are analyzed and found to be comparable with that of standard antennas. Hence this antenna can be offered as a compact antenna system with reduced area requirements.

## 4.2.5 Comparison of the Single Stub Microstrip Antenna (SSMA) and Dual Stub Microstrip Antenna (DSMA)

The two antenna designs discussed so far are found to be providing good area reduction and cross-polar level performance. Table 4.10 illustrates the various characteristics of two geometries.

*Table 4.10 Comparison of the characteristics of the SSMA and DSMA*

| Property | SSMA | DSMA |
|----------|------|------|
| Resonant Frequencies | 1.41 GHz ($f_1$) <br> 1.61 GHz ($f_2$) | 1.254 GHz ($f_1$) <br> 1.482 ($f_2$) |
| 3 dB Beamwidth – E-Plane <br> H-Plane | $112^0\ 124^0$ <br> $82^0\ 88^0$ | $108^0\ 114^0$ <br> $88^0\ 90^0$ |
| Directivity | 7.08 dB | 6.91 dB |
| 2:1 VSWR Bandwidth | 1.8 ($f_1$) 2.1 ($f_2$) | 1.71 ($f_1$) 2.2 ($f_2$) |
| % Area reduction | 50 <br> 36 | 61 <br> 45 |
| Total Area of patch | $16cm^2$ | $16cm^2$ |

## 4.3 THREE STUB MICROSTRIP ANTENNA (TSMA)

Dual-frequency operation of microstrip antennas has been widely used in portable communication systems. For such portable systems, as miniaturization of the communication equipment is of prime importance, the design of compact antenna systems becomes essential.

The studies are extended by including one more tuning stub to achieve further area reduction without considerable reduction in gain. This modified structure possesses three tuning stubs and is named as ' TSMA' (Three Stub Microstrip Antenna). The modified structure consists of a square patch with a square slot at the centre having three tuning stubs centered in the square patch to lower the frequencies of the dual band operation. The third stub arm is placed at a location exactly perpendicular to the existing two identical stubs in the DSM Antenna.

## 4.3.1. Antenna Geometry

The geometry of the three-stub microstrip antenna is given in Fig 4.18.
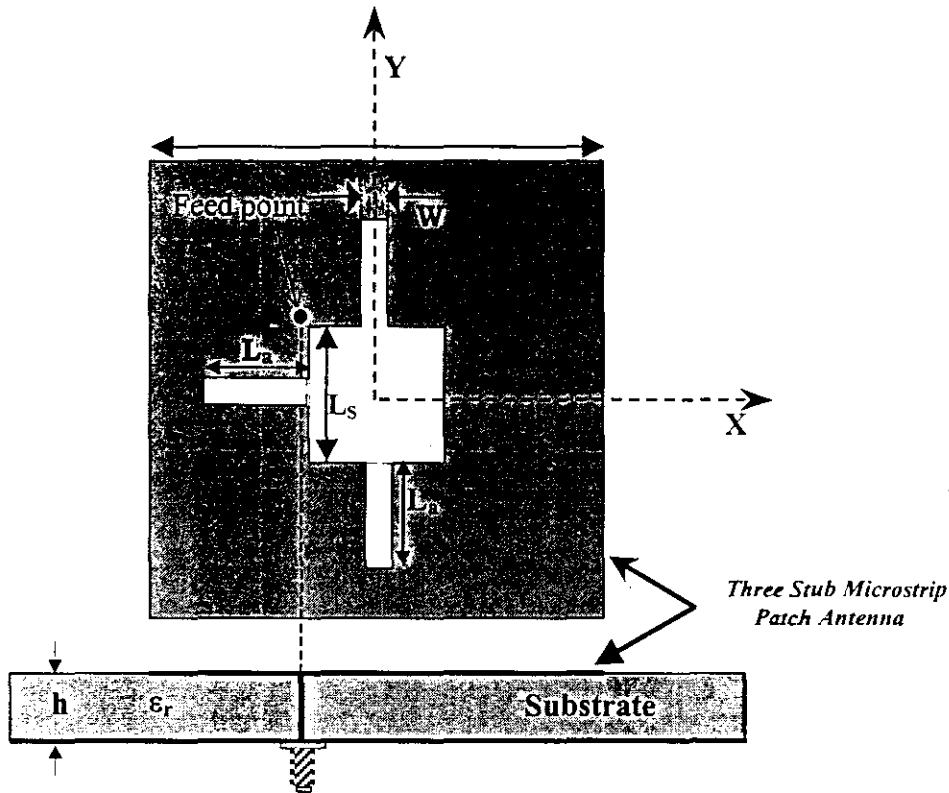


*Figure 4.18 Geometry of the three stub slotted Microstrip Patch Antenna for Dual Frequency Operation $L_P=4cm, L_S=1.0cm, L_a=1.0cm, W_a=0.2cm, \varepsilon_r=4.28$*

The antenna is initially simulated using IE3D and it is experimentally implemented and tested using the microwave antenna measurement system. The dimension of the three-stub antenna is optimised for perfect matching. It is observed that perfect matching

occurs when the third stub is equal in dimensions to the existing two. The feed location of the antenna is chosen along the diagonal of the square patch as in the earlier two cases.

In a typical case, $L_S$, $L_a$, and $W_a$ are chosen to be 1.2 cm, 1.0 cm and 0.2 cm respectively. Here, also like in the previous cases, two distinct frequencies are excited with considerable impedance bandwidth required for applications in communication antenna systems.

### 4.3.2 Antenna Return Loss Characteristics

The scattering parameter measurements on the antenna with suitably selected patch dimensions, gave two distinct frequencies with opposite polarization. The fundamental resonance frequency of the unslotted standard square patch is ~ 1.79GHz (f). In the absence of the tuning stubs ($L_S$=1.2 cm, $L_a$=$W_a$=0) it is observed that the antenna is resonating at 1.63 GHz, whereas the introduction of the three stubs initiates an additional resonance frequency at 1.21 GHz $(f_1)$. The return loss characteristic for the typical design is shown in figure 4.19.
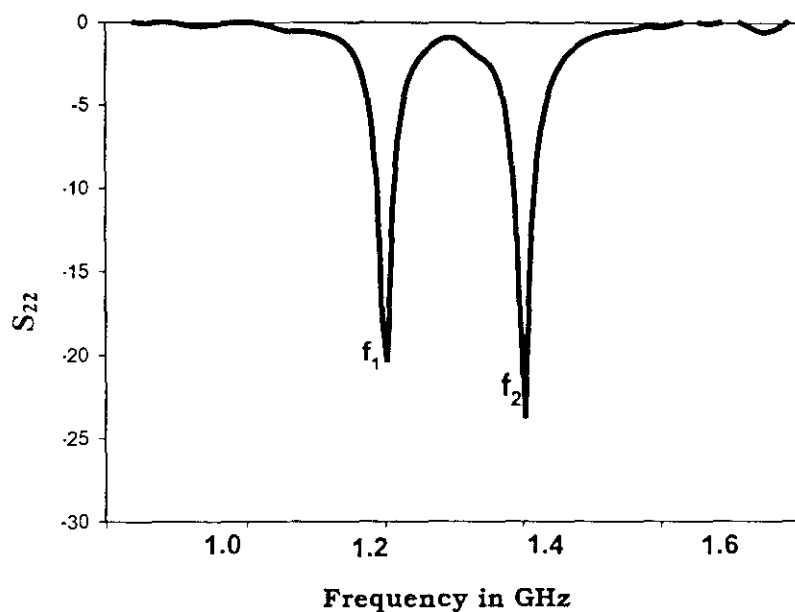


Figure 4.19 Return loss characteristics of the three stub Microstrip patch antenna
$L_P=4cm, L_S=1.0cm, L_a=1.0cm, W_a=0.2cm, \varepsilon_r=4.28$

It is also observed that the second resonance frequency falls to 1.389 GHz $(f_2)$ from 1.63 GHz. Thus it provides an area reduction of the order of 63% and 52 % respectively for the dual resonant modes.

### 4.3.3 Frequency Tuning and its dependence on Antenna parameters

Frequency tuning can be carried over a wide band of frequencies with this modified structure. As in the previous cases, the variation of TSM Antenna resonance with respect to changes in antenna parameters is initially simulated and then experimentally verified. The simulation results are presented in section 5.9.3.

### 4.3.3.1 Variation of resonant frequencies with respect to slot length 'L$_s$' and stub arm length 'L$_a$'

By varying the central slot length 'L$_s$' and stub arm length 'L$_a$', it can be observed that the slot is effectively increasing the patch dimensions and hence lowering the resonant frequencies. Both the resonant frequencies are well below the resonant frequency of the standard rectangular patch. Table 4.11 shows the effect of stub length 'L$_a$' and stub width 'W$_a$' on the resonance frequencies on the TSMA.

**Table: 4.11** *Variation of* $TM_{10}$ *(f$_1$) and* $TM_{01}$ *(f$_2$) mode frequencies with slot length 'L$_s$' stub arm length 'L$_a$'*

| L$_P$ (cm) | L$_S$ (cm) | W$_a$ (cm) | L$_{a1}$=L$_{a2}$=L$_{a3}$ =La (cm) | h (cm) | $\epsilon_r$ | Frequency $f_1$ (GHz) | Frequency $f_2$ (GHz) | Frequency Ratio (f$_2$/f$_1$) |
|---|---|---|---|---|---|---|---|---|
| 4 | .8 | 0.2 | 0.2 | 0.16 | 4.28 | 1.285 | 1.536 | 1.195 |
|   |    |     | 0.4 |      |      | 1.271 | 1.522 | 1.197 |
|   |    |     | 0.6 |      |      | 1.266 | 1.503 | 1.187 |
|   |    |     | 0.8 |      |      | 1.254 | 1.488 | 1.191 |
|   |    |     | 1.0 |      |      | 1.233 | 1.474 | 1.195 |
|   |    |     | 1.2 |      |      | 1.220 | 1.462 | 1.198 |
|   |    |     | 1.4 |      |      | 1.214 | 1.454 | 1.197 |
| 4 | 1 | 0.2 | 0.2 | 0.16 | 4.28 | 1.254 | 1.459 | 1.163 |
|   |    |     | 0.4 |      |      | 1.239 | 1.438 | 1.161 |
|   |    |     | 0.6 |      |      | 1.226 | 1.417 | 1.158 |
|   |    |     | 0.8 |      |      | 1.16  | 1.401 | 1.152 |
|   |    |     | 1.0 |      |      | 1.210 | 1.389 | 1.148 |
|   |    |     | 1.2 |      |      | 1.204 | 1.381 | 1.147 |
|   |    |     | 1.4 |      |      | 1.193 | 1.377 | 1.154 |
| 4 | 1.2 | 0.2 | 0.2 | 0.16 | 4.28 | 1.244 | 1.437 | 1.149 |
|   |    |     | 0.4 |      |      | 1.232 | 1.411 | 1.145 |
|   |    |     | 0.6 |      |      | 1.207 | 1.395 | 1.155 |
|   |    |     | 0.8 |      |      | 1.189 | 1.377 | 1.158 |
|   |    |     | 1.0 |      |      | 1.177 | 1.361 | 1.156 |
|   |    |     | 1.2 |      |      | 1.170 | 1.348 | 1.152 |

From the table we can see that by trimming the stub parameters the operating frequency can be brought to a minimum value of 1.17 GHz ($f_1$) and 1.348 GHz ($f_2$). It can be inferred that this novel design is capable of providing an area reduction of 66% and 54 % for the TSMA configuration.
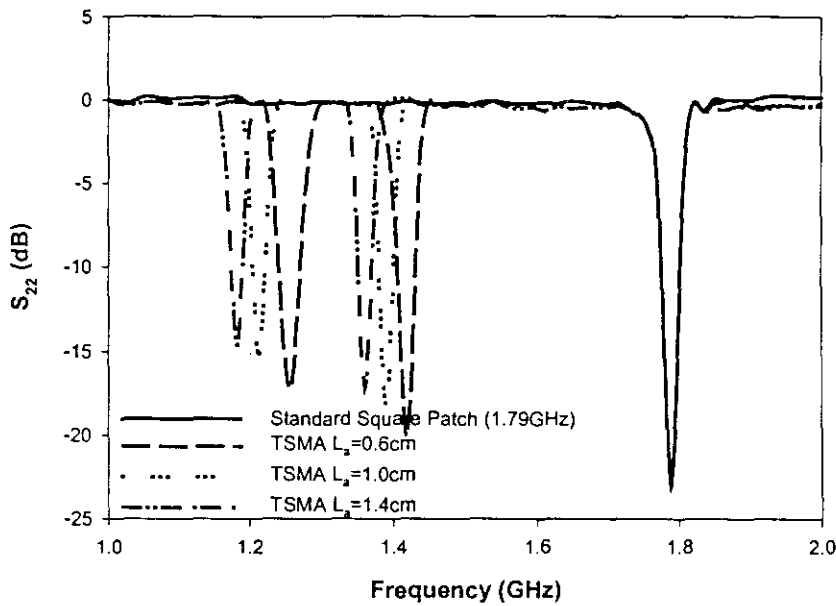
*Figure 4.20 illustrating decrease in resonance frequency with respect to stub arm length 'L$_a$' L$_p$=4.0 cm, L$_S$=1.0 cm, W$_a$=0.2 cm, ε$_r$=4.28*

The variation of resonant frequency with respect to stub arm length 'L$_a$' is plotted in figure 4.20, keeping the rest of the antenna dimensions fixed. From the figure it is seen that both the resonant frequencies decrease considerably with respect to increase in stub arm length (L$_a$). Two modes are excited with good impedance matching using a single probe feed. Due to the slot geometry in the patch, the excited patch surface current paths in both the TM$_{10}$ and TM$_{01}$ modes are increased, which effectively lowers the resonant frequencies of the two modes. This implies that, at a fixed dual frequency operation, the required antenna size can be reduced significantly. The frequency ratio is found to be unaffected by the change in 'L$_a$' alone. But, changing the various parameters of the slot and stub arm, the frequency ratio can be tuned effectively.

Figure 4.21 illustrates the variation in resonance frequency with respect to stub arm length 'L$_a$', for different central slot lengths 'L$_S$'. Here also, as in the case of DSM Antenna, it can be seen that the resonance frequency decreases with increase in stub length 'L$_a$'.

The frequency ratio seems to be unaffected by changing 'L$_a$' alone, but by changing the various parameters of slot and stubs the frequency ratio can be tuned effectively.

### 4.3.3.2 Impedance Bandwidth

The impedance bandwidth and ratio of the resonance frequencies are studied by varying the stub arm length (L$_a$). Table 4.12 depicts the impedance bandwidth and frequency ratio of the three-stub patch antenna.
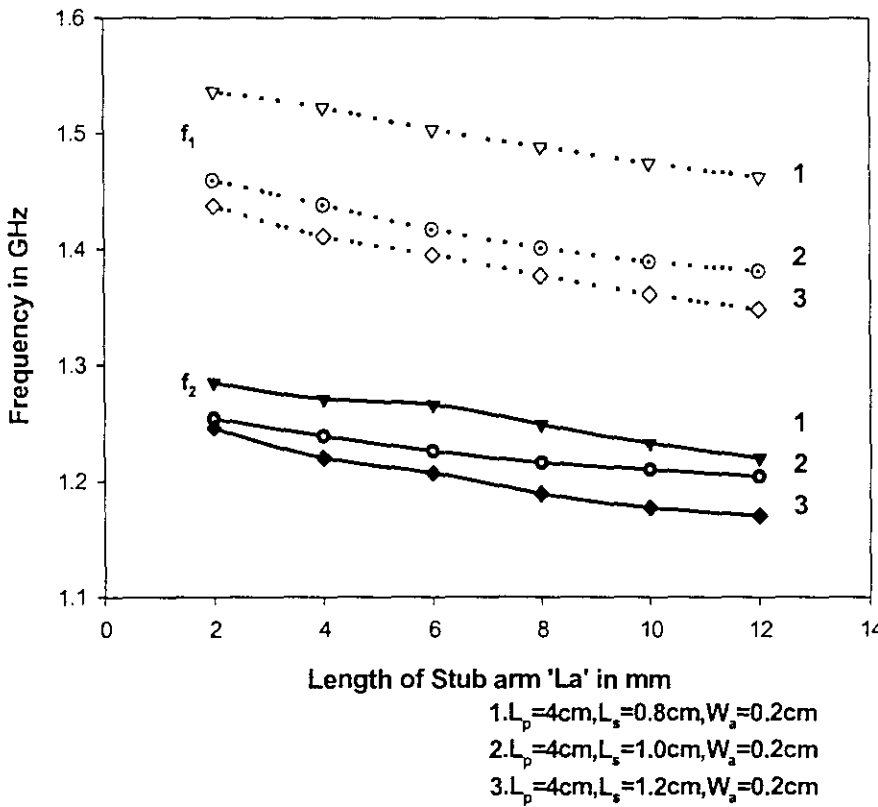


Figure 4.21 Experimental variation of TM$_{10}$ and TM$_{01}$ mode
frequencies for various values of L$_s$

*Table 4.12 Impedance Bandwidth variation and frequency Ratio with respect to 'L$_a$'*

| Tuning stub length (L$_a$) cm | 0.2 | 0.4 | 0.6 | 0.8 | 1.0 | 1.2 |
|---|---|---|---|---|---|---|
| $f_1$ (MHz) | 1254 | 1239 | 1226 | 1216 | 121 | 1204 |
| BW$_1$ (%) | 1.821 | 1.775 | 1.81 | 1.792 | 1.8 | 1.788 |
| $f_2$ (MHz) | 1459 | 1438 | 1417 | 1401 | 1389 | 1381 |
| BW$_2$ (%) | 2.14 | 2.13 | 2.045 | 2.162 | 2.14 | 2.095 |
| $f_2/f_1$ | 1.163 | 1.161 | 1.152 | 1.148 | 1.147 | 1.154 |

From the table it is clear that the TSM Antenna possess almost constant impedance bandwidth across the entire band of operation.

### 4.3.3.3 Transmission Characteristics

The two-port $S_{21}$ measurements are conducted and it confirms the dual polarisation characteristic of the slot antenna. The measured transmission characteristics are shown in figure 4.22. The curve shows the dual polarisation nature of the TSMA, which finds applications in communication systems in which a compact and low cost single antenna can be used for both Transmission (Tx) and Reception (Rx). The $S_{21}$ studies reveal that the cross-polarisation levels are better than -20 dB, which is also evident from the radiation patterns plotted in figure 4.22
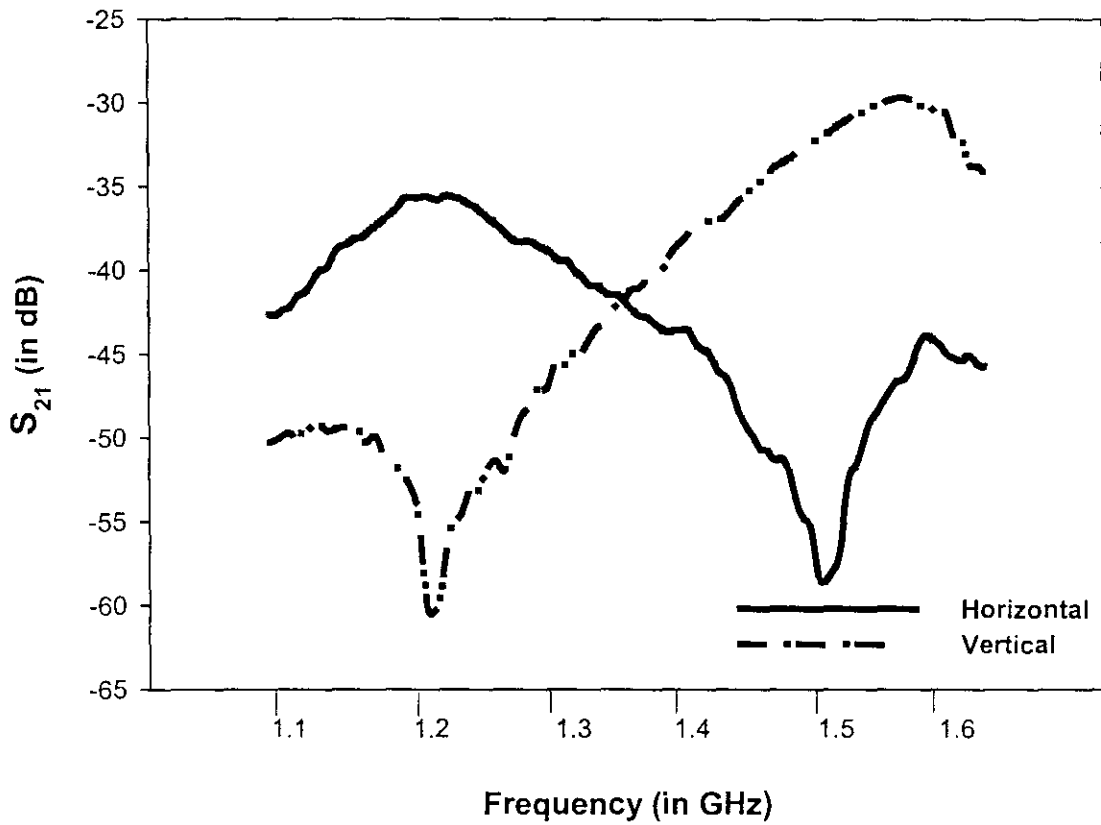
*Figure 4.22* The Dual-Polarisation Characteristics of the TSMA
$L_P=4$ cm, $L_S=1.0$ cm $L_a=1.2$ cm, $W_a=0.2$ cm

## 4.3.4 Radiation Pattern

The co-polar and cross-polar radiation patterns of this TSMA in the principal planes are taken at different frequency points in the operating frequency band of each antenna. The measured co-polar and cross-polar radiation pattern at the central frequencies of a typical TSMA configuration is shown in figure 4.23. Good cross-polar level of ~ -20 dB is observed with this design which helps up to minimize cross-talk in communication systems.

### H-Plane

### E-Plane



$f_1=1216MHz$

$f_2=1401MHz$
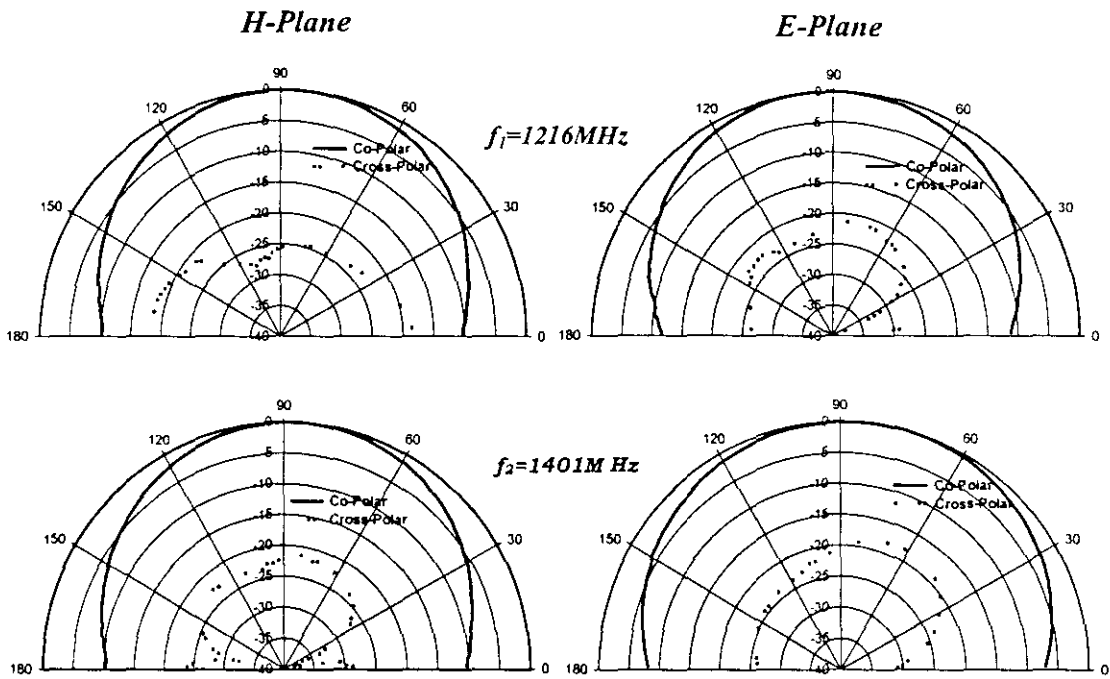
*Figure 4.22 Measured H-plane and E-plane Radiation Pattern of the slotted Square Antenna embedded with 3 stubs $L_p=4cm$, $Ls=1.0cm$ $La=0.8cm$, $Wa=0.2cm$*

## 4.3.5 Antenna Gain

Antenna gain measurements are conducted after calibrating the network analyser with a wideband horn. Rectangular microstrip antennas resonating at the same two frequencies of the TSMA are fabricated on the same substrate. The $S_{21}$ plot directly gives the relative gain of the antenna with respect to the standard rectangular patch antenna. The gain plots of two typical TSM antenna configurations are given in figure 4.24. It shows that there is only very slight reduction in gain for the TSMA compared to the equivalent rectangular patch antenna.
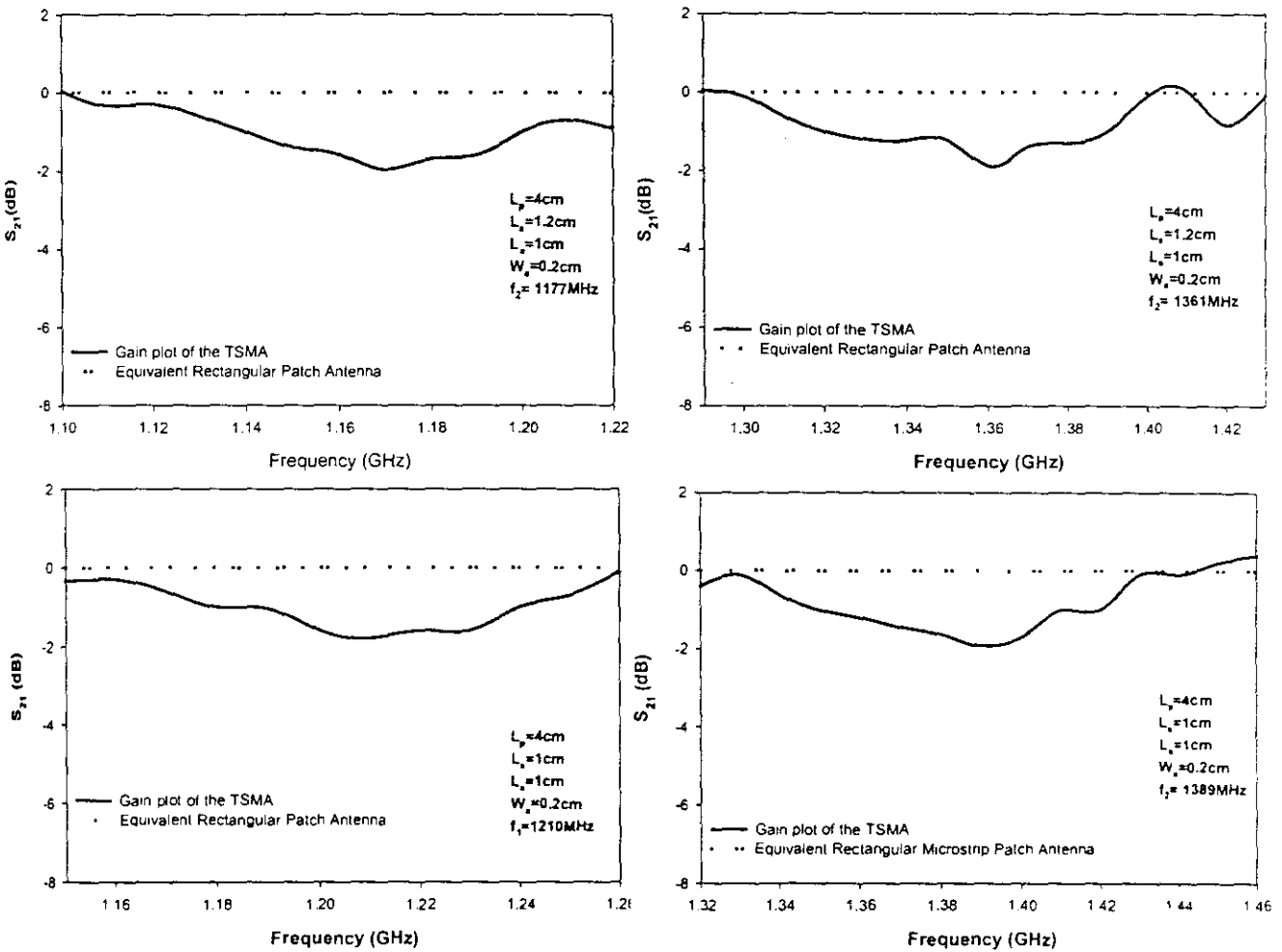
*Figure 4.24 S₂₁ plots for the Three Stub Microstrip Antenna(TSMA) having different configurations, with respect to standard rectangular microstrip patch antennas fabricated on the same substrate and resonating at the same frequency.*

Since the area of the patch has reduced considerably, by the introduction of the third stub, the antenna gain is reduced by ~2 dB, with respect to the equivalent rectangular patch Antenna operating at the same frequency and fabricated on the same substrate. This reduction in gain is negligible compared to the reduction in antenna patch area, which extends up to 64 % and 52 % for the TSMA geometry.

Table 4.14 illustrates the reduction in patch area for the two resonant modes. The resonance frequency and its percentage reduction, physical area of the Three-stub microstrip antenna ($A_{TSMA}$) and the equivalent rectangular patch antenna ($A_{eqnt.rect}$) are

given in table 4.14. The effective reduction in patch area is calculated using the

formula. $\dfrac{A_{eqnt.rect} - A_{TSMA}}{A_{eqnt.rect}}$

***Table 4.14*** *The resonant frequencies, % of area reduction, physical area of the TSMA ($A_{TSMA}$) and corresponding equivalent rectangular patch antenna ($A_{eqnt.rect}$) for various dimensions (h=0.16cm, $\varepsilon_r$=4.28)*

| $L_P$, $L_S$, $W_a$ (cm) | $L_a$ (cm) | Frequency $f_1$ (GHz) | Frequency $f_2$ (GHz) | Area of the eqnt. Rectangular Patch Patch ($A_{eqnt.rect}$) cm$^2$ | | Area of the TSMA ($A_{TSMA}$) cm$^2$ | Percentage Reduction in area $\dfrac{A_{eqnt.rect} - A_{TSMA}}{A_{eqnt.rect}}$ | |
|---|---|---|---|---|---|---|---|---|
| | | | | $A_{eqnt.Rect}$ ($f_1$) | $A_{eqnt.Rect}$ ($f_1$) | | $f_1$ | $f_2$ |
| | 0.2 | 1.285 | 1.536 | 38.6 | 26.95 | 16.0 | 58.5 | 40.6 |
| | 0.4 | 1.271 | 1.522 | 39.4 | 27.5 | 16.0 | 59 | 41.8 |
| | 0.6 | 1.266 | 1.503 | 39.7 | 28.2 | 16.0 | 59.7 | 43.3 |
| 4,0.8,0.2 | 0.8 | 1.254 | 1.488 | 40.5 | 28.7 | 16.0 | 60.5 | 44.3 |
| | 1.0 | 1.233 | 1.474 | 42 | 29.3 | 16.0 | 61.9 | 45.4 |
| | 1.2 | 1.220 | 1.462 | 42.8 | 29.8 | 16.0 | 62.6 | 46.3 |
| | 1.4 | 1.214 | 1.454 | 43.2 | 30 | 16.0 | 63 | 46.7 |
| | 0.2 | 1.254 | 1.459 | 40.5 | 29.9 | 16.0 | 60.5 | 46.5 |
| | 0.4 | 1.239 | 1.438 | 41.5 | 30.7 | 16.0 | 61.4 | 47.9 |
| | 0.6 | 1.226 | 1.417 | 42.4 | 31.7 | 16.0 | 62.3 | 49.5 |
| 4,1.0,0.2 | 0.8 | 1.216 | 1.401 | 43 | 32.4 | 16.0 | 62.8 | 50.6 |
| | 1.0 | 1.210 | 1.389 | 43.5 | 33 | 16.0 | 63.2 | 51.5 |
| | 1.2 | 1.204 | 1.381 | 44 | 33.4 | 16.0 | 63.6 | 52.1 |
| | 1.4 | 1.193 | 1.377 | 44.8 | 33.57 | 16.0 | 64.3 | 52.3 |
| | 0.2 | 1.244 | 1.437 | 41.17 | 30.8 | 16.0 | 61 | 48.1 |
| | 0.4 | 1.232 | 1.411 | 41.97 | 31.97 | 16.0 | 61.9 | 50 |
| 4, 1.2, 0.2 | 0.6 | 1.207 | 1.395 | 43.74 | 32.71 | 16.0 | 63.4 | 51 |
| | 0.8 | 1.189 | 1.377 | 45.1 | 33.6 | 16.0 | 64.5 | 52.4 |
| | 1.0 | 1.177 | 1.361 | 46 | 34.4 | 16.0 | 65 | 53.5 |
| | 1.2 | 1.170 | 1.348 | 46.56 | 35 | 16.0 | 65.6 | 54.3 |

From table it is seen that the metallic area of the three stub design decreases as the resonant frequency decreases. For operation at 1.21 GHz and 1.389 GHz we need to design two conventional rectangular patch antennas having overall area of 43.5 cm$^2$ and 33 cm$^2$ respectively. But, these two frequencies can be excited from a single planar radiating structure with a three stub loaded slot inserted in to a square patch having overall dimension of 16 cm$^2$ only.

Another property of this design that is evident from table 4.14 is the frequency tuning technique developed without increasing the overall size. Frequency tuning through reduction of resonant frequencies is achieved by adjusting the length 'L$_a$' and width 'W$_a$' of the tuning stubs. The stub arm is found to be the key element in controlling the antenna resonance and range of dual frequency operation. The patch and the central slot dimension affect the fundamental TM$_{01}$ mode, whereas the fundamental TM$_{10}$ mode is fully characterized by the tuning stub parameters.

## 4.4 FOUR STUB MICROSTRIP ANTENNA (FSMA)

An extended structure with two pair of stub arms is designed and analyzed. In this design the length of the second pair of stub arms is selected to be only half of the first pair. As in the earlier designs, the representative name given to this geometry is 'FSMA' (Four Stub Microstrip Antenna).

### 4.4.1. Antenna Geometry

The geometry of the FSM Antenna is illustrated in figure 4.25. The design parameters of the basic geometry and the square slot and the first two stub arms are exactly as studied in section 4.2 on DSM Antennas. The first pair of stub arms is identical with length '$L_{a1}$'. The second pair of stub arms is having length half of '$L_{a2}$' ($L_{a2}=0.5\ L_{a1}$).
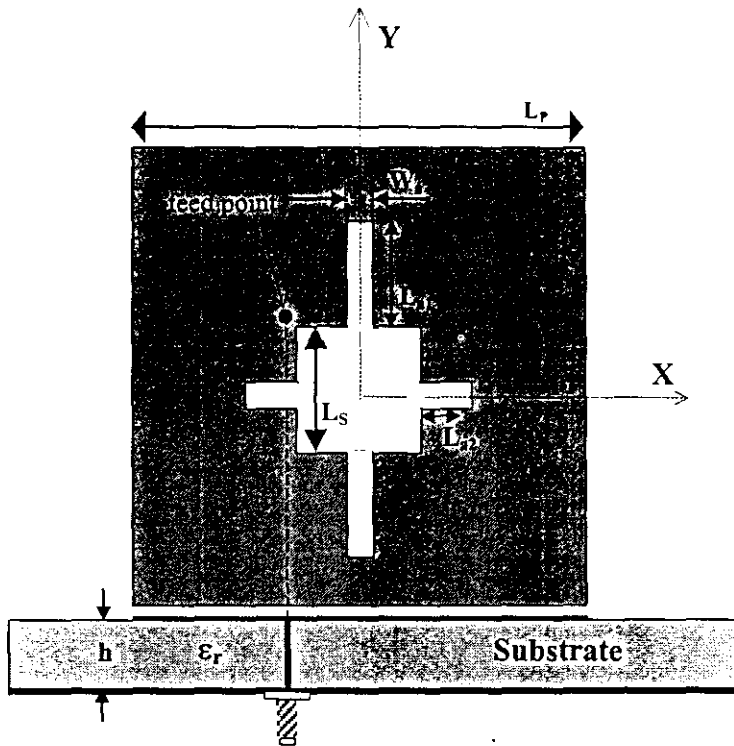


*Figure 4.25* Geometry of the Four Stub Microstrip Antenna
$Lp=4\ cm, Ls=1.2cm. L_{a1}=0.8cm, L_{a2}=0.4cm,\ W_a=0.15\ cm,\ \varepsilon_r=4.28,\ h=0.16\ cm$

106

## 4.4.2 Antenna Resonance Frequency Characteristics

The antenna geometry is simulated using IE3D. To study the resonance of FSM Antenna one port scattering parameters ($S_{11}$) are analyzed. A typical antenna design with specifications $L_P$, $L_S$, $L_{a1}$, $L_{a2}$ and $W_a$ having values 4 cm, 1.2 cm, 1.0 cm and 0.15 cm respectively is fabricated and tested using the network analyzer. The width of the two pair of stubs is kept uniform at 0.15 cm. (0.05cm less from the earlier designs to reduce deterioration in gain).

The $S_{11}$ plot of the design is given in figure 4.26. From this plot, it can be seen that the dual operating frequencies of the FSMA has been reduced to a 1.15 GHz and 1.38 GHz. As seen in the previous three sections, even though resonance frequencies has lowered considerably, the net area of the square patch remains exactly the same at 16cm$^2$, resulting in enhanced area reduction characteristics.
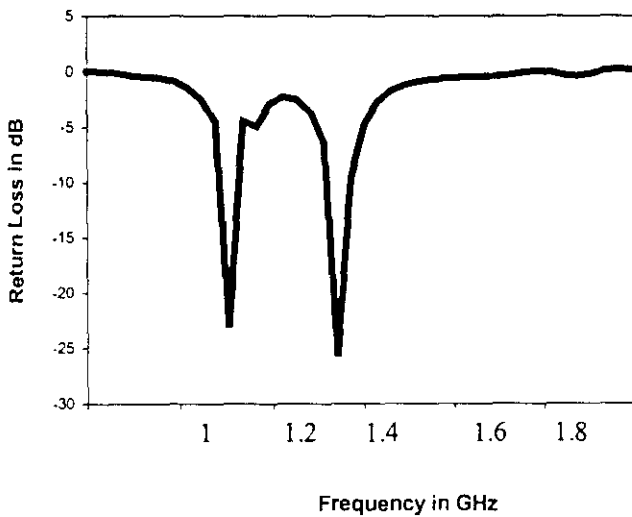
*Fig 4.26. Measured return loss ($S_{11}$) for the FSM dual frequency dual polarized with Lp=4cm,Ls=1.2cm, $L_{a1}$=0.8cm, $L_{a2}$=0.4cm, $W_a$=0.15 mm, $\varepsilon_r$=4.28 h=0.16cm*

The FSMA design, simulated using IE3D for an optimum design, is fabricated and experimentally tested. Table 4.15 illustrates the experimental return loss values.

The table illustrates the reduction in resonance frequencies with respect to increase in length of the pair of stub arms.

*Table 4.15 FSMA Resonance Frequencies for different 'L_{a1}', 'L_{a2}' and 'L_S'*

| $L_P, L_S, L_{a1}, L_{a2}, W_a$ (cm) | FSMA Dual Resonance Frequencies | |
|---|---|---|
| | $f_1$ (GHz) | $f_2$ (GHz) |
| 4,1.0, 0.8,0.4, 0.15 | 1.17 | 1.38 |
| 4,1.2, 1.0,0.5, 0.15 | 1.146 | 1.378 |

A comparison of the Single Stub Microstrip Antenna and the Four Stub Microstrip Antenna is illustrated in figure 4.27. The figure also shows the resonance frequency of a standard equivalent rectangular patch antenna. The SSMA geometry is providing an area reduction of 50 % and 36 % compared to the standard square patch. At the same time the four-stub patch antenna is capable of providing about 67% and 55 % of patch area reduction.
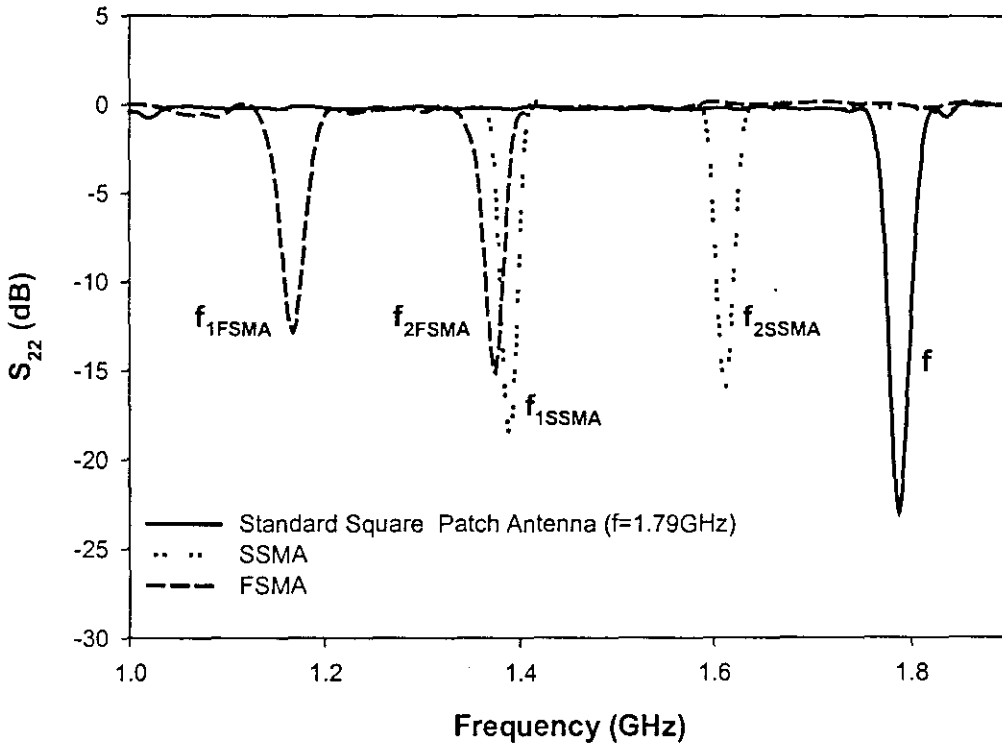


*Figure 4.27 Graph showing the comparison of the resonance frequencies of the FSMA, SSMA and the Standard square Patch Antenna*

### 4.4.3 Radiation Pattern

The radiation pattern of the FSMA has been measured using the experimental set-up described in the section 3.4 of the methodology chapter. Figure 4.28 illustrates the radiation pattern of the two resonance frequencies of the Four Stub Microstrip Antenna.
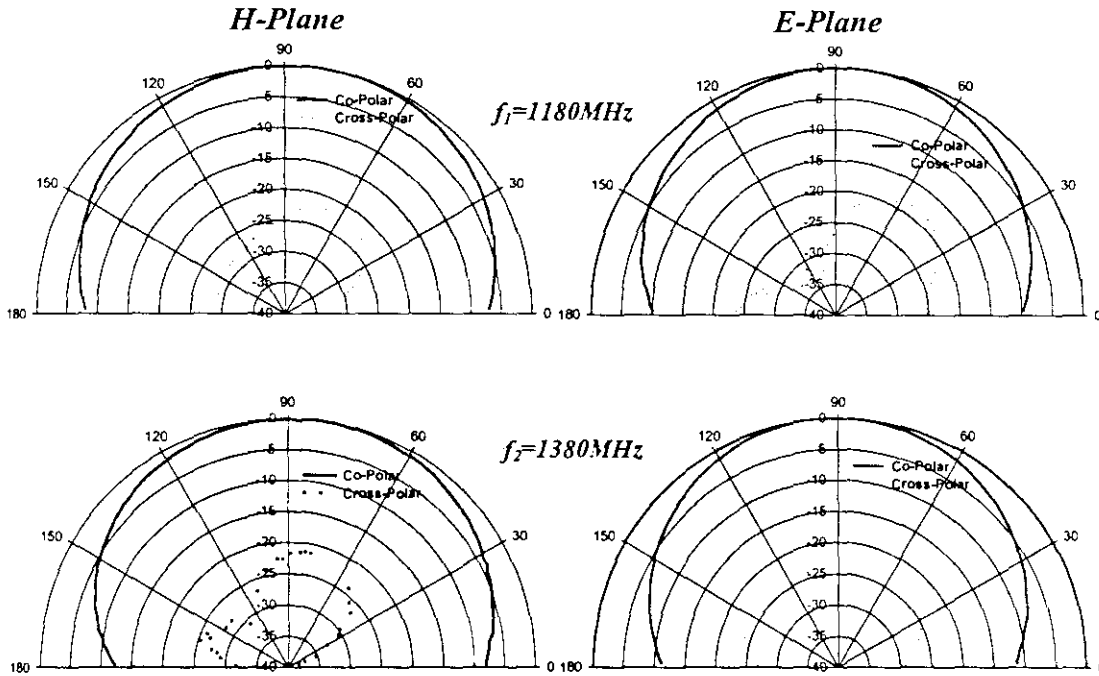


**Figure 4.28** *Measured H-plane and E-plane Radiation Pattern of the Four Stub Microstrip Antenna embedded $L_p=4cm$, $L_s=1.2cm$ $L_{a2}=1.0cm$, $L_{a2}=0.5cm$, $W_a=0.15cm$*

In FSMA since the metallic area has further reduced considerably the gain of the patch has deteriorated below the limits characterized for antenna radiation. Hence, the design has certain practical limitations as far as its application aspects are concerned.

# CAPACITOR LOADING TECHNIQUE FOR SLOTTED PATCH ANTENNAS FOR FREQUENCY TRIMMING

The trend of any maturing electrical technology is towards smaller size, lighter weight, lower cost and increased complexity. Microwave technology has been moving in such a direction during the last couple of decades with the development of Microwave Integrated Circuits and Antennas. This technology serves to replace bulky and expensive coaxial components with small and inexpensive planar components. Microwave Integrated Circuitry can incorporate transmission lines, discrete resistors, capacitors and inductors.

Similarly lumped elements for microstrip antennas can also be realized in the length 'l' of the component under the condition that 'l' < $\lambda/10$. Capacitors can be implemented in a patch antenna in many ways. A short transmission line stub can provide a shunt capacitance in the range of 0 to 0.1pF. A single gap or interdigital set of gaps in a transmission line can provide a series capacitance up to about 0.5pF. Greater values (up to about 25pF) can be obtained by using a metal-insulator-metal sandwich, either in monolithic or in chip form.

High performance surface mountable capacitor (C 06 0603) is used for the measurements reported in this section.

Recently, in literature one can find a number of publications reporting the characteristics of probe fed slot-loaded short-circuited patch antennas and antennas loaded with reactive components like capacitors [163,168]. In order to meet the miniaturization of the mobile communication equipments, the design of such dual frequency antennas with reduced area become significant loaded with reactive components that enhance the overall system efficiency.

## 4.5 CAPACITOR LOADED SINGLE STUB MICROSTRIP ANTENNA (CSSMA)

As a next step in this study, a capacitor mounted frequency-tuning method is implemented and investigated for controlling the operating frequency and cross-polar

110

level of the proposed Single Stub Microstrip Antenna. The frequency control is achieved by placing microwave chip capacitors at appropriate locations within the antenna geometry. The antenna geometry nomenclature adopted here is an extension the first geometry, and it is **CSSMA** -Capacitor Mounted Single Stub Microstrip Antenna'.

### 4.5.1 Antenna Geometry

The geometry of the proposed CSSM Antenna is shown in figure 4.29. The capacitor is seen mounted at the bottom of the tuning stub arm of the central slot geometry. With this technique, the required antenna size is reduced significantly for operation at a fixed frequency by maintaining a simple geometry, avoiding the series insertion of a number of tuning stubs, which makes the geometry more complicated. To demonstrate the capability of such a capacitor loading technique, two related designs, for a slotted square antenna are studied. Two different mechanisms, a probe feed and a microstrip line feed are implemented and analyzed.

### 4.5.2 Resonance Characteristics

The dual frequency design consists of a square microstrip antenna coaxially fed along the diagonal with a chip capacitor mounted at the bottom of the single tuning stub. This design provides enhanced patch area reduction and with good cross-polarization levels, by incorporating a capacitor in to the simple geometry described in section 4.1. with a single tuning stub ideal for satellite communications systems, without compromising antenna gain considerably. This modified antenna design can be used as a compact antenna system where limited size is a major requirement. With the studies done on the SSM and DSM antennas, it has been experimentally demonstrated that the tuning stubs are having an important role in effectively trimming the resonant frequency of the proposed microstrip antenna. Due to the frequency tuning ability of the stub, it is expected that with a proper length, the resonant mode in the direction parallel to the stub can have a lower resonant frequency than that in the direction perpendicular to the stub orientation. A number of publications reporting the characteristics of probe-fed slot-loaded short-circuited microstrip antennas and antennas loaded with chip capacitors are available [163,168]. Thus, by mounting a chip capacitor of low capacitance, the overall antenna size can be reduced significantly for operation at a fixed frequency, with

negligible drop in gain. It is also seen that the antenna cross-polarization level can be considerably enhanced which finds wide applications in avoiding cross talk in communication systems. The capacitor-loaded antenna is tested using the HP 8510C vector Network Analyzer. It is observed that the first resonance frequency falls drastically to 1.19 GHz ($f_{1c}$). It is also noted that, by mounting the capacitor, only the first resonant frequency is affected, and the second resonant frequency ($f_{2c}$) remains almost invariant. An equivalent circuit taken along the diagonal of the square slot antenna is the parallel resonant circuit; when the loading capacitor is connected to the equivalent circuit, the resonant frequency decreases.

Both the resonant frequencies are well below the resonant frequency of the standard square patch. The optimum feed position remains practically the same even when capacitor is loaded and the stub-length is varied. The radiation patterns are plotted for various capacitor values and it is seen that at both the resonance frequencies radiation patterns are broad, having orthogonal polarizations and a cross-polar level better than -30 dB.
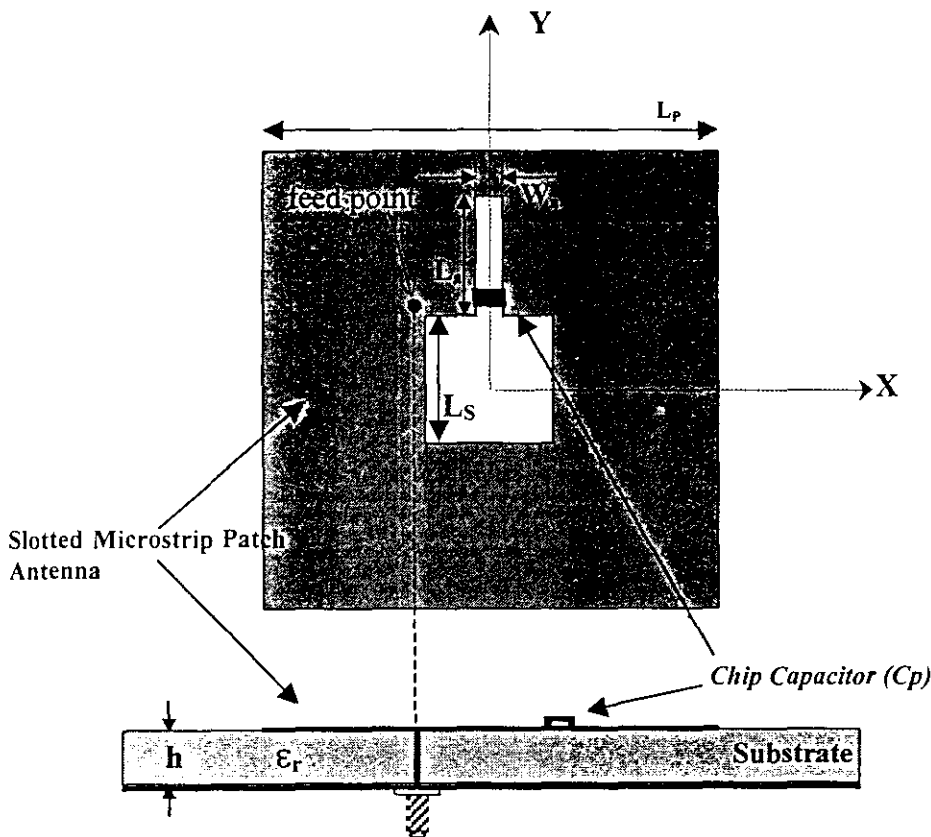


*Figure 4.29  Capacitor loaded Single stub Microstrip (CSS) Antenna*
*L$_P$=4cm,  L$_S$=1.2 cm L$_a$=1.2 cm,  W$_a$=0.2cm,  C$_p$=5pF*

## 4.5.2.1 Return Loss

In the discussion of the SSMA, the antenna characteristics have been optimised by systematically varying its stub parameters, length 'L$_a$' and width 'W$_a$'. In such an optimised SSM Antenna design with dimensions L$_P$=4cm, L$_S$=1.2 cm, L$_a$=1.2 cm and W$_a$=0.2 cm, a capacitor is loaded and the antenna return loss is measured, which is given in figure 4.30.
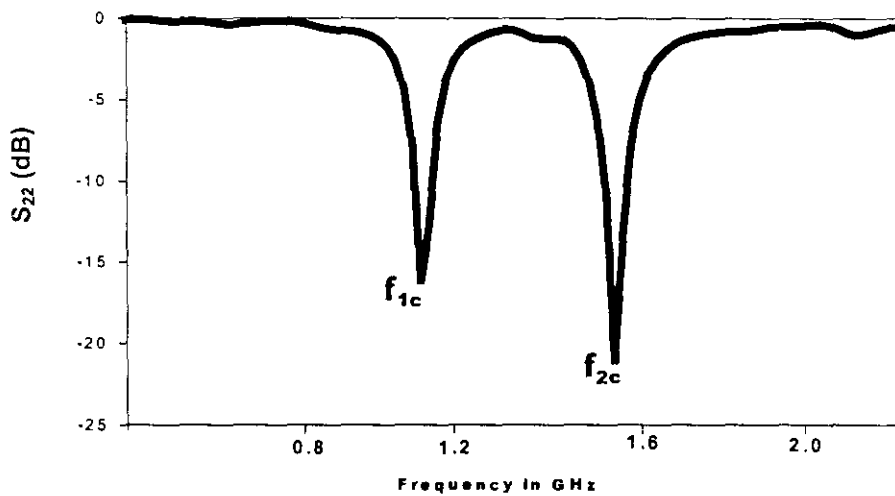


*Figure 4.30 Return loss plot of the Capacitor Single Stub Microstrip (CSSM) Antenna*

The return loss characteristics reveals that as a result of capacitor loading upon the SSM Antenna, the resonant frequency reduces to 1.19 GHz and 1.59 GHz. This modified design provides an area reduction of 64 % and 36 % respectively for the two resonant modes compared to an equivalent standard rectangular patch antenna operating at the two frequencies. The analysis is repeated by mounting capacitors of various values and it be is found that the capacitor loading can be used to extend the frequency tuning technique further to a low frequency band. The analysis of the frequency trimming technique by mounting various capacitors presented in the following section.

## 4.5.3 Radiation Pattern

The radiation pattern of the capacitor loaded antenna has been studied in detail. The pattern measurement set-up and the method adopted is the same as explained in the earlier antenna designs.

Figure 4.31 shows the radiation pattern at the two frequencies of the Capacitor mounted Single Stub Microstip Antenna (CSSMA). The radiation pattern of the CSSMA is compared with the radiation pattern of the single stub antenna without capacitor plotted in section 4.1.4. The comparison reveals that there is a considerable increase in cross-polar level and it can be directly understood as a direct outcome of the capacitor mounting.

*H-Plane*        *E-Plane*

$f_1=1133\ MHz$

$f_2=1571\ MHz$
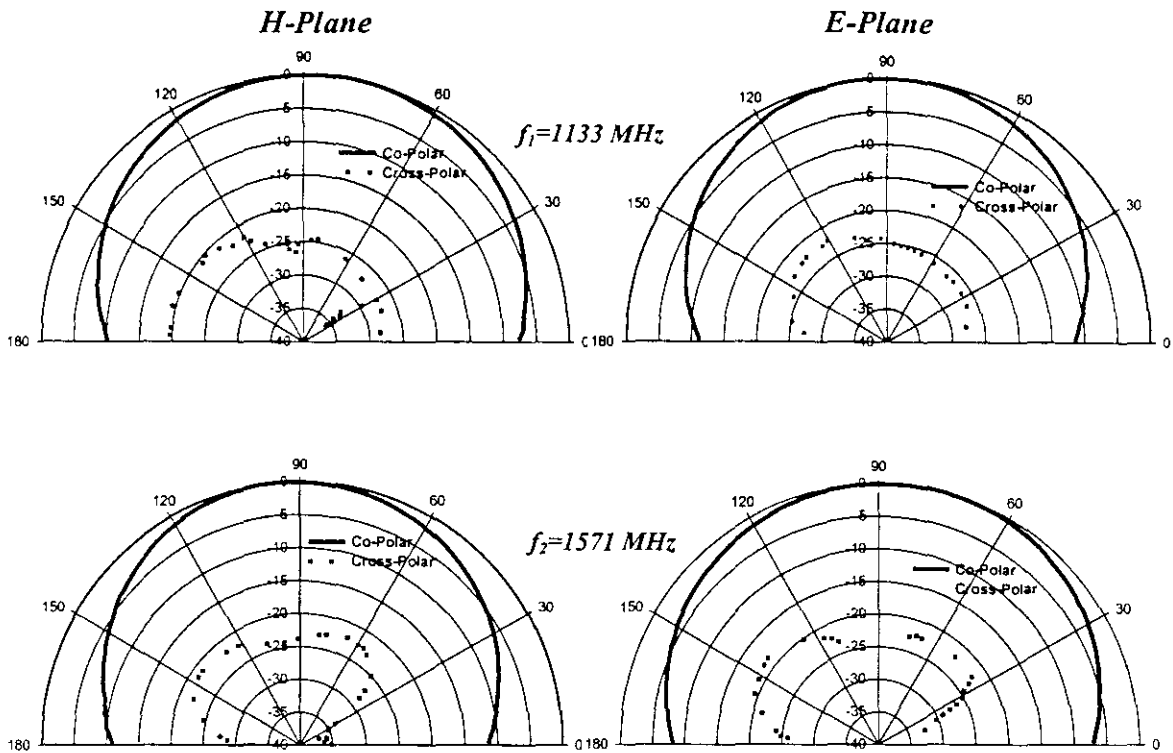
*Figure 4.31 Radiation Pattern of the CSSMA*
$L_P=4\ cm, L_S=1.2\ cm,\ L_a=1.2\ cm,\ W_a=0.2cm, Cp=10pF$

A frequency varying patch antenna with a capacitor loading technique is developed. Here, the operating frequency can be varied over a broad range by either varying the stub arm parameters as described in section 4.1 or by assigning capacitors of

### 4.5.4 Antenna Gain

Gain transfer method has been implemented for measuring the relative gain of the proposed CSSMA. Standard rectangular microstrip antennas resonating at the same frequency as that of the selected antennas have been fabricated on the same substrate. By using a wideband-ridged horn as the transmitter, an $S_{21}$ THRU calibration is done using the rectangular patch antennas as the receiver. The CSSMA then replaces the rectangular patch antenna and the transmission characteristic is measured. The measured $S_{21}$ will give the relative gain of the new antenna design with respect to the standard rectangular patch antenna. The relative gain of the antenna for the two resonance frequencies is plotted in figure 4.32.
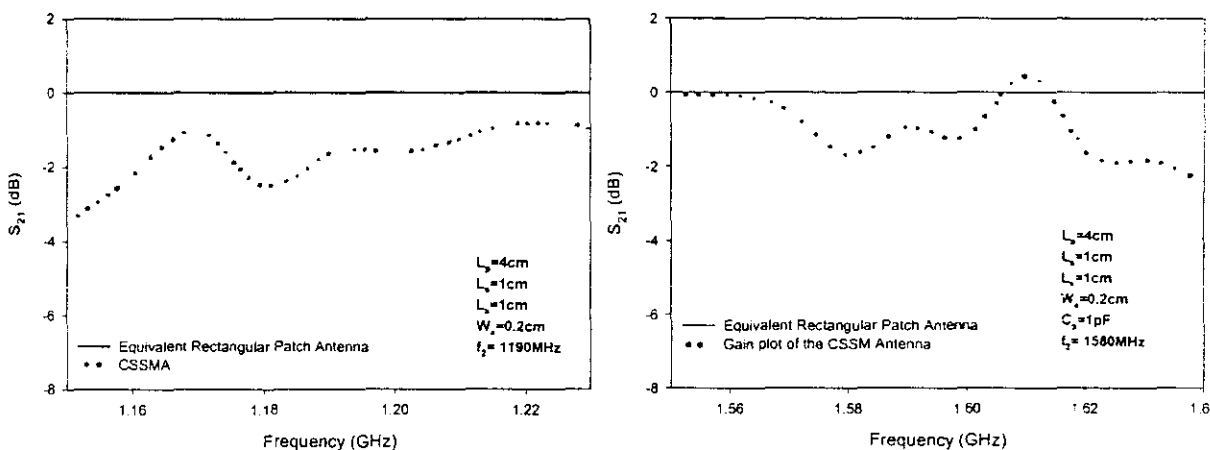


**Figure 4.32**    *$S_{21}$ plots for a typical Capacitor mounted single stub (CSSM) antenna configuration for different central slot and stub arm lengths with respect to standard rectangular microstrip patch antennas fabricated on the same substrate and resonating at the same frequency*

From the gain plots of the SSMA and CSSMA we can observe that the radiating power is not significantly reduced by the capacitor mounting.

The polarisation characteristic of the antenna is analysed in detail. The typical polarisation curve of the antenna is plotted in figure 4.33. It is evident from the figure that the capacitor mounting has not affected the orthogonal polarisation nature of the antenna.
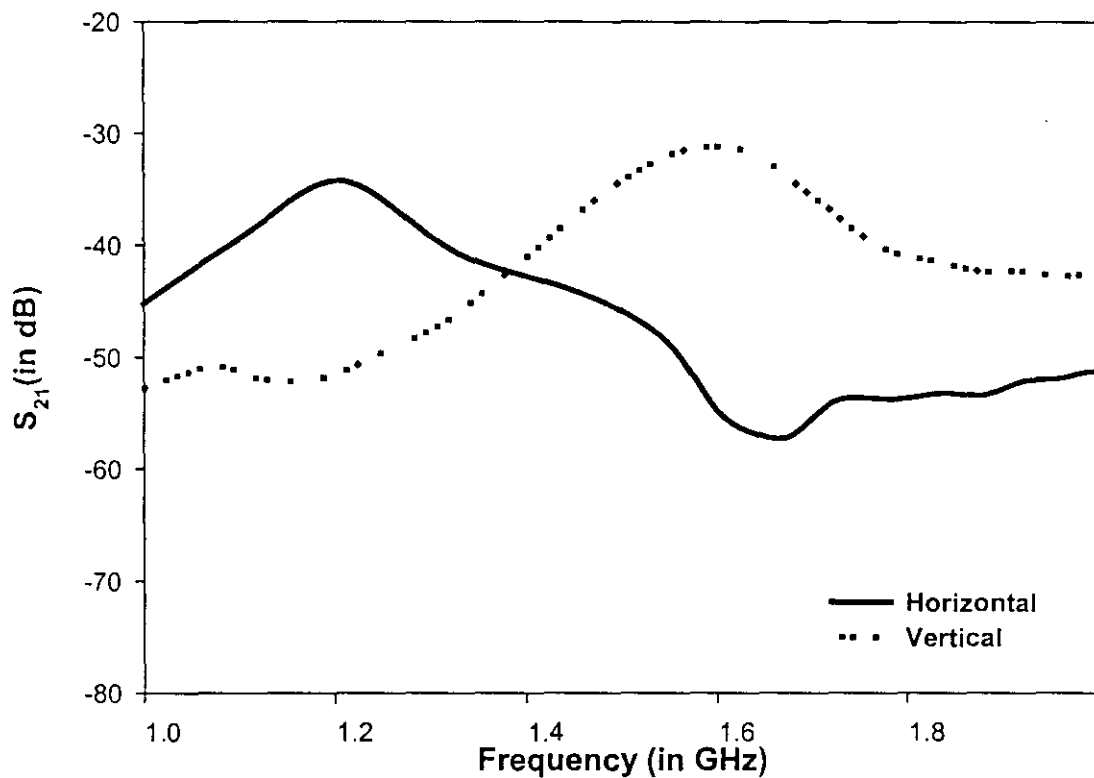


*Figure 4.33* $S_{21}$ *Orthogonal Polarisation of the CSSMA*
$L_P=4$ *cm,* $L_S=1.2$ *cm,* $L_a=1$ *cm,* $W_a=0.2$ *cm,* $Cp=2.2$ *pF*

## 4.6 CAPACITOR LOADED DUAL STUB MICROSTRIP ANTENNA (CDSMA)

Once the effect of capacitor loading on the SSM Antenna is established studies are extended to analyse the effect of capacitor loading on a dual stub antenna and its various characteristics. In the CDSMA also it was observed that the antenna is exhibiting dual frequency dual polarized operation and enhanced patch area reduction characteristics.

The geometry of the CDSMA is illustrated in figure 4.34. The design and feed characteristics are exactly as in the case of CSSMA.
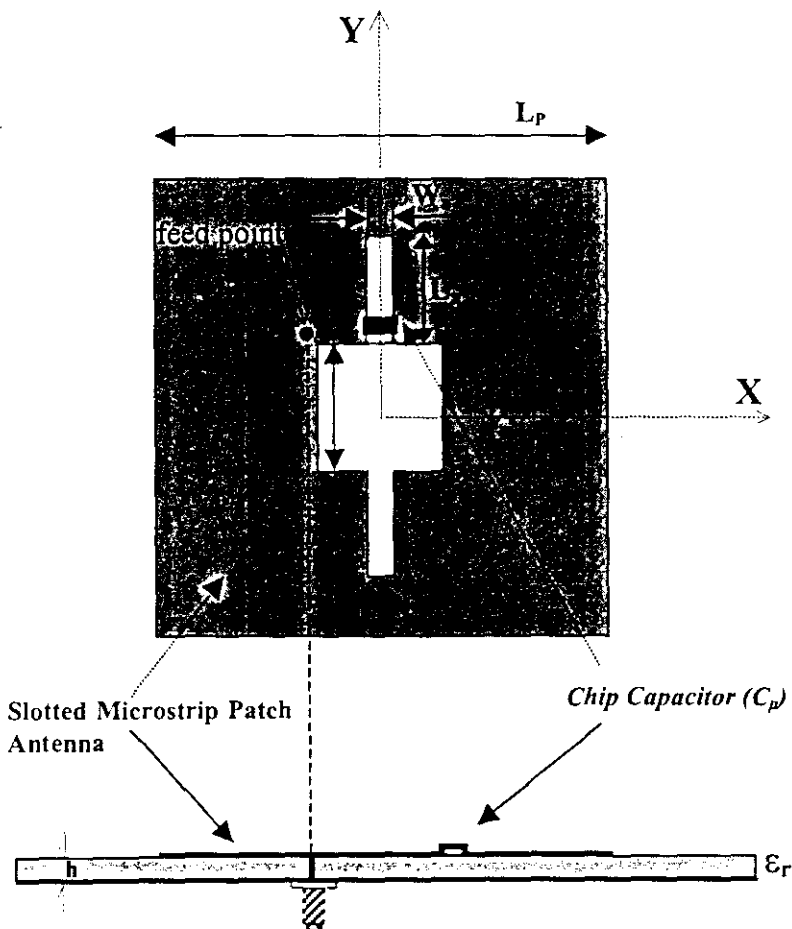
*Figure 4.34 Geometry of the Capacitor Mounted Dual Stub Microstrip Antenna*
$L_P=4cm, L_S=1.2cm, L_a=1.2cm, W_a=0.2cm, C_P= 10pF$

## 4.6.1. Antenna Resonant Modes and Return Loss

The resonant modes of the DSM Antenna have been already studied in detail as well as effect of variation in antenna dimensions on its performance.

In the discussion of the DSM Antenna we have optimised the stub parameters by systematically varying its length '$L_a$' and width '$W_a$'. In such an optimised DSM antenna prototype with parameters $L_P$=4 cm, $L_S$=1.2 cm, $L_a$=1.2 cm and $W_a$=0.2 cm, a capacitor is loaded and the antenna return loss measured.

The capacitor is mounted towards the base of the first arm and the variation of return loss characteristics is studied. The return loss characteristic of the CDSMA is plotted in figure 4.35, which gives a comparison in reduction in resonance frequency with respect to a standard square patch and the DSM Antenna. From the figure we can see that the capacitor mounting affects the lower resonance frequency ($TM_{10}$) of the DSMA and the second resonance ($TM_{01}$) is only slightly affected.
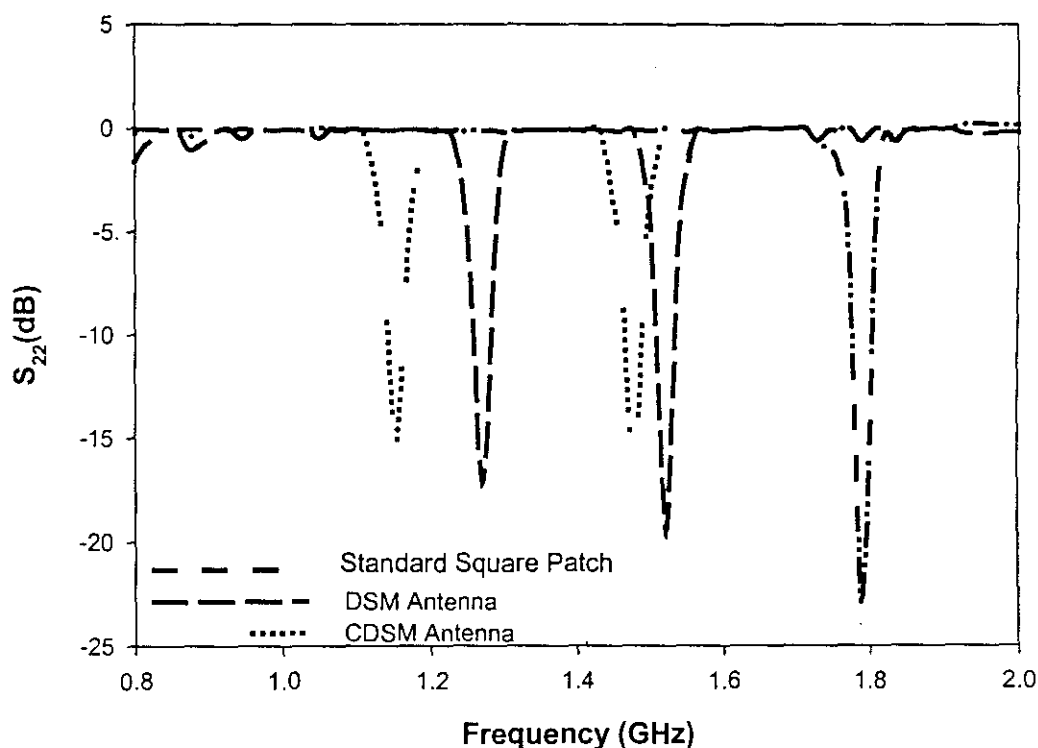


*Figure 4.35 Return Loss Characteristics of the CDSM Patch Antenna*
$L_p$=4cm, $L_s$=1.2cm, $L_a$=1cm, $W_a$=0.2cm, $Cp$=4.7pF

The return loss characteristics reveals that the capacitor loading on DSM Antenna causes the antenna resonant frequency to fall to 1.148 GHz and 1.489 GHz. This modified design provides an area reduction of 67 % and 44 % for the two resonant modes compared to a standard rectangular patch antenna operating at the two frequencies.

Table 4.17 depicts the variation in resonant frequencies with respect to different capacitor values. From the table it can be seen that the when the value of the capacitor is changed from 1 to 22 pF the $TM_{10}$ mode frequency moves from 1.163 to 1.091 GHz.

*Table. 4.17 ilustrates the variration in resonance frequency for different capacitor values and the %area reduction ($A_{CDSMA}=16$ cm$^2$)*

| $L_p$, $L_s$, $L_a$,$W_a$ (cm) | Resonance Frequency without capacitor loading (GHz) | | $C_p$ (pF) | Resonance Frequency with capacitor Loading (GHz) | | Area of the equivalent Rectangular Patch $A_{eqnt.rect}$ (cm$^2$) | | Percentage Reduction in Patch Area $\dfrac{A_{eqnt.rect} - A_{CDMSA}}{A_{eqnt.rect}}$ % | |
|---|---|---|---|---|---|---|---|---|---|
| | $f_1$ | $f_2$ | | $F_1$ | $f_2$ | $f_1$ | $f_2$ | $f_1$ | $f_2$ |
| 4,1.2, 1.0, 0.2 | 1.274 | 1.512 | 1 | 1.163 | 1.505 | 47.12 | 28 | 66 | 42.8 |
| | | | 4.7 | 1.148 | 1.488 | 48.36 | 28.74 | 67 | 44 |
| | | | 10 | 1.113 | 1.477 | 51.5 | 29.2 | 68.9 | 45.2 |
| | | | 22 | 1.091 | 1.472 | 53.5 | 29.4 | 70 | 45.6 |

## 4.6.2 Transmission Characteristics

The Polarisation of the antenna was also studied using the $S_{21}$ method by with a standard wide band horn as the transmitter and the test (CDSMA) antenna as the receiver. The $S_{21}$ plot revealing the polarisation of the antenna is shown in figure 4.36.
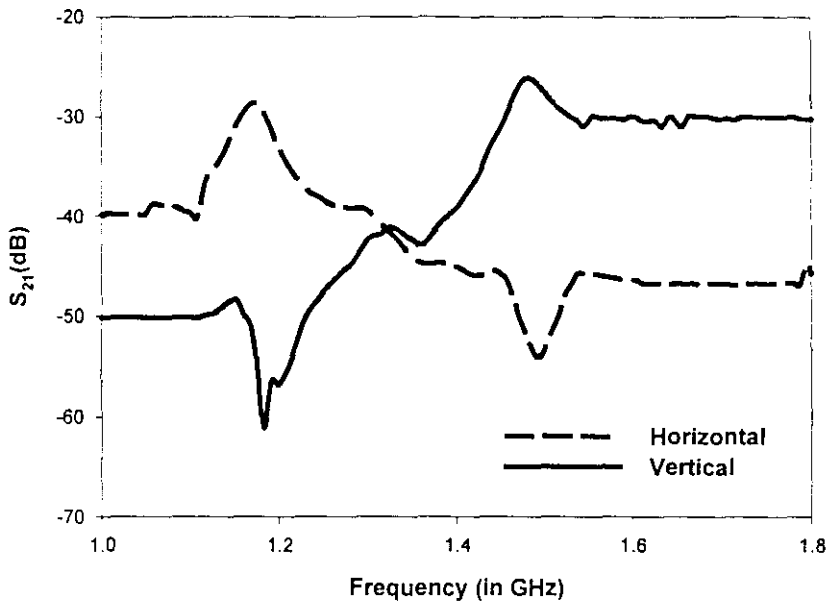
*Figure 4.36* $S_{21}$ *plot showing the orthogonal Polarisation of the CDSMA*
$L_p=4cm$, $L_s=1.2cm$, $L_p=1cm$, $W_a=0.2cm$, $Cp=4.7\,pF$

### 4.6.3 Radiation Pattern

The radiation pattern of the CDSM Antenna is measured using the experimental set-up described in Chapter III, at different frequency points in the operating frequency band of CDSMA. A typical capacitor mounted (Cp=4.7 pF) patch antenna with dimensions $L_P=4cm$, $L_S=1.2cm$, $L_a=1cm$ and $W_a=0.2cm$ is measured and it is plotted in figure 4.37.
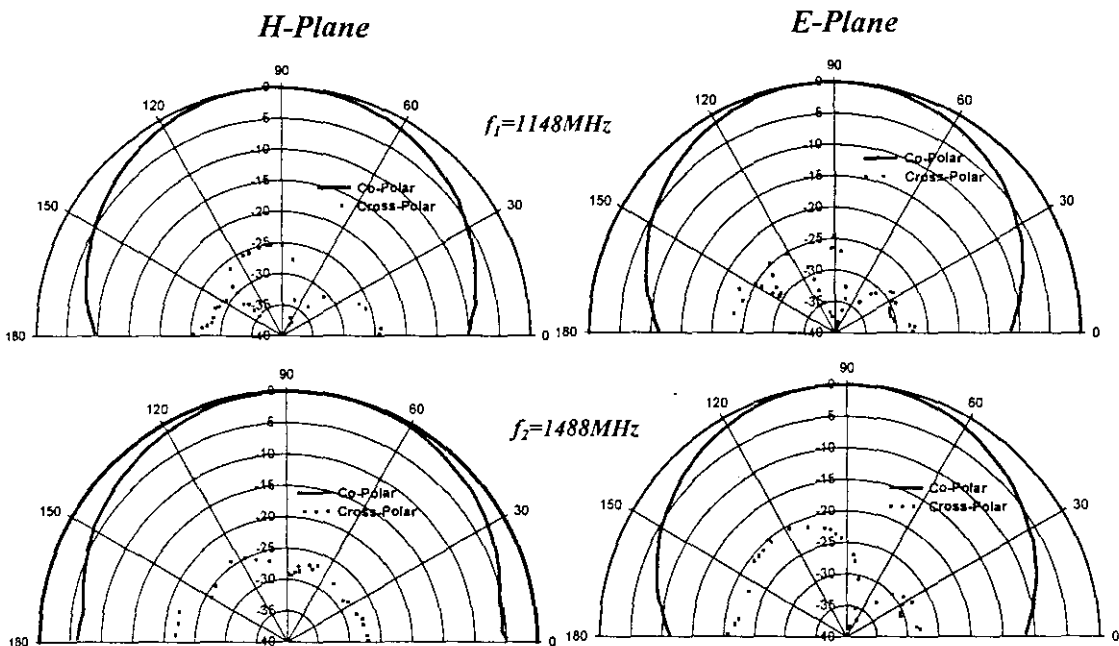


*Figure 4.37 Radiation Pattern of the CDSM Patch Antenna*
$L_p=4cm$, $L_s=1.2cm$, $L_p=1cm$, $W_a=0.2cm$, $Cp=4.7\,pF$

121

### 4.6.4 Gain

The relative gain of the Capacitor loaded Dual Stub antenna can be measured. The typical gain plots of a standard TSA has been measured and is plotted in figure 4.38.



*Figure 4.38 $S_{21}$ plots for a typical Capacitor Mounted Dual Stub Microstrip (CDSM) antenna configuration with respect to standard rectangular microstrip patch antenna fabricated on the same substrate and resonating at the same frequency*

## 4.7 CAPACITOR MOUNTED THREE STUB MICROSTRIP ANTENNA (CTSMA)

A modified design with a capacitor introduced into the TSMA is designed and studied. Similar to the earlier designs, CTSMA also provides a dual frequency, dual polarised operation and extended area reduction characteristics. The antenna return loss, radiation characteristics and gain are also analyzed.

### 4.7.1 Antenna Geometry

Figure 4.39 shows the geometry of the proposed CTMSA. The substrate has a relative permittivity of $\varepsilon_r$ and height h. The slot geometry centered with respect to the square patch, having three tuning arms with a capacitor (1 pF) loaded at the base of the first arm, which helps to maximize the excitation of dominant mode of the antenna.
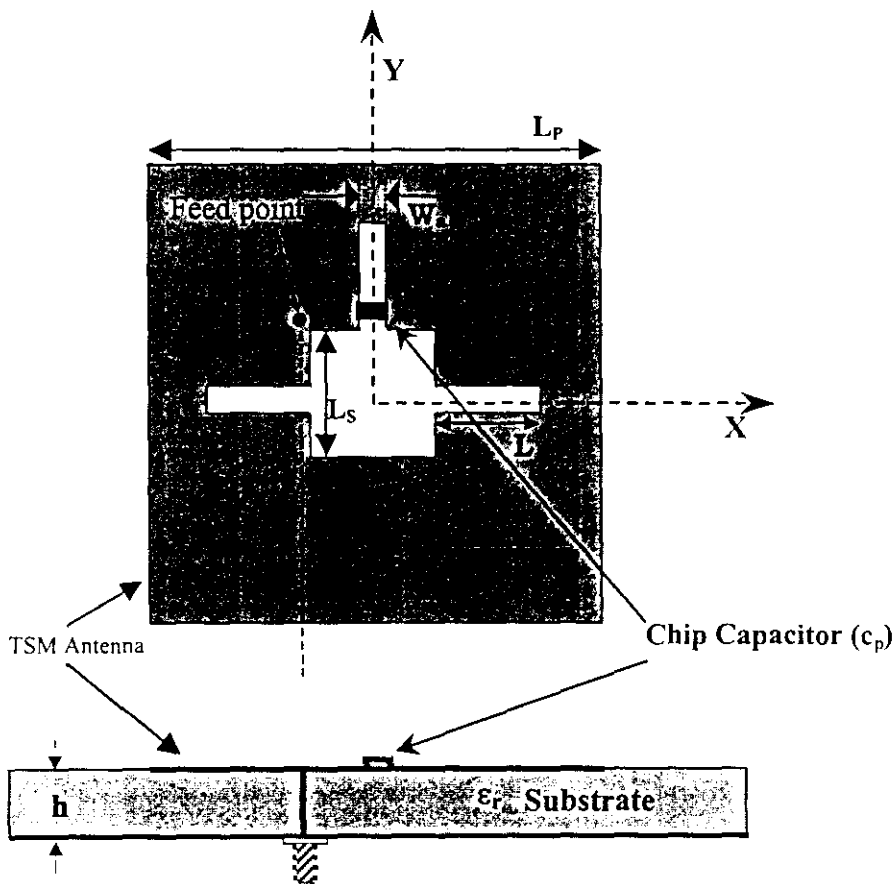


*Figure 4.39 Geometry of TSMA for Dual Frequency Operation*
*$L_P=4cm, L_S=1.2cm, L_a=1.2cm, W_a=0.2cm, Cp=10pF$*

## 4.7.2 Antenna Return Loss Characteristics

The antenna one-port scattering parameters are analyzed. Figure 4.40 illustrates the dual frequency operation of the CTSMA. In section 4.3 we have optimized the antenna parameters and characteristics of Three stub Microstrip antenna (TSMA). The return loss plot of the unslotted 4x 4cm$^2$ square patch is also shown.
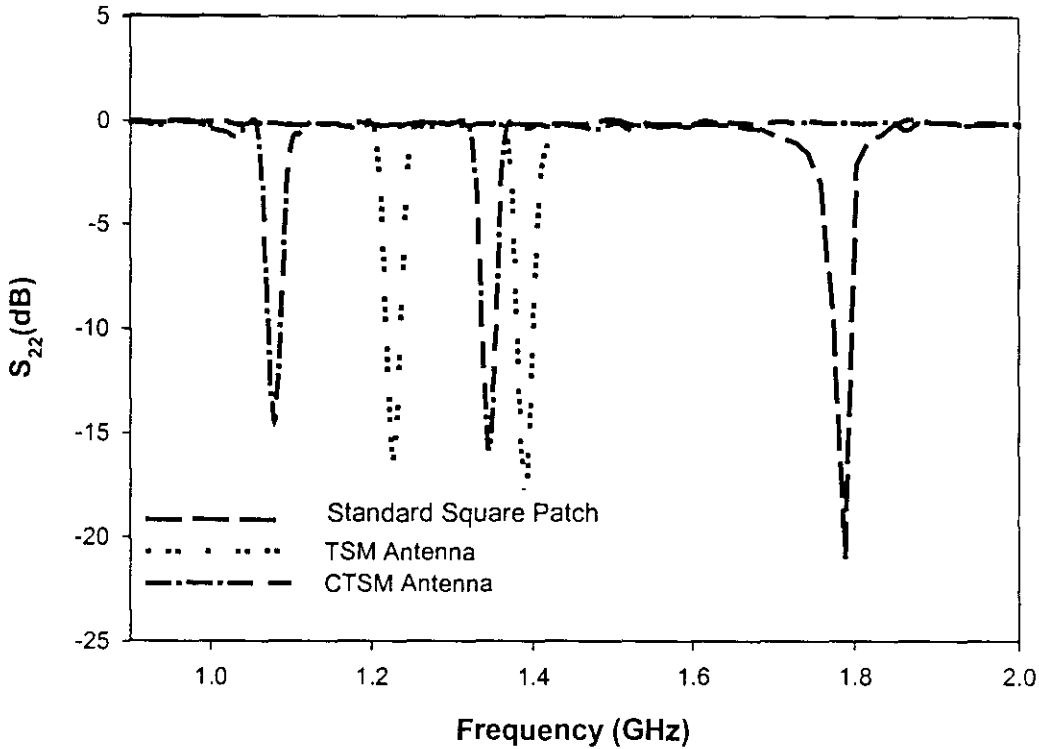


*Figure 4.40 Return Loss Characteristics of the CTSM Patch Antenna*
$L_p$=4cm, $L_s$=1.2cm, $L_a$=1cm, $W_a$=0.2cm, Cp=4.7pF

The return loss characteristics reveals that the capacitor loading on TSM Antenna causes the antenna resonant frequency to fall to 1.085 GHz and 1.366 GHz. This modified design provides an area reduction of 72% and 53 % for the two resonant modes compared to an equivalent rectangular patch antenna operating at the two frequencies. The capacitor is mounted towards the base of the first arm and the variation of return loss characteristics is analysed. The studies are repeated by varying the capacitor values. The plot shown above gives a comparison in reduction in resonance frequency with respect to a standard rectangular patch and a typical TSM Antenna.

From the figure we can see that the capacitor mounting affects the lower resonance frequency ($f_1$) of the TSMA and the second frequency ($f_2$) is only slightly affected.

When the value of the capacitor is varied from 1 pF to 20 pF, the corresponding reduction in frequency is illustrated in Table 4.19. From the table it can be seen that the when the value of the capacitor is changed from 1 to 22 pF the $TM_{10}$ mode frequency moves from 1.163 to 1.091 GHz with a reduction of 72 MHz.

*Table. 4.18 ilustrates the variration in resonance frequency of a CTSM Antenna for different capacitor values*

| $L_P, L_S, L_a, W_a$ (cm) | Resonance Frequency without capacitor loading | | $C_p$ (pF) | Resonance Frequency with capacitor Loading (GHz) | |
|---|---|---|---|---|---|
| | $f_1$ (GHz) | $f_2$ (GHz) | | $f_1$ (GHz) | $f_2$ (GHz) |
| 4,1.2,1.0, 0.2 | 1.21 | 1.389 | 1 | 1.114 | 1.380 |
| | | | 4.7 | 1.089 | 1.373 |
| | | | 10 | 1.065 | 1.366 |
| | | | 22 | 1.051 | 1.359 |

### 4.7.3 Radiation Pattern

The measured H- and E-plane radiation patterns are shown in figure 4.50.The antenna gain on the axis is 3.59dBi for the TSM antenna at the operating frequency of 1.21 GHz and 3.17dBi for a capacitor mounted TSM antenna at a resonating frequency of 1.089GHz. This shows that there is only a slight reduction in antenna gain with the loading capacitor method. A typical capacitor mounted (Cp=4.7 pF) patch antenna with dimensions $L_P$=4cm, $L_S$=1.2cm, $L_a$=1cm and $W_a$=0.2cm is measured and it is plotted in figure 4.41.
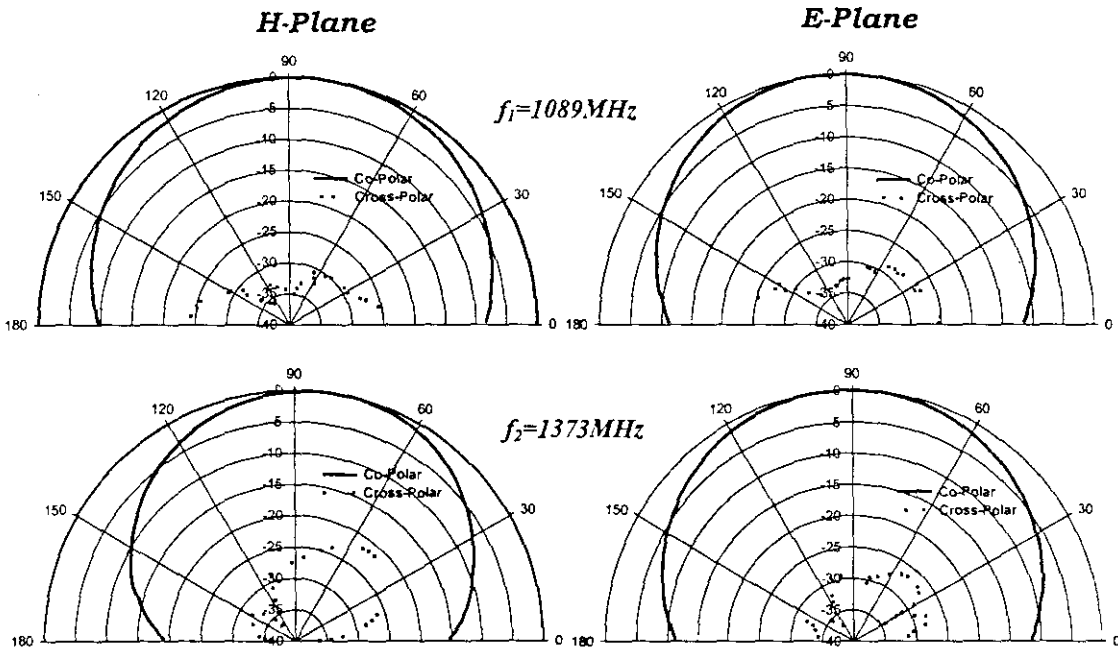
*Figure 4.41* Radiation pattern for a typical Capacitor mounted Three Stub Microstrip Antenna (CTSMA) configuration $L_p=4cm$, $L_s=1.2cm$, $L_a=1cm$, $W_a=0.2cm$, $Cp=4.7pF$

## 4.7.4 Gain

As described in section 4.1.5 of the single Stub patch antenna the relative gain of the Capacitor loaded Dual Stub antenna can be measured. The typical gain plots of a standard TSA has been measured and is plotted in figure 4.42.
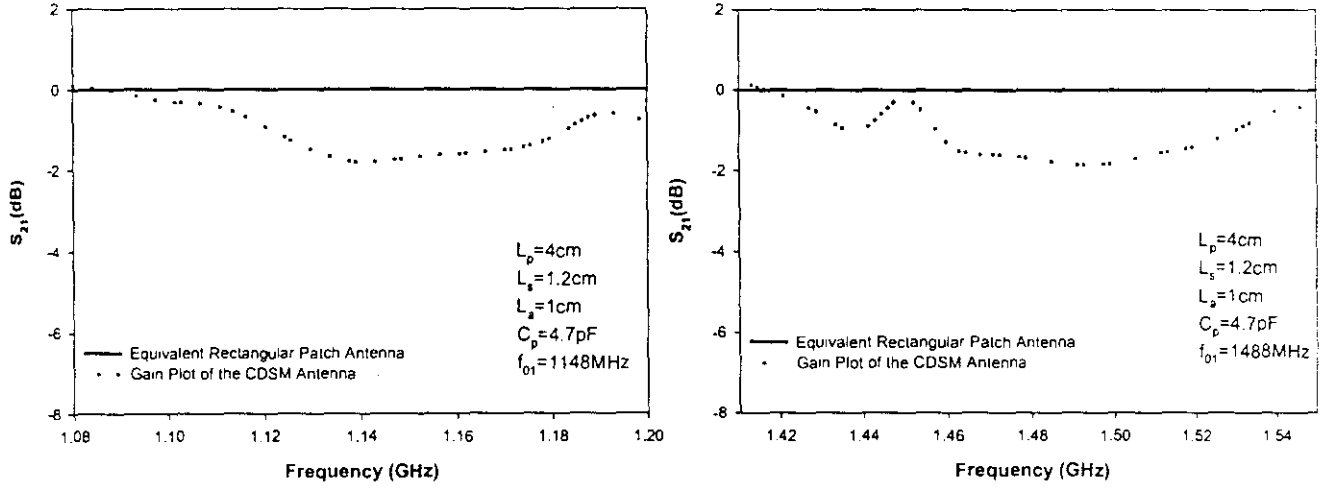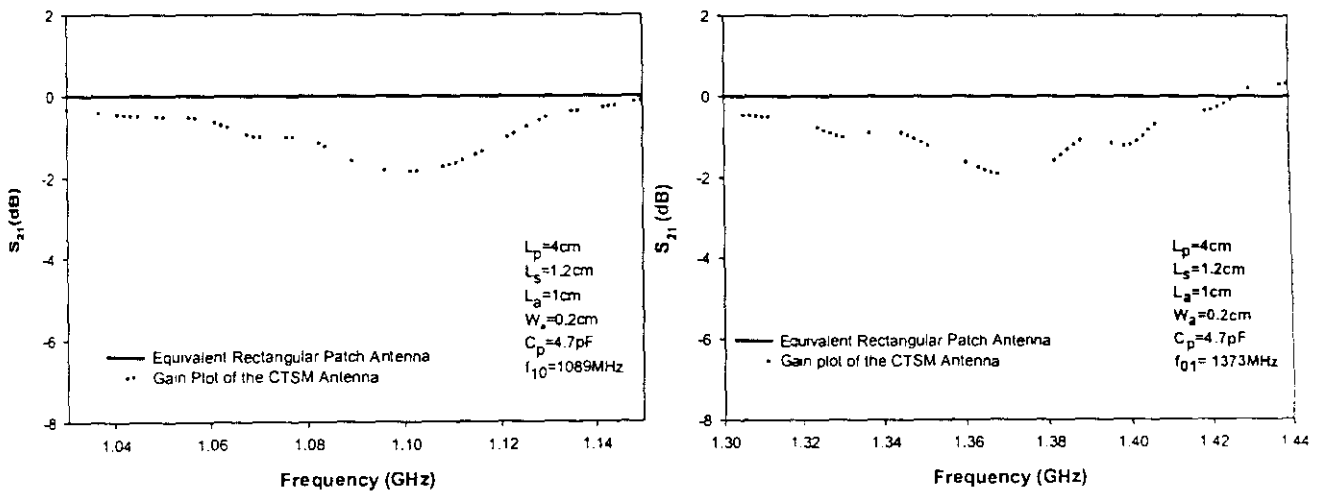


*Figure 4.42* $S_{21}$ plots for a typical Capacitor Mounted Three Stub Microstrip Antenna (CTSMA) configuration with respect to standard rectangular microstrip patch antenna fabricated on the same substrate and resonating at the same frequency

The area reduction feature of the CTSMA is analyzed by varying the capacitor values and the corresponding area reduction characteristics are analyzed and presented in table 4.19.

*Table. 4.19 The resonant frequencies, percentage of area reduction, physical area of the CTSMA ($A_{CTSMA}$) and corresponding equivalent rectangular patch antenna ($A_{eqnt.rect}$) for various dimensions (h=0.16cm, $\varepsilon_r$=4.28)*

| $L_p$, $L_s$, $L_a$,$W_a$ (cm) | $C_p$ (pF) | Resonance Frequency with capacitor Loading (GHz) | | Area of the equivalent Rectangular Patch ($A_{eqnt.rect}$) cm$^2$ | | Area of the CTSSMA cm$^2$ | Percentage Reduction in Patch Area % $\dfrac{A_{eqnt.rect} - A_{CTSMA}}{A_{eqnt.rect}}$ | |
|---|---|---|---|---|---|---|---|---|
| | | $f_1CTSMA$ | $f_2CTSMA$ | $f_1CTSMA$ | $f_2CTSMA$ | | $f_1CTSMA$ | $f_2CTSMA$ |
| 4,1.2, 1.0, 0.2 | 1 | 1.114 | 1.380 | 51.4 | 33.4 | 16 | 69 | 52 |
| | 4.7 | 1.089 | 1.373 | 53.8 | 33.8 | 16 | 70.2 | 52.7 |
| | 10 | 1.058 | 1.366 | 57 | 34.12 | 16 | 72 | 53 |
| | 22 | 1.039 | 1.359 | 59.88 | 34.5 | 16 | 73 | 53.6 |

From the table 4.19 it is clear that the capacitor loading has further extended the frequency tuning of the design for operation at a lower frequency band. The typical design provides an area reduction of 72% and 53 % for the two resonant modes in comparison to a standard rectangular patch operating at the same frequency.

Since, the FSMA geometry is already having a reduced antenna gain, the results of capacitor loading on FSMA is not included.

From the above experimental observations, it is found that the new slotted square microstrip patch antenna is a compact, dual frequency dual polarized antenna. The radiation characteristics are comparable to that of an equivalent rectangular microstrip antenna. The stub arm is found to be the key element in tuning the frequency characteristics of the design. The capacitor loading in found to have further extended the frequency tuning to a low frequency band.

**CHAPTER V**

---

**THEORETICAL INTERPRETATIONS**

# THEORETICAL INTERPRETATIONS

*A direct three-dimensional Finite-Difference Time-Domain (FDTD) method is applied to the full-wave analysis of the various slot loaded Microstrip Patch Antennas. The accuracy of the analysis is validated through experiments and IE3D electromagnetic modelling. An FDTD code that can be used for calculating the scattering parameters as well as the current and field distribution over the surface and edges is generated.*

## 5.1 INTRODUCTION

A theoretical analysis of the slotted microstrip patch antenna is presented in this chapter. The analysis is based on the FDTD method. It is a computationally efficient means of directly solving the Maxwell's time dependent curl equations, or their integral equations using finite difference technique. In this chapter, the frequency dependant scattering parameters have been calculated for the antenna geometries under consideration. The continuous distribution of electromagnetic fields in a finite volume of space is sampled at different points in a space and time lattice. The analysis can accurately determine the antenna resonant frequency and the current distribution. The calculated results are presented and compared with experimental measurements for the SSMA, DSMA, TSMA and FSMA geometries.

## 5.2 The theoretical Approach

An FDTD algorithm for the analysis of the antenna characteristics is generated. The antenna geometry is divided into cells for which necessary boundary conditions are applied. The finite difference time-domain (FDTD) technique permits the analysis of interactions of electromagnetic waves with material bodies of any desired shape.

### 5.2.1 Key Elements in FDTD Modelling Theory

The direct time-domain solutions of Maxwell's equations using the FDTD technique for the analysis of electromagnetic wave interactions with arbitrary material structures appear to be suitable for simulating planar patch geometries that are too large or too complex for simulation by any other principal numerical technique available today. The FDTD technique helps in modelling electromagnetic wave interactions by applying to the respective differential operators of the curl equations simple second order accurate central-difference approximations for the space and time derivatives of the electric and magnetic fields. Space and time discretization are selected to bound errors in the sampling process and to ensure numerical stability of the problem. The electric and magnetic components are

129

interleaved in space to permit a natural satisfaction of the tangential field continuity conditions at media interfaces.

The FDTD methods are applied in the present work for analysis and solving the Maxwell's equations for microstrip antennas. Applications of FDTD techniques to various electromagnetic problems are available in the literature [176-178]. In the case of arbitrary shaped patches, application of Yee algorithm has been found to be extremely accurate in predicting the current and field distributions across the patch [179]. However, when time domain electromagnetic field equations are solved using finite difference techniques in unbounded space, there needs to be a method applied for limiting the domain in which the field is computed [180]. Although the FDTD method is very successful in predicting the impedance and scattering parameters of antennas over a wide frequency band with the application of fast Fourier Transform, one practical difficulty with this method is that for devices that contain small structures or strongly varying fields, very fine meshes needs to be used. Since a finer mesh means longer computing time and larger memory. An improved method for reducing the number of time steps is implemented [181]. The technique is based on using a source with an internal resistance to excite the circuit.

FDTD method is used extensively for the solution of two and three-dimensional scattering problems. Recently, this method has also been used for effectively calculating the frequency dependent characteristics of microstrip circuit discontinuities. Analysis of the microstrip discontinuities is of great significance since more complicated geometries can be realized by interconnecting microstrip lines with these discontinuities and using transmission line and network theory. For simulating patch antennas, if the discontinuities are so close to each other the use of network concepts will not be accurate due to interaction of transient waves [182]. So, for the accurate analysis of the patch antenna structures it is necessary to simulate the entire structure in one computation. In the time domain analysis, a broadband pulse may be used as the excitation and the frequency domain parameters can be calculated over the entire frequency range of interest by Fourier transform of the transient results [177].

The basic steps presented in this section consists of the analysis of Yee algorithm based on Maxwell's Equation and the equivalent set of Finite Difference Equations:

Maxwell's curl Equations in an isotropic medium are:

$$\frac{\partial B}{\partial t} + \nabla \times E = 0 \tag{5.1}$$

$$\frac{\partial D}{\partial t} - \nabla \times H = J \tag{5.2}$$

$$B = \mu H \tag{5.3}$$

$$D = \varepsilon E \tag{5.4}$$

In a rectangular coordinate system, (5.1) and (5.2) are equivalent to the following system of scalar equations:

$$-\frac{\partial B_x}{\partial t} = \frac{\partial E_z}{\partial y} - \frac{\partial E_y}{\partial z} \tag{5.5}$$

$$-\frac{\partial B_y}{\partial t} = \frac{\partial E_x}{\partial z} - \frac{\partial E_z}{\partial x} \tag{5.6}$$

$$\frac{\partial B_z}{\partial t} = \frac{\partial E_z}{\partial y} - \frac{\partial E_y}{\partial x} \tag{5.7}$$

$$\frac{\partial D_z}{\partial t} = \frac{\partial H_z}{\partial y} - \frac{\partial H_y}{\partial z} - J_z \tag{5.8}$$

$$\frac{\partial D_y}{\partial t} = \frac{\partial H_x}{\partial z} - \frac{\partial H_z}{\partial x} - J_y \tag{5.9}$$

$$\frac{\partial D_z}{\partial t} = \frac{\partial H_y}{\partial x} - \frac{\partial H_x}{\partial y} - J_z \tag{5.10}$$

The boundary condition appropriate for a perfectly conducting surface is that the tangential components of the electrical fields vanish [180]. This condition also implies that the normal

131

component of the magnetic field vanish on the surface. The conducting surface may therefore be approximated by a collection of surfaces of cubes, the sides of which are parallel to the coordinate axis. Plane surfaces, perpendicular to the x-axis will be chosen so as to contain points where, $E_x$ and $E_y$ are defined.

The basic Yee algorithm helps us to solve both electric and magnetic fields in time and space using the coupled Maxwell's curl equations instead of solving either one of these with a wave equation [1]. This is similar to the combined-field integral equation formulation of Method of Moments.

The grid points for the E-field and H-field are chosen as shown in figure 5.1
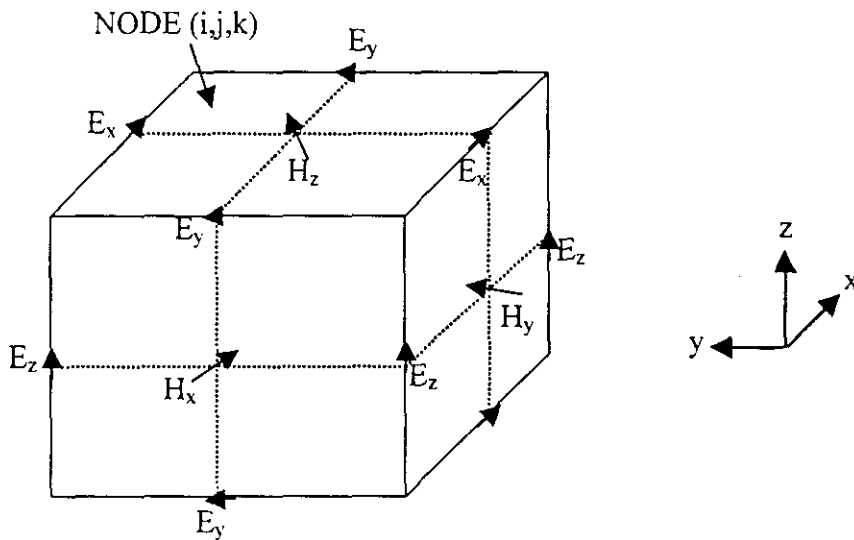


*Figure 5.1* *Field Component Placement in the FDTD unit cell*

The Yee algorithm centres its $\bar{E}$ and $\bar{H}$ components in a three dimensional space so that every $\bar{E}$ component is surrounded by four circulating $\bar{H}$ components, and every $\bar{H}$ component is surrounded by four circulating $\bar{E}$ components.

If the interface is parallel to one of the grid coordinate axis continuity of tangential $\bar{E}$ and $\bar{H}$ components is maintained across an interface of dissimilar materials. At the beginning of the problem, we can specify the material permittivity and permeability at each field component location. For a square Yee-mesh, this yields a 'stepped', approximation of the surface and internal geometry of the patch antenna with a space resolution set by the size of the unit cell.

The FDTD method is formulated by discretizing Maxwell's curl equation over a finite volume and approximating the derivatives with centred difference approximations. Conducting surfaces are treated by setting tangential electric field components to 0. The walls of the mesh are treated separately to prevent reflections from mesh termination.

## 5.3 ANALYSIS OF THE PRESENT DESIGN USING FDTD METHOD

The configuration of the new slot-loaded patch antenna along with the coordinate system is shown in figure 5.2. The antenna consists of a square patch on one side of a dielectric substrate of thickness '$h$' and relative dielectric constant '$\varepsilon_r$'. The antenna parameters and the different steps considered for implementing FDTD method and the obtained results are detailed below. Once the method has been successfully implemented for the single stub design (SSMA), the work was extended to the remaining 2, 3 and 4 stub geometries.
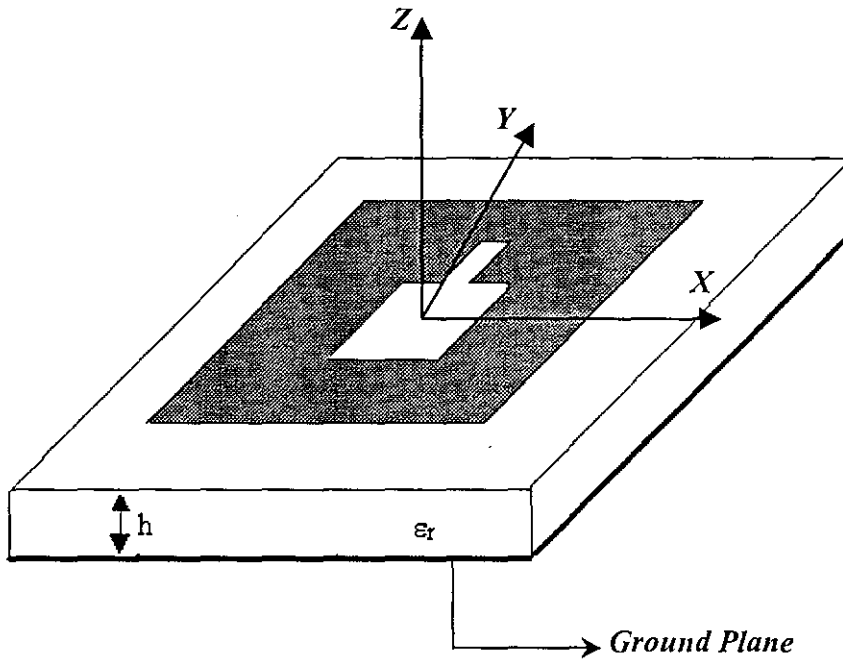
*Figure 5.2* *Configuration of the new Compact Single Stub Microstrip Patch Antenna*

## 5.4 FDTD PROBLEM DEFINITION AND PROPERTIES OF DIELECTRIC SUBSTRATE USED

In the present analysis, space grid size is selected such that the electromagnetic field does not vary significantly over one increment. For this, the linear dimensions of the grid must be only a fraction of the wavelength. For computational stability, it is necessary to satisfy the condition between the space increments $\Delta x = \Delta y = \Delta z$, and the time increment $\Delta t$. The notations used for the analysis are generalized into three spatial dimensions; a space point in a uniform rectangular lattice is represented as;

$$(i, j, k)=(i\Delta x, j\Delta y, k\Delta z) \qquad (5.11)$$

Here, $\Delta x$, $\Delta y$ and $\Delta z$ are the lattice space increments in the x, y and z coordinate directions, and i, j and k are integers.

134

The FDTD computational electromagnetic modelling provides a means to prototype a complex antenna design on a computer. The Single stub Microstrip Patch Antenna design is partitioned into six rectangular geometries and the formulation of the FDTD method begins by considering the differential form of Maxwell's two curl equations that govern the propagation of fields in microstrip structures.

The aim in the present analysis is to accurately and efficiently model the stub loaded frequency tunable antenna geometries with coaxial feed by the implementation of FDTD techniques. For the proposed geometry a simple coaxial model with an internal source resistance [181] is considered. This provides accurate results while significantly reducing the number of time steps required for convergence.

## 5.5 FDTD Source Excitation and Principal Equations

The volume in which the microstrip patch simulation for the antenna geometries is to be performed is depicted in figure 5.3. The analysis depends on the volumetric sampling of the unknown electric and magnetic fields within and surrounding the structure of interest, and over a period of time, which is given in figure 5.3. At time t=0, the fields are assumed to be identically zero throughout the computational domain. As its frequency spectrum is also Gaussian in nature, a Gaussian pulse is used for the excitation and will therefore provide frequency domain information from dc to the desired cut-off frequency by adjusting the width of the pulse. As the structure becomes complicated, tens or even hundreds of thousands of time steps may be required for the FDTD calculations to converge, especially for transient excitation.

For simplicity of analysis, the media are assumed to be piecewise uniform, isotropic and homogenous. The structure is assumed to be loss less, [176] (no volume currents or finite conductivity). Based on these assumptions, Maxwell's curl equations may be written as:

$$\mu \frac{\partial H}{\partial t} = -\nabla \times E \qquad (5.12)$$

$$\varepsilon \frac{\partial E}{\partial t} = \nabla \times H \qquad (5.13)$$

In order to find an approximate solution to this set of equations, the problem is discretized over a finite three-dimensional computational domain with appropriate boundary conditions enforced on the microstrip mesh walls.

The six field locations are considered to be interleaved in space as shown in figure 5.1, which is a drawing of the FDTD unit cell [179]. Here since the domain in which the field has to be computed is unbounded, an absorbing boundary condition by using a mesh of limited size, but one large enough to fully contain the obstacle has to be applied.

FDTD antenna or microstrip transient calculations are excited by a voltage source in which the internal source resistance is zero. These sources can be implemented in an FDTD code for calculating the current and field distribution from a microstrip structure. The electric field at the mesh edge where the source is located is determined by a Gaussian pulse, which is significantly greater than zero amplitude for only a very short fraction of the total computation time.

Once the pulse amplitude drops the source voltage becomes essentially zero, any reflection from the antenna, which return to the source, is totally reflected back. The introduction of a source with the inclusion of an internal source resistance to excite the FDTD calculation provides an additional loss mechanism to dissipate this energy introduced into the calculation space [181] which in turn results in reducing the FDTD calculation time appreciably.

To simulate a voltage source excitation, it is necessary to impose the vertical electrical field, $E_z$, in a square region above the ground plane, as shown in figure 5.3.

The remaining electric field components on the source plane are to be set zero. An excitation scheme is generated to simulate a magnetic wall directly on the source plane using image theory, then the remaining electric field components on the source plane can be calculated using the finite-difference equations, with minimum source distortion. The launched wave has nearly unit amplitude and is Gaussian in time which is given by:

$$E_z = f_s(t) = e^{-(t-t_0)/T^2} \qquad (5.14)$$

This excitation will result in the fundamental mode only propagating down the microstrip patch in the desired frequency range of interest.

The antenna design under investigation is having conducting ground plane and a single dielectric substrate with metallisation on top as in the conventional microstrip configuration. These electric conductors are assumed to be perfectly conducting and have zero thickness and are treated by setting the electric field components that lie on the conductors to be zero. The edge of the conductor should be modelled with electric field components tangential to the edge lying exactly on the edge of the microstrip as shown in figure 5.3.

### 5.5.1 Finite Difference Equations

To obtain discrete approximations of these continuous partial differential equations, the central difference approximation is used on both the time and space first order partial differentiations. The single stub slotted geometry is divided into fixed rectangular field locations and each conducting surfaces are treated by setting tangential electric field components to zero. These six field locations are considered to be interleaved in space as illustrated in figure 5.1. The entire computational domain is obtained by stacking these rectangular cubes, into a larger rectangular volume. The $\hat{x}$, $\hat{y}$, and $\hat{z}$ dimensions of the unit cell are $\Delta x$, $\Delta y$, and $\Delta z$, respectively. Here the centered differences are realised in the
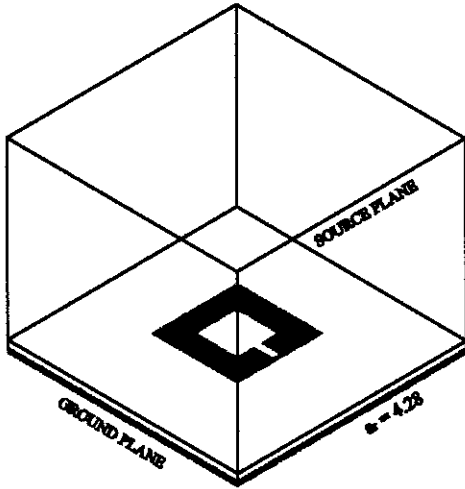
(i) SSMA
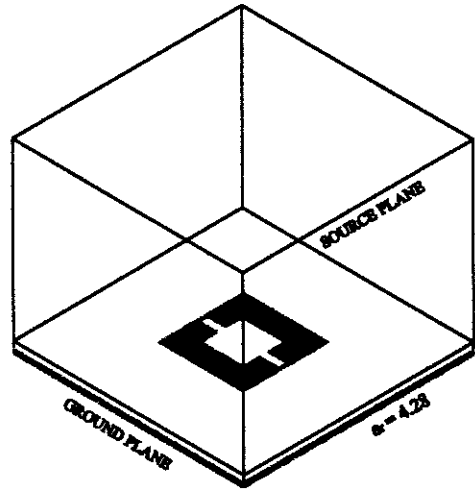
(ii) DSMA
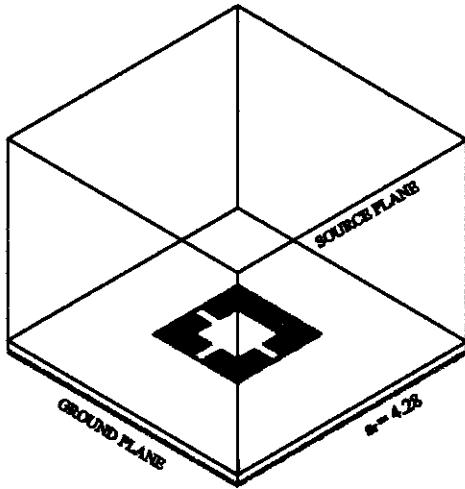
(iii) TSMA
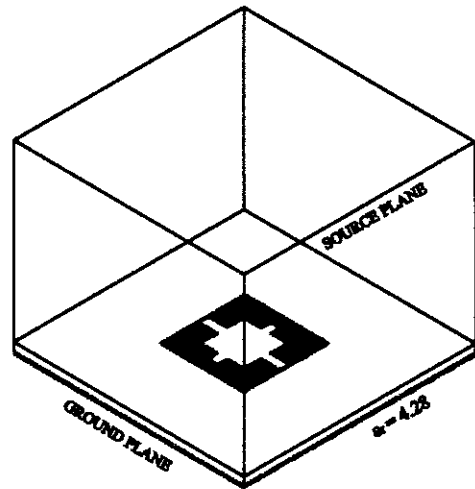
(iv) FSMA
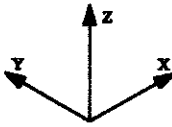
Figure 5.3  Computational domain

calculation of each field component and that continuity of tangential field components is hence automatically satisfied.

As there are only six unique field components within the unit cell, the six field components touching the shaded upper eighth of the unit cell in figure 5.1 are considered to be a unit node with subscript indices i, j and k corresponding to the node numbers in the $\hat{x}, \hat{y}$, and $\hat{z}$ directions.

This notation implicitly assumes the $\pm$ ½ space indices and thus simplifies the notation. The time steps are indicated with the superscript *n*. We can rewrite the explicit finite difference approximations to (5.12) and (5.13) as:

$$H_x^{n+1/2}{}_{i,j,k} = H_{xi,j,k}^{n-1/2} + \frac{\Delta t}{\mu \Delta z}(E_{yi,j,k}^n - E_{yi,j,k-1}^n) - \frac{\Delta t}{\mu \Delta y}(E_{zi,j,k}^n - E_{zi,j-1,k}^n)$$

$$(5.15)$$

$$H_y^{n+1/2}{}_{i,j,k} = H_y^{n-1/2}{}_{i,j,k} + \frac{\Delta t}{\mu \Delta x}(E_z^n{}_{i,j,k} - E_z^n{}_{i-1,j,k}) - \frac{\Delta t}{\mu \Delta z}(E_x^n{}_{i,j,k} - E_x^n{}_{i,j,k-1})$$

$$(5.16)$$

$$H_z^{n+1/2}{}_{i,j,k} = H_z^{n-1/2}{}_{i,j,k} + \frac{\Delta t}{\mu \Delta y}(E_x^n{}_{i,j,k} - E_x^n{}_{i,j-1,k}) - \frac{\Delta t}{\mu \Delta x}(E_y^n{}_{i,j,k} - E_y^n{}_{i-1,j,k})$$

$$(5.17)$$

$$E_x^{n+1}{}_{i,j,k} = E_x^n{}_{i,j,k} + \frac{\Delta t}{\varepsilon \Delta y}(H_z^{n+1/2}{}_{i,j+1,k} - H_z^{n+1/2}{}_{i,j,k}) - \frac{\Delta t}{\varepsilon \Delta z}(H_y^{n+1/2}{}_{i,j,k+1} - H_y^{n+1/2}{}_{i,j,k})$$

$$(5.18)$$

$$E_y^{n+1}{}_{i,j,k} = E_y^n{}_{i,j,k} + \frac{\Delta t}{\varepsilon \Delta z}(H_x^{n+1/2}{}_{i,j,k+1} - H_x^{n+1/2}{}_{i,j,k}) - \frac{\Delta t}{\varepsilon \Delta x}(H_z^{n+1/2}{}_{i+1,j,k} - H_z^{n+1/2}{}_{i,j,k})$$

$$(5.19)$$

$$E_z^{n+1}{}_{i,j,k} = E_z^n{}_{i,j,k} + \frac{\Delta t}{\varepsilon \Delta x}(H_y^{n+1/2}{}_{i+1,j,k} - H_y^{n+1/2}{}_{i,j,k}) - \frac{\Delta t}{\varepsilon \Delta y}(H_x^{n+1/2}{}_{i,j+1,k} - H_x^{n+1/2}{}_{i,j,k})$$

$$(5.20)$$

The half time steps indicate that the E and H are alternatively calculated in order to achieve centered differences for the time derivatives. In these equations, the permittivity and permeability are set to the appropriate values depending on the location of each field component. For the electric field components on the dielectric air-interface the average of two permittvities $(\varepsilon_0 + \varepsilon_r)/2$, is used [183].

Due to the use of these centered differences, the error is second order in both the space and time steps; i.e., if $_\Delta x$, $_\Delta y$, and $_\Delta z$ and $_\Delta t$ are proportional to $_\Delta l$, then the overall error will be O $(_\Delta l)^2$. The maximum time step that may be used is limited by the stability criterion of the finite difference equations:

$$\Delta t \leq \frac{1}{V_{max}}\left(\frac{1}{\Delta x^2} + \frac{1}{\Delta y^2} + \frac{1}{\Delta z^2}\right)^{-1/2} \qquad (5.21)$$

Where, $V_{max,}$ is the maximum velocity of light within the computational volume. Typically, $V_{max}$, will be the velocity of light in free space unless the entire volume is filled within the dielectric. These equations will allow the appropriate solution of E(r,t) and H(r,t) in the volume of the computational domain or mesh; however, special consideration is required for the source, the conductors and the mesh walls. All of the $\bar{E}$-computations in the three dimensional space of interest are completed and stored in memory for a particular time point using $\bar{H}$-data previously stored in the system memory. The reverse process is repeated for the $\bar{H}$-computations.

The equations for individual unit cells are identical for lossy dielectric, perfect conductor and free space. The FDTD implementation uses pulse excitation, which provides a wide band of frequencies with a single fast Fourier Transform.

### 5.5.2 Absorbing Boundary Conditions for the Finite-Difference Approximation

When time-domain electromagnetic field equations are solved using finite-difference techniques in unbounded space, there must be a method for limiting the domain

in which the field is computed. This is achieved by truncating the mesh in $\hat{x}, \hat{y}$, and $\hat{z}$ directions and applying absorbing boundary conditions at its artificial boundaries to simulate the unbounded surroundings. One of the six mesh boundaries is a ground plane and its tangential electric field values are forced to be zero. The tangential electric field components on the remaining five mesh walls are represented as if the outgoing waves are not reflected using the absorbing boundary conditions. In this approach, the pulses on the microstrip patch will be incident normally to the mesh walls. This results in a simple approximate continuous absorbing condition that the tangential field on the outer boundaries will obey the one-dimensional wave equation in the direction normal to the mesh wall. For the $\hat{y}$ normal wall the one-dimensional wave equation is:

$$\left(\frac{\partial}{\partial y} - \frac{1}{v}\frac{\partial}{\partial t}\right)E_{\tan} = 0 \qquad (5.22)$$

The above equation is the first approximate boundary condition [180] and it may be easily discretized using only few field components on or just inside the mesh wall, yielding an explicit finite difference equation.

$$E_0^{n+1} = E_1^n + \frac{v\Delta t - \Delta y}{v\Delta t + \Delta y}(E_1^{n+1} - E_0^n) \qquad (5.23)$$

Here, $E_0$ represents the tangential electric field components on the mesh wall and $E_1$ represents the tangential electric field components on node inside the mesh wall. This normal incidence assumption is not valid for the fringing fields, which are propagating tangential to the walls, so the sidewalls should be far enough in order to make the fringing fields negligible at the walls. Moreover, radiation will not be exactly normal to the mesh walls. Second order absorbing boundary conditions that account for oblique incidence will not work on the mesh walls where the microstrip is incident because these absorbing boundary conditions are derived in uniform space.

The finite difference equations (5.15-5.20) are used with the above boundary and source conditions to simulate the propagation of a broadband Gaussian pulse on the microstrip patch is applied.

The important aspects of the time-domain algorithm are as follows:

- Initially (at t=n=0) all fields are 0.
- The following steps are repeated until the response is $\approx$ 0:

    Gaussian Impulse is imposed on Port 1.

    $H^{n+1/2}$ is calculated from FD equations.

    $E^{n+1}$ is calculated from FD equations.

    Tangenital E is set to 0 on conductors.

    Save desired field equations.

    $n \rightarrow n+1$

- Compute the scattering matrix coefficients from time domain results.

Here the reflections from the microstrip patch will be reflected by the source wall. This is avoided by placing the source wall patch at a sufficient distance from the source, and after the Gaussian pulse has been fully launched, the absorbing boundary condition is turned ON at the boundary walls.

To excite an FDTD calculation with a voltage source mentioned above, which corresponds to an electric field E in the Z-direction at a certain mesh location $i_s\Delta x$, $j_s \Delta y$, and $k_s\Delta z$. To converge the FDTD calculation time steps at a faster rate, a source resistance is included along with the voltage source and the equivalent circuit is depicted in figure 5.4
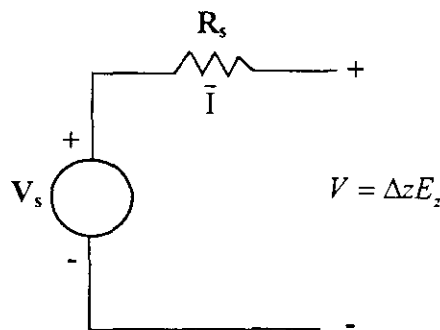


*Figure 5.4 FDTD Source with source Resistance 'R$_s$'*

If the source resistance R$_s$, is set to zero, then the usual FDTD electric field at the source location is given by:

$$E_s^n(i_S, j_S, k_S) = V_S(n\Delta t) / \Delta z \qquad (5.24)$$

where, V$_s$ is the Gaussian Pulse.

With the source resistance included, the calculation of the source field $E_s^n(i_s, j_s, k_s)$ becomes complicated. To find the terminal voltage and the source field, the current through the source must be determined by applying Ampere's circuital law. The current through the source is given by:

$$I_S^{n-1/2} = [H_x^{n-1/2}(i_S.j_S - 1.k_S) - H_x^{n-1/2}(i_S.j_S.k_S)]\Delta x + [H_y^{n-1/2}(i_S.j_S.k_S) - H_y^{n-1/2}(i_S - 1.j_S.k_S)]\Delta y$$
$$(5.25)$$

Now, by applying Ohm's law, to the circuit of figure 5.4, the electric field source is given by,

$$E_s^n(i_S.j_S.k_S) = V_S(n\Delta t) / \Delta z + I_S^{n-1/2} R_S / \Delta z \qquad (5.26)$$

The value of the source resistance cannot be made too large. Instabilities can also occur due to neglecting the displacement current through the FDTD cell containing the source.

The value of the internal resistance does not appear to be critical. A reasonable choice of for R$_s$ is to implement the value of the characteristic impedance depending on the particular microstrip patch geometry.

### 5.5.3 Calculation of Scattering Parameters

The frequency dependant scattering matrix coefficients can be calculated.

$$[V]^r = [S] \quad [V]^i \qquad (5.27)$$

Where, $[V]^r$ and $[V]^i$ are the reflected and incident voltage vectors, and $[S]$ is the scattering matrix. It is assumed that this field value is proportional to the voltage considering the propagation of the fundamental mode. To obtain the scattering parameters $S_{11}(w)$, the incident and reflected waveforms must be known. The FDTD simulation calculates the sum of the incident and the reflected waveforms. To obtain the incident waveform, calculation is performed using only port 1 of the patch, which will now be of infinite extent and the incident waveform is noted. This incident waveform is then subtracted from the total waveform (incident + reflected) to yield the reflected waveform for port1. The scattering parameters, $S_{jk}$, can be calculated by simple Fourier Transform of the transient waveform as;

$$S_{jk}(w) = \frac{FT[V_j(t)]}{FT[V_k(t)]} \qquad (5.28)$$

Here the reference planes are selected with enough distance from the patch discontinuities to eliminate evanescent waves. These distances are included in the definition of the circuit so that no phase correction is performed for the scattering coefficients. For all of the circuits considered, the only unique coefficients are in the first column of the scattering matrix such as $S_{11}(w)$, $S_{21}(w)$, $S_{31}(w)$...etc.

The numerical analysis has been computed based on the FDTD code formulated in Matlab 5.3. The operating frequency range is from 1 to 2 GHz. The patches are fabricated on copper clad substrates with $\varepsilon_r$=4.28, and h=0.16cm.

The four basic patches are analysed and the computations are performed by varying the central slot length '$L_s$', and stub length' '$L_a$'. These configurations are named for convenience, based on the configuration and dimension of the slotted patch in the experimental chapter itself.

## 5.6 ANALYSIS OF COAXIALLY FED STUB LOADED SQUARE MICROSTRIP ANTENNAS

The exact dimensions of the four basic microstrip antenna geometries analysed are shown in figure 5.5.

Simulation of the patch involves the direct application of finite-difference equations, along with source excitation and boundary conditions. To precisely model the thickness of the substrate, $\Delta z$ is chosen so that three nodes exactly match the thickness. An additional 13 nodes, in the Z-direction, are used to model the free space above the substrate. In order to correctly model the dimensions of the antenna, $\Delta x$ and $\Delta y$ have been chosen so that an integral number of nodes will exactly fit the square patch under study. For accurate excitation of the fundamental mode, sufficient numbers of unit cells are modelled to match the thickness of the stub arm width 'W$_a$'. The coaxial SMA feeding cell is identified uniquely for perfect impedance matching. The feed is oriented along a z-directed electric field just above the ground plane and directly below the patch, as marked in figure 5.6. Here, the perfectly conducting ground plane is at the bottom, the dielectric substrate is shown as unfilled squares, the mesh edge where the electric field feed is located is shown as an arrow, and the conducting meshes, are shown filled. The field transition from the electric field feed (arrow) to the microstrip patch at the top was used to provide a relatively smooth connection from the single electric field location to the microstrip.

The space steps used are $\Delta x=0.025cm$, $\Delta y=0.025\ cm$, and $\Delta z=0.04\ mm$ and the total mesh dimensions are 200 x200 x16 in the $\hat{x}$, $\hat{y}$, and $\hat{z}$ directions respectively. The square patch antenna dimension for the FDTD analysis is $160\Delta x\ X\ 160\ \Delta y$. The feed point is located along the diagonal of the square patch.

The time step used is 0.91 ps. The Gaussian half-width is T=15 ps, and the time delay $T_0$ is set to be 2T so that the Gaussian will start at approximately 0. An internal source resistance (Rs=50$\Omega$) is also incorporated into the geometry. This helps us to reduce the computational time significantly thereby enhancing computational efficiency.
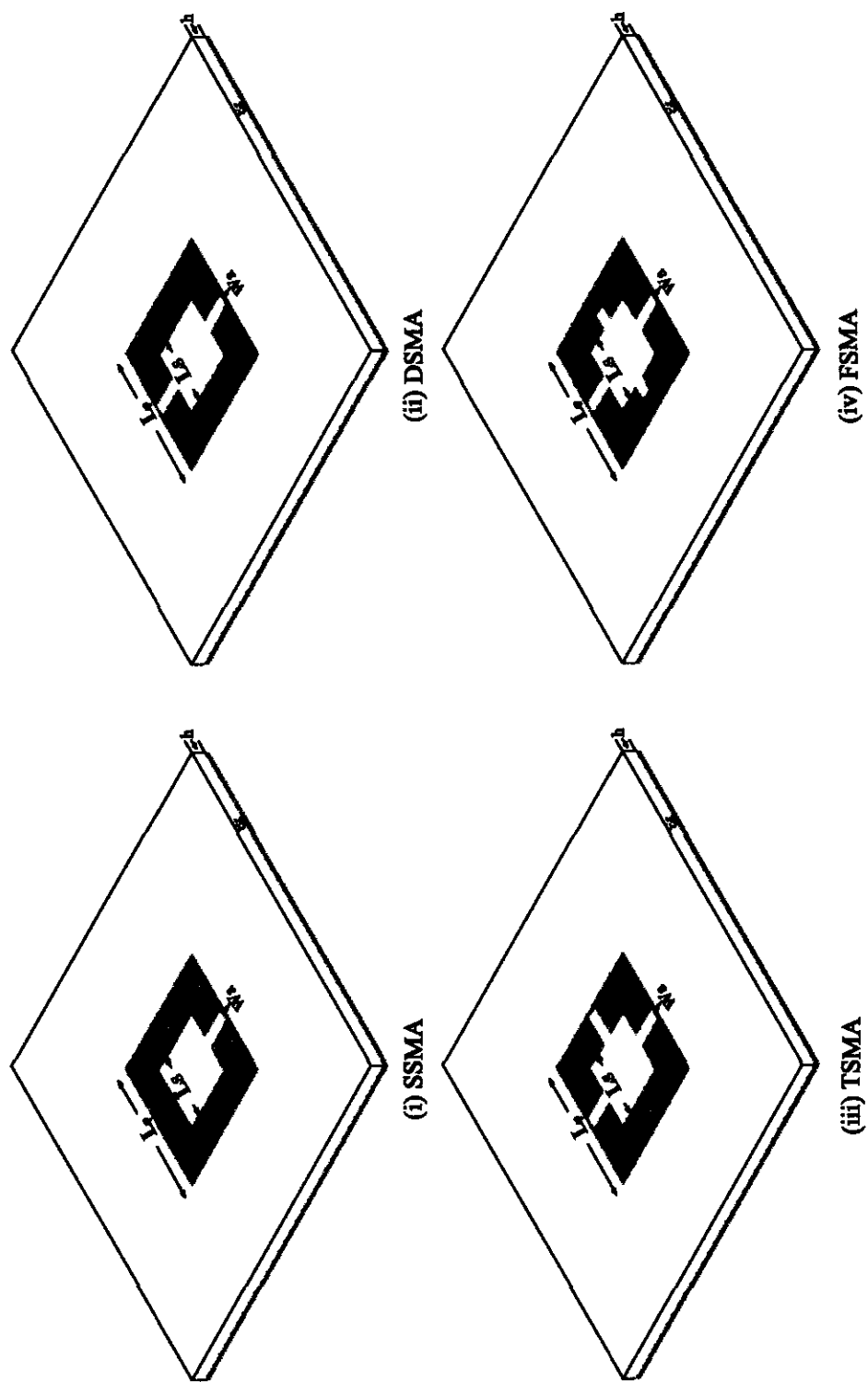
*Figure 5.5 Coaxial fed microstrip antenna parameters*

$L_p = 4cm, L_s = 1.2cm, L_a = 1cm, W_a = 0.2cm, L_{a1} = 1cm, L_{a2} = 0.5cm, h = 0.16cm, \varepsilon_r = 4.28$

(i) SSMA

(ii) DSMA

(iii) TSMA

(iv) FSMA
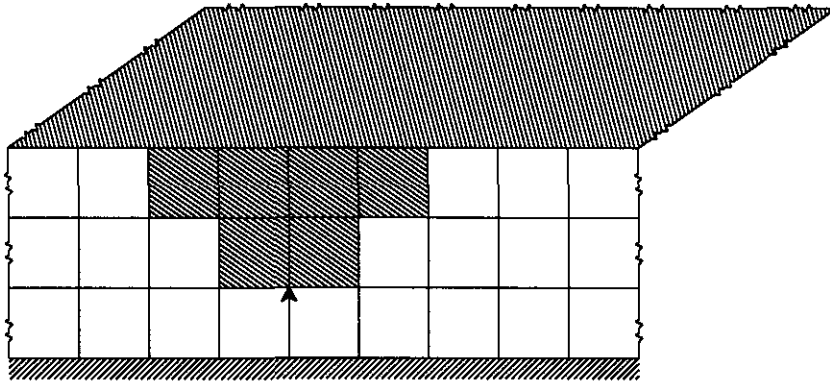
***Figure 5.6*** *Detail of the stair-cased FDTD mesh transition from the electric field source location to the microstrip patch antenna*

For a voltage source excitation, an appropriate vertical electric field $E_z$ needs to be imposed, in a square region below the patch, as shown in figure 5.3. The remaining electric field components on the source plane can be calculated by supplying appropriate boundary conditions. An electric wall modelling can be implemented so that the remaining electric field components on the source wall of the mesh are set to be 0. A demerit of this type of excitation is that a sharp magnetic field is induced tangential to the source wall. This results in some distortion of the launched pulse.

## 5.7 COMPARISON OF THE THEORETICAL AND EXPERIMENTAL RESULTS

The scattering coefficients of the various antenna designs were simulated using the present theory. The theoretically predicted and experimentally observed results are compared and the percentage error is calculated as:

$$\text{Percentage Error} = \frac{f_{experimental} - f_{theoretical}}{f_{experimental}} \times 100$$

### 5.7.1 Analysis of SSMA

The table 5.1 gives a comparison of the calculated and measured resonant frequencies of the Single Stub Microstrip Antenna. The table also provides the variation of resonance frequencies with the central slot length '$L_s$' and stub arm length '$L_a$'.

*Table 5.1 Calculated and Measured Return Loss Comparison for the Proposed Single Stub Microstrip slotted Antenna*

| $L_P, L_S, W_a$ (cm) | $L_a$ (cm) | h (cm) | $\varepsilon_r$ | $TM_{10}$ mode frequency ($f_1$) (GHz) | | | $TM_{01}$ mode frequency ($f_2$) (GHz) | | |
|---|---|---|---|---|---|---|---|---|---|
| | | | | Measured | Calculated | % error | Measured | Calculated | % error |
| | 0.2 | | | 1.525 | 1.536 | 0.72 | 1.631 | 1.6379 | 0.42 |
| | 0.4 | | | 1.514 | 1.534 | 1.32 | 1.627 | 1.6297 | 0.17 |
| | 0.6 | | | 1.472 | 1.459 | 0.88 | 1.623 | 1.6194 | 0.22 |
| 4, 0.8, 0.2 | 0.8 | 0.16 | 4.28 | 1.463 | 1.473 | 0.68 | 1.622 | 1.616 | 0.37 |
| | 1.0 | | | 1.443 | 1.446 | .2 | 1.62 | 1.628 | 0.49 |
| | 1.2 | | | 1.426 | 1.4302 | .29 | 1.617 | 1.6201 | 0.19 |
| | 0.2 | | | 1.507 | 1.5099 | 0.19 | 1.622 | 1.66291 | 0.43 |
| | 0.4 | | | 1.480 | 1.4862 | 0.42 | 1.614 | 1.6228 | 0.54 |
| | 0.6 | | | 1.450 | 1.4587 | 0.6 | 1.597 | 1.604 | 0.43 |
| 4, 1, 0.2 | 0.8 | 0.16 | 4.28 | 1.433 | 1.4351 | 0.15 | 1.611 | 1.62 | 0.55 |
| | 1.0 | | | 1.411 | 1.4159 | 0.34 | 1.604 | 1.5967 | 0.49 |
| | 1.2 | | | 1.390 | 1.399 | 0.64 | 1.609 | 1.6059 | 0.19 |
| | 0.2 | | | 1.487 | 1.4942 | 0.48 | 1.594 | 1.5981 | 0.25 |
| | 0.4 | | | 1.459 | 1.46 | 0.68 | 1.589 | 1.5825 | 0.41 |
| | 0.6 | | | 1.441 | 1.4432 | 0.14 | 1.577 | 1.5717 | 0.35 |
| 4, 1.2, 0.2 | 0.8 | 0.16 | 4.28 | 1.419 | 1.425 | 0.42 | 1.561 | 1.5646 | 0.23 |
| | 1.0 | | | 1.407 | 1.4125 | 0.39 | 1.560 | 1.5581 | 0.51 |
| | 1.2 | | | 1.387 | 1.3808 | 0.44 | 1.553 | 1.5561 | 0.20 |

A prototype fabricated out of the copper clad sheet exhibited a dual frequency operation at 1.41 GHz and 1.61 GHz. Using the FDTD code the design have been analysed and the results are found to be showing good agreement with the experimental $S_{22}$ results. From table 5.1 it is clear that the frequency tuning nature of the single stub antenna can be predicted accurately using the present theory.

The stub length variations mainly influence the lower resonant frequency $(f_1)$. This has already been established experimentally, which is again confirmed using the present theory. Figure 5.7 shows the $S_{22}$ plots obtained using the present theory and that is compared with the experimental result. The plot also contains the $S_{22}$ plot of the antenna simulation using IE3D electromagnetic modelling technique. The details of the IE3D simulation techniques and the results obtained are presented and analysed in detail in section 5.9 of this chapter.

The FDTD scattering coefficient result, shown in figure 5.7 depicts good agreement with the experimental and simulated data. The operating resonance at 1.41 GHz and 1.61 GHz is almost identical shown by both theory and measurement. This result is a significant advancement over planar circuit techniques, which without empirical treatment will allow only $|S_{11}|=1.0$ because they do not allow for radiation. The resonance frequency calculated using planar circuit techniques would be prone to errors in the effective dimensions of the patch.
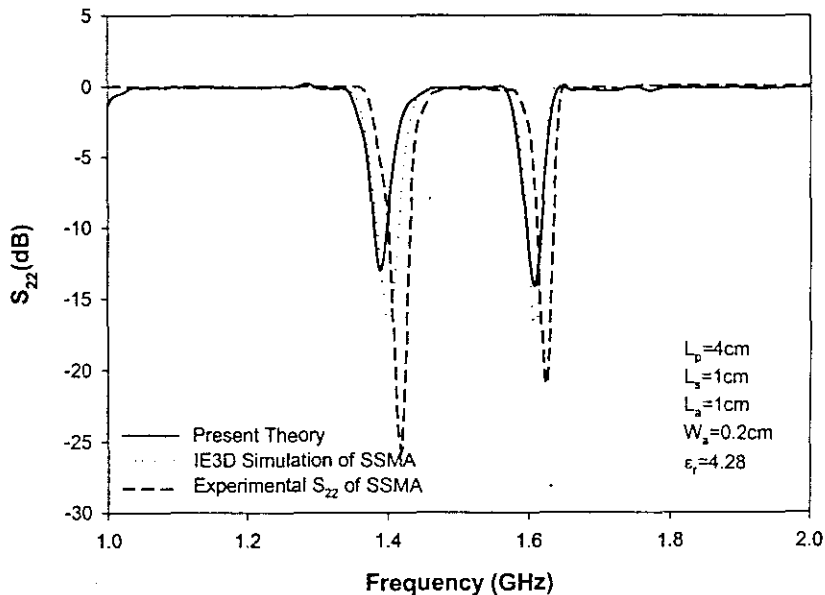


*Figure 5.7 Showing the return loss comparison curves of the single stub microstri Antenna using the FDTD (present theory), IE3D simulation and the experimenta results.*

## 5.7.2 Analysis of DSMA

The Single stub antenna is now restructured into Dual Stub Microstrip Antenna for enhanced area reduction achievement. In this section, the FDTD results of the DSMA are presented.

Table 5.2 show the comparison between the present theory and the measured values for various DSMA configurations.

***Table 5.2*** *Calculated and Measured Return Loss Comparison for the Proposed Dual Stub Microstrip (DSMA) slotted Antenna*

| $L_p, L_S, W_a$ (cm) | $L_a$ (cm) | h (cm) | $\varepsilon_r$ | $TM_{10}$ mode frequency $(f_1)$ (GHz) | | | $TM_{01}$ mode frequency $(f_2)$ (GHz) | | |
|---|---|---|---|---|---|---|---|---|---|
| | | | | Measured | Calculated | % error | Measured | Calculated | % error |
| 4, 0.8, 0.2 | 0.2 | 0.16 | 4.28 | 1.345 | 1.3424 | 0.19 | 1.576 | 1.5784 | 0.15 |
| | 0.4 | | | 1.339 | 1.3444 | 0.41 | 1.569 | 1.574 | 0.32 |
| | 0.6 | | | 1.327 | 1.3339 | 0.52 | 1.544 | 1.5479 | 0.25 |
| | 0.8 | | | 1.311 | 1.3194 | 0.64 | 1.531 | 1.54 | 0.59 |
| | 1.0 | | | 1.304 | 1.3118 | 0.59 | 1.519 | 1.531 | 0.79 |
| | 1.2 | | | 1.292 | 1.2985 | 0.50 | 1.491 | 1.5007 | 0.65 |
| 4, 1, 0.2 | 0.2 | 0.16 | 4.28 | 1.322 | 1.3245 | 0.19 | 1.549 | 1.5402 | 0.57 |
| | 0.4 | | | 1.301 | 1.3091 | 0.62 | 1.530 | 1.5336 | 0.24 |
| | 0.6 | | | 1.292 | 1.2981 | 0.47 | 1.512 | 1.5183 | 0.42 |
| | 0.8 | | | 1.278 | 1.2838 | 0.45 | 1.497 | 1.4949 | 0.15 |
| | 1.0 | | | 1.262 | 1.2693 | 0.58 | 1.492 | 1.4839 | 0.54 |
| | 1.2 | | | 1.253 | 1.2597 | 0.53 | 1.489 | 1.484 | 0.34 |
| 4, 1.2, 0.2 | 0.2 | 0.16 | 4.28 | 1.315 | 1.3219 | 0.52 | 1.533 | 1.545 | 0.78 |
| | 0.4 | | | 1.297 | 1.3035 | 0.50 | 1.518 | 1.524 | 0.39 |
| | 0.6 | | | 1.274 | 1.2809 | 0.54 | 1.503 | 1.5119 | 0.59 |
| | 0.8 | | | 1.268 | 1.2759 | 0.62 | 1.489 | 1.4951 | 0.41 |
| | 1.0 | | | 1.254 | 1.2579 | 0.31 | 1.477 | 1.488 | 0.74 |
| | 1.2 | | | 1.250 | 1.263 | 1.04 | 1.461 | 1.4632 | 0.15 |

The table reveals the comparison between the theoretical and experimental values. Figure 5.8 illustrates a typical case from this table in which three return loss curves can be seen, from which one corresponds to the present theory, another one to the experimental result and a third curve representing the IE3D analysis, which is explained in detail in next section.
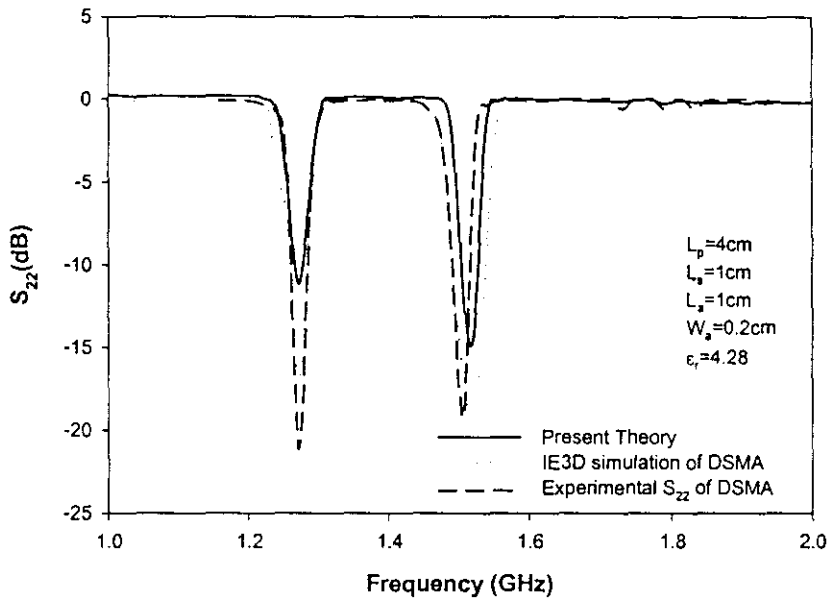


*Figure 5.8 Showing the return loss comparison curves of the Dual Stub Microstri Antenna using the FDTD (present theory), IE3D simulation and the experimenta results.*

The plot reveals good matching theoretical, experimental and simulated results. The DSMA antenna is providing an area reduction of 61 and 45 % for the two resonance modes.

## 5.7.3 Analysis of TSMA

The Three Stub Microstrip Antenna is also analysed using the FDTD method. The third stub is oriented in a direction perpendicular to the two existing stub arms as explained earlier in the experimental section.

A comparison of the theoretical and the measured return loss characteristics is given in table 5.3 for various values of the central slot length "$L_s$", and Stub arm length '$L_a$'.

**Table 5.3** *Calculated and Measured Return Loss Comparison for the Proposed Triple Stub Microstrip (TSM) slotted Antenna*

| $L_P, L_S, W_a$ (cm) | $L_a$ (cm) | h (cm) | $\varepsilon_r$ | $TM_{10}$ mode frequency ($f_1$) (GHz) | | | $TM_{01}$ mode frequency ($f_2$) (GHz) | | |
|---|---|---|---|---|---|---|---|---|---|
| | | | | Measured | Calculated | % error | Measured | Calculated | % error |
| 4, 0.8, 0.2 | 0.2 | 0.16 | 4.28 | 1.285 | 1.2884 | 0.26 | 1.536 | 1.5412 | 0.33 |
| | 0.4 | | | 1.271 | 1.2671 | 0.31 | 1.522 | 1.5204 | 0.11 |
| | 0.6 | | | 1.266 | 1.272 | 0.47 | 1.503 | 1.5069 | 0.26 |
| | 0.8 | | | 1.254 | 1.2566 | 0.20 | 1.488 | 1.4821 | 0.40 |
| | 1.0 | | | 1.233 | 1.2343 | 0.11 | 1.474 | 1.4774 | 0.23 |
| | 1.2 | | | 1.220 | 1.2263 | 0.51 | 1.462 | 1.4681 | 0.42 |
| 4, 1, 0.2 | 0.2 | 0.16 | 4.28 | 1.254 | 1.267 | 1.03 | 1.459 | 1.4655 | 0.45 |
| | 0.4 | | | 1.239 | 1.2479 | 0.72 | 1.438 | 1.4406 | 0.18 |
| | 0.6 | | | 1.226 | 1.2344 | 0.68 | 1.417 | 1.4193 | 0.16 |
| | 0.8 | | | 1.16 | 1.1681 | 0.69 | 1.401 | 1.3991 | 0.14 |
| | 1.0 | | | 1.210 | 1.2011 | 0.73 | 1.389 | 1.3921 | 0.22 |
| | 1.2 | | | 1.204 | 1.2072 | 0.26 | 1.381 | 1.3832 | 0.16 |
| 4, 1.2, 0.2 | 0.2 | 0.16 | 4.28 | 1.244 | 1.2463 | 0.18 | 1.437 | 1.4392 | 0.15 |
| | 0.4 | | | 1.232 | 1.2383 | 0.51 | 1.411 | 1.4146 | 0.25 |
| | 0.6 | | | 1.207 | 1.2136 | 0.54 | 1.395 | 1.4001 | 0.37 |
| | 0.8 | | | 1.189 | 1.1935 | 0.62 | 1.377 | 1.44 | 0.46 |
| | 1.0 | | | 1.177 | 1.1737 | 0.28 | 1.361 | 1.3672 | 0.46 |
| | 1.2 | | | 1.170 | 1.1763 | 0.54 | 1.348 | 1.3515 | 0.26 |

From the table it can see be seen that the frequency tunability of the TSMA is also verified using the present theory.

For comparison, a plot of the $S_{22}$ characteristics of the antenna plotted using the three available methods are plotted in figure 5.9
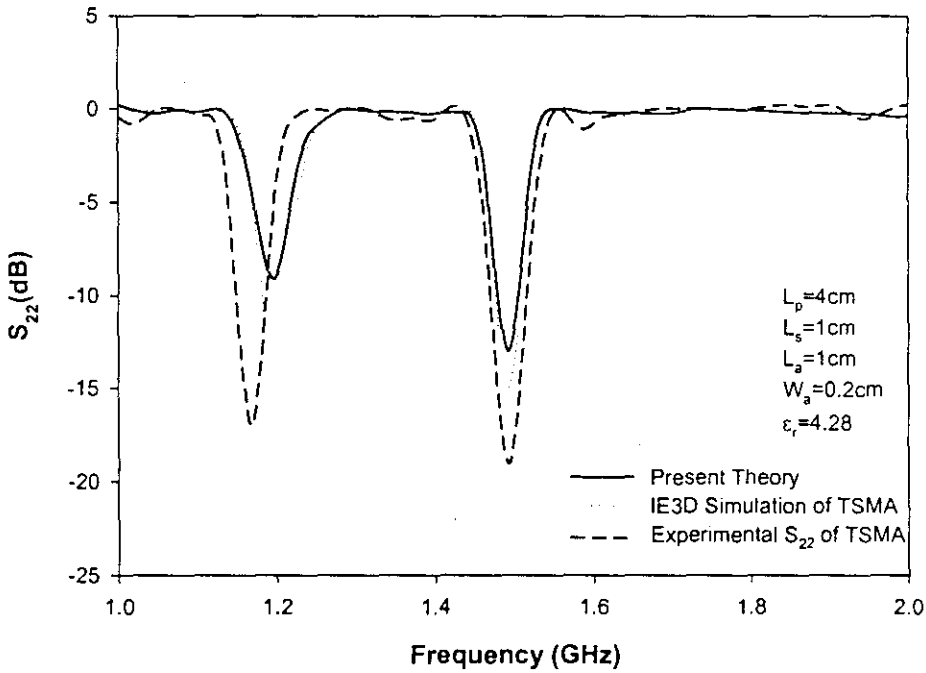


*Figure 5.9 Showing the comparison of scattering coefficient results of the FDTD calculation, the IE3D simulation and the experimental $S_{22}$ of TSMA*

The next geometry to be checked using the FDTD simulation is the four stub Microstrip Antenna (FSMA). In section, 4.4 it has been shown that the antenna is designed with a characteristic difference from the first three geometries in that the second pair of stub arms are only half that of the other pair. Figure 5.10 illustrates the comparison of return loss results obtained using the FDTD method and IE3D simulation result, which is verified also with experimental return loss.



$L_p$=4cm
$L_s$=1cm
$L_{a1}$=1cm
$La_2$=0.5cm
$W_a$=0.2cm
$\varepsilon_r$=4.28

——— Present Theory
IE3D Simulation of FSMA
– – – Experimental $S_{22}$ of FSMA
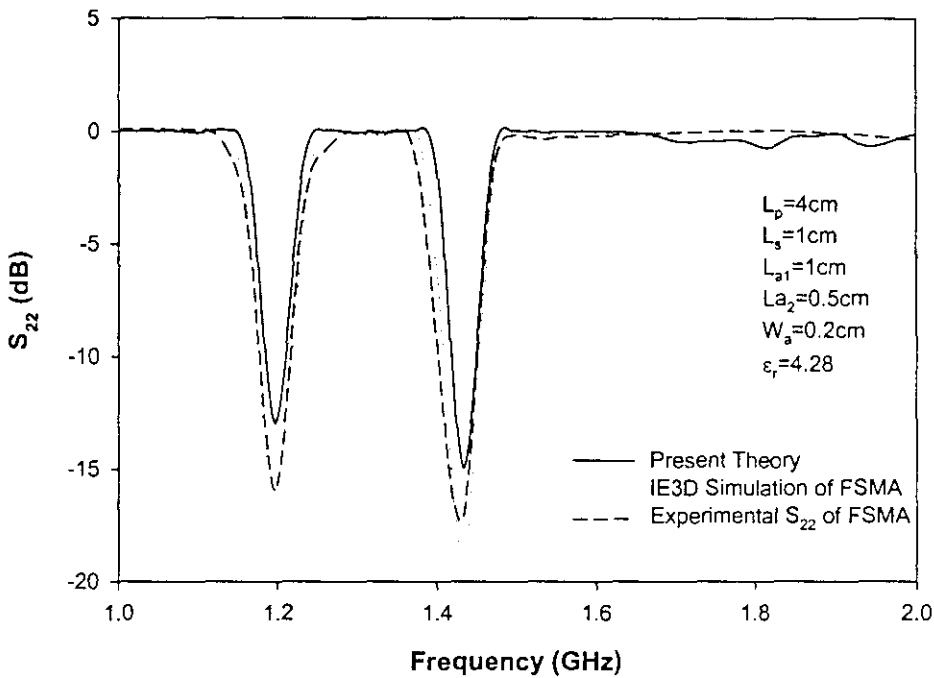
*Figure 5.10 Showing the return loss comparison curves of the Four Stub Microstrip Antenna using the FDTD (present theory), IE3D simulation and the experimental results.*

## 5.8 ELECTRIC FIELD VARIATION

The electric field variation along the periphery of the antenna is required to identify the mode of operation, which can help to predict the radiation patterns, power radiated, etc. The field variation in the surface of the patch is modelled using the FDTD technique and it is compared with the experimentally observed resonance modes. The modelling of the electric field variation has been studied for the above mentioned geometries and a typical case is presented. The electric field variation computed using the FDTD code is plotted in figure 5.11 (i). The analysis of the figure reveals that at the lower resonance frequency, one half wave variation along the X-direction, $TM_{10}$ mode is generated. At the higher resonance frequency there is no field variation along the X-direction, and one half wave variation along Y-direction. The same mode characteristics are observed in all the geometries. The results are exact agreement with the experimentally predicted modes using the electric probe measurement technique [173].

FDTD provides a simple and direct solution to various natural and caused problems. It can effectively model 3D complex geometry interacting with electromagnetic or acoustic-driven graphics and images ...



RELATIVE E-FIELD

DISTANCE ALONG LENGTH, Lp (MM)

DISTANCE ALONG WIDTH, Lp (MM)
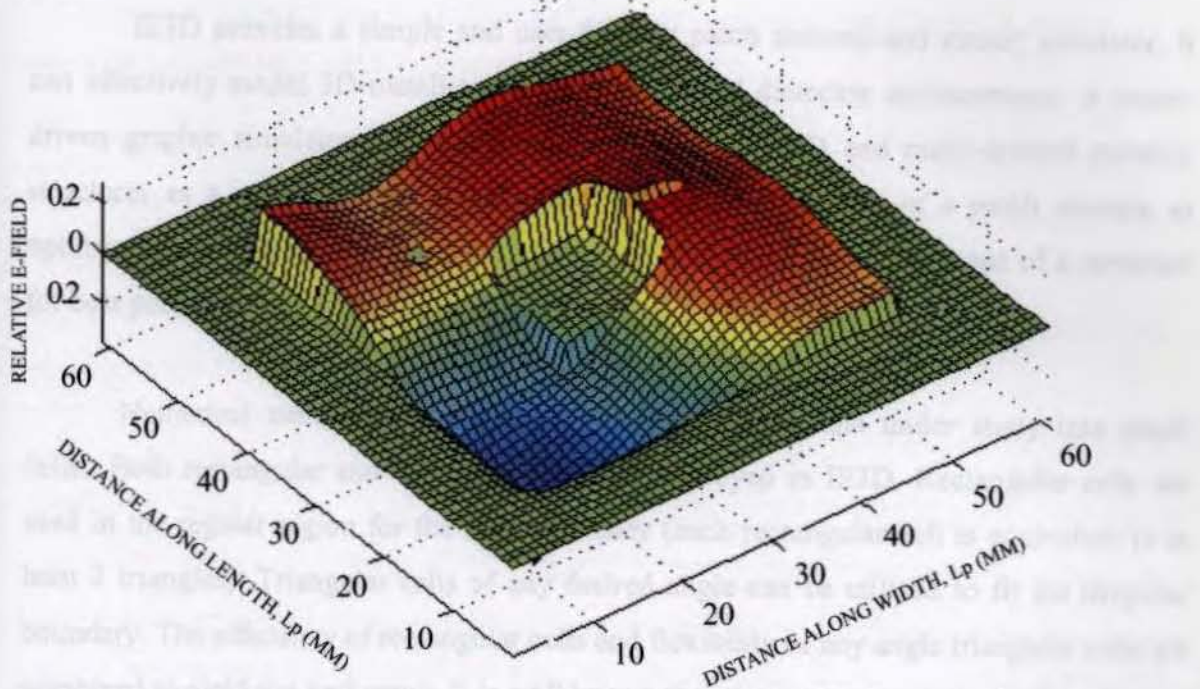
**Figure 5.11 (i)** *3-Dimensional Current Distribution on the surface of the Single Stub Microstrip Patch Antenna* $L_p$=*4cm,* $L_s$=*1.0cm,* $L_a$=*1.0cm* $W_a$=*0.2cm*



DISTANCE ALONG WIDTH, Lp (MM)

DISTANCE ALONG LENGTH, Lp (MM)
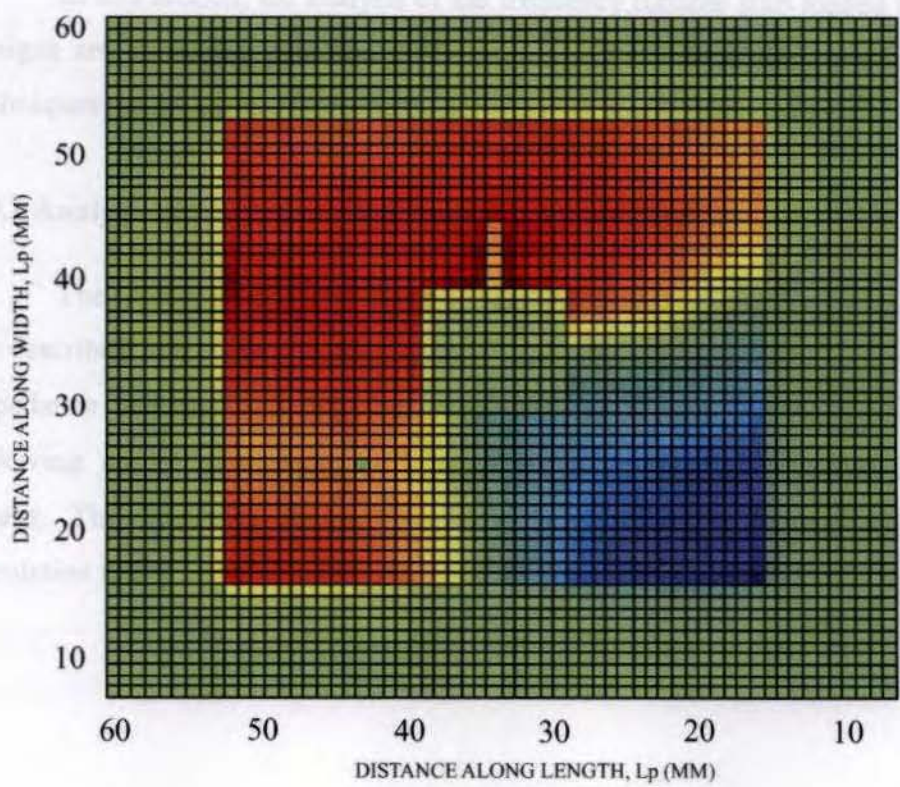
**Figure 5.11 (ii)** *2-D current Distribution in SSMA*

## 5.9 IE3D ELECTROMAGNETIC SIMULATION: MODELING AND ANALYSIS

IE3D provides a simple and user-friendly patch antenna and circuit simulator. It can effectively model 3D metallic structures in layered dielectric environments. A menu-driven graphic simulator allows interactive assembly of 3D and multi-layered metallic structures as a set of polygons. IE3D allows defining the shape of a patch antenna as optimization variables. The built-in optimizer is able to optimize the shape of a structure for best performance.

Numerical simulation requires sub-dividing the antenna under study into small cells. Both rectangular and triangular cells are employed in IE3D. Rectangular cells are used in the regular region for the best efficiency (each rectangular cell is equivalent to at least 2 triangles). Triangular cells of any desired angle can be utilized to fit the irregular boundary. The efficiency of rectangular cells and flexibility of any angle triangular cells are combined to yield the best result. It is well known that current concentrates on the edges of metallic strips. Precise modeling of the high current concentration along the edges is critical to accurate simulation of printed circuits. The simulator programming has been explained in detail with figures in Chapter III.

In this section, the analysis of the frequency tunable stub loaded microstrip antenna designs are simulated with the IE3D electromagnetic modelling results. The simulation techniques are mentioned elsewhere in chapter III.

### 5.9.1 Analysis of Single Stub Microstrip Antenna (SSMA)

The SSMA is simulated using IE3D. The simulation procedure and its various steps are described in the methodology chapter. The tool can be used to analyse the return loss, impedance variation and radiation pattern of the Single Stub Microstrip Antenna. The following section illustrates the comparison between the simulated and experimental results. The frequency tuning technique developed here is also validated using the simulation tool.

## 5.9.1.1 Resonant Frequency variation with respect to Central Slot length 'Ls' and Stub Arm Length 'L$_a$' – Simulation Results

The antenna dimensions L$_P$, L$_S$, L$_a$ and W$_a$ are properly selected and typical designs are analysed. The present design has been simulated using the IE3D and the results of the simulation are compared with the experimental results as shown in Table 5.4.

*Table 5.4 Simulated and Measured resonance frequency Comparison for the Novel Single Stub Microstrip Antenna L$_P$=4 cm, W$_a$=0.2 cm*

| L$_s$, L$_a$ (cm) | h (cm) | $\varepsilon_r$ | TM$_{10}$ mode frequency (f$_1$) (GHz) | | TM$_{01}$ mode frequency (f$_2$) (GHz) | |
|---|---|---|---|---|---|---|
| | | | Measured | Simulated | Measured | Simulated |
| 0.8,0.2 | 0.16 | 4.28 | 1.525 | 1.528 | 1.631 | 1.6399 |
| 0.8,0.4 | 0.16 | 4.28 | 1.514 | 1.5229 | 1.627 | 1.637 |
| 0.8,0.6 | 0.16 | 4.28 | 1.472 | 1.493 | 1.623 | 1.6345 |
| 0.8,0.8 | 0.16 | 4.28 | 1.463 | 1.4705 | 1.622 | 1.634 |
| 0.8,1.0 | 0.16 | 4.28 | 1.443 | 1.454 | 1.620 | 1.641 |
| 0.8,1.2 | 0.16 | 4.28 | 1.426 | 1.4305 | 1.617 | 1.638 |
| 1.0,0.2 | 0.16 | 4.28 | 1.507 | 1.5132 | 1.622 | 1.625 |
| 1.0,0.4 | 0.16 | 4.28 | 1.480 | 1.4842 | 1.614 | 1.622 |
| 1.0,0.6 | 0.16 | 4.28 | 1.450 | 1.4414 | 1.601 | 1.4738 |
| 1.0,0.8 | 0.16 | 4.28 | 1.433 | 1.447 | 1.597 | 1.5906 |
| 1.0,1.0 | 0.16 | 4.28 | 1.411 | 1.43 | 1.611 | 1.6081 |
| 1.0,1.2 | 0.16 | 4.28 | 1.390 | 1.387 | 1.604 | 1.618 |
| 1.2,0.2 | 0.16 | 4.28 | 1.487 | 1.4951 | 1.609 | 1.6139 |
| 1.2,0.4 | 0.16 | 4.28 | 1.459 | 1.4646 | 1.601 | 1.6098 |
| 1.2,0.6 | 0.16 | 4.28 | 1.441 | 1.454 | 1.589 | 1.6006 |
| 1.2,0.8 | 0.16 | 4.28 | 1.419 | 1.4218 | 1.578 | 1.601 |
| 1.2,1.0 | 0.16 | 4.28 | 1.407 | 1.4164 | 1.566 | 1.5716 |
| 1.2,1.2 | 0.16 | 4.28 | 1.387 | 1.392 | 1.558 | 1.567 |

The table shows good agreement with the simulated and experimental results. The results are verified in the same manner for different dielectric substrates having different thickness. The major achievement in this study is the design of a frequency-tuning stub. The simulation is also performed to verify the frequency tunability. The simulated and measured results for various stub lengths ($L_a$) of the single stub antenna for different combinations of $L_s$ are shown in figure 5.12.
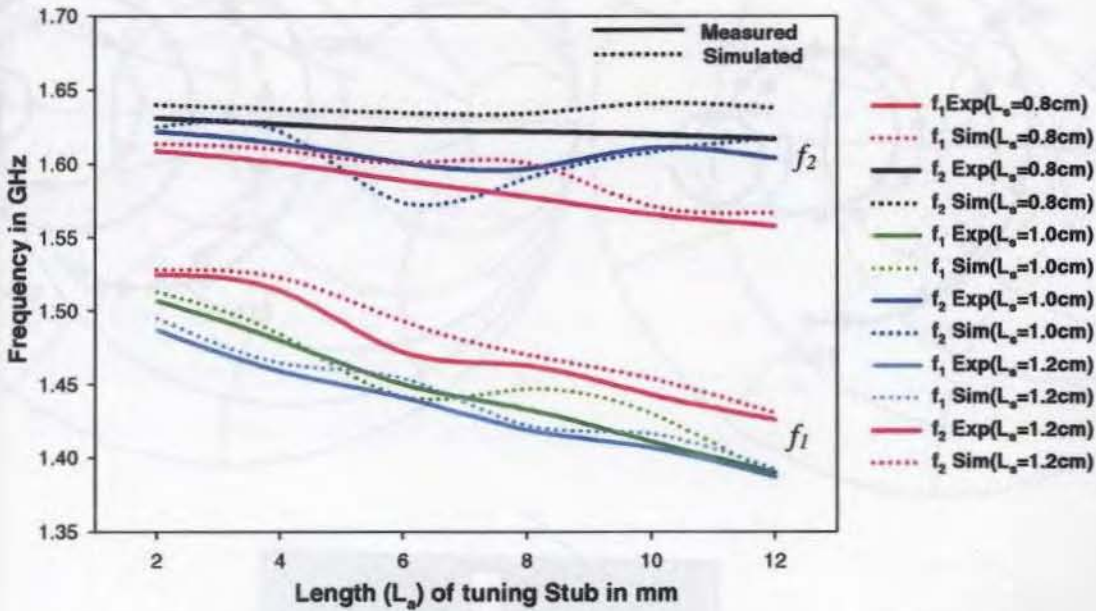


**Figure5.12** *Experimental and Simulated Results of the TM$_{10}$ and TM$_{01}$ resonance frequencies of the Single Stub Microstrip Antenna $L_p=4cm$, $W_a=0.2cm$*

By exciting the single stub slotted patch antenna, the desired mode can be generated. The input impedance also varies with location of the feed point. For the TM$_{10}$ mode (half wave variation of electric field along the side dimension of the patch), a variation of input impedance from a minimum value to a maximum value is observed, when the feed is moved along the diagonal. Figure 5.13 shows the impedance loci of a typical SSMA configuration with a coaxial feed along the diagonal line of the patch. Both the experimental and simulated results are included in the smith chart. In both cases it can be seen that the impedance at resonance varies from a minimum to a maximum value as we

move from the centre of the patch along the diagonal towards the edges. The frequencies are marked on the figures in MHz scale.
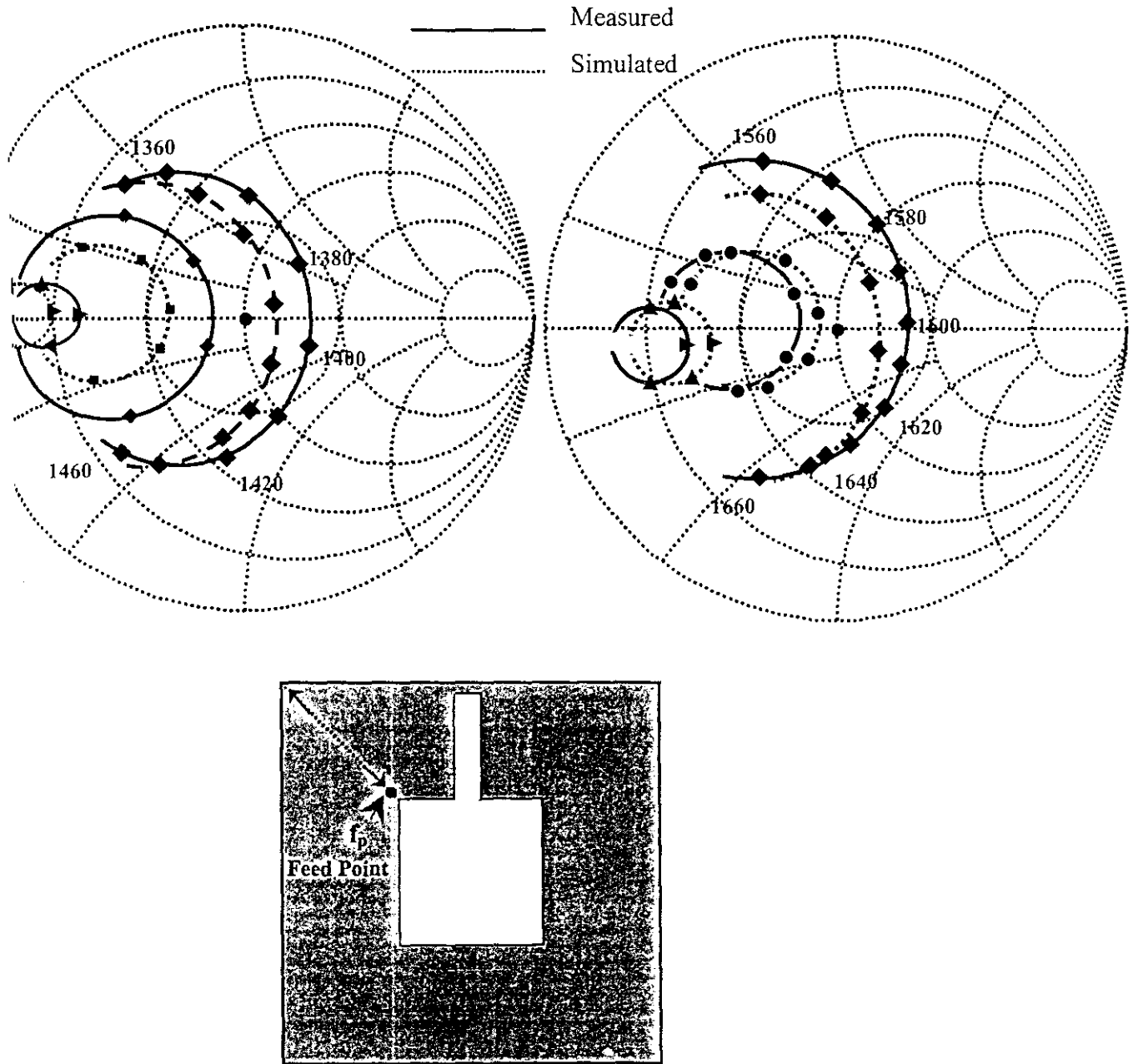


*Figure 5.13 Variation of input impedance with feed location for the $TM_{10}$ and $TM_{01}$ modes $L_p=4cm, L_s=1.0cm, L_a=1.0cm W_a=0.2cm$*

The proposed SSMA design excites two modes in its simulation analysis, in which one is the fundamental $TM_{10}$ mode, characterised by the stub arm parameters '$L_a$' and '$W_a$' and the $TM_{01}$ mode corresponding to the patch dimension 'Ls' and the central square slot length '$L_s$'. This frequency tuning antenna design provides a frequency ratio ($f_2/f_1$) of the two frequencies as low as 1.06, which makes the proposed antenna design suitable for applications where a low frequency ratio is required.

## 5.9.1.2 Radiation Pattern Simulation

The radiation characteristics of the SSMA have been simulated using IE3D and it is compared with the experimentally obtained radiation patterns. Figure 5.14 represents the simulated and the corresponding measured radiation patterns for a typical SSMA configuration. The beam width along the E and H planes at 1.61 GHz are 112 and $82^0$ respectively; the corresponding values at 1.41 GHz are 124 and $88^0$, respectively. Bandwidths of 1.8 and 2.1 % respectively, have been obtained in the two bands. The radiation pattern is plotted for various stub lengths for comparison and it is observed that in all cases the antenna offers good cross-polarization characteristics.
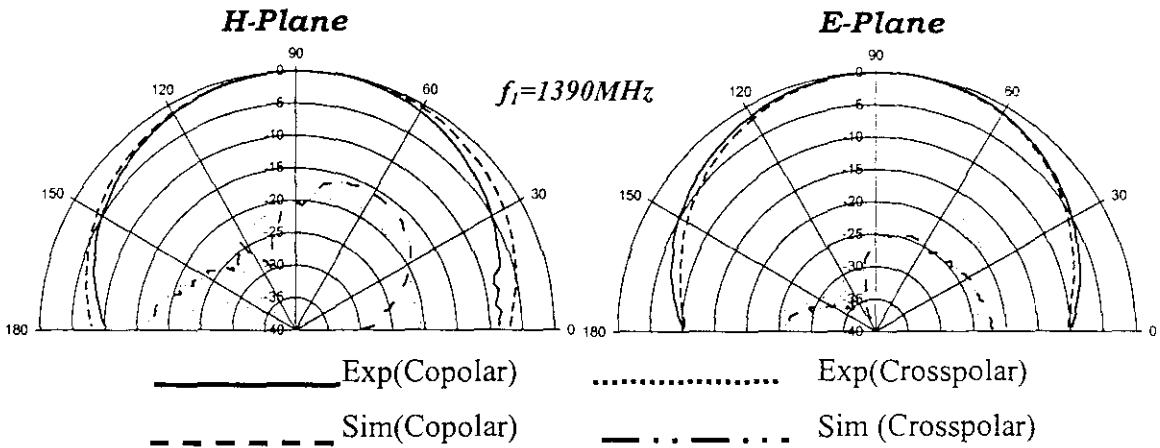


*Fig 5.14(i) Simulated and Experimental Radiation patterns of the Single Stub Microstrip Patch Antenna. $L_p$= 4 cm, $L_s$ = 1.2cm, $L_a$= 1.2cm*

H-Plan                    E-Plan

$f_2=1618MHz$

_____ Exp(Copolar)          .................... Exp(Crosspolar)

_ _ _ _ _ _ Sim(Copolar)      _ .. _ _ ... Sim (Crosspolar)
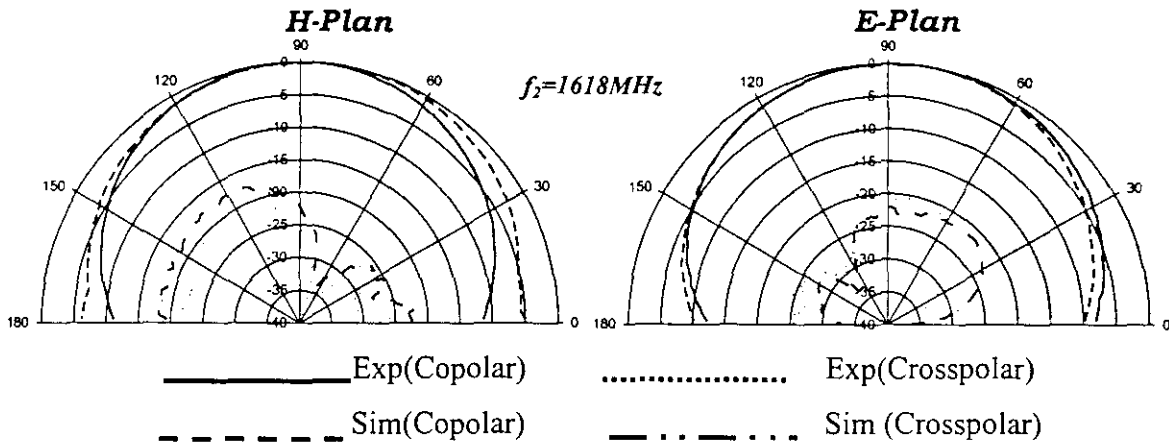
*Fig 5.14(ii) Simulated and Experimental Radiation patterns of the Single Stub Microstrip Patch Antenna. $L_p$ = 4 cm, $L_s$ = 1.2cm, $L_a$ = 1.2cm*

## 5.9.2 Analysis of Dual Stub Microstrip Antenna (DSMA)

An effective approach, to increase the electric length by optimizing the shape of the microstrip antenna so that its size can be reduced for a given frequency, has been dealt in this dual stub design. After realizing the significance of the tuning stub in the frequency tuning characteristics, the investigations are extended by the dual stub geometry (DSMA). Recently, there has been an increased interest in minimizing microstrip antennas for their applications in mobile communications and monolithic microwave integrated circuits. Based, on the slot antenna theory, if the total length of the slot approximately equals half of the effective wavelength, it will resonate and produce radiation. The main objective of the extended dual stub arm simulation analysis is to enhance the patch area reduction without considerable reduction in antenna gain.

## 5.9.2.1 Resonant Frequency variation with respect to Central Slot length 'Ls' and Stub Arm Length 'La' – Simulation Results

The design is simulated for various antenna designs with different slot and stub parameters and the corresponding frequency variations are studied. The results are verified for both coaxial feeding and microstrip feeding. In both cases good matching is obtained between experimental and simulated results. It is also observed that the resonance

163

frequencies have reduced considerably with regard to the single stub microstrip antenna. The tuning stubs that make the frequency trimming possible caused the further area reduction. Table 5.5 illustrates the measured and simulated resonance frequency comparison of the Dual Stub Microstrip Antenna with coaxial feeding technique.

*Table 5.5* *Comparison of simulated and measured resonance frequencies of the DSMA* $L_p=4cm$, $W_a=0.2cm$

| $L_s$, $L_a$ (cm) | h (cm) | $\varepsilon_r$ | $TM_{10}$ mode frequency $(f_1)$ (GHz) | | $TM_{01}$ mode frequency $(f_2)$ (GHz) | |
|---|---|---|---|---|---|---|
| | | | Measured | Simulated | Measured | Simulated |
| 0.8,0.2 | 0.16 | 4.28 | 1.525 | 1.528 | 1.631 | 1.6399 |
| 0.8,0.4 | 0.16 | 4.28 | 1.514 | 1.5229 | 1.627 | 1.637 |
| 0.8,0.6 | 0.16 | 4.28 | 1.472 | 1.493 | 1.623 | 1.6345 |
| 0.8,0.8 | 0.16 | 4.28 | 1.463 | 1.4705 | 1.622 | 1.634 |
| 0.8,1.0 | 0.16 | 4.28 | 1.443 | 1.454 | 1.620 | 1.641 |
| 0.8,1.2 | 0.16 | 4.28 | 1.426 | 1.4305 | 1.617 | 1.638 |
| 1.0,0.2 | 0.16 | 4.28 | 1.507 | 1.5132 | 1.622 | 1.625 |
| 1.0,0.4 | 0.16 | 4.28 | 1.480 | 1.4842 | 1.614 | 1.622 |
| 1.0,0.6 | 0.16 | 4.28 | 1.450 | 1.4414 | 1.601 | 1.4738 |
| 1.0,0.8 | 0.16 | 4.28 | 1.433 | 1.447 | 1.597 | 1.5906 |
| 1.0,1.0 | 0.16 | 4.28 | 1.411 | 1.43 | 1.611 | 1.6081 |
| 1.0,1.2 | 0.16 | 4.28 | 1.390 | 1.387 | 1.604 | 1.618 |
| 1.2,0.2 | 0.16 | 4.28 | 1.487 | 1.4951 | 1.609 | 1.6139 |
| 1.2,0.4 | 0.16 | 4.28 | 1.459 | 1.4646 | 1.601 | 1.6098 |
| 1.2,0.6 | 0.16 | 4.28 | 1.441 | 1.454 | 1.589 | 1.6006 |
| 1.2,0.8 | 0.16 | 4.28 | 1.419 | 1.4218 | 1.578 | 1.601 |
| 1.2,1.0 | 0.16 | 4.28 | 1.407 | 1.4164 | 1.566 | 1.5716 |
| 1.2,1.2 | 0.16 | 4.28 | 1.387 | 1.392 | 1.558 | 1.567 |

Table 5.5 shows good agreement between the simulated and experimental resonance frequencies. The characteristics of frequency tunability of the antenna is also be verified using this electromagnetic modelling tool. A graph showing the experimental and simulated resonance with respect to stub arm length ($L_a$) for various central slot lengths ($L_s$) are shown in figure 5.15. The frequencies are marked on the smith chart in MHz scale.
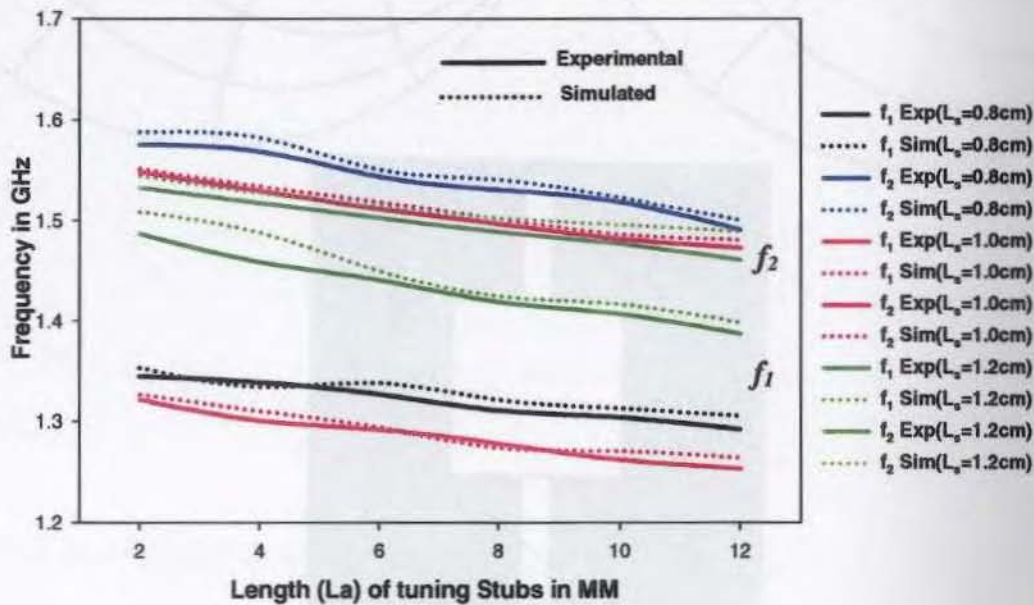


***Figure 5.15*** *Experimental and Simulated Results of the resonance frequencies of the Dual Stub Microstrip Antenna $L_p=4cm$, $W_a=0.2cm$*

The impedance characteristics of the dual stub antenna have been simulated using IE3D and it is experimentally verified using the HP 8510C vector network analyser. The feed point can be either coaxial or microstrip. Figure 5.16 illustrates experimental and simulated impedance loci of a typical Dual Stub Antenna design with a coaxial type feeding along the diagonal line of the patch.
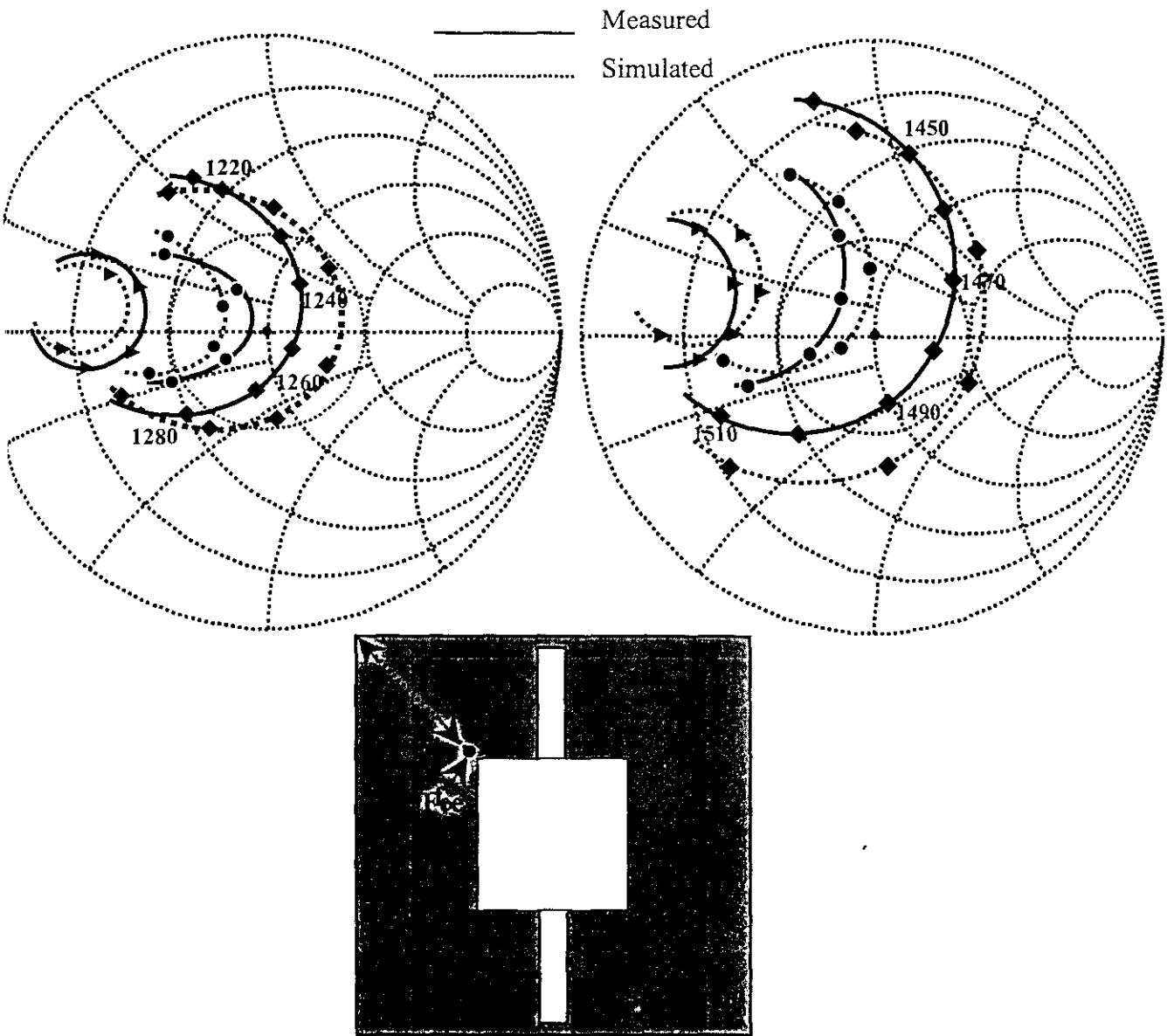
*Figure 5.16 Variation of input impedance with feed location for the $TM_{01}$ and $TM_{10}$ modes $L_p=4cm, L_s=1.0cm, L_a=1.0cm\ W_a=0.2cm, h=0.16cm, \varepsilon_r=4.28$*

## 5.9.2.2 Radiation Pattern

The radiation characteristics of the proposed SSMA has been simulated using IE3D and an antenna of the same physical dimensions is fabricated and tested using the automatic radiation pattern measurement set-up. Figure 5.17 illustrates the IE3D simulated and experimentally measured radiation patterns for the antenna.

166

| | |
|---|---|
| —————— Exp(Copolar) | ·············· Exp(Crosspolar) |
| — — — — — Sim(Copolar) | — ·· — ··· Sim(Crosspolar) |
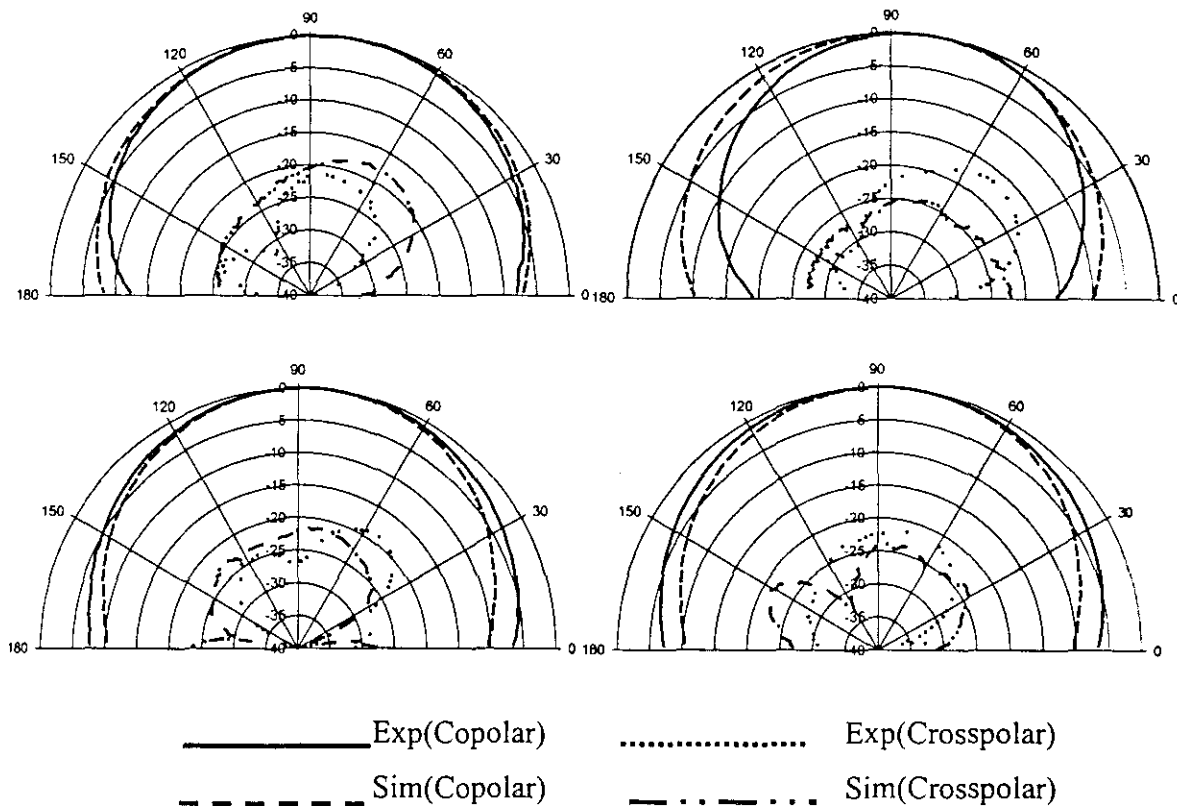
*Fig 5.17* Simulated and experimental Radiation patterns of a typical design of the DSM Antenna $L_p$ = 4.0 cm, $L_s$ = 0.8 cm, $L_a$=1.0 cm, $W_a$= 0.2 cm

## 5.9.3 Analysis of the Three Stub Microstrip Antenna (TSMA)

The three stub Microstrip antenna also has been extensively studied using both simulation and experimental techniques. IE3D is an Electromagnetic simulator that computes the effects of the electrostatic and electromagnetic fields of the metallic patch. The S-parameters of the proposed geometry has been analyzed extensively using this technique.

**5.9.3.1 Resonant Frequency variation with respect to Central Slot length 'Ls' Stub Arm Length 'L$_a$' – Simulation Results**

The Three Stub Microstrip Antenna (TSMA) design provides enhanced area reduction features in comparison to the SSMA and DSMA designs at the cost of nominal reduction in antenna gain. The patch is simulated using IE3D package for various combinations of the antenna dimensions to verify the significance of the three uniform stubs in frequency tuning. The frequency tunability of the antenna is also verified using the IE3D modeling.

This design is providing an enhanced patch area reduction, which is having several advantages in communication systems where compact antenna systems are required for reducing the overall dimension of the system.

The simulated and measured return loss characteristics are compared in figure 5.18 for a typical antenna design, that reveals the exact matching between the simulated and experimental results.
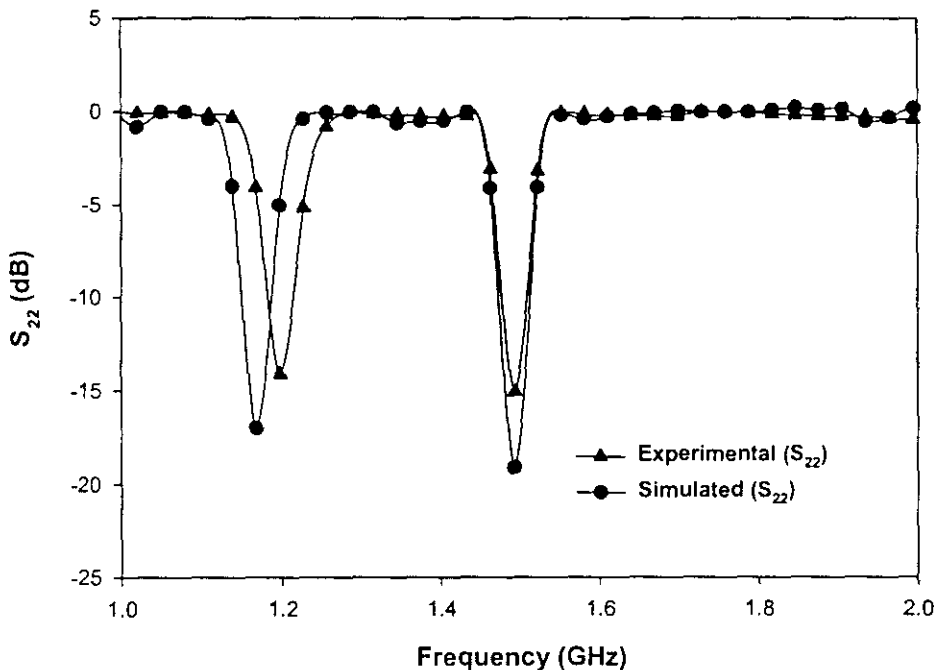


*Figure 5.18* Comparison of Simulated and Measured Return Loss curves of the Three Stub Microstrip Antenna (TSMA)  $L_s=4cm, L_s=1cm, L_a=1cm, W_a=0.2cm$

The characteristic input impedance of the new TSM antenna is analyzed. This antenna is also capable of sufficient impedance matching at both operating frequencies with a single feed position. The smith chart showing the input impedance variation shown in figure 5.19 reveals that if the feed position is fixed, the antenna with a larger slot dimension has larger input impedance. i.e., as the slot length increases, the feed position for impedance matching needs to be moved toward the centre of the patch along the diagonal of the patch.
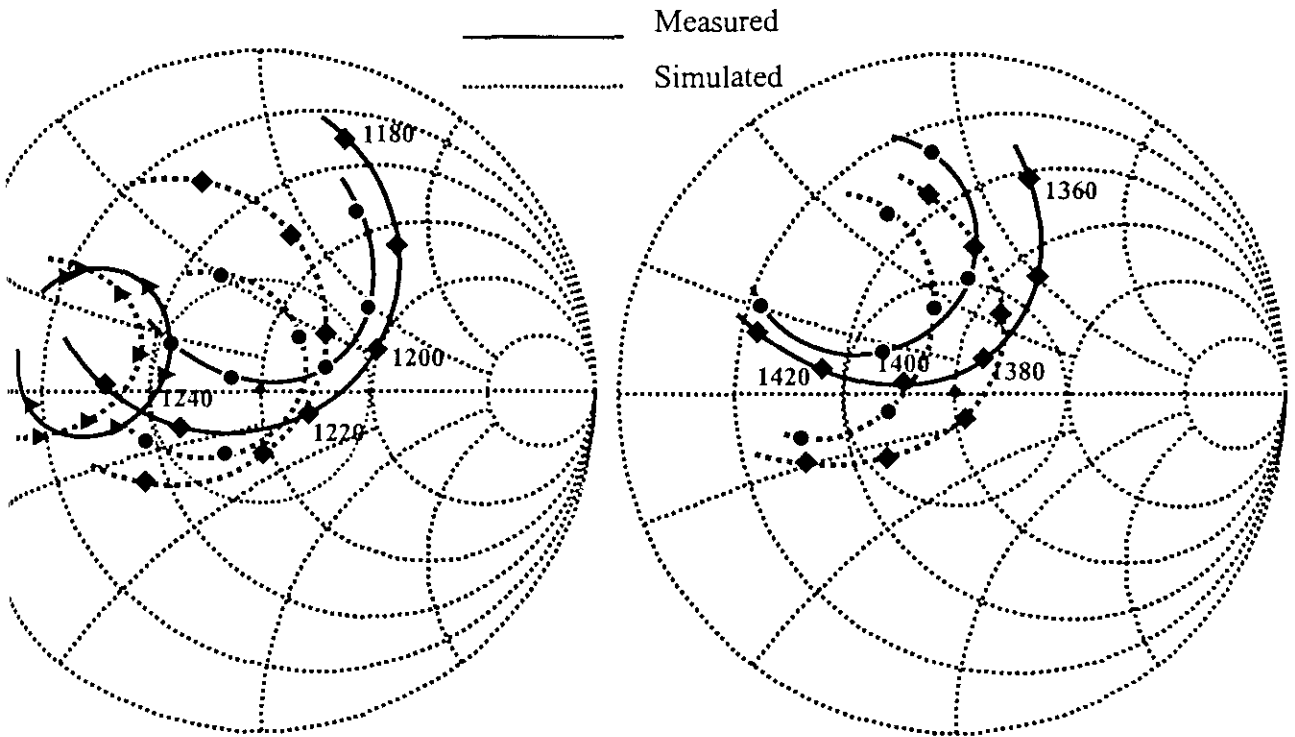


*Figure 5.19 Variation of input impedance with feed location for the TM$_{01}$ and TM$_{10}$ modes L$_s$=4cm,L$_s$=1cm,L$_a$=1cm,W$_a$=0.2cm,h=0.16cm, $\varepsilon_r$=4.28*

## 5.9.3.2 Radiation Pattern

IE3D can model probe-fed antennas accurately and efficiently. Here, the triple stub antenna radiation pattern is simulated using the IE3D tool and verified in comparison to the measured pattern at the two resonance frequencies.

The measured and simulated co-polar and cross-polar pattern at the corresponding central frequencies of a typical configuration is plotted in figure 5.20. The TSMA simulated and measured antenna radiation pattern comparison reveals good agreement in cross-polar level that has already been demonstrated in the section 4.3.2.3 of the experimental chapter.
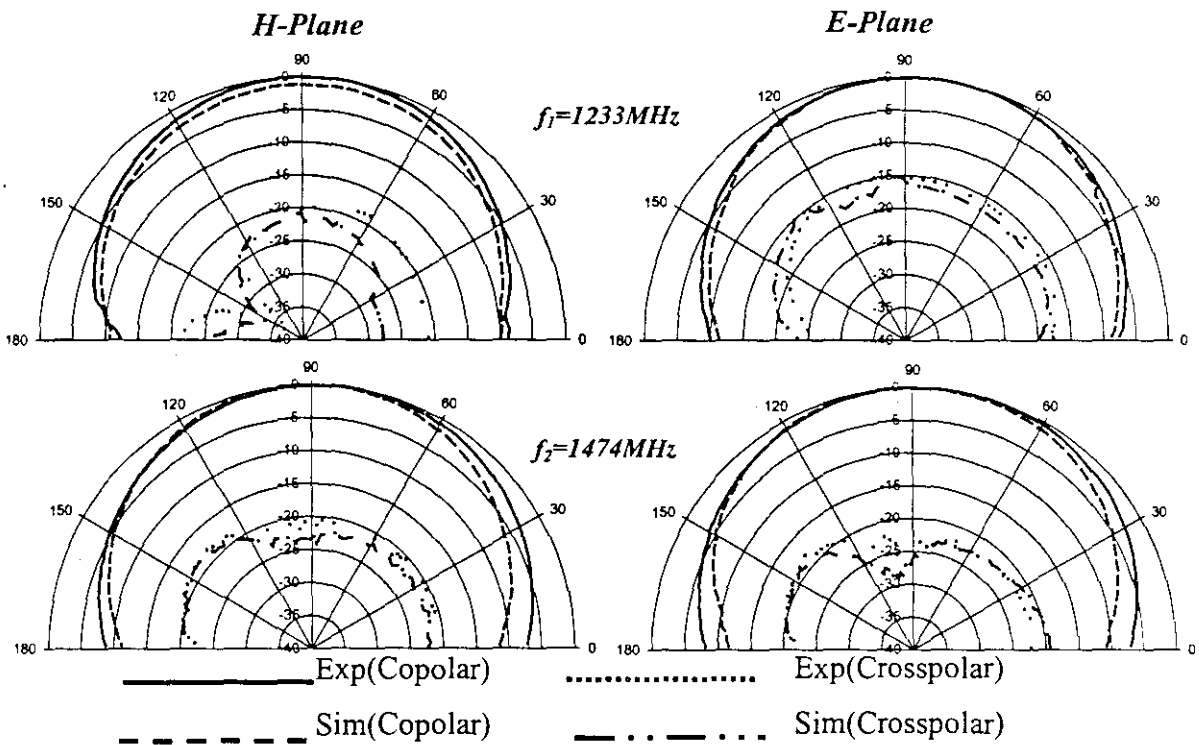


*Fig 5.20 The simulated and experimental Radiation patterns of a typical design of the Triple stub slotted Patch Antenna* $L_p$= 4.0cm, $L_s$ = 0.8cm, $L_a$=1.0cm, $W_a$= 0.2cm

## 5.9.4 Analysis of FSMA

The IE3D simulation results of the FSMA geometry have been discussed in this section.

The design has been simulated using IE3D for various combinations of $L_S$, $L_{a1}$ and $L_{a2}$, which are the key dimensions found to be capable of sufficient frequency trimming.

Table 5.4 gives a comparison between the experimental and simulated resonance frequencies of the FSMA.

*Table 5.4 FSMA-Comparison of Simulation and Experimental Results*

| $L_P, L_S$, Wa (cm) | h (cm) | $L_{a1}, L_{a2}$ | $TM_{10}$ mode frequency ($f_1$) (GHz) | | $TM_{01}$ mode frequency ($f_2$) (GHz) | |
|---|---|---|---|---|---|---|
| | | | Measured | Simulated | Measured | Simulated |
| 4,1.0, 0.2 | 0.16 | 0.8,0.4 | 1.18 | 1.17 | 1.374 | 1.38 |
| 4,1.2, 0.2 | 0.16 | 1.0,0.5 | 1.139 | 1.146 | 1.368 | 1.378 |

Table reveals that the simulation and experimental results are in close agreement. Since the antenna gain is considerably reduced due to the enhanced increased patch area reduction, the antenna suffers certain practical limitations. This operational disadvantage regarding the gain of the antenna has been introduced in section 4.4.2 in the experimental discussions.

The new slot loaded microstrip antenna has been analyzed for specific antenna characteristics, which are resonance frequency, mode of operation, field distribution along periphery, radiation pattern, input impedance etc. The different antenna configurations are treated with FDTD method and the results obtained are in compared with experimental results. Excellent agreement is achieved between the theoretical calculations and the experimental results.
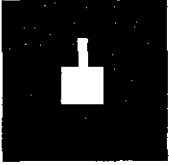
# CONCLUSIONS

*Outcome of the analysis performed on novel slotted microstrip patch antennas resonating at two frequencies and providing orthogonal polarisations is discussed. The conclusions drawn from the experimental and theoretical investigations carried out on these compact microstrip antennas are presented here. Suggestions for further work on these antennas are also suggested.*

## 6.1    INFERENCES FROM EXPERIMENTAL INVESTIGATIONS

Detailed analysis of the four types (SSMA, DSMA, TSMA, FSMA) of stub loaded patch antennas has been carried out. The objective of the study is to design a frequency tuning technique by employing slotted stubs in the square patch antenna. As there is no overall increase in patch size, miniaturisation of the antenna has been achieved through this frequency tuning method. From the comprehensive experimental investigations, it is found that the stub loaded slotted antenna is resonating at two lower frequencies compared to standard square microstrip patch antenna.

The design of SSMA consists of a square slot with an extended stub arm inserted in a square patch. The stub arm is identified to be the key element of the structure, determining the antenna resonance characteristics and range of dual frequency operation. The tuning stub is characterised by its length 'L$_a$' and width 'W$_a$', which play a crucial role in the frequency tunability of the antenna. The antenna is simulated using IE3D initially. The optimum designs were fabricated and verified experimentally. From the simulated and experimental results, the antenna is found to have a dual frequency, dual polarized nature with good cross-polar levels at both the resonance frequencies. The frequency ratio can be varied substantially by adjusting the stub arm parameters. The dual resonance frequencies of the Single Stub Microstrip Antenna (SSMA) are found to be decreasing with the stub arm length 'L$_a$'. The two resonant modes excited in the patch are TM$_{10}$ and TM$_{01}$ modes. By varying 'L$_a$', the TM$_{10}$ frequency lowers appreciably, and TM$_{01}$ mode frequency remains almost unaffected as evident from figure 4.4. The length 'La' is systematically varied to analyse the frequency tuning capability of the antenna. Studies were also conducted by varying the size of the square patch 'L$_P$'. The effect of variations in central slot width 'L$_S$' and stub width 'W$_a$' on antenna resonance frequency is also investigated. The studies conducted by selecting substrates of different dielectric constant and thickness establish that in this design, both the resonant frequencies decreases with increase in the dielectric constant and thickness.

From the study it is clear that the SSMA operating at the TM$_{10}$ and TM$_{01}$ frequencies requires less area compared to an equivalent standard rectangular patch antennas operating at the corresponding frequencies and fabricated on the same substrate. The antenna provides an area reduction of ~50 % for the TM$_{10}$ frequency and 36 % for the TM$_{01}$ frequency.

The detailed study of the antenna radiation pattern indicates that the antenna has 3 dB beam width and cross-polar level similar to those of rectangular patch antennas. The cross-polar level in most of the cases is found to be better than 15 dB. The impedance bandwidth is also comparable to that of the standard rectangular patch. Gain of the antenna shows a slight reduction of ~1.4 dB compared to the gain of an equivalent rectangular patch fabricated on the same dielectric substrate.

In the Dual Stub Microstrip Antenna (DSMA) one more stub arm is introduced for further studies. The geometry has been simulated using IE3D design and the occurrence of dual resonance is verified experimentally. Here, the pair of stub arms is playing a crucial role in the frequency tuning technique and patch area reduction. The DSMA design has further reduced the patch area as can be seen from its resonance frequency characteristics. Typical DSMA provides two frequencies providing a patch area reduction of 61 % and 45 % compared to the equivalent rectangular patches operating at the corresponding frequencies and fabricated on the same substrate.

Gain of DSMA shows a slight reduction of ~1.7 dB compared to the gain of an equivalent rectangular patch. The radiation pattern of the DSMA exhibits a good cross-polar level, better than 20 dB.

A third stub arm, which is placed at right angles to the existing dual stub, in TSMA further reduces the resonant frequencies. The typical TSMA excites two lower frequencies providing an area reduction of 64 % and 52 % respectively in comparison to standard rectangular patch antennas operating at the same frequencies. The $S_{21}$ studies of the TSMA antenna reveal the orthogonal polarisation nature of this design.

Incorporation of one more stub to the TSMA geometry results in a Four Stub Microstrip Antenna (FSMA), which has some operational disadvantages regarding its gain due to the considerable reduction in the metallic patch area.

By inserting high performance surface mountable chip-capacitors to the above designs, extended dual frequency tuning is possible.

In the Capacitor Mounted Single Stub Microstrip Antenna (CSSMA), analysis of the variation in resonance characteristics for different capacitor mounting indicates a further reduction in resonance frequencies and patch area. Patch area reduction of 64 % and 36 % has been achieved for the two resonant modes. The analysis indicates that the capacitor loading has extended the frequency tuning to a lower frequency band. Further frequency tuning is possible by adjusting the stub arm parameters.

The cross-polar level in CSSMA is found to be better than 20 dB, which is appreciably good in comparison to the SSMA design. The design also exhibits orthogonal polarisation.

The analysis of chip-Capacitor mounted DSMA (CDSMA) shows that considerable frequency tuning can be achieved. Figure 4.35 illustrates the reduction in resonance frequency of the CDMSA in comparison to DSMA as well as with an equivalent rectangular patch antenna. The comparison shows a reduction in patch area by 66 % and 46 % for the $TM_{10}$ and $TM_{01}$ modes. Here also, resonance frequency tuning is influenced by the value of the capacitor as well as the stub arm parameters. The study of the radiation characteristics reveals that the antenna gain has nominal reduction as a result of capacitor loading.

The TSMA design incorporated with the Capacitor (CTSMA) loading provides further reduction in resonance frequencies.Considerable frequency trimming is possible by adjusting the capacitor values as well as the tuning stub parameters. The characteristics of this CTSMA is portrayed in figure 4.40 for a comparison with TSMA and an equivalent rectangular patch.

## 6.2 INFERENCES FROM THEORETICAL INVESTIGATIONS

A method based on the finite difference time-domain (FDTD) technique is used for the analysis of the SSMA, DSMA, TSMA and FSMA antenna configurations. The analysis

computes the resonance frequency and electric field variation along the periphery of the patch. An FDTD code that can be used for calculating the scattering parameters as well as the current and field distribution over the surface and edges is developed. The resonance characteristics of the SSMA, DSMA and TSMA designs and their comparison with experimental results are given in Table 5.1, 5.2 and 5.3 respectively. Both the experimental and theoretical results are in good agreement with error only less than one percentage. This error can be attributed to the fabrication tolerances and non-homogeneity of the dielectric substrates. The field distribution across the periphery of the patch is simulated using the present theory. A typical 3-dimensional field variation obtained from the analysis of the SSMA design is shown in figure 5.11. From the nature of the field variation the mode of excitation of the antenna is identified. The analysis of the 3-D plot confirms the resonance modes evaluated using the electric probe measurement technique.

The SSMA, DSMA, TSMA and FSMA designs are also simulated using IE3D electromagnetic modelling tool and the results are presented in section 5.9.

The presence of the mode due to the field variation along the length of the patch is confirmed by measuring the electric field variation at the patch surface, at the corresponding resonance frequency. The probe measurements showed that there are two distinct resonant modes, ($TM_{10}$ and the $TM_{01}$) based on the current distribution. This result indicates the possibility of using this antenna as a dual frequency orthogonally polarized antenna.

The developed dual frequency dual polarised antenna can be used for personal and satellite communication applications. One of the main features, which qualifies this antenna to be used in such systems is its frequency reduction characteristics without increasing the physical dimension of the patch. The stub arm is identified as the key element in determining the antenna resonance characteristics and range of dual frequency operation.

A cross-polar level of better than −20 dB obtained for the orthogonal modes, $TM_{10}$ and $TM_{01}$, makes the antenna suitable in communication systems where a single compact patch antenna is used for both Transmission (Tx) and Reception (Rx). Chip-capacitor loading can effect a further enhancement in cross-polar levels up to −25 dB.

A significant advantage of this antenna is a versatile frequency tuning feature, which is effected by variations in the tuning stub parameters and mounting chip-capacitors.

## 6.3 SCOPE FOR FURTHER WORK

The stub loaded frequency tunable antennas finds applications in systems where a compact antenna that can excite dual resonance from a single radiating structure, is required.

The antenna geometry can be developed into an active array for satellite communication applications. By interconnecting higher value chip-capacitors and similar other active antenna elements, the range of operation can be extended to other bands also. This antenna can effectively replace conventional rectangular microstrip patch antennas in applications like phased arrays.

Capacitor mounted geometries can be incorporated in MMIC designs or in adaptive antenna elements for obtaining any desirable resonance frequency, impedance, polarisation, and pattern characteristics.

Like other microstrip antennas, this design also suffers from poor impedance bandwidth. The Bandwidth enhancement of this design would be an interesting topic for future work. It can be achieved by using shaped geometries or stacked configurations.

## Appendix A

## MEASUREMENT OF DIELECTRIC CONSTANT OF CERTAIN PLANAR DIELECTRIC MATERIALS USING FREE SPACE AND CAVITY PERTURBATION METHODS

### A.1 Introduction

The determination of dielectric constant is very significant in Ground penetrating Radar (GPR) studies.Generally free-space methods are considered suitable for frequencies in the microwave and millimeter wave region. Dielectric studies are of great significance in the present era of satellite communication. Wireless communication uses free space waves and its magnitude cane be deteriorated by the reflections from the atmosphere.

Free space methods are very popular for determining the dielectric properties because it has got wide operation frequency range extending up to the millimeter wave region. Component dimensions limit the operational freedom of the frequency analysis in other conventional methods. This method also provides a complete contact-less and non-destructive environment and also here the measurements can be performed even in strong magnetic and electric fields.

In transmission line methods, a sample of the dielectric material is placed either between the outer and inner conductor of a coaxial line or inside a waveguide. The sample when placed at the end of the waveguide may be terminated with either a short or some known impedance.

The HP 8510 C vector Network Analyzer is used for calibration in the $S_{21}$ mode for the analysis of the dielectric substrate. The change in reflected microwave power and the dielectric constant of the material is studied.

## A.2 Methodology and Theory

At microwave frequencies, a standing wave pattern will be developed along a transmission line when there is a load connected to it that is not equal to the line's characteristic impedance. The standing wave pattern is composed of the sum of the voltage wave incident on load $E_i$ and the voltage wave reflected form this load or device under test, $E_r$. At the load, the ratio of $E_r$ to $E_i$, and the phase angle between them are uniquely determined by the load impedance. This ratio, called the reflection coefficient is therefore a convenient measure of the deviation of the load impedance from the characteristic impedance.

$$\Gamma = \frac{Er}{Ei} = \rho \angle \phi$$

where $\rho$ is the magnitude and $\phi$ is the phase angle.

Bistatic method is implemented for studying the dielectric properties of materials. The experimental set showing the arrangement is shown in figure A-1. There two pyramidal horns are mounted on a stand in exact phase alignment with the substrate mount. The exact phase measurements can be obtained by electronically scanning for accurate phase matching of transmission lines used so the signals are in the correct phase relationships needed for proper system operation.

Automatic network analyzer methods can also be considered as transmission line methods because the sample is held in a transmission line and dielectric constant is determined by measuring the reflection and/or

transmission coefficient. The scattering parameters are measured with a vector network analyzer. (HP 8510 C) consisting of a synthesized sweeper and an S-parameter test set. The block diagram of the network analyzer and its function is given in Chapter 3.

## A.3 Bistatic Time Domain Methods

The bistatic time domain methods are modern techniques for the material characterization because of its widespread use in determination of dielectric constant at microwave frequencies.

Time Domain methods are broadly classified into two categories.

(a). Reflection methods

(b). Transmission methods

Reflection methods are basically used in electrical engineering for locating the faults in cables known as the "Time Domain Reflectometry". The measurement of reflection coefficient and the time delay gives the type and distance and of the fault from the secondary end. The reflection and transmission methods time domain techniques are collectively called "Time Domain Spectroscopy" (TDS). Time domain measurement methods have also been used for performing broad band measurement on filters, directional couplers, amplifiers and studying the electronic system response to lightning and EMP.

Although TDS is basically a time domain technique, the data is usually converted to the frequency domain using a Fast Fourier Transform (FFT) analysis.

The reflection/transmission measurements at different frequencies are carried out using HP 8510 C Network Analyzer The material (Acrylic sheet, FRP etc.) is mounted on a positioner. The transmitting and receiving antennas are mounted side by side with normal incidence to the sheet of material as depicted

in figure A-1. The antennas are then connected to the ports of the S – parameter set up which is interfaced with 8510C Network Analyzer and computer. Using time domain gating option of the Network Analyzer, the unwanted reflection can be fully eliminated.
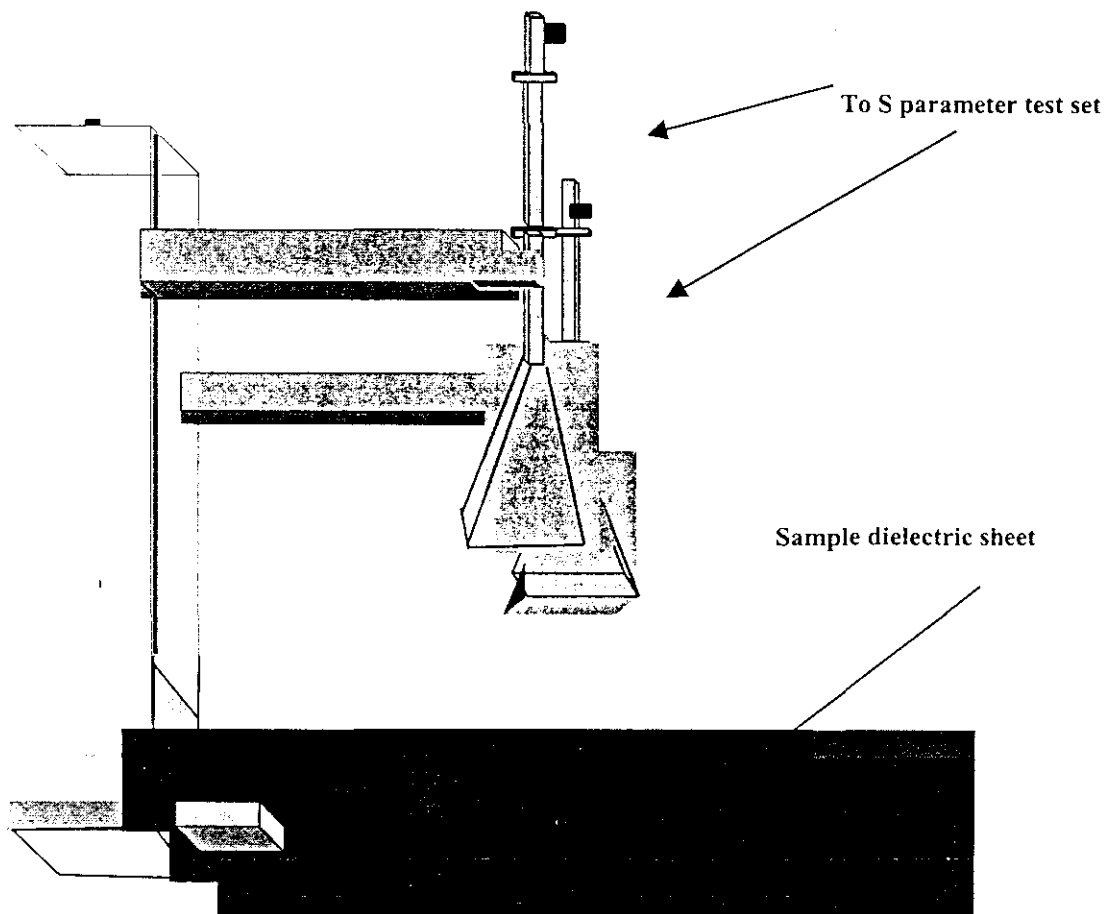


*Figure A-1. Experimental Set up to study the microwave reflection from various samples*

## A.4 Experimental Results

The investigations are mainly focused on the following studies:

1. Reflection studies of certain medium loss materials over the wide frequency band of 6 GHz to 18 GHz.

2. Dielectric studies of those materials in the S-Band using cavity resonator method.

The network analyzer is calibrated using the TMSO calibration technique described earlier for bistatic measurement and analysis. First the reflection response for wood in the C-band is calculated in the C-band. Horn. It was initially calibrated for the frequency range of 4.4 GHz to 8 GHz using standard techniques and the repeatability was confirmed. Later, the same methodology was adopted for the X and Ku bands and there frequency response is also analyzed . The frequency response, characteristics of wood, FRP and Acrylic is illustrated in A-2

The experiment is conducted for the entire frequency range from 6 to 18 GHz. For transmission of microwave power across these bands two horn antennas are utilized. So the small amounts mismatch of reflected power at the band endpoints is accounted owing to the horn dimension changeover.
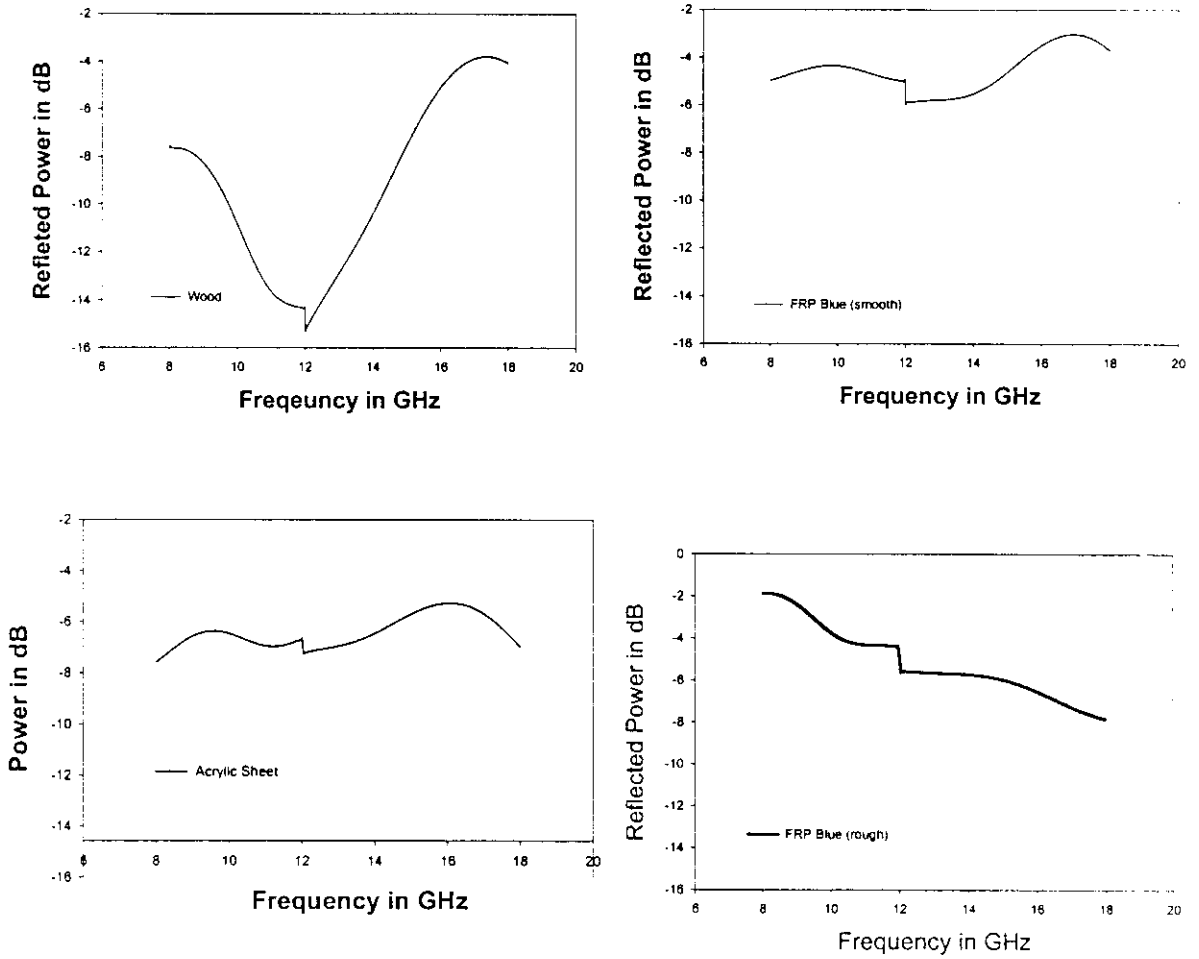
*Figure A-2* The frequency response curve showing the reflected power of the various substrates

## A.5 Measurement of Real and Imaginary parts of Complex Permittivity

The real and imaginary parts of the complex permittivity of the samples taken for reflection studies were measured using the cavity resonator technique. The method of measurement of complex permittivity based on the cavity perturbation technique is following the assumption that "the electric field in the perturbing sample is equal to the electric field of the empty cavity". The inner wall of the S-band cavity is silvered to reduce the wall losses. The resonator is of transmission type, since power is coupled into/out through separate irises.

The rectangular waveguide cavity resonator is connected to the two ports of the HP 8517B S parameter test set of the measuring system. The block diagram of the experimental set up is shown in figure A-3. An rectangular waveguide cavity is shown in figure A-4. In the cavity shown in figure, we can insert the sample of a specific dimension depicted below, and can be connected to the network analyzer.

```
+------------------------+        +------------------------+
|      HP 8341B          |        |      HP 8510 C         |
|   SWEEP OSCILLATOR     |--------|   NETWORK ANALYSER     |
+------------------------+        +------------------------+
            |
+------------------------+
|      HP 8517B          |
| S-PARAMETER TEST SET   |
+------------------------+
            |
+------------------------+
|   CAVITY RESONATOR     |
+------------------------+
```
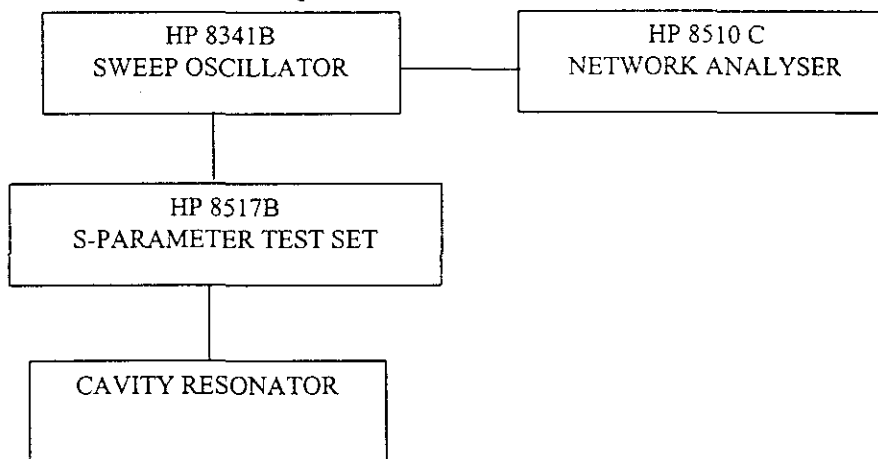
The procedure for determination of complex permittivity is described as follows.

1. The resonance frequency $f_t$ and unloaded Q-factor $Q_t$ of the cavity resonator are measured with the empty cavity resonator at the position of the maximum electric field.

2. The material is positioned at the maximum electric field . the resonance frequency $f_s$ and the loaded Quality factor $Q_s$ are measured.
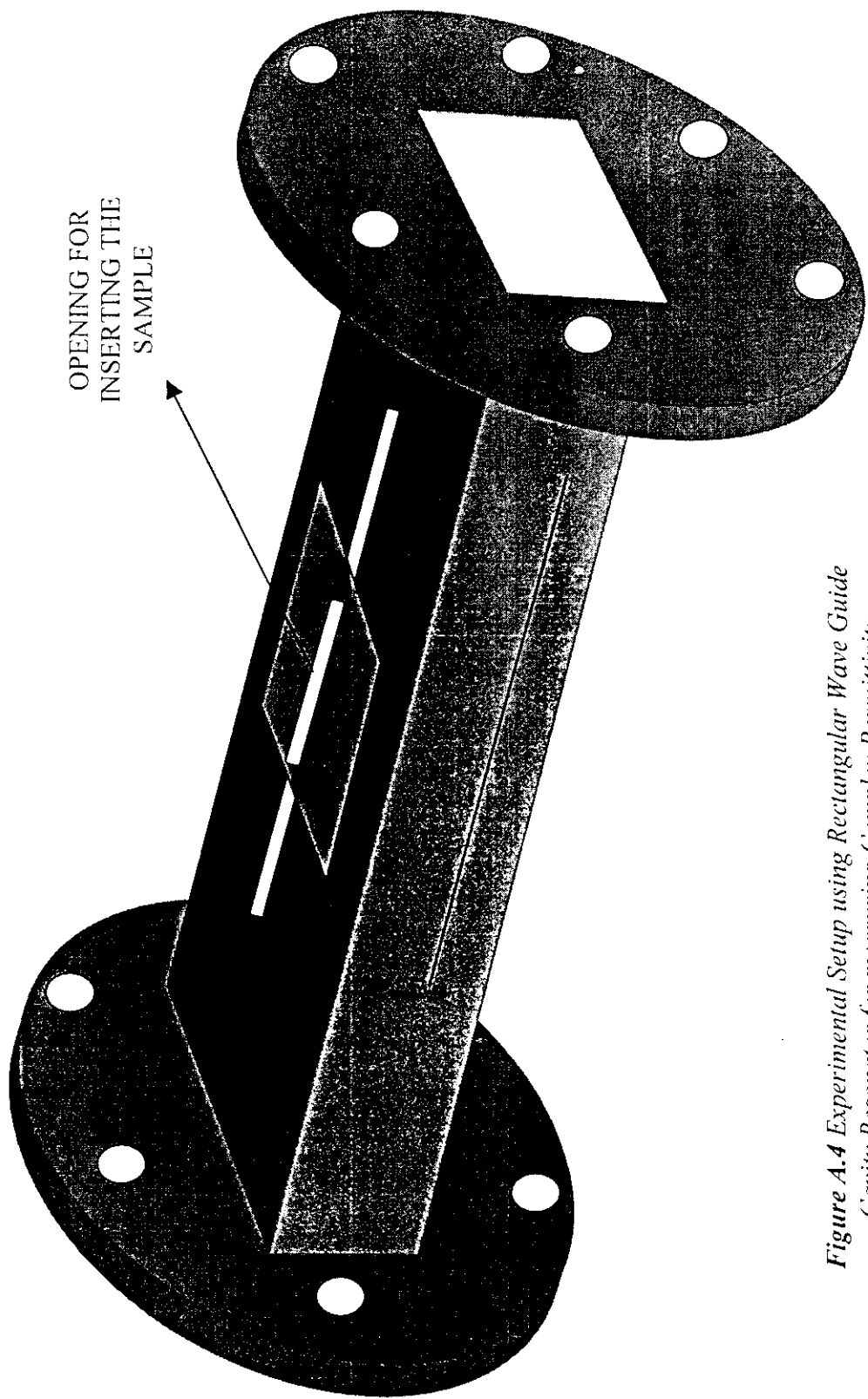
OPENING FOR
INSERTING THE
SAMPLE

*Figure A.4 Experimental Setup using Rectangular Wave Guide
Cavity Resonator for measuring Complex Permittivity*

3. Knowing the volume of the material inserted in to the cavity resonator the permittivity can be calculated.

The real part of permittivity $\varepsilon'_r$ is calculated as

$$\varepsilon'_r - 1 = \frac{(f_t - f_s)}{2f_s}\left[\frac{v_c}{v_s}\right]$$

the imaginary part is

$$\varepsilon''_r = \frac{v_c}{4v_s}\left[\frac{1}{Q_s} - \frac{1}{Q_t}\right]$$

where $v_c$ and $v_s$ are the volumes of the cavity and the sample respectively.

Dimension of the Samples used:

1.  Red FRP            :    Thickness – 1.33 mm, Breadth – 2mm

2.  Blue FRP           :    Thickness – 1.3 mm, Breadth – 2mm

3.  Green FRP          :    Thickness – 0.9 mm, Breadth – 2mm

4.  Transparent FTP    :    Thickness – 1.3 mm, Breadth – 2mm


The experiments were conducted for the S, C and X band cavities. Table A-1 illustrates the real and imaginary part of the dielectric constant corresponding to the various resonances in the S-band.

The real and imaginary part of dielectric constant is measured in the S, C and X cavities and it is plotted in figures A-5 (a) and (b).

*Table A-1 Real and Imaginary part of Dielectric Constant for various samples*

|          | Frequency | Real  | Imaginary | Loss |
|----------|-----------|-------|-----------|------|
| FRPBLUE  | 2.4405    | 4.100 | .213      | .052 |
|          | 2.6856    | 3.930 | .216      | .055 |
|          | 2.9719    | 3.953 | .239      | .060 |
|          | 3.2883    | 4.314 | .241      | .056 |
|          | 3.6266    | 4.255 | .303      | .071 |
| FRPTRANS | 2.4405    | 4.221 | .227      | .054 |
|          | 2.6856    | 4.161 | .229      | .055 |
|          | 2.9719    | 4.174 | .229      | .060 |
|          | 3.2883    | 4.347 | .254      | .058 |
|          | 3.6266    | 4.294 | .319      | .074 |
| FRPGREEN | 2.4405    | 4.058 | .231      | .057 |
|          | 2.6856    | 4.504 | .231      | .051 |
|          | 2.9719    | 4.275 | .256      | .060 |
|          | 3.2883    | 4.454 | .258      | .058 |
|          | 3.6266    | 4.400 | .323      | .073 |
| FRPRED   | 2.4405    | 3.649 | .210      | .058 |
|          | 2.6856    | 3.736 | .234      | .066 |
|          | 2.9719    | 3.571 | .234      | .066 |
|          | 3.2883    | 3.681 | .236      | .064 |
|          | 3.6266    | 3.593 | .296      | .082 |
| FRPBRWN  | 2.4405    | 4.059 | .177      | .044 |
|          | 2.6856    | 4.058 | .178      | .044 |
|          | 2.9719    | 3.931 | .198      | .050 |
|          | 3.2883    | 4.179 | .198      | .047 |
|          | 3.6266    | 4.157 | .248      | .060 |
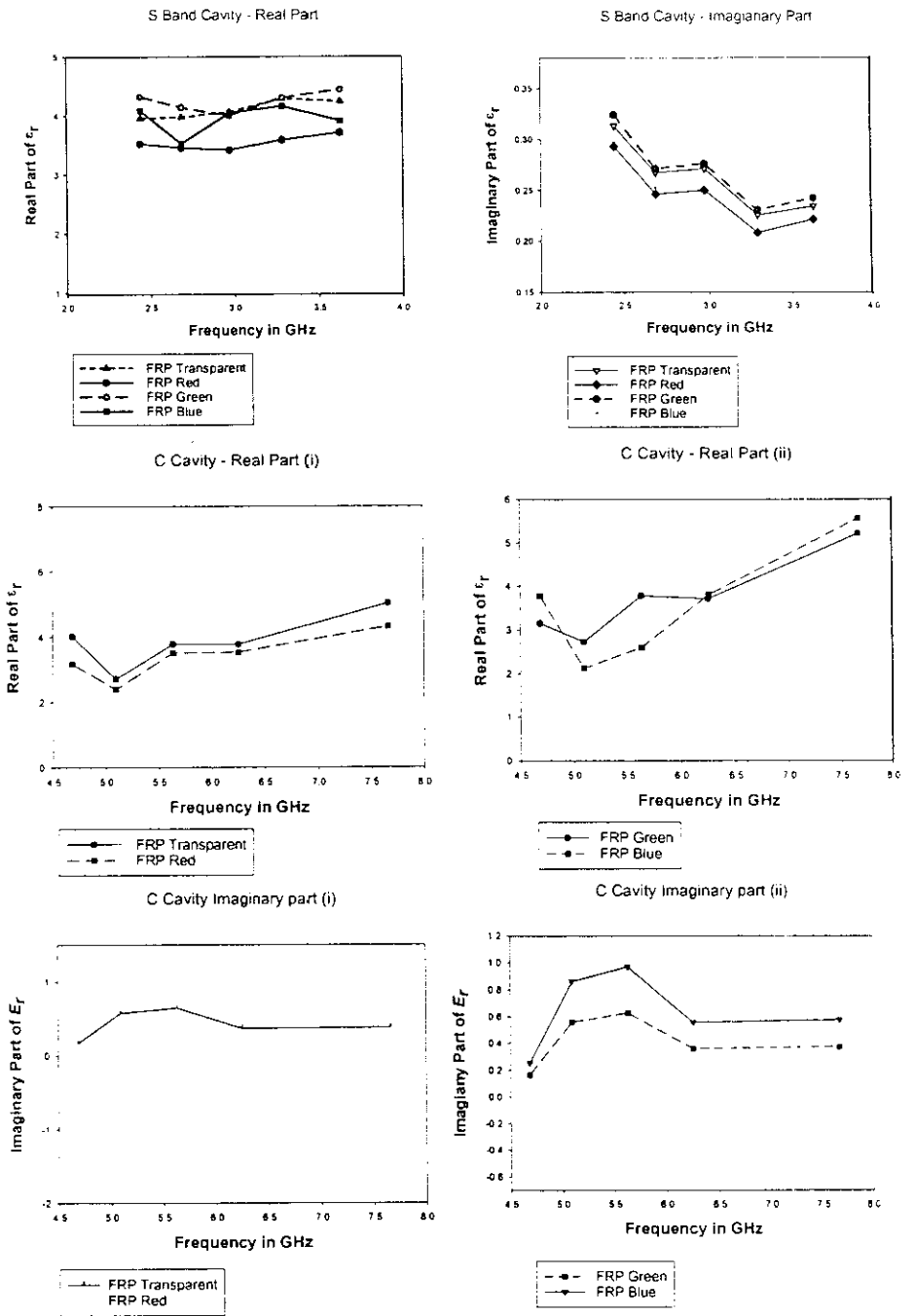
*Figure A-5 (a)* Real and Imaginary part of complex permittivity in the S and C bands
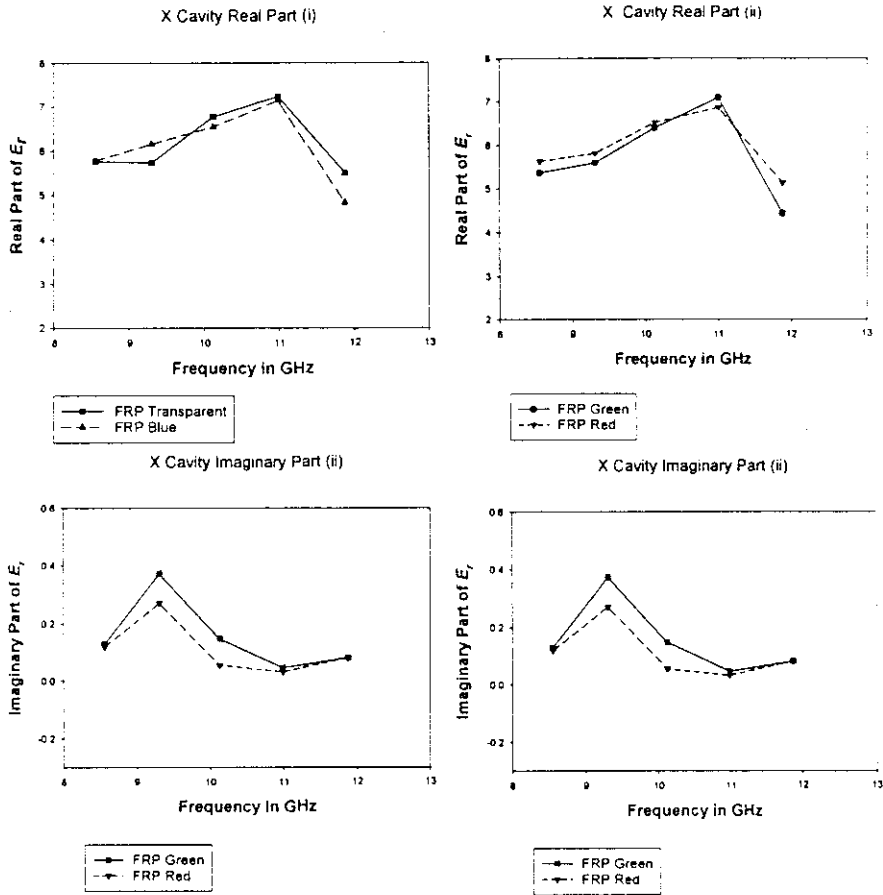
*Figure A-5 (b) Real and Imaginary part of complex permittivity in the X-band*

**Conclusion**

The study is aimed at analyzing the dielectric property of certain dielectric substrates. The reflected power from the dielectric samples and the real and imaginary part of the dielectric constant is presented for various frequency bands. Both time-domain and cavity perturbation techniques are employed for the measurements.

# REFERENCES

1. Taflove, A., *Computational Electrodynamics*. I ed, Boston: Artech House.

2. J.D.Kraus, *Antennas:Our Electronic Eyes & Years*. Microwave Journal, Jan 1989: p. 77-92.

3. C.A.Balanis, *Antenna Theory:Analysis and design*. Second ed. 1997, New York: John Wiley & sons Inc.

4. J.C.Bose, *On the Selective Conductivity and Exhibited by Certain Polarizing Substances*. Proc. of the Royal Society, 28 Jan1897. **LX**: p. 433-436.

5. J.D.Kraus, *Antennas*. Second ed. 1997: Tata MCGraw-Hill.

6. Deschamps, G.A. *Microstrip Microwave Antennas*. in *3rd USA symposium*. 1953.

7. Howell, J.Q. *Microstrip Antennas*. in *Intl. Symposium Antennas & Porpagation Soc*. 1972. WIlliamburg.

8. R.E.Munson, *Conformal Microstrip Antennas and Phased Arrays*. IEEE Trans. Antennas & propagation, 1974. **AP-22**: p. 74-77.

9. I.J.Bahl and P.Bhartia, *Microstrip Antennas*. 1980, Boston: Artech House.

10. J.R.James and P.S.Hall, *Handbook of Microstrip Antennas*. Series IV. 1989, London: Peter Peregrinus IEE.

11. A.G.Derneryd, *Linear Microstrip Antenna*. Chalmer Univ. Technol., Report, Goteborge,Sweden, 1975. **TR 7505**.

12. J.H.Richmond, *A wiregrid Model for Scattering by Conducting Surfaces*. IEEE Trans. Antennas & Propagation, 1966. **AP-14**(Nov): p. 782-786.

13. A.J.Parfitt and T.S.Bird, *Phased Array Antenna Analysis and using Time Delay beam Steering and hybrid FDTD method*. Electronics Letters, 2000. **36**(2): p. 108-110.

14. A.Reineix and B.Jecko, *Analysis of Microstrip Patch Antennas using Finite Difference Time-Domain method*. IEEE Trans. Antennas & Propagation, 1989. **Ap-37**(Nov): p. 1361-1369.

15. Software, Z., *IE3D Users Manual*. Vol. 7.0. 2001: Zeland.

16. H.Gulton and G.Bassinot, *Flat Aerial for Ultra High Frequencies*, in *Patent*. 1955: France.

17. E.V.Byron. *A New Flush-Mounted Antenna Element for Phased Array Applications.* in *Phased Array Antenna Symposium.* 1970.

18. G.G.Sanford. *Conformal Microstrip Phased Array for Aircraft Tests with ATS-6.* in *National Electronic Conference.* 1974.

19. H.D.Weinschel. *Cylindrical Array of Circularly Polarized Microstrip Antennas.* in *IEEE AP-S Society International Symposium on Antennas & Propagation.* 1975.

20. J.R.James and C.J.Wilson, *Microstrip Antennas and Arrays:Part-I-Fundamental action and Limitations.* IEE Proc of Microwaves, Opt and Antennas, 1977. **1**: p. 165-174.

21. T.E.Nowicki. *Microwave Substrates, Present and Future.* in *Workshop on Printed Circuit Antenna Tech.* 1979. Las Cruces.

22. G.R.Traut, *Clad Laminates of PTFE composites for Microwave Antennas.* ibid, 1979. **27**: p. 1-17.

23. A.G.Demeryd, *Linearly Polarized Microstrip Antennas.* IEEE Trans. Antennas and Propagation, 1976. **AP-24**: p. 846-851.

24. P.K.Agarwal and M.C.Bailey, *An Analysis Technique for Microstrip Antennas.* IEEE Trans. Antennas & Propagation, 1977. **AP-25**: p. 756-759.

25. Y.T.Lo, D.Solomon, and W.F.Richards, *Theory and Experiment of Microstrip Antennas.* IEEE Trans. Antennas & Propagation, 1978: p. 53-55.

26. Y.T.Lo, W.F.Richards, and D.D.Harrison, *Improved Theory for Microstrip Antennas.* Electronics Letters, 1979. **15**: p. 42-44.

27. Y.T.Lo, D.Solomon, and W.F.Richards, *Theory and Experiments on Microstrip Antennas.* IEEE Trans. Antennas & propagation, 1979. **AP-27**: p. 137-145.

28. N.G.AlexoPoulos, N.K.Uzunoglu, and I.E.Rana. *Radiation by Microstrip Patches.* in *IEEE International Symp on Antennas & propagation.* 1979.

29. J.R.Mosig and F.E.Gardiol. *The Near field of an Open Microstrip Structure.* in *IEEE AP-S International Symp on Antennas & Propagation.* 1979.

30. E.L.Newmann, *Strip Antennas in a Dielectric Slab.* IEEE Trans. Antennas & Propagation, 1978. **AP-26**: p. 647-653.

31. E.L.Newmann and D.M.Pozar, *Electromagnetic Modelling of Composite Wire and Surface Geometries*. IEEE Trans. Antennas & Propagation, 1978. **AP-26**: p. 784-787.

32. P.Hammer, D.V. Bouchante, and D.Verschraevan, *A model for Calculating the Radiation Fields of Microstrip Antennas*. IEEE Trans. Antennas & Propagation, 1979. **AP-27**: p. 267-270.

33. K.R.Karver and E.L.Coffey, *Theoretical Investigation of the Microstrip Antenna*. Physic. and Sci. Lab., New Mexico State University Tech Report, 1979. **PT 00929**.

34. C.M.Butler. *Analysis of Coax-fed Circular Microstrip Antenna*. in *Workshop on Printed Circuit Antenna Techniques*. 1979. New Mexico State Univ, Las Cruces.

35. C.M.Butler and E.K.Yung, *Analysis of a Terminated Parallel Plate Waveguide with a slot in its upper plate*. Ann. Telecommunication., 1979. 34(9).

36. S.A.Long, *et al.*, *Impedance of a Circular Disc Printed Circuit Antenna*. Electronics Letters, 1978. **14**: p. 684-686.

37. L.C.Chen, *et al.*, *Resonant Frequency of a Circular Disc Printed Circuit Antenna*. IEEE Trans. Antennas & Propagation, 1977. **AP-25**: p. 595-596.

38. S.Bartley and D.Huebner. *A Dual-Beam Low Sidelobe Microstrip Antenna*. in *IEEE AP-S Intl Symposium on Antennas & Propagation*. 1979.

39. J.Yee and W.Furlong. *An Extremely Lightweight Fuselage Integrated Phased Array for Airborne Applications*. 1979. Workshop on Printed Circuit Antenna Technology.

40. F.Cipolla. *A 7.5 GHz Microstrip Phased Array for Aircraft to Satellite Communications*. in *Workshop on Printed Circuit Antenna Technology*. 1979.

41. L.Murphy. *SEASAT and SIR-A Microstrip Antennas*. in *Workshop on Printed Circuit Antenna Tech*. 1979.

42. M.Weiss and R.Cassel. *Microstrip Millimeter Wave Antenna Study*. in *CORADCOM Tech Report*. 1979.

43. K.R.Carver. *Practical Analytical Techniques for the Microstrip Antenna*. in *Workshop on Printed Circuit Antenna Tech*. 1979. New Mexico State Univ., Las Cruces.

44.   C.Wood, *Curved Microstrip lines as Compact Wideband Circularly Polarized Antennas*. IEE Journal of Microwaves Opt and Antennas, 1979. **3**: p. 5-13.

45.   J.W.Mink. *Circular Ring Microstrip Antenna Elements*. in *IEEE AP-S International Symposium on Antennas & Propagation*. 1980. Quebec City Canada.

46.   R.Chandha and K.C.Gupta, *Green's Functions for Triangular Segments In Planar Microwave Circuits*. IEEE Trans of Microwave Theory and Tech., 1980. **MTT-28**: p. 1139-1143.

47.   L.C.Shen, *The Elliptical Microstrip Antenna with Circular Polarisation*. IEEE Trans. Antennas & Propagation, 1981. **AP-29**: p. 95-99.

48.   S.A.Long, *et al.*, *An Experimental Study of the Circular Polarised Elliptical Printed Circuit Antenna*. IEEE Trans on Antennas & Propagation, 1981. **AP-29**: p. 267-270.

49.   R.Chandha and K.C.Gupta, *Green's Function for Circular Sectors, annular Rings and annular sectors in planar microwave circuits*. IEEE Trans. on Microwave Theory Tech., 1981. **MTT-29**: p. 68-71.

50.   E.H.Newmann and P.Tulyathan, *Analysis of Microstrip Antennas using Moment methods*. IEEE Trans. on Antennas and Propagation, 1981. **AP-29**: p. 47-53.

51.   K.R.Carver and J.W.Mink, *Microstrip Antenna Technology*. IEEE Trans. Antennas & Propagation, 1981. **AP-29**: p. 2-24.

52.   T.Itoh and W.Menzel, *A full-wave analysis method for Open Microstrip Structures*. IEEE Trans. Antennas & Propagation, 1981. **AP-29**: p. 63-68.

53.   K.C.Gupta, *Two-Dimensional Analysis of Microstrip Circuits and Antennae*. J.IEEE, 1981. **28**(7): p. 346-364.

54.   C.wood, *Improved Bandwidth of Microstrip Antennas using Parasitic Elements*. IEE.Proc. Pt. H, 1980. **127**: p. 231-234.

55.   W.C.Wilkinson. *A Class of Printed Circuit Antennas*. in *IEEE AP-S Antennas and Propagation International Symposium*. 1974.

56.   H.G.Oltman and D.A.Huebner, *Electromagnetically Coupled Microstrip Dipoles*. IEEE Trans. Antennas & Propagation, 1981. **AP-29**: p. 151-157.

57.  M.D.Deshpandey and M.C.Bailey, *Input Impedance of Microstrip Antennas.* IEEE Trans. Antennnas & Propagation, 1982. **AP-30**: p. 645-650.

58.  Poddar, D.R., J.S.Chatterjee, and S.K.Choudhary, *On some Broad band Microstrip Resonators.* IEEE Trans. Antennas & Propagation, 1983. **AP-31**: p. 193-194.

59.  Y.T.Lo, W.F.Richards, and D.Harrison, *An Improved Theory for Microstrip Antennas and Applications.* RADC-TR-79-Tech Report, 1979. **I**: p. 111.

60.  N.Das and J.S.Chatterjee, *Conically Depressed Microstrip Patch Antenna.* IEE Proc.Pt.H, 1983. **130**: p. 193-196.

61.  N.Das and J.S.Chatterjee, *Quarterwave Microstrip Antenna on ferriMagnetic Substrate.* Electronic Letters, 1981. **17**: p. 441-442.

62.  M.S.Lee and S.S.Lee, *Design of Wideband Quasi-Log-Periodic Microstrip Antenna.* J.of Korean Inst. of Electron. Engg, 1983. **20**: p. 40-44.

63.  A.Henderson and J.R.James, *Design of Microstrip Antenna feeds-PartI-Estimation of raidation Loss and Implications.* IEE Proc.pt.H, 1981. **128**: p. 19-25.

64.  C.Wood, *Analysis of Circular Microstrip Patch Antennas.* IEE Proc.Pt.H, 1981. **128**(2).

65.  A.K.Brown, *Cross-Polarization Characteristics of Linear Comb line Microstrip Antennas.* Electronics Letters, 1980. **16**: p. 743-744.

66.  I.J.Bahl, P.Bhartia, and S.S.Stuchly, *Design of a Microstrip Antenna with covered with a Dielectric layer.* IEEE Trans. Antennas & Propagation, 1982. **AP-30**: p. 314-318.

67.  E.Lier and K.R.Jakobsen, *Rectangular Microstrip Patch Antennas with infinite and Finite Ground Plane Dimensions.* IEEE Trans. Antennas & Propagation, 1983. **AP-31**: p. 978-984.

68.  E.F.Kuester, R.T.Johak, and D.C.Chang, *The Thin Substrate Approximation for Reflection from the End of Slab loaded parallel plate Waveguide with application to Microstrip Patch.* IEEE Trans. Antennas & Propagation, 1982. **AP-30**: p. 910-917.

69. D.M.Pozar, *Input Impedance and Mutual Coupling of Rectangular Microstrip Antennas*. IEEE Trans. Antennas & Propagation, 1982. **AP-30**: p. 1191-1196.

70. P.C.Sharma and K.C.Gupta, *Analysis and Optimized Design of Single Feed Circularly Polarized Microstrip Antennas*. IEEE Trans. Antennas & Propagation, 1983. **AP-31**: p. 949-955.

71. C.C.Liu, J.Shmoys, and A.Hessel, *E-Plane Performance Trade-offs in Two Dimensional Microstrip Patch Element Phased Arrays*. IEEE Trans Antennas & Propagation, 1982. **AP-30**: p. 1201-1205.

72. B.B.Jones, F.Y.M.Chow, and A.M.Seeto, *The synthesis of Shaped Patterns with Series Fed Microstrip Array*. IEEE Trans. Antennas & Propagation, 1982. **AP-30**: p. 1206-1212.

73. Y.Suzuki and T.Chiba, *Computer Analysis Method for arbitrarily shaped Microstrip Antenna with Multiterminals*. IEEE Trans. Antennas & Propagation, 1984. **AP-32**: p. 585-590.

74. E.Lier, *Improved Formulas for Input Impedance of Coax Fed Microstrip Patch Antennas*. IEE Proc. Pt.H, 1982. **129**: p. 161-164.

75. E.F.Kuester and D.C.Chang, *A Geometrical Theory for the Resonant Frequencies and Q-Factors of Some Triangular Microstrip Patch Antennas*. IEEE Trans. Antennas & Propagation, 1983. **AP-31**: p. 27-33.

76. P.B.katehi and N.G.Alexopoulos, *On the Effect of Substrate Thickness and Permittivity on Printed Circuit Dipole Properties*. IEEE Trans. Antennas & Propagation, 1983. **AP-31**: p. 34-39.

77. J.Ashkenazy, P.Perlmutter, and D.Treves, *A Modular Approach for the Design of Microstrip Array Antennas*. IEEE Trans. Antennnas & Propagation, 1983. **AP-31**: p. 190-193.

78. Krowne, C.M., *Cylindrical Rectangular Microstrip Antennas*. IEEE Trans. Antennas & Propagation, 1983. **AP-31**: p. 194-199.

79. J.R.Mosig and F.E.Gardiol, *Anlytical and Numerical Technique using Green's Function Treatment of Microstrip Antennas and Scatterers*. IEE Proc. Pt.H, 1983. **130**: p. 175-182.

80. Ronald.R.DeLyser, D.C.Chang, and E.F.Kuester, *Design of a Log Periodic Strip Grating Microstrip Antenna.* Int'l Journal of Microwave and Millimeter wave Computer Aided Design, 1993. 3(2): p. 143-150.

81. J.S.Dahele and K.F.Lee, *Effect of Substrate Thickness on the Performance of a Circular Disc Microstrip Antenna.* IEEE Trans. Antennas & Propagation, 1983. **AP-31**: p. 358-360.

82. S.N.Prasad and S.Mahapatra, *A New MIC Slot line Aerial.* IEEE Trans. Antennas & Propagation, 1983. **AP-31**: p. 525-527.

83. J.Huang, *The Finite Ground Plane Effect on the Microstrip Antenna Radiation Pattern.* IEEE Trans. Antennas & Propagation, 1983. **AP-31**: p. 649-652.

84. P.C.Sharma and K.C.Gupta, *Analysis and Optimized Design of Single Feed Circularly Polarized Microstrip Antennas.* IEEE Trans. Antennas & Propagation, 1983. **AP-31**: p. 949-955.

85. D.M.Pozar, *Considerations for Millimeter Wave Printed Antennas.* IEEE Trans. Antennas & Propagation, 1983. **AP-31**: p. 740-747.

86. W.F.Richards, J.D.Ou, and S.A.Long, *A Theoretical and Experimental Investigation of annular, annular sector and Circular Sector Microstrip Antennas.* IEEE Trans. Antennas & Propagation, 1984. **AP-32**: p. 864-867.

87. H.Pues and V.D. capelle, *Accurate Transmission-Line Model for the Rectangular Microstrip Antenna.* IEE Proc. Part H, 1984. **131**: p. 334-340.

88. palaniswami, V. and R. Garg, *Rectangular Ring and H-Shaped Microstrip Antennas-Alternatives to Rectangular Patch Antennas.* 1985, 1985. **21**(19): p. 874-876.

89. D.L.Sengupta, *Approximate Expression for the Resonant Frequency of a Rectangular Patch Antenna.* Electronics Letters, 1983. **19**: p. 834-835.

90. K.Y.Wu and J.F.Kauffman. *Radiation Pattern Computations for Cylindrical Rectangular Microstrip Antennas.* in *IEEE AP-S Int'l Symposium on Antennas & Propagation.* 1983. Houston,Tx.

91. N.H.Sabhani and B.V.Rao, *Analysis of a Microstrip Dipole Antenna.* Electronics Letters, 1984. **20**: p. 116-118.

92. P.S.Bhatnagar, *et al.*, *Experimental Study on Stacked Triangular Microstrip Antennas*. Electronics Letters, 1985. **22**: p. 864-865.

93. K.S.Fong, H.F.Pues, and M.J.Withers, *Wideband Multilayer Coaxial Fed Microstrip Antenna Element*. Electronics Letters, 1985. **21**: p. 497-499.

94. A.De and B.N.Das, *Input Impedance of Probe Excited Rectangular Microstrip Patch Radiator*. IEE Proc.Part II, 1984. **131**: p. 31-34.

95. C.J.Prior and P.S.Hall, *Microstrip Disc Antenna with a Short-Circuited Annular Ring*. Electronics Letters, 1985. **21**: p. 719-721.

96. J.R.Mosig and F.E.Gardiol. *The Effect of Parasitic Elements on Microstrip Antennas*. in *IEEE AP-S Int'l Symposium on Antennas & Propagation*. 1985. Vancouver.

97. G.Kumar and K.C.Gupta, *Non-Radiating Edges and Four Edges Gap Coupled Multiple Resonator Broadband Microstrip Antennas*. IEEE Trans. Antennas & Propagation, 1985. **AP-33**: p. 588-593.

98. T.Morioka, S.Araki, and K.Hirasawa, *Slot Antenna with Parasitic Element for Dual band Operation*. Microwave & Optical Technology Letters, 1997. **33**(25): p. 2093-2094.

99. Palanisamy, V. and R.Garg, *Analysis of Circularly Polarized Square Ring and Crossed Strip Microstrip Antennas*. IEEE Trans. Antennas & Propagation, 1986. **AP-34**: p. 1340-1346.

100. Aanandan, C.K. and K.G. Nair, *Compact Broadband Microstrip Antenna*. Electronics Letters, 1986. **22**(20): p. 1064-1065.

101. Hall, P.S., *Multioctave Bandwidth Log-Periodic Microstrip Antenna Array*. IEE Proc.Pt.H, 1986. **133**: p. 127-136.

102. Benalla, A. and K.C. Gupta, *Transmission Line Model for Two port rectangular Microstrip Patch Antennas with ports at Non-radiating Edges*. Electronics Letters, 1987. **23**: p. 882-884.

103. D.M.Pozar, S.M.V., *A Rigerous Analysis of a Microstripline fed Patch Antenna*. IEEE Trans. on Antennas & Propagation, 1987. **AP-35**: p. 1343-1350.

104. H.Y.Yang and N.G.Alexopoulos, *Gain Enhancement Methods for Printed Circuit Antennas Through Multiple Superstrates.* IEEE Trans. Antennas & propagation, 1987. **AP-35**: p. 860-863.

105. A.Reineix and B.Jecko, *Analysis of Microstrip patch Antennas Using FDTD method.* IEEE Trans. Antennas & Propagation, 1989. **AP-37**: p. 1361-1369.

106. A.Benalla and K.C. Gupta, *Multiport Network Approach for Modelling the Model Coupling Effects in Microstrip Patch Antennas and Arrays.* **AP-37**, 1989 (148-452).

107. J.L.Drewniak and P.E.Mayes, *ANSERLIN:A Broadband, Low Profile Circularly Polarized Antenna.* IEEE Trans. Antennas & Propagation, 1989. **AP-37**:
   p. 281-288.

108. Wang, J.J.H. and V.K.Tripp, *Design of Multioctave Spiral Mode Microstrip Antennas.* IEEE Trans. Antennas & Propagation, 1991. **AP-39**: p. 332-335.

109. Lee, D.H.G., M.Kanda, and D.C.Chang, *Characteristics of Iris-Fed Millimeter wave Rectangular Microstrip Patch Antenna.* NBS TN-1063 Tech. Report Nat.Bur Stand W'DC, 1983: p. 44.

110. E.Penard and J.P.Daniel, *Open and Hybrid Microstrip Antennas.* IEE Proc.Pt. II, 1984. **131**: p. 38-44.

111. D.L.Sungupta, *Resonant Frequency of a Tunable Rectangular Patch Antenna.* Electronics Letters, 1984. **20**: p. 614-615.

112. N.G.Alexopoulos, *Criteria for Nearly Omnidirectional Radiation Patterns from Printed Antennas.* IEEE Trans. on Antennas & Propagation, 1985. **AP-33**:
   p. 195-205.

113. Q.Zhang, Y.Fukuoka, and T.Itoh, *Analysis of a Suspended Patch Antenna using Electromagnetically Coupled Inverted Microstrip Feed.* IEEE Trans. on Antennas & Propagation, 1985. **AP-33**: p. 895-899.

114. Y.Hara. *An Omnidirectional Vertical Shaped Beam Three Phased Microstrip Slot Array Antenna.* in *IEEE AP-S Int'l Symposium on Antennas & Propagation.* 1984. Boston,MA.

115. J.Venkataraman and D.C.Chang, *Input Impedance of a Probe-Fed Rectangular Microstrip Patch Antenna.* Electromagnetics, 1983. **3**: p. 387-399.

116.    D.M.Pozar, *Microstrip Antenna Aperture Coupled to a Microstrip Line.* Electronics Letters, 1985. **21**: p. 49-50.

117.    J.L.Kerr. *Microstrip Antenna Developments.* in *Workshop on Printed Circuit Antenna Tech.* 1979. New Mexico State University, Las Cruces.

118.    D.H.Schaubert and F.G.Farrar. *Some Conformal Printed Circuit Antenna Designs.* in *Workshop on Printed Circuit Antenna Tech.* 1979. New Mexico State Univ, Las Cruces.

119.    J.McIlvenna and N.Kernweis. *Variations on the Circular Microstrip Antenna Calculations.* in *Workshop on Printed Circuit Antenna Tech.* 1979. New mexico State Univ. Las Cruces.

120.    S.A.Long and M.D.Walton, *A Dual Frequency Stacked Circular Microstrip Antenna.* IEEE Trans. on Antennas & Propagation, 1979. **AP-27**: p. 270-273.

121.    H.Weinschel and K.Carver. *A Medium Gain Circularly Polarized Microstrip VHF Antenna for Marine DCP Communication to the GOES satellite System.* in *IEEE AP-S Int'l Symposium on Antennas & propagation.* 1976.

122.    K.Itoh and N.Goto, *Dual Frequency Circularly Polarised Microstrip Antennas Composed of Strips and Slots.* IEE Proc.Pt.H, 1983. **130**: p. 170-174.

123.    B.F.Wang and Y.T.Lo, *Microstrip Antennas for Dual-Frequency Operation.* IEE Proc. Pt.H, 1985. **132**: p. 938-943.

124.    Y.Suzuki and T.Chiba, *Improved Theory for Single fed Circularly Polarized Microstrip Antenna.* Trans.Inst.Electron. and Commn Engg, Japan Sect.E, 1985. **E-68**: p. 76-82.

125.    A.J.Svitak, D.M.Pozar, and R.W.Jackson, *Optically Fed Aperture Coupled Microstrip Patch Antennas.* IEEE Trans. on Antennas & Propagation, 1992. **41**: p. 85-90.

126.    A.A.Kishk, *Analysis of Spherical Annular Microstrip Antennas.* IEEE Trans. Antennas & Propagation, 1993. **AP-41**: p. 338-343.

127.    T.Kashiwa, T.Onishi, and I.Fukai, *Analysis of Microstrip Antennas on a Curved Surface Using the conformal grids FDTD Method.* IEEE Trans. on Antennas & Propagation, 1994. **AP-42**: p. 423-427.

128. K.F.Lee, *et al.*, *On the Role of Substrate Loss Tangent In the Cavity Model Theory of Microstrip Patch Antennas.* IEEE Trans. on Antennas & Propagation, 1994. **AP-42**: p. 110-112.

129. S.Dey, *et al.*, *Analysis of Cavity Backed printed Dipole.* Electronics Letters, 1994. **30**(3): p. 173-174.

130. K.F.Tong, *et al.*, *Two -Layer five-Patch Broadband Microstrip Antennas.* Electronic Letters, 1995. **31**(19): p. 1621-1622.

131. Elazar, G. and M.Kisliuk, *Microstrip Liner Slot Array Antenna for X-Band.* IEEE Trans. on Antennas & Propagation, 1988. **36**(8): p. 1144-1147.

132. T.Huynh and K.F.Lee, *Single layer Single Patch Wideband Microstrip Antenna.* Electronics Letters, 1995. **31**(16): p. 1310-1312.

133. H.An, B.K.J.C.Nauwelaens, and A.R.V.D. Capelle, *Broadband Active Microstrip Antenna Design with the Simplified Real Frequency Technique.* IEEE Trans. on Antennas & Propagation, 1994. **AP-42**: p. 1612-1619.

134. D.M.Pozar and S.M.Duffy, *A Dual-band Circularly Polarised Aperture-Coupled Stacked Microstrip Antenna for Globa Positoning Satellites.* IEEE Trans. on Antennas & Propagation, 1997. **AP-45**: p. 1618-1625.

135. K.L.Wong and W.-H. Hsu, *Braodband Triangular Microstrip Antenna with U-Shaped Slot.* Electronics Letters, 1997. **33**(25): p. 2085-2087.

136. Lu, J.H., *Single Feed Dual Frequency Rectnagular Microstrip Antenna with pair of step Slots.* Electronics Letters, 1999. **35**(5): p. 354-355.

137. Lu, J.H., *Novel Dual_Frequency Design of Single Feed Equilateral Triangular Microstrip Antenna.* Microwave & Optical Technology Letters, 1999. **22**(2): p. 133-136.

138. Yang, K.-P., K.L. Wong, and J.H. Lu, *Compact Circularly Polarized Triangular Microstrip Antenna with Y-Shaped Slot.* Microwave & Optical Technology Letters, 1999. **20**(1): p. 31-34.

139. Lu, J.-H., *Single Feed Circularly Polarized Triangular Microstrip Antenna with Zigzagged Edges.* Microwave & Optical Technology Letters, 1999. **22**(5): p. 340-342.

140. Y.X.Guo, K.M.Luk, and K.F.Lee, *U-Slot Circular Patch Antennas with L-Probe feeding.* Electronics Letters, 1999. **35**(20): p. 1694-1695.

141. P.M.Bafrooei and L.Shafai, *Charactierics of Single and Double Layer Microstrip Square Ring Antennas.* IEEE Trans. on Antennas & Propagation, 1999. **AP-47**(10): p. 1633-1639.

142. Jan, J.-Y. and K.L.Wong, *Single Feed Dual Frequency Circular Microstrip Antenna with an Open Ring Slot.* Microwave & Optical Technology Letters, 1999. **22**(3): p. 157-159.

143. Lu, J.-H. and K.L.Wong, *Compact Dual Frequency Circular Microstrip Antenna with an Offset Circular Slot.* Microwave & Optical Technology Letters, 1999. **22**(4): p. 254-256.

144. Sze, J.-Y. and K.L.Wong, *Single layer Single Patch Broadband Rectagular Microstrip Antenna.* Microwave & Optical Technology Letters, 1999. **22**(4): p. 234-236.

145. Sze, J.-Y. and K.L.Wong, *Broadband rectangular Microstrip Antenna with a Pair of tooth-Brush Shaped Slots.* Electronics Letters, 1998. **34**: p. 2186-2187.

146. Lu, J.-H. and K.L.Wong, *Dual Frequency Rectangualr Microstrip Antenna with Embedded Spur lines and Integrated Reactive Loading.* Microwave & Optical Technology Letters, 1999. **21**(4): p. 272-274.

147. Ying, K.-P. and K.L.Wong, *Inclined Slot Coupled Compact Dual Frequency Microstrip Antenna With Cross-Slot.* Electronics Letters, 1998. **34**(24): p. 321-322.

148. C.M.Mak, K.M.Luk, and K.F.Lee, *Proximity Coupled U-Slot Patch Antenna.* Electronics Letters, 1998. **34**(8): p. 715-716.

149. Chen, H.-D., *A Dual-Frequency Rectangular Microstrip Antenna with a Circular Slot.* Microwave & Optical Technology Letters, 1998. **18**(2): p. 130-132.

150. Huang, C.-Y., J.-Y. Wu, and K.-L. Wong, *Slot-Coupled Microstrip Antenna for Broadband Circular Polarisation.* Electronics Letters, 1998. **34**(9): p. 835-836.

151. Chen, W.-S., C.-K. Wu, and K.L. Wong, *Compact Circularly Polarised Microstrip Antenna with Bent Slots.* Electronics Letters, 1998. **34**(13): p. 1278-1279.

152. Wong, K.L., S.-T. Fang, and J.H. Lu, *Dual Frequency Equilateral triangular Microstrip Antenna with a Slit.* Microwave & Optical Technology Letters, 1998. **19**(5): p. 348-350.

153. Wu, C.-K., K.L. Wong, and W.-S. Chen, *Slot-coupled Meandered Microstrip Antenna for Compact Dual Frequency Operation.* Electronics Letters, 1998. **34**(11): p. 1047-1048.

154. Lu, J.-H. and K.L. Wong, *Slot-Loaded Meandered Rectangular Microstrip Antenna with Compact Dual Frequency Operation.* Electronics Letters, 1998. **34**(11): p. 1048-1049.

155. K.L.Wong and J.-Y. Sze, *Dual-Frequency Slotted Rectangular Microstrip Antenna.* Electronics Letters, 1998. **34**(14): p. 1368-1370.

156. Tseng, W.-J., C.S. Hu, and S.-J. Chung, *Planar Retrodirective Array Reflector using Dual-Slot Antenna.* Electronics Letters, 1998. **34**(14): p. 1374-1375.

157. Wong, K.-L. and W.-S. Chen, *Slot-Loaded Bow-Tie Microstrip Antenna for Dual Frequency Operation.* Electronics Letters, 1998. **34**(18): p. 1713-1714.

158. K.M.Luk, R.Chair, and K.F.Lee, *Small Rectangular Patch Antenna.* Electronics Letters, 1998. **34**(25): p. 2366-2367.

159. Z.M.Xie, *et al., Efficient Modelling of Multiple Wideslots On coaxial Antenna.* Electronics Letters, 1999. **35**(14): p. 1121-1122.

160. R.Waterhouse, *Small Microstrip patch Antenna.* Electronics Letters, 1995. **31**(8): p. 604-605.

161. S.Dey and R. Mittra, *Compact Microstrip Patch Antenna.* Microwave & Optical Technology Letters, 1996. **13**(1): p. 12-14.

162. J.S.Baligar, U.K.Revankar, and K.V.Acharya, *Broadband Stacked Annular Ring Coupled shorted Circular Microstrip Antenna.* Electronics Letters, 2000. **36**(21): p. 1756-1757.

163. Hong, C.-S., *Small Annular Slot Antenna with Capacitor Loading.* Electronics Letters, 2000. **36**(2): p. 110-111.

164. E.Lee, P.S.Hall, and P.Gardner, *Compact Dual Band Dual Polarisation Microstrip Patch Antenna.* Electronics Letters, 1999. **35**(13): p. 1034-1036.

165. C.Luxey, *et al.*, *Dual-Frequency Operation of CPW Fed Antenna Controlled by Pin-Diodes*. Electronics Letters, 2000. **36**(1): p. 2-3.

166. K.L.Wong and Y.-F. Lin, *Small Braodband Rectangular Microstrip Antenna with Chip-Resistor Loading*. Electronics Letters, 1997. **33**(19): p. 1593-1594.

167. Y.X.Guo, K.M.Luk, and K.F.Lee, *Dual-Band Slot Loaded Short-Circuited Patch Antenna*. Electronics Letters, 2000. **36**(4): p. 289-291.

168. M.C.Liang, *et al.*, *Capacitor Loaded Frequency Controlled Scheme for Circular Patch Antennas*. Electronics Letters, 2000. **36**(21): p. 1757-1758.

169. Chiou, T.-W., H.-C. Tung, and K.L. Wong, *A Dual Polarisation Wideband Circular Patch Antenna with Hybrid feeds*. Microwave & Optical Technology Letters, 2000. **26**(1): p. 37-39.

170. Tong, K.-F., *et al.*, *A Broadband U-Slot Rectangular Patch Antenna on a Microwave Substrate*. IEEE Trans. on Antennas & Propagation, 2000. **48**(6): p. 954-960.

171. Desclos, L., *Size Reduction of Planar Patch Antenna by Means of Slot Insertion*. Microwave & Optical Technology Letters, 2000. **25**(2): p. 111-113.

172. Chia-LuanTang, J.-Y. Chiou, and K.-L. Wong, *Broadband Dual-Frequency V-Shaped patch Antenna*. Microwave & Optical Technology Letters, 2000. **25**(2): p. 121-123.

173. J.H.Dahale and A.L.Cullen, *Electric Probe Measurements on Microstrip*. IEEE Trans. Microwave Theory and Techniques, 1980. **MTT-28**(Feb): p. 98-104.

174. Inc., T.M., *The Matlab 5.3 Users Manual*. 1999. **R11**.

175. Zeland, *IE3D Users Manual*. Vol. Release 7. 1999, CA.

176. David.M.Sheen, *et al.*, *Application of Three-Dimensional Finite-Difference Time-Domain Method to the Analysis of Planar Microstip circuits*. IEEE Trans. on Microwave Theory and Techniques, 1990. **38**(7): p. 849-857.

177. Taflove, A., *Reinventing Electromagnetics:Emerging Applications of FDTD Computation*. IEEE Computational Science and Engineering, 1995: p. 24-34.

178. R.Luebbers, *et al.*, *A Frequency-Dependant Finite-difference Time-Domain Formulation for Dispersive Materials*. IEEE Trans. on Electromagnetic Combatibility, 1999. **32**(3): p. 222-227.

179. Kane.S.Yee, *Numerical Solution of Initial Boundary Value Problems Involving Maxwell's Equations in Isotropic Media.* IEEE Trans. on Antennas & Propagation, 1966. **AP-14**(3): p. 302-307.

180. G.Mur, *Absorbing Boundary Conditions for the Finite-Difference Approximation of the Time-Domain Electromagnetic field Equations.* IEEE Trans. on ELectromagnetic Compatibility, 1981. **EMC-23**(4): p. 377-382.

181. R.J.Luebbers and H.S.Langdon, *A Simple Feed Model that Reduces Time Steps Needed for FDTD Antenna and Microstrip Calculations.* IEEE Trans. on Antennas & Propagation, 1996. **AP-44**(7): p. 1000.

182. Jose.A.Perada, *et al., Numerical Dispersion and Stability Analysis of the FDTD Technique in Lossy Dielectrics.* IEEE Microwave and Guided Wave Letters, 1998. **8**(7): p. 245-248.

183. X.Zhang and KK.Mei, *Time-Domain Finite-difference Approach to the Calculation of the Frequency Dependant Characteristics of Microstrip Discontinuities.* IEEE Trans. on Microwave Theory Techniques, 1988. **36**: p. 1775-1787.

**INTERNATIONAL JOURNALS**

1. **GS Binoy,** C K Aanandan, P Mohanan, K Vasudevan & K G Nair "Single Feed Dual Frequency Dual Polarised Slotted Square Microstripantenna", *"Microwave & Optical Technology Letters"*, **Texas, USA,** Vol 25 No 6, June20, 2000 pp 395-397

2. **GS Binoy**, C K Aanandan, P Mohanan, K Vasudevan "Compact dual frequency dual polarised slotted microstrip patch antenna", *"Microwave and Optical Technology Letters"*, **Texas, USA,** Vol 29 No. 1 April 5 2001 pp 60-62

3. **GS Binoy**, C K Aanandan, P Mohanan, K Vasudevan "Dual Frequency Dual Polarised Slot-Coupled Compact Microstrip Antenna For Communication Systems", Accepted for publication in *International Journal of Electronics*, London, UK

4. **GS Binoy**, C K Aanandan, P Mohanan, K Vasudevan, "Slot-Coupled Square Microstrip Antenna for Compact Dual Frequency Operation", *Microwave and Optical Technology Letters"*, **Texas, USA,** Vol 32, No1. January 5 2002 pp 7-9

5. **G S Binoy,** C K Aanandan, P Mohanan and K Vasudevan, "A Novel patch antenna with chip capacitor loading for communication Systems", communicated to **Electronics Letters, UK**

**INTERNATIONAL PROCEEDINGS**

6. **GS Binoy**, C K Aanandan, P Mohanan, & K.Vasudevan, "Dual band Square MicrostripAntenna Embedded With A Shaped Slot", Proc of the International symposium on Antennas Propagation and Electromagnetic theory, Vol No.I Page No 6-9. **(ISAPE-2000)** China.

7. **GS Binoy**, C K Aanandan, P Mohanan, & K Vasudevan " Dual Band Square Microstrip Antenna Embedded With A Placard Shaped Slot", Proc of the International symposium on Antennas &Propagation **(ISAP2000)**, Tokyo Institute of Technology, Japan.

8. **G S Binoy**, C K Aanandan, P Mohanan & K Vasudavan "Square Microstrip Slot Antenna with Chip Capacitor Loading for Dual Frequency Operation", Proceedings of the **IEEE AP-S** Symposium on Antennas and Propagation, Boston, Massachusetts, USA from 8-13 July 2001.

9. **G S Binoy** and K Vasudevan "Dual Frequency Square Microstrip Slot Antenna with Chip Capacitor Loading for EMI Shielding", accepted for presentation in the forthcoming **EMC 2002** to be held at Wroclaw, Poland from June 25-28 2002.

10. **G S Binoy,** C K Aanandan, P Mohanan and K Vasudevan, "Analysis Of A Compact Microstrip Patch Antenna With Tuning Stubs For Dual Frequency Trimming And Dual Polarization", abstract submitted to **PIERS-2002** , to be held at Cambridge, MA, USA in July 2002.

## NATIONAL PROCEEDINGS

11. **G S Binoy,** C K Aanandan, P Mohanan & K Vasudavan, "Capacitor Loaded Square Slot Antenna for Dual Frequency Operation", Proceedings of the National Symposium on Antennas and Propagation", **APSYM 2000,** CUSAT, Cochin December 2000.pp 82-85

12. I N Jawahar, **G S Binoy,** P Mohanan, & M T Sebastian: A Novel Method for Tuning the Microwave Dielectric properties by Stacked Dielectric Resonatiors", Proceedings of **APSYM-2000,** CUSAT, Cochin, December 2000 pp 173-175

13. **G S Binoy,** C K Aanandan, P Mohanan & K Vasudavan "Slot-loaded Square Dual Frequency Dual Polarised Square Microstrip Antenna ", Proceedings of the National Symposium on Advances in Elctronics,"**ELECTRO-2001**", IT, BHU, Varanasi, January 4-6, 2001.

14. S Mridula, **G S Binoy,** C K Aanandan, P Mohanan & K Vasudavan, "Multi-layer Bow-Tie Microstip Antenna", Proceedings of National Conference on Technology Convergence for Information Communication and Entertainment.**NICE-2001,** Cochin, February 2001 pp. 195-197

15. **GS Binoy,** C K Aanandan, P Mohanan & K Vasudevan "Analysis Of A Three Stub Slotted Square Microstrip Antenna For Dual Frequency And Dual Polarisation Operation ", Proceedings of the National Conference on "Microwaves, Antennas & Propagation , '**Microwaves-2001**', Nov 2-4 at Jaipur Organised by SSJS PG College.JP.pp.130-133.

16. **GS Binoy,** C K Aanandan, P Mohanan & K Vasudevan, "Design of A Symmetric Slot Antenna For Dual Frequency Dual Polarization Operation" Proc. of **NCC-2002,** organized by IIT, Mumbai, from Jan 26-27, 2002.

17. **G S Binoy** & K Vasudevan, " Design of Square Patch Antennas with Dual Frequency Operation with reduced area for Mobile Communication Systems". Proceedings of the 14th State Science Congress held at CUSAT, Cochin, Kerala, India from 29-31 January 2002 pp. 506-509.

18. **G S Binoy,** P Mohanan & K Vasudevan, "A novel patch antenna design for satellite and mobile communication Systems", accepted **for** presentation at the forthcoming national Seminar on Interactive Integrated Technological Advancement-Recent Trends (IITART) to be held at College of Engineering, Trivandrum, from July 5-6, 2002.

# BINOY G S – Brief Resume

| *Permanent Address* | *Present Address* |
|---|---|
| 'Saral', TC 15/1205<br>Kukkilia Lane<br>Jagathy<br>Trivandrum<br>Kerala -695014, India<br>Phone  : 91 471 320754<br>E-mail : binoygs@yahoo.com | Senior Research Fellow, Department of Electronics,<br>Cochin University of Science and Technology,<br>Cochin-682 022, Kerala, India<br>Phone: 91 484 576814, Fax: 91 484 575800<br>E-mail: binoygs@cusat.ac.in |

**Objective:** To involve in Research and Development activities in the field of Microstrip Antennas for satellite and mobile communication systems, Computational Electromagnetics, Microwave Propagation, Material Characterization and Microwave Devices.

## EDUCATION

(a)     *PhD in Microwave Electronics (Antennas)-* Thesis submitted by **June 2002**

(b)     Master of Science in Physics- ***Kerala University, Kerala, India (July 1997)***

(c)     Bachelor of Education - ***Kerala University, Kerala, India*** (August 1998)

(d)     *Bachelor of Science in Physics-* ***Kerala University, Kerala, India*** (July 1995)

## COMPUTER PROFICIENCY

**Operating Systems**     DOS, WINDOWS 9*/NT, LINUX

**Technical Applications** PUFF, IE3D, FIDELITY, MATHEMATICA, MATLAB

**Languages**     C, HP BASIC

## AWARDS OBTAINED

❖ **Young Scientist Travel Grant Support** by CSIR, Government of India. As part of award, participated in the IEEE AP-S Antennas & Propagation Symposium held at Boston, Massachusetts, USA during July 2001. Candidate has also presented his research paper in that scientific event.

❖ Selected for the **Young Collaborator Programme** at the The Abdus Salam International Center for Theoretical Physics ( ICTP), Trieste, Italy. Participated in the 'SCHOOL ON DATA AND MULTIMEDIA COMMUNICATIONS USING  TERRESTRIAL AND SATELLITE RADIO LINKS', during February - March 2001.

❖ **URSI Young Scientist Award** support for attending and presenting a research paper at the EMC 2002 at Poland Wrocalw.